REPORT DOCUMENTATION PAGE	READ INSTRUCTIONS BEFORE COMPLETING FORM

1. REPORT NUMBER 79-270D	2. GOVT ACCESSION NO. AD-A106782	3. RECIPIENT'S CATALOG NUMBER

4. TITLE (and Subtitle) Transient Effects in Turbulence Modelling.	5. TYPE OF REPORT & PERIOD COVERED THESIS/DISSERTATION
	6. PERFORMING ORG. REPORT NUMBER

7. AUTHOR(s) David Roy Boyle	8. CONTRACT OR GRANT NUMBER(s)

9. PERFORMING ORGANIZATION NAME AND ADDRESS AFIT STUDENT AT: Massachusetts Institute of Technology	10. PROGRAM ELEMENT, PROJECT, TASK AREA & WORK UNIT NUMBERS

11. CONTROLLING OFFICE NAME AND ADDRESS AFIT/NR WPAFB OH 45433	12. REPORT DATE Dec 1979
	13. NUMBER OF PAGES 272

14. MONITORING AGENCY NAME & ADDRESS(If different from Controlling Office)	15. SECURITY CLASS. (of this report) UNCLASS
	15a. DECLASSIFICATION/DOWNGRADING SCHEDULE

16. DISTRIBUTION STATEMENT (of this Report)

APPROVED FOR PUBLIC RELEASE; DISTRIBUTION UNLIMITED

NOV 6 1981

17. DISTRIBUTION STATEMENT (of the abstract entered in Block 20, if different from Report)

20 OCT 1981

18. SUPPLEMENTARY NOTES

APPROVED FOR PUBLIC RELEASE: IAW AFR 190-17

FREDRIC C. LYNCH, Major, USAF
Director of Public Affairs
Air Force Institute of Technology (ATC)
Wright-Patterson AFB, OH 45433

19. KEY WORDS (Continue on reverse side if necessary and identify by block number)

20. ABSTRACT (Continue on reverse side if necessary and identify by block number)

ATTACHED

81 10 27 224

DTIC FILE COPY

TRANSIENT EFFECTS IN TURBULENCE MODELLING

by

DAVID ROY BOYLE

B.S., University of Cincinnati
(1971)

M.S., Georgia Institute of Technology
(1972)

SUBMITTED IN PARTIAL FULFILLMENT
OF THE REQUIREMENTS FOR THE
DEGREE OF

DOCTOR OF PHILOSOPHY

at the

MASSACHUSETTS INSTITUTE OF TECHNOLOGY

December 1979

© David Roy Boyle

Signature of Author _____
Department of Nuclear Engineering
December 26, 1979

Certified by _____
Michael W. Golay
Thesis Supervisor

Accepted by _____
Allan F. Henry
Chairman, Department Committee
on Graduate Students

TRANSIENT EFFECTS IN TURBULENCE MODELLING

by

DAVID ROY BOYLE

Submitted to the Department of Nuclear Engineering
on December 24, 1979 in partial fulfillment of the
requirements for the Degree of Doctor of Philosophy in
Nuclear Engineering

ABSTRACT

Measurements of turbulence field data are reported for recirculat-
ing water flows under steady-state and transient flow conditions in an
improved 1/15 scale FFTF outlet plenum test-cell. A dual-channel
Laser Doppler Anemometer is used, and a unique method for performing
transient measurements is developed and analyzed. The experimental
behavior is predicted with a modified version of the VARR-II fluid
dynamics code, and the suitability of using the steady-state turbulence
model closure assumptions for analysis of transient flows is evaluated.
A relationship between $K-\sigma$ and $K-\epsilon$ turbulence models is derived, and the
two models are found to be nearly equivalent.

Steady-state and transient mean velocity data are well-predicted
throughout most of the test-cell. Calculated spatial distributions
of the scalar turbulence quantities are qualitatively similar for
both models; however, the predicted distributions do not match the data
over major portions of the flow area. The $K-\sigma$ model provides better
estimates of the turbulence quantity magnitudes.

The predicted results are found to be highly sensitive to small
changes in the turbulence model free parameters and to depend heavily
on the levels of inlet turbulence. A parametric analysis shows that
important differences observed between prediction and measurement
cannot be significantly reduced by simple changes to the model's
constants.

The transient analysis indicates that, for the coast-down rate,
flow-speeds, and geometry used in this experiment, the turbulence
model closure assumptions are adequate. An approximate method is
described for determining the applicability of this conclusion to
other flows.

Thesis Supervisor: Dr. Michael W. Golay
Title: Associate Professor of Nuclear Engineering
Thesis Reader: Dr. Neil E. Todreas
Title: Professor of Nuclear Engineering

TRANSIENT EFFECTS IN TURBULENCE MODELLING

by

DAVID ROY BOYLE

Submitted to the Department of Nuclear Engineering
on December 24, 1979 in partial fulfillment of the
requirements for the Degree of Doctor of Philosophy in
Nuclear Engineering

ABSTRACT

Measurements of turbulence field data are reported for recirculating water flows under steady-state and transient flow conditions in an improved 1/15 scale FFTF outlet plenum test-cell. A dual-channel Laser Doppler Anemometer is used, and a unique method for performing transient measurements is developed and analyzed. The experimental behavior is predicted with a modified version of the VARR-II fluid dynamics code, and the suitability of using the steady-state turbulence model closure assumptions for analysis of transient flows is evaluated. A relationship between K-σ and K-ϵ turbulence models is derived, and the two models are found to be nearly equivalent.

Steady-state and transient mean velocity data are well-predicted throughout most of the test-cell. Calculated spatial distributions of the scalar turbulence quantities are qualitatively similar for both models; however, the predicted distributions do not match the data over major portions of the flow area. The K-σ model provides better estimates of the turbulence quantity magnitudes.

The predicted results are found to be highly sensitive to small changes in the turbulence model free parameters and to depend heavily on the levels of inlet turbulence. A parametric analysis shows that important differences observed between prediction and measurement cannot be significantly reduced by simple changes to the model's constants.

The transient analysis indicates that, for the coast-down rate, flow-speeds, and geometry used in this experiment, the turbulence model closure assumptions are adequate. An approximate method is described for determining the applicability of this conclusion to other flows.

Thesis Supervisor: Dr. Michael W. Golay
Title: Associate Professor of Nuclear Engineering
Thesis Reader: Dr. Neil E. Todreas
Title: Professor of Nuclear Engineering

ACKNOWLEDGEMENTS

TABLE OF CONTENTS

LIST OF TABLES

LIST OF FIGURES

NOMENCLATURE

$\alpha, \alpha_1, \Gamma, \Gamma_1$ constants appearing in transport equations of K-σ model

α_x, d_z donor cell coeficients

β_o relaxation factor

C_1, C_2, C_μ constants appearing in transport equations of K-ϵ model

ΔL optical path length difference

ϵ turbulent energy dissipation rate

f_c RC circuit cut-off frequency

f_D Doppler frequency (Hz)

K turbulent kinetic energy

ℓ length scale or Prandtl's mixing length

L_c laser coherence length or characteristic length

λ wavelength of laser light

n_i index of refraction of substance i

N_2 number of fringes in the measuring volume

ω frequency in radians

ω_D Doppler frequency (radians)

ω_o frequency of laser

ω_1 frequency of Doppler shifted light

ω_2 frequency of reference beam light

P pressure

Re Reynolds number, defined with respect to inlet duct

ρ density of the fluid

σ turbulent kinematic viscosity

$\sigma_K, \sigma_\epsilon$ effective turbulent Prandtl number for transport of K and ϵ

t time

$T_{int.}$ integration time

$t_{trans.}$	transient time scale
$t_{turb.}$	turbulence time scale
τ	integration time constant for RC-circuit
θ	half angle of the beam intersection
$\overline{U}$	mean velocity (vertical or X direction)
U_c	characteristic velocity
$\overline{U}_e$	ensemble averaged velocity
$\overline{U}_i$	velocity component in i-direction
$\overline{U}_t$	time averaged velocity
$\overline{u_i' u_j'}$	kinematic Reynolds stresses
$\overline{u' v'}$	kinematic shear stress
u', v', w'	fluctuating velocity components
$\overline{V}$	mean velocity (horizontal or Y direction)
$\overline{W}$	mean velocity in Z direction
X_i, X_j	general Cartesian coordinate

CHAPTER ONE

INTRODUCTION

1.0 Overview

Accurate design of many types of fluid-flow and heat-transfer equipment is aided by accurate knowledge of the fluid velocities, temperatures and turbulence intensities that develop within the particular mechanical component under study. Knoweldge of these parameters permits detailed estimates of such important quantities as local heat-transfer coefficients, pressure-drops, fluid/solid mechanical interactions forces, and thermal shock effects. One important area where this information is needed is in the design of the outlet plenum region of a liquid-metal-cooled fast breeder reactor (LMFBR).

The efficient heat transfer characteristics of liquid metal coolant, combined with the relatively high bulk temperature change across the core (approx. 300°F), present thermal shock problems for nozzles and other above-core mechanical components in the event of a reactor scram from full power, with or without pump coast-down [1]. In an effort to mitigate these effects, current outlet plena designs provide for a large inventory of "hot" coolant above the core, and a "chimney-like" entrance to the outlet plenum. The chimney forces the relatively cool core-outlet flow to mix with the existing high temperature fluid in the plenum so that the average temperature of the fluid contacting the high-temperature

structure is raised to some safe value.

One method of predicting the success of this design is to solve numerically the applicable fluid dynamics equations. A number of computer programs exist for this purpose, and newer versions and updates of these codes are currently evolving. For the turbulent flow case (the most likely and hence most practical), all such codes employ a turbulence model to compensate for the fact that averaged versions of the Navier-Stokes equations present more unknowns that independent equations. Turbulence models, then, are just additional equations (they may be algebraic or differential) that close the set of equations which describe a particular problem, thereby allowing a solution to be obtained.

The turbulence models currently being used vary widely in their complexity. In general, they all depend to some degree on heuristic reasoning for their derivation, and contain adjustable constants (model free parameters) that are set based on existing experimental data. Although the majority of current models employ free parameters that were obtained from steady-state flow experiments, they are, of necessity, being used to solve transient problems like the LMFBR outlet plenum flow described above.

The purpose of this work is to examine the applicability of an essentially steady-state turbulence model to the solution of transient flow problems. The method used is to perform flow-mapping measurements during a transient in a simple geometry similar to the LMFBR outlet plenum configuration. A comparison is then made between the measurements and the code calculations to determine the accuracy of the model's

predictions. In this way it is possible to determine situations in which the models are fundamentally inadequate, to identify vital input data requirements for accurate calculations, and to guide improvements in the models for application to transient flows.

1.1 Background

This effort is part of a larger program, the overall goal of which is the validation and improvement of calculational methods for analysis of LMFBR outlet plenum flow transients. The most general situation involves a transient in both flow-rate and fluid temperature occurring in three-dimensional space. The approach taken for assessment of the various calculational models and methods has been to separate the relatively complex general transient into its more readily studied parts. Results are compared to the numerical predictions for that particular flow situation. In this way, individual effects of the various physical parameters on the model's predictions can be isolated and studied. For example, two previous projects have dealt respectively with two-dimensional steady-state isothermal flows [2] and with two-dimensional thermally mixing flows [3]. This effort considers two-dimensional transient flows under isothermal conditions. Follow-on work has begun on two-dimensional thermal transients and three-dimensional steady isothermal flows.

1.2 Scope

In this work a lab-scale outlet plenum test-cell, with internal dimensional ratios that simulate the Fast Flux Test Facility (FFTF), is

considered experimentally and computationally. Isothermal water flow transients are produced in the test-cell, and Plexiglas side-wall construction permits measurement of turbulence field quantities throughout the cell by a Laser Doppler Anemometer (LDA).

The LDA, and its associated electronics, is arranged to measure two orthogonal velocity components, turbulent kinetic energy (TKE), and the velocity cross correlation (proportional to Reynolds Stress) simultaneously at any point within the test-cell. At a number of different locations, the values of these quantities are recorded during a flow shut-down transient that is repeated successively to permit ensemble averaging of the recorded values. The result is a record of the mean fluid velocity components and the turbulence field parameters throughout the test-cell as a function of time during a transient. Details of the measurement technique, data reduction, and the method for achieving a repeatable flow transient are presented in Sec. 3.

For the computational work, the VARR-II computer code is used to generate predictions of the same turbulence field parameters measured above. VARR-II is a two-dimensional time-dependent thermal-hydraulic code that employs a unique two equation turbulence model, and was developed for designer use in the LMFBR programs. Flow map "snapshots" of velocity vectors and values of the primary turbulence quantities are produced by the code at various times during a numerical shut-down transient that is matched to the experimentally determined plenum inlet flows. These data are then compared with the experimental results.

In order to generate a shut-down transient, in either the experimental or numerical case, an initial steady state flow pattern must

be established. In a previous work, Chen [4] has considered the steady-
state case in essentially the same geometry, with mixed results. He
suggested that departure from turbulence isotropy in the experimental
test-cell, along with insufficient knowledge of detailed inlet conditions,
could explain some of the poor predictions produced by VARR-II.
Accordingly, the test-cell inlet has been modified in this effort to
improve the degree of isotropy, flow symmetry, and velocity profile
control in order to determine their effect on code performance. In
addition to the transient data, therefore, detailed steady-state
measurements were also accomplished, as were steady-state computer runs.
A number of numerical experiments were performed for the steady-state
case to investigate the effects of mesh size, boundary conditions,
turbulence model constants, and the artificial diffusion term that
accompanies full donor cell differencing.

CHAPTER TWO

LITERATURE REVIEW

2.0 Introduction

The basis for the computational analysis of turbulent flows is the
so-called "turbulence model" that relates the complex small-scale motions
in the flow to the large-scale mean quantities that are more readily
calculated on reasonably sized machines. This review begins with a
brief description of the types and characteristics of available turbulence
models. The question of transient influence on model performance is
subsequently addressed as a rationale for the experiment itself. Finally,
recent work at Argonne National Laboratory (ANL) on a related experiment
and computational scheme is reviewed to put this effort in context.

2.1 Turbulence Models

Mathematical predictions of isothermal turbulent flows begin with
the well-known conservation equations for mass and momentum. This set
of partial differential equations (pde) is generally agreed to be "exact"
in the sense that its solution completely and correctly describes the flow
of a single-phase Newtonian fluid. However, for turbulent flows, this
equation set cannot be solved analytically. Direct recourse to finite
difference formulations and digital computers proves impractical because
the exceedingly small spatial scale of turbulent fluctuations requires

a very fine grid and the number of mesh points needed for the simplest problem exceeds present computer capabilities by two to three orders of magnitude [5].

On the assumption that the important effects of turbulence may be accounted for by average or statistical measures of the fluctuating quantities, an approximate method for computing turbulent flows is commonly used. Following Reynolds' classic time-averaging of the Navier-Stokes Equations, the instantaneous velocity is decomposed into its mean and fluctuating parts and substituted into the "exact" equations; these equations are ensemble averaged, resulting in a new set of partial differential equations for the mean quantities [6]. Since all of the dependent variables in this set of equations are averaged quantities, they do not vary nearly as rapidly over space as the original turbulent fluctuations; therefore, the problem of an excessively fine grid for the finite difference formulation is overcome. However, the new set of equations so obtained is not complete, that is, there are now more unknowns than independent equations. The averaging process produces these additional unknowns in the form of correlations or mean products of fluctuating quantities. In the case of isothermal incompressible flow, which is dealt with in this work, the unknown correlation that arises is $\overline{u'_i u'_j}$, the so-called Reynolds Stress.

In effect, all of the influence of the turbulence on the mean motion is contained in this term. In order to close the set of averaged equations, a relationship between $\overline{u'_i u'_j}$, and one or more of the other mean quantities is required. The non-linear nature of the applicable equations is such that an exact mathematical derivation of the

required relation is impossible. Therefore, an equation, or set of equations, must be developed to specify the new unknowns in terms of the other variables, and thereby permit the solution of the averaged equation set. These relational equations are turbulence models.

2.1.1 Types of Models

Turbulence models are usually classified by the number of transport type pde's they involve. The motivation for going to more complex models (more equations) lies in the hope of improved generality and reduced reliance on empirical prescriptions for solutions to engineering turbulence flow problems. The five major categories of turbulent-flow pde models are succinctly described by W. C. Reynolds [7]:

1. Zero-equation models -- models using only the pde for the mean velocity field, and no turbulence pde's.

2. One-equation models -- models involving an additional pde relating to the turbulence velocity scale.

3. Two-equation models -- models incorporating an additional pde related to a turbulence length scale.

4. Stress-equation models -- models involving pde's for all components of the turbulent stress tensor.

5. Large-eddy simulations -- computations of the three-dimensional time-dependent large-eddy structure and a low-level model for the small-scale turbulence.

Launder and Spalding [8] give a clear and definitive treatment of these models, their derivation, advantages, and shortcomings. They also show that, for recirculating flows, the two-equation model is the simplest

that can provide realistic predictions of the quantities that the designer needs to know. Since the experiment in this work involves recirculating flow, a two-equation turbulence model is used for the computer predictions.

2.1.2 Two-Equation Models

Two-equation models attempt to determine turbulent kinetic energy (TKE = K) and length scale (ℓ) from transport equations. These two quantities, in turn, specify the turbulent viscosity (σ), which relates the unknown Reynolds Stress to mean velocity gradients, the basic goal of all turbulence models. Early work in this area has shown that the turbulence length scale, ℓ, does not diffuse as the gradient of ℓ, and so transport equations for this quantity have not produced successful models. Accordingly, it has become standard practice to write the second transport equation for some other quantity that is related to ℓ, usually either the turbulent energy dissipation rate (ε), or directly in terms of σ itself.

The turbulence model used in VARR-II takes the latter approach and is a so-called K-σ model developed by J. H. Stuhmiller [9]. The alternative K-ε model, such as used in the TEACH-T code [10], was not employed directly in this work since TEACH-T is a steady-state code. However, a mathematically equivalent model (fully described in Sec. 4) was derived for use in VARR-II and results are reported for both model types.

2.2 Transient Effects

A common method for generating the additional transport equations that form the turbulence model is described by Bradshaw [11]. Exact transport equations for the quantities of interest can be formed by operating on the

averaged momentum equations. These exact equations contain unknown corre-
lations, each of which must be modelled in terms of known mean variables
before the solution can proceed. This process, necessarily approximate,
entails a degree of heuristic reasoning based on diverse factors such as
experience, phenomenological studies and the mathematical properties of
tensors. Whichever closure assumptions are used, the resulting model
equations contain constants, or free parameters, that must be set by experi-
ment. Empirical results used to determine values for these free parameters
necessarily come from available data largely derived from steady-state
experiments. Bradshaw has noted that "unsteady flows present no extra
problems in turbulence modelling as long as the total transport term is
no larger than in corresponding steady flows." [12] This is clearly true
for the exact formulations; e.g., the transport equation for quantity ξ
is

$$\frac{\partial \xi}{\partial t} + U_i \frac{\partial \xi}{\partial X_i} = \text{production} + \text{diffusion} - \text{dissipation} . \qquad (2.1)$$

total transport term

Strictly speaking, the magnitude of the transport term, not the relative
contributions of its components, determines the physics of the situation.

However, when the unknown terms in the right-hand side of Eq. 2.1
are modelled, the free parameters are established independently via
different experiments. Generally the decay of isotropic turbulence is
considered to determine a portion of the unknown constants, and then the
remaining free parameters are specified by homogeneous shear flow experi-
ments where the transport terms vanish completely. Reynolds and Cebeci
[13] point out that this procedure implies the assumption that the same

empirical input suffices for both types of flow.

Of more direct importance to this work are Stuhmiller's closure approximations for the K-σ model used in the VARR code. His unique development considers a single wavenumber of the turbulence frequency spectrum. Physical interpretation of the interactions with other wavenumbers leads to linearized forms of the equations of motion for the fluctuating quantities. The concept of simulated fluctuations at a single wave number makes explicit solution of the linearized equations possible. Stuhmiller suggests that an advantage of this approach is that it preserves the dynamical relation between fluctuations in addition to the root mean square amplitude of the correlations. However, the assumption of zero, or nearly zero, time derivatives is an essential feature of his complex development. Stuhmiller addresses this point, and partially motivates the current work, when he states that his assumption of constant mean flow is an approximation that must be assessed by comparison with experiment.

2.3 Related Outlet Plenum Studies

An extensive series of experimental and analytical studies of thermal hydraulic behavior in LMFBR outlet plena is currently underway at Argonne National Laboratory (ANL). The ANL reports on this work are numerous; a recent article by Howard and Carbajo [14] references a number of the relevant papers. Experiments performed in this series were in more prototypic (3-D, cylindrical) geometries and on a larger scale than used in the current work. Simultaneous temperature and flow transients were examined and the effects of the important dimensionless groups studied. Based on this work, calculational techniques have been developed, MIX [15]

and Plenum-3 [16] for example, that feature much shorter run times than detailed fluid dynamics codes such as VARR-II.

MIX uses the vorticity stream-function formulation and a zero-equation turbulence model that specifies a constant turbulent viscosity from experiment. Plenum-3 uses a lumped-parameter approach that separates the outlet plenum into three vertically stacked regions and solves the conservation equations in each region. The code predictions are generally assessed by comparing fluid temperature data at a number of key locations within the plenum. Agreement between codes of this type and experiment has been good, better in fact than more complex, longer running codes, such as VARR-II [17].

The experiments performed in the ANL series primarily measured fluid temperatures and did not provide detailed velocity and/or turbulence field data. Overall evaluation of the more sophisticated turbulence models, such as that used in VARR, as well as improvements in the model free parameters, can be more effectively accomplished from a data base of specific turbulence field measurements. For example, a recent article by N. Markatos [18] describes the application of a K-ε two-equation model to the transient flow of liquid sodium in a geometry similar to that used in the current work. Turbulence model performance is not directly discussed in his paper. However, the overall code predictions are found to be "in qualitative agreement with expectations," pointing out the sparsity of detailed experimental data on turbulent recirculating flows in this geometry.

25

CHAPTER THREE

EXPERIMENTAL WORK

3.0 Introduction

Measurements of turbulence field parameters (TFP), i.e., two velocity

components ($\overline{U}$ and $\overline{V}$), turbulent kinetic energy (TKE $= \dfrac{\overline{u'2} + \overline{v'2}}{2}$), and

Reynolds Stress ($\overline{u'v'}$), have been made in a plexiglas-walled test cell

that is a two-dimensional stylized model of an LMFBR outlet plenum. The

measurements were made with a dual-channel Laser Doppler Anemometer (LDA)

which is described in detail in Sec. 3.2. For a typical measurement

sequence, flow conditions in the test cell were initially established at

a predetermined "full" or steady-state flow rate; measurement of the TFPs

were made to determine the initial or steady-state values; then a repeat-

able flow transient was induced that caused the inlet flow rate to decrease

to 32.5% of its initial value in 120 seconds. During this flow coast-down

the values of the TFPs were recorded electronically. The same transient

measurement was repeatedly performed at 42 locations throughout the cell so

that ensemble averages could be calculated for all the TFPs during the flow

transient. At 37 additional locations, steady-state measurements were

made to provide a more detailed description of the full-flow field. The

net result of this process is a series of time-sequenced "snapshot" plots

of velocity vectors and a record of the values of average TKE and Reynolds

Stress as a function of time during the transient. These data are

presented and discussed in Sec. 5.

This chapter describes the hydraulic and electronic details of the experimental apparatus. Moreover, since turbulence measurements in the presence of mean flow transients are not commonly made, the specific measurement technique used and its effect on accuracy are also presented.

3.1 Hydraulics

3.1.1 General Description of Loop

A schematic view of the hydraulic loop is shown in Fig. 3.1. The loop is closed and filled with distilled water. The filter and de-mineralizers are used to maintain water purity and thereby to inhibit corrosion and provide a controlled concentration of scattering particles for use by the LDA. Two pumps are mounted in parallel to provide a variety of flow rates. The five hp pump was used in this experiment to obtain the maximum possible initial inlet Reynolds No.

The heat exchanger served a dual purpose. Initially it functioned as a heat source to raise the loop temperature to 110°F; from that point it became a heat sink and maintained isothermal fluid conditions by dissipating pump-heat during the prolonged experimental runs. The parallel-mounted rotameters were useful for providing gross indications of flow-transient repeatability and for monitoring flow rates during and between runs. A more precise measure of the repeatability factor involved the LDA measurements themselves and is discussed in Sec. 3.1.2. Each transient run began with both flow meters indicating 100%, and at the end of the run, flow had decreased monotonically to 32.5% indicated on the larger rotameter.

3.1.2 Repeatable Flow Transient Generator--(RFTG)

The turbulence parameters measured in this experiment were obtained by constructing ensemble averages (see Sec. 3.3 for details) of the time-varying fluid flow properties measured by the LDA. This necessarily required a flow transient that could be faithfully repeated a large number of times. Further, the transient to be measured had to be initiated automatically so that the data recorder always collected data from the same time base for each run.

The technique selected is illustrated in Fig. 3.2. A two-inch (air-to-open, spring-to-close) diaphragm control valve with a Moore Valve Positioner/Controller was installed at the outlet of the pump down stream of the flow meters. During the steady-state (full flow) period, an air signal is supplied via the three-way solenoid valve to the instrument port of the valve controller. The amount of valve travel is proportional to the air pressure at this port. By regulating this source of air to the valve controller the steady-state flow rate can be repeatably set at any initial value desired. This initial charge of air was accurately checked for repeatability with a Heise pressure gauge throughout the experimental period. At the start of the transient, the solenoid is energized, and air is permitted to slowly bleed out of the valve controller instrument port (and parallel-connected surge-tank) through a micrometer-adjusted needle valve. The micrometer setting determines the rate of air pressure decrease at the instrument port and thereby the valve closure speed, and ultimately, the fluid flow rate. This simple system fulfills the automatic requirement, and has been tested for repeatability with excellent results.

Two methods were used to check and maintain the flow-transient repeatability throughout the data collection period. The flow-meters were one source of information for determining repeatability of initial and final flow rates. A more accurate determination was made at each measurement point by using the output voltage of the LDA Frequency Trackers to insure that the initial velocity at a point was the same (within 1%) as the previous run. This was particularly useful after an overnight shut-down. In such a case, the LDA measuring volume was not moved from the last point measured until the loop was fully warmed up and the steady-state velocity at that point had stabilized to the same value (within 1%) that had been recorded on the previous day.

The repeatability of the shape of the flow transient as a function of time was ascertained by visual readings of the flow meters during repetitive valve close-downs with a fixed needle-valve setting for various rates of closure. Flow rates were recorded at ten-second intervals during a number of identical runs; the average value at each sample time was then used to form a plot of mean flowrate vs. time. The individual flowrates at each point in time formed a population whose standard deviation was less than 2% of the mean at points of worst agreement, thereby indicating a reliable replication of transient shape. Further, during the many hundreds of transients repeated during the period of experimental data-taking, key flowrate values were always observed to occur at the same time during the transient.

3.1.3 FFTF Test Cell

The test cell used in this experiment is a stylized two-dimensional

model of an LMFBR outlet plenum designed to exhibit the recirculating flow
and turbulent mixing characteristics of that geometry. Measurements made
in this test cell during a 120 second coast-down transient are compared to
VARR-II computer predictions in Sec. 5.

The FFTF test cell is a 1/15 scale model of a two-dimensional diametral
section of the Fast Flux Test Facility (FFTF) reactor outlet plenum (Fig.
3.3). It is constructed of a machined aluminum frame, two inches in depth,
with plexiglas face-plates to permit the transmission of light for the
Laser Doppler Anemometer. This cell is essentially the same device used
by Chen for steady-state experiments, and reported on in reference [19].
However, discrepancies in Chen's data (discussed below) suggested a number
of modifications to the cell, primarily in the inlet region. The following
describes those modifications and their effects on the data.

Since measurements and calculations are carried out in only half the
cell, flow symmetry across the cell center-line must be obtained initially
and maintained throughout the transient. Lack of flow symmetry in the
unmodified test cell used by Chen is the most likely reason that cell-scale
mass balances obtained from his data are not consistent. The modifications
needed to alleviate this problem were found to be:

(a) change from one inlet channel to three (each independently
valved);

(b) installation of throttling valves on each outlet;

(c) installation of four-level rigid grids and a shaped
entrance at the bottom of the chimney.

These modifications are sketched and noted in Fig. 3.3. The three
inlet channels, each valved separately, markedly reduce the center-line jet

velocity experienced in the original cell. The outlet valves permit balancing of the flow resistances in the two outlet channels. The shaped entrance region eliminates the sharp-edged entrance effects of the original cell, and the four layers of stainless grid suppress the turbulence intensity, further flatten the velocity distribution, and produce nearly isotropic turbulence at the cell inlet.

The improvement in flow symmetry obtained by these changes is indicated by cell-scale vertical mass balances that were made at each horizontal plane of measurement in the test cell at full flow conditions. With perfect flow symmetry and truly two-dimensional flow, exact correspondence between upflow and downflow should obtain at each horizontal plane listed in Table 3.1. Overall agreement is good, significantly improved from the unmodified case, but severe deterioration of the mass balance is still observed near the top of the cell. This discrepancy is likely caused by three-dimensional effects that become more important in the upper region of the cell. Velocity measurements off the cell center-plane show that the missing downflow is being pushed outside of the normal measurement plane in this region (see Appendix E for details). As a result, velocity predictions by strictly two-dimensional fluid dynamics codes, such as VARR-II, would not be expected to conform to the measurements made in this part of the test cell. Although these three-dimensional effects appear to be unavoidable at the top of the cell, cross-wise velocity measurements and the mass balance data suggest they are far less important over the main body of the recirculating region.

Another area of concern regarding Chen's data is that the highly-peaked velocity distribution at the inlet exhibited an inflection point

indicating that the flow was not fully developed. This condition contri-
buted to the significant anistropy of the turbulence in the inlet region,
and has been remedied by the modifications performed on the new cell.
Since the turbulence model used in VARR is based on the assumption of
roughly isotropic turbulence, the improved isotropy of the modified inlet
can be expected to yield measurements closer to the code predictions. This
was found to be the case and is discussed more fully in Sec. 5. It should
be noted that truly isotropic turbulence can rarely be expected in real
engineering flow situations. As such, it is usually preferable that a
hydrocode of this type not exhibit extreme sensitivity to inlet turbulence
levels.

3.2 Laser Doppler Anemometer (LDA)

3.2.1 General Description

A dual-channel Laser Doppler Anemometer (LDA), operating in the
reference-beam mode, was used to make the measurements of instantaneous
velocity components in this experiment. The dual-channel designation
indicates that the LDA performed simultaneous measurements of two
orthogonal velocity components at each point in the test cell. The
reference-beam mode refers to the optical configuration used in the set-up
and is discussed in what follows. The equipment and optical system used
in this experiment are basically the same as that used by Chen and reported
on in detail in reference [20]. However, some important modifications were
made to the laser and to the signal processing equipment that improved
overall system performance, and these are described in detail throughout
Sec. 3.2.3.

3.2.2 Theory of Operation

The basic principle of the Laser Doppler Anemometer is that the frequency of light observed emanating from a moving source will be changed depending on the velocity of the light-source relative to the observer. In the same fashion, the familiar "Doppler" effect causes an apparent change of pitch (or frequency) in the whistle of a fast train that is in relative motion to an observer. Yeh and Cummins [21] first demonstrated the feasibility of using the LDA to measure fluid velocities in the laboratory in 1964. Since that time the technique has been studied, refined and commercialized. As a result, manufactured LDA systems are readily available in modular form that permit relatively easy alignment and straightforward operation. A detailed discussion of the theory of operation of the LDA is available from many good sources, e.g. [22], [23], or [24]. Chen's report [25] also includes a general synopsis of the theory. Such details will not be repeated here, but the major advantages of the LDA over conventional fluid flow measuring devices such as the hotwire or pitot tube bear repeating:

    (1) the measurement is performed with laser beams; no probes disturb the flow;

    (2) the measuring volume is small enough to provide a high degree of spatial resolution;

    (3) no calibration is required;

    (4) fluid velocity is linearly proportional to the Doppler shift;

    (5) the directional sensitivity is ideal for simultaneous measurements in two orthogonal directions.

The major disadvantage of the LDA in an experiment of this nature is the possible failure to account for a number of sources of error that can modify the raw system output signal significantly. These factors are addressed in Appendix B, "Error Analysis."

3.2.3 Experimental Arrangement

The basic components of the LDA used in this experiment are:

(1) light source (laser)

(2) light scattering particles

(3) system to focus and collect the light (optics)

(4) method of monitoring the Doppler shift or frequency
     (frequency tracker)

These components are described below in general and treated in detail only insofar as they differ from the set-up used by Chen [26].

3.2.3.1 Laser

A Spectra-Physics Model 164 Argon Ion laser, capable of a maximum power of 2 watts, was used as the light source. The laser was tuned to the green line at a wavelength of 5145 Å.

A Spectra Physics Model 589 Air Spaced Etalon was installed in the cavity of the Argon Laser system. The purpose of the etalon is to inhibit longitudinal oscillations in all but one laser frequency. Operation in the single mode permitted by the etalon results in a much improved coherence length (L_c) for the laser. A long coherence length is required for LDA operations when split-beam path lengths are not exactly equal, which is the case for the dual channel measurements being performed in this

experiment. For the DISA optical unit configured for dual channel measurements, optical path length differences (ΔL) on the order of 5-6 cm. occur. This length is unacceptably close to the 10-20 cm. coherence length of the Argon laser when operated without single frequency etalon. Installation of the etalon increases the coherence length to about 10 meters, thus satisfying the requirement that $L_c \gg \Delta L$ for the optimal signal-to-noise ratio [27].

3.2.3.2 Light Scattering Particles

The theory of operation of the LDA states that the Doppler frequency measured is specifically associated with a light-scattering particle and actually yields the particle velocity rather than the fluid velocity. It is therefore essential that the scattering particles used in a particular flow situation follow the fluid motion directly, or that the velocity of the scattering particles can be related to the fluid velocity in a reliable fashion. In turbulent water flows, "natural" seeding is generally acceptable for most LDA applications. That is, the microscopic organisms and suspended matter normally present in ordinary tap water are used as light scattering particles. As mentioned in Sec. 3.1.1, tap water was not used in the experiment because of corrosion problems, and so artificial seeding was required.

The properties of the seed that determine its ability to closely follow the water velocity are its shape, size, and relative density ratio. Reference [28] reviews various methods of calculating the motion of particles in a turbulent fluid flow. The authors demonstrate that smooth, small particles of density equal to the fluid are best. In this experiment,

polystyrene latex spheres (diameter $\simeq$ .5 μm, specific gravity = 1.05),
which meet all three criteria, are used and can be safely assumed to follow
the velocity fluctuations exactly.

Light scattering ability is a second criteria to be considered.
Although the individual particles are quite small, reference-beam operation
achieves its highest signal-to-noise ratio for high scattering particle
concentration, which places many particles in the measuring volume at any
given time. This high particle concentration, combined with the excess
laser power available, provided acceptable signals throughout the experiment.

3.2.3.3 Optical Arrangement

The three basic modes of LDA optical arrangement refer to the
method by which the Doppler frequency shift is amplified and detected.
They are:

      (1)   reference beam mode;

      (2)   dual beam or fringe mode;

      (3)   single beam or two scattered beam mode [29] .

The dual beam mode seems to be the most generally used method for water
flows with commercially available LDA systems. However, the requirement
to measure two velocity components simultaneously, while achievable with
the dual beam or fringe method, was most easily and directly met with the
reference beam mode. Further, the excess power available from the Argon
laser made it possible to get good signals with the high particle
concentrations needed for reference beam operations.

The reference beam arrangement used in this experiment is illustrated
schematically in Fig. 3.4. The original laser beam is divided by a 90/10

beam-splitter and the weak beam is directed to the acousto-optic Bragg Cell. This beam is shifted in frequency by 40 MHz in the Bragg Cell and then passes through an adjustable neutral density filter that allows external control of its intensity. The frequency-shifted beam is split again, and the two resulting beams are made parallel to the unshifted beam and arranged so that an end view of the beams places the three spots on three corners of a square. The two frequency-shifted beams, reduced in intensity, are on opposite ends of the diagonal; these are the reference beams. The third, high intensity, beam is referred to as the scattering beam. This three-beam group is then focused by a lens (focal length = 300 mm.), and their point of mutual intersection defines the measuring volume. The scattering particles in the flow pass through the measuring volume, are illuminated by the bright scattering beam, and the light reflected from these moving particles is shifted in frequency depending on the velocity of the particle. This Doppler shifted light is of low amplitude and the extent of the frequency change is very small when compared to the original laser frequency. In other words, the Doppler frequency cannot be readily deduced from this weak signal alone. A simplified description of the process by which this signal is amplified and made useable in the reference beam mode follows.

Recall that this weak signal is produced by particles moving with the flow that are illuminated by the high-intensity scatter beam. The reference beam for each of the two orthogonal velocity components is much weaker than the scatter beam and light scattered by particles from this beam does not contribute to the Doppler shifted light reaching the photo-multiplier tube (PMT) detector. However, the reference beam is aligned

directly on the axis of the PMT and thereby produces a non-Doppler-shifted signal whose amplitude can be adjusted by the external neutral density filter control. Therefore, two light signals arrive at the PMT:

(1) $A \cos\omega_1 t$ - Weak amplitude Doppler shifted light reflected from particles passing through the strong scattering beam, where

$$\omega_1 = \omega_0 \pm \omega_D \quad \text{(sign indicates velocity sense)},$$

$$\omega_D = \text{Doppler frequency},$$

$$\omega_0 = \text{original laser light}$$

(2) $B \cos\omega_2 t$ - Strong amplitude signal produced by reference beam aimed directly at PMT, where

$$\omega_2 = \omega_0 - 40 \text{ MHz, because of Bragg cell}$$
$$\text{induced frequency shift.}$$

The PMT is a square-law detector. The output of an ideal square-law detector resulting from the combination of the two signals described above is:

$$I(t) = (A \cos\omega_1 t + B \cos\omega_2 t)^2$$

$$= A^2 \cos^2\omega_1 t + AB[\cos(\omega_1+\omega_2)t + \cos(\omega_1-\omega_2)t] + B^2 \cos^2\omega_2 t.$$

$$(3.1)$$

If this signal is low-pass filtered to remove frequencies above $(\omega_1-\omega_2)$, or if the electronic equipment cannot respond to frequencies in the optical range--basically an equivalent phenomenon--the resulting PMT output becomes:

$$I(t) = A^2 + B^2 + AB \cos(\omega_1 - \omega_2)t, \qquad (3.2)$$

where

$$\omega_1 - \omega_2 = \omega_0 \pm \omega_D - (\omega_0 - 40) = 40 \pm \omega_D$$

The constant, or d.c., part of the signal can be blocked, and only the frequency $(40 \pm \omega_D)$, amplified by the strong signal B, remains.

This is the heterodyne principle that the reference beam mode exploits. This relatively strong signal is then directed to the frequency trackers for further processing (Sec. 3.3). It is not necessary for the reference beam to pass through the measuring volume, but this procedure reduces vibration problems and makes for easier alignment.

The component of particle (or fluid) velocity that is measured is in the plane formed by the reference and scatter beams and perpendicular to the bi-sector of their intersection angle [30]. As a result, the three-beam arrangement described above, with two PMTs, permits measurement of two orthogonal velocity components simultaneously.

3.2.3.4 Point Positioning

The measuring volume location, or X-Y coordinate position in the test cell, is controlled by fixing the test cell and moving the laser and associated optics as an integral unit. This is accomplished, as shown in Fig. 3.5, by anchoring the laser, optics and PMTs to a milling-machine base which provides precise 3-axis maneuverability. While this arrangement makes alignment problems more tedious, fixing the location of the test cell is preferred because changing the position of the flexible hoses that are attached to the test cell can affect the flow pattern in the cell.

Measurements were made at the various X-Y coordinate locations on the cell center-plane. Because of index of refraction effects, the center-plane was located by moving the measuring volume (beam intersection) from the inside surface of one plexiglas face to the other, recording the translation distance, and then moving back one-half this distance.

3.3 Signal Processing

3.3.1 General Description

Frequency tracking was used as the method for converting the PMT signal into a continuous voltage that is proportional to fluid velocity. Simultaneous measurement of two velocity components requires two independent frequency trackers. The DISA model 55L20 and TSI model 1090 trackers were used, which allowed a side-by-side comparison of the two systems. Although both units are frequency trackers, they differ in their fundamental method of following the varying Doppler frequency. The DISA system uses a phase discriminator [31], while TSI incorporates a phase-locked loop to perform this function [32]. Further, the two trackers differ somewhat in manual control features, input filtering, and output signal characteristics. For this turbulent water flow, using the reference beam mode, the DISA tracker, with more frequency ranges, a finer Voltage-Controlled-Oscillator frequency selection capability, and a narrow-band input filter was found to have more flexibility and a less noisy output for most measuring situations encountered. However, the TSI tracker was able to maintain track on the poorest signals, when DISA could not, and with proper filter-ing of the output signals, the electronic noise problem could be overcome.

A schematic diagram of the analog portion of the electronic layout is shown in Fig. 3.6. As indicated in the sketch, the two trackers used a common 40 MHz oscillator. In Sec. 3.2.3.3 it was shown that the Doppler frequency is contained in a signal from the PMT whose frequency is $(40 \pm \omega_D)$MHz. The "40" in this expression arises from the nominal 40 MHz frequency shift imposed on both reference beams by the single Bragg Cell in the optical unit. Since the Bragg Cell is driven by a single 40 MHz oscillator, maximum accuracy is obtained if that same signal drives the local oscillator which is used in each tracking system to extract ω_D from $(40 \pm \omega_D)$. Therefore, the two tracking systems were modified to use the identical 40 MHz driver for their individual local oscillators.

3.3.2 Low Pass Filtering

The phase-locked loop configuration of the TSI tracker and its larger IF bandwidth (15% fixed on TSI vs. .5% to 8% variable on DISA) is thought to be the reason that the TSI system could better maintain track on rapidly varying signals of poor quality. However, although the average value of the frequency tracked in these cases was the correct average Doppler frequency, the tendency to track noise within the IF bandwidth range was apparent. As a result, the output voltage of the TSI tracker required low-pass filtering to remove these high-frequency noise contributions prior to making the mean square and correlation measurements. Though most important when operating on the middle frequency range, the low-pass filter was installed for all measurements.

The filter used was designed and built in-house as part of the project. It is an active dual-channel state-variable low-pass filter

with precision adjustable gain, damping, and cut-off frequency. Both channels are buffered to provide an input impedance of 10^8 ohms, and the filtering characteristics are exactly matched so that the outputs from both trackers are treated equally. In water flows, very little turbulent energy is contained in fluctuations above 500 Hz; consequently, the low-pass cut-off was conservatively set at 1 KHz. This value effectively filtered out the high frequency noise while preserving the real turbulent energy contribution to the mean square measurements.

The adjustable gain feature of the filter was crucial to the transient measurements of TKE. Since it is not possible to change the range switch on the averaging RMS voltmeters in the midst of a transient, it is necessary that the initial RMS value register near the top of the particular range selected so that its value can be accurately recorded throughout the transient. Once the steady-state RMS value of the signal from each channel had been established, the filter gain controls were manipulated to bring the values near the top of their respective ranges to give maximum coverage and accuracy during the transient.

3.3.3 Analog Instrumentation

The output signal from each tracker is a fluctuating voltage whose average value (or d.c. component) is proportional to the mean fluid velocity in the component direction associated with that tracker ($\overline{U}$ and $\overline{V}$). The mean square value of the fluctuating part of this output signal, corrected for broadening errors as discussed in Appendix B, is twice the turbulence kinetic energy (TKE) associated with a particular direction ($\overline{u'^2}$ and $\overline{v'^2}$). Finally, the averaged product of the two fluctuating

components is the Reynolds stress ($\overline{u'v'}$).

Standard commercial averaging/integrating devices were used to produce the five time-averaged quantities discussed above. The hardware layout is as shown in Fig. 3.6, and a complete list of the electronic equipment is given in Table 3.2.

In addition to a digital or meter read-out of the measured quantities, each device produces an analog voltage that is proportional to the time-average being performed. These five analog signals were digitized and recorded during each transient. The characteristics of these signals, their relationship to true mean values, and the selection of the time constant for the required integration is discussed in Sec. 3.4.

3.4 Transient Data Collection and Analysis Method

3.4.1 General

The measurement of mean turbulence parameters during a flow transient presents the problem of correctly defining the quantities actually measured. The basic assumption underlying the calculational prediction of turbulent flows is that equations for _average_ values of the fluctuating turbulence quantities adequately describe the flow. The predictions of a typical fluid dynamics code, such as VARR, are given in terms of average or mean values. Therefore, for purposes of comparison, the quantities of interest to be obtained from an experiment must also be average values. The problem in the case of a transient experiment is that the very existence of the transient makes the normal method of forming mean values from turbulence data invalid.

This difficulty can be clearly seen by considering the definitions of the two common types of averages applicable to turbulence:

(1) Time-Average

$$\overline{U}_t \equiv \underset{T \to \infty}{Limit} \quad \frac{1}{2T} \int_{-T+t}^{T+t} U(t')dt' \quad ,$$

(2) Ensemble or "Probability" Average

$$\overline{U}_e \equiv \frac{\sum\limits_{i=1}^{N} U_i(t)}{N} = \int_{-\infty}^{+\infty} U(t)p(U)dU \quad ,$$

where p(U) is the normalized probability density function which satisfies: .

$$\int_{-\infty}^{+\infty} p(U)dU = 1 \quad .$$

Also note, in the theory of turbulence, $\overline{U}_t = \overline{U}_e$, the so-called "ergodic hypothesis."

In the more common experimental situation of steady-state turbulent flow, the appropriate average values are obtained by method (1), the time-average technique. For the steady-state case, $\overline{U}_t$ is a function of T and not of t. The integration time, T, is taken large enough so that $\overline{U}_t$ is constant. This method is preferred to the ensemble or probability approach because it avoids the very large number of experimental repetitions (N) and does not require that p(U) be known.

However, because of the requirement that $\overline{U}_t$ be constant, the time-average method, strictly applied, is not appropriate for a transient experiment where all mean turbulence quantities are expected to vary with

time. Also, since p(U) is not known, the probability average is not useful. The ensemble average, therefore, is the correct method for cases where the average value of a fluctuating quantity may itself be a function of time. Indeed, though Reynolds' classic time-averaging of the Navier-Stokes equations recasts them into a more computationally tractable form, strictly speaking, it is the <u>ensemble</u>-averaged forms of these equations that are solved when the time derivatives are not identically zero.

In principle, application of the ensemble approach is straightforward. However, for transient measurements at fifty or so different locations, the total number (N) of transient runs required to form statistically valid averages would be impractically large. Further, the speed, cost and data-storage capability of the recording equipment required for such an effort are discouragingly high.

Accordingly, a method of approximating the true averages, similar to that used for the measurement of turbulence in atmospheric and ocean flows [33], was devised. In such cases, time-averages are made with averaging times (T) that are large with respect to the period of turbulent fluctuations, but small when compared to the time-scale of the diurnal or tidal variations which, strictly speaking, cause the mean values so obtained to be functions of time. A typical example occurs in the measurement of ocean flows where turbulent components on the order of 1 Hz are observed super-imposed on tidal variations which exhibit periods of 12 to 24 hours. Appli-cation of time-averaging in this case gives a mean value which is essentially constant during the averaging period.

Mathematically, the criteria to be met for successful application of the above approximation is:

$$t_{turb} \ll T_{int} \ll t_{trans};$$

where

t_{turb} = Time scale of turbulent fluctuations,

T_{int} = Integration time,

t_{trans} = Time scale of flow transient.

The objective in this experiment was to minimize t_{trans} so that time derivatives and their effects on the flow would be enhanced. This constraint led to a T_{int} which, though considerably larger than t_{turb}, was not so large as to produce a smooth, pseudo-constant $\overline{U}_t(t)$, and, naturally, was small enough to follow the imposed transient to within a known small error. This time-averaged signal was recorded for a series of identical transients, and then a single set of the five ensemble-averaged functions of time was formed from this data.

The averaging method employed, therefore, was a combination of ensemble and time-averaging techniques. The time-averaging served to decrease the frequency and amplitude of the fluctuating signal to be digitized; this permitted the use of a slower and less expensive data collection system, as well as a reduction in the number of transient runs needed to get a statistically suitable ensemble average. Six to seven transient runs at each position generally yielded standard deviations that did not significantly improve with additional runs.

Use of this pseudo-ensemble averaging technique entails a degree of error that depends on a number of factors. These are discussed and analyzed in detail in Sec. 3.4.3. A schematic illustration of the method is shown in Fig. 3.7.

3.4.2 A-to-D Conversion and Data Recording

The five analog signals depicted as average outputs in Fig. 3.6 are actually time-varying analog voltages (e.g. $\overline{U}_t(t)$ in Fig. 3.7). In order to form the ensemble averages described above, these voltages must be recorded for a series of identical transient runs, and then the values at each point in time mathematically averaged to give the final output (e.g. $\overline{U}_e(t)$ in Fig. 3.7).

This procedure was accomplished by a five channel A-to-D converter that sampled and digitized all five outputs at ten second intervals throughout each transient run. The digital values were transferred to magnetic tape at the experimental site for later processing by a previously-available Tektronix 4051 mini-computer. The Tektronix 4924 cassette tape recorder, fully compatible with both the 4051 and the in-house A-to-D, was used for data storage.

The A-to-D was designed and constructed in-house as part of the project. This permitted tailoring of the five input channels to the precise requirements of the experiment, and provided a high degree of accuracy and flexibility at a relatively low cost. General features of the device include:

(1) Digitization of 1 to 5 channels simultaneously;

(2) 8-bit A-to-D conversion;

(3) Variable sampling time (.1 sec. to 25.5 sec.);

(4) Buffered inputs capable of digitizing the voltage ranges 0 to 10, 3 to 5, 4 to 6, 0 to -1, and -1 to +1 with maximum accuracy;

(5) Input buffer amp accuracy better than $\pm$ 0.1%;

(6) External Programming Capability.

A complete description of the design and operation of the A-to-D converter is included as Appendix D.

3.4.3 Averaging Method Error Analysis

The use of the special averaging technique, described at the end of Sec. 3.4.1, introduces an error in the mean value of the quantity measured. The errors discussed in this section refer only to those caused by the averaging technique itself, and do not include the experimental errors covered in Appendix B. The method-related inaccuracies are a function of:

(1) The nature of RC integration networks;

(2) The integration time, T_{int};

(3) The shape of the average magnitude vs. time curve for the quantity being measured.

3.4.3.1 RC-Integration Characteristics

All five analog channels of experimental data were averaged via standard RC-network integration. The solution to the differential equation describing the response of a simple RC-circuit to an impressed voltage, $V_i(t)$, may be written:

$$V_0(t) = V_i(t) - e^{-t/\tau} \int_0^t \left[\frac{d}{dt'} V_i(t')\right] e^{t'/\tau} dt' - \left[V_i(o) - V_0(o)\right] e^{-t/\tau} \quad (3.3)$$

where

τ = RC (integration time constant),

V_0 = Output Voltage (ideally, the average value of $V_i(t)$ at the time, t)

Generally, for this experiment, where transients are begun from initial steady-state conditions, $V_i(0) = V_0(0)$. Then given any $V_i(t)$, Eq. 3.3 defines the output of the RC-circuit as a function of t and τ Comparison of this $V_0(t)$ with the known ensemble-average of $V_i(t)$ specifies the error caused by the special averaging technique employed in this experiment.

In order to use Eq. 3.3, an analytic expression for $V_i(t)$ is required. The stochastic nature of turbulent velocity fluctuations does not permit straightforward application of Eq. 3.3 to real turbulence. However, the fact that any function can be expressed as a Fourier series suggests that a sinusoidal approximation can be used to bound the errors involved and determine the relationship of input signal frequency, ω, and functional-shape to the error.

For example, consider the idealized case of a mild coast-down transient, where the mean velocity and the amplitude of the velocity fluctuations are assumed to decay linearly. In such a case, the instantaneous voltage, proportional to instantaneous velocity, may be approximated by:

$$V_i(t) = A-Bt + C(1-Dt) \sin \omega t, \qquad (3.4)$$

where, generally $(A-Bt) > 10 [C(1-Dt)]$ for all t.

Eq. 3.3 gives, as the output of an RC averaging circuit receiving Eq. 3.4 as input,

$$V_0(t) = A-Bt \qquad \text{Correct ensemble average}$$

$$+ \frac{C}{1+\omega^2\tau^2} [\sin \omega t - \omega t \cos \omega t] \qquad \text{Error due to a circuit acting as a low pass filter}$$

$$+ \frac{CD\tau}{(1+\omega^2\tau^2)^2} [(1-\omega^2\tau^2)\sin\omega t - 2\omega\tau\cos\omega t]$$

Error due to imposed transient

$$+ B\tau - \frac{CDt}{1+\omega^2\tau^2} [\sin\omega t - \omega\tau\cos\omega t]$$

$$+ e^{-t/\tau} \left[\frac{C\omega\tau}{1+\omega^2\tau^2} \left[\frac{2D\tau}{1+\omega^2\tau^2} - 1 \right] - B\tau \right]$$

Exponential Lag Term

$$(3.5)$$

The error contribution to the TKE measurements is somewhat different; in this case the mean square amplitude of the fluctuations is of interest. A simplified representation during a linear transient is:

$$V_i(t) = (\alpha - \beta t) \sin^2\omega t. \tag{3.6}$$

Application of Eq. 3.3 gives:

$$V_0(t) = \frac{1}{2} (\alpha - \beta t)$$

Correct ensemble average.

$$+ \frac{\alpha}{\frac{1}{(\omega\tau)^2} + 4} \left[\frac{\sin^2\omega t - \frac{1}{2}}{\omega^2\tau^2} \right]$$

Error due to circuit acting as a low pass filter.

$$- \frac{\alpha \sin 2\omega t}{\left[\frac{1}{(\omega\tau)^2} + 4 \right]^2} \left[\frac{1}{(\omega\tau)^3} + \frac{4}{\omega\tau} \right]$$

$$+ \frac{\beta}{\left[\frac{1}{(\omega\tau)^2} + 4\right]^2} \left[8\tau + \frac{6}{\omega^2\tau} - \frac{8}{\omega}\sin 2\omega t + \left(\frac{1-4\omega^2\tau^2}{\omega^4\tau^3}\right)\sin^2\omega t\right]$$

Error due to
imposed transient
amplitude.

$$+ \frac{\beta t\,\sin 2\omega t}{\left[\frac{1}{(\omega\tau)^2} + 4\right]^2}\left[\frac{1}{(\omega\tau)^3} + \frac{4}{\omega\tau}\right] - \frac{\beta t}{\frac{1}{(\omega\tau)^2} + 4}\left[\frac{\sin^2\omega\tau - \frac{1}{2}}{\omega^2\tau^2}\right]$$

$$- \frac{e^{-t/k}}{\left[\frac{1}{(\omega\tau)^2} + 4\right]^2}\left[\frac{2\alpha}{(\omega\tau)^2} + 8\alpha + \frac{6\beta}{\omega^2\tau} + 8\beta\tau\right]$$

Exponential lag term.

$$(3.7)$$

Both of the simplified input signals produce a relatively complicated output which consists of the "correct"* mean value plus some error terms. Fortunately, most of the error terms are negligibly small for the frequencies and averaging time-constants of interest; this will be demonstrated in what follows. Moreover, those errors which are not insignificant are functions of the experimental parameters and can be minimized and bounded by proper experimental design. In fact, these particular error effects ultimately determine the type and rate of the transient that can be measured via the pseudo-ensemble averaging method.

---

*Correct in the sense that an ensemble average of these input signals, where phase angles are random, gives the same mean function of time.

3.4.3.2 Optimal Integration Time Constant (τ)

Inspection of Eqs. 3.5 and 3.7 shows that selection of the best value of τ is a problem in optimization. A small value of τ minimizes the transient-related error, while a large value of τ is needed to reduce the frequency-related error. Since transient effects are of primary interest, the lowest value of τ consistent with expected turbulent fluctuation frequencies, allows the fastest flow shut-down rate and represents the optimum value for this experiment.

The smallest useable value of τ is limited by the tendency of the RC-circuit to act as a low-pass filter and thereby fail to integrate that portion of turbulent energy contained in the lower frequency fluctuations. The cut-off frequency, f_c, of the RC-network determines the lowest frequency of a periodic signal that is accurately integrated. For good integration of periodic signals (less than 1% error), Ref. [34] shows that the lowest frequency in the input signal, f_i, must satisfy

$$f_i > 100 \ f_c, \tag{3.8}$$

where $f_c = \frac{1}{2\pi RC}$. In terms of the circuit time constant, $\tau = RC$, proper integration occurs for input signals that satisfy

$$f_i > \frac{100}{2\pi\tau} \tag{3.9}$$

Therefore, $\tau = 10$ sec., the value used in this experiment, assures us of properly integrating all turbulence energy contained in fluctuations with frequency greater than about 1.6 Hz.

A related effect, where random signals are being processed, is

discussed in the operating manual for the mean-square voltmeters [35].
The expression for minimum τ in this case is

$$\tau \geq \frac{2}{4B(\frac{B}{2f_0})} \cdot \frac{1}{\epsilon^2} \quad , \tag{3.10}$$

where

B = Bandwidth in Hz;

f_0 = Center frequency;

ϵ = Desired error.

For ϵ = .01, B = 500, and f_0 = 250, conservative values for turbulence in water, Eq. 3.10 gives $\tau \geq 10$ seconds, thereby confirming our earlier estimate.

An order of magnitude study of those error terms in Eqs. 3.5 and 3.7 that are frequency related reveals that, with τ = 10 and turbulent fluctuations of frequency $\geq$ 2 Hz, the worst-case error magnitude is of order 10^{-3}. This estimate was computed with values of C, D and β matched to the experiment. Further, as the minimum frequency is raised modestly, the error magnitude drops dramatically.

In theory, given the nature of the analog devices used to perform the time-averaging, the pseudo-ensemble method will succeed when the fluctuations are Gaussian [36]. However, since turbulence fluctuations are only approximately Gaussian, a simple experiment was performed to determine the magnitude of this effect, as well as to evaluate the overall error introduced by use of the optimized time constant. Accordingly, the standard turbulence quantities were measured one inch above the chimney inlet at full steady-state flow, and averaged in two different ways. The experiments

produced a negligible difference (~1%) between the true time-average
($\tau = 100$ sec.) and the pseudo-ensemble-average ($\tau = 10$ sec.) values for both
mean velocities and turbulence intensities.

3.4.3.3 Transient Shape Effects

For a transient experiment, the minimum useable value of τ, with
respect to frequency related errors, is also the optimum choice. This can
be seen by noticing that those parts of the error terms in Eqs. 3.5 and 3.7
that are related to the imposed transient amplitude are increased as τ
increases. Once τ is established, the only parameters that control the
error magnitude are those that determine the transient speed (B, β, and D
in the case of Eqs. 3.5 and 3.7).

The mechanical characteristics of the control valve produced a
transient shape (i.e. plot of flowrate vs. time) that was roughly congruent
to that produced by most mean quantities measured in the experiment
(e.g. Fig. F.1). The form of this curve can be closely approximated by a
third-order polynomial, and this analytic expression used with Eq. 3.3 to
estimate the size of the error term. Since τ has been constrained to be
large enough to keep frequency related errors negligible, one may simplify
the analysis by omitting the periodic part of $V_i(t)$. This is permissible
because of the linearity of the differential equation that describes the
RC network. The frequency-related error term is simply superimposed on the
shape-related error, and therefore can be treated separately. In this case,
the analytic approximation to the shape-related part of the input signal
is

$$V_i(t) = at^3 + bt^2 + 1 \tag{3.11}$$

where,

$$a = 4.672 \times 10^{-7} \quad ;$$

$$b = -9.872 \times 10^{-5} \quad ;$$

$$0 \leq t \leq 140 \text{ secs.}$$

Using Eq. 3.3,

$$V_0(t) = at^3 + bt^2 + 1 \qquad \text{Correct ensemble average.}$$

$$- 6a\left(\frac{\tau t^2}{2} - \tau^2 t + \tau^3\right)$$

Error due to transient shape and rate.

$$- 2b(\tau t - \tau^2)$$

$$+ e^{-t/\tau}(6a\tau^3 - 2b\tau^2) \quad \text{Exponential lag term.} \tag{3.12}$$

The shape related error is a function of time. For $\tau = 10$ seconds, and a and b matched to the experimental data, the worst-case error is about 7% of the steady-state (t=0) value. Fortunately, the performance of the averaging devices can be markedly improved by a simple translation of the time variable, i.e., let

$$t^* = t - \tau ,$$

then Eq. 3.12 becomes

$$V_0(t^*) = a(t^*)^3 + b(t^*)^2 + 1$$

$$+ a\tau^2\left[3(t^*+\tau) + \tau(6e^{-(t^*+\tau)/\tau} - 5)\right]$$

$$+ b\tau^2\left[1 - 2e^{-(t^*-\tau)/\tau}\right]. \tag{3.13}$$

In essence, the fixed time lag introduced by the RC-network has been compensated for, and only the curvature-related errors are left. The resulting worst-case error, associated with the shape effect for the standard transient, is now less than 1% of the steady-state initial magnitude, an acceptable value.

The mathematical time translation is accomplished in the experiment and carried over into the calculations as follows:

(1) τ is fixed for all five averaging devices, for all runs, and at all locations.

(2) The recorded inlet measurements, which have the time-lag built in, are used to define the time-dependent inflow values for the code.

(3) All comparisons between code and experiment are made in t*-space.
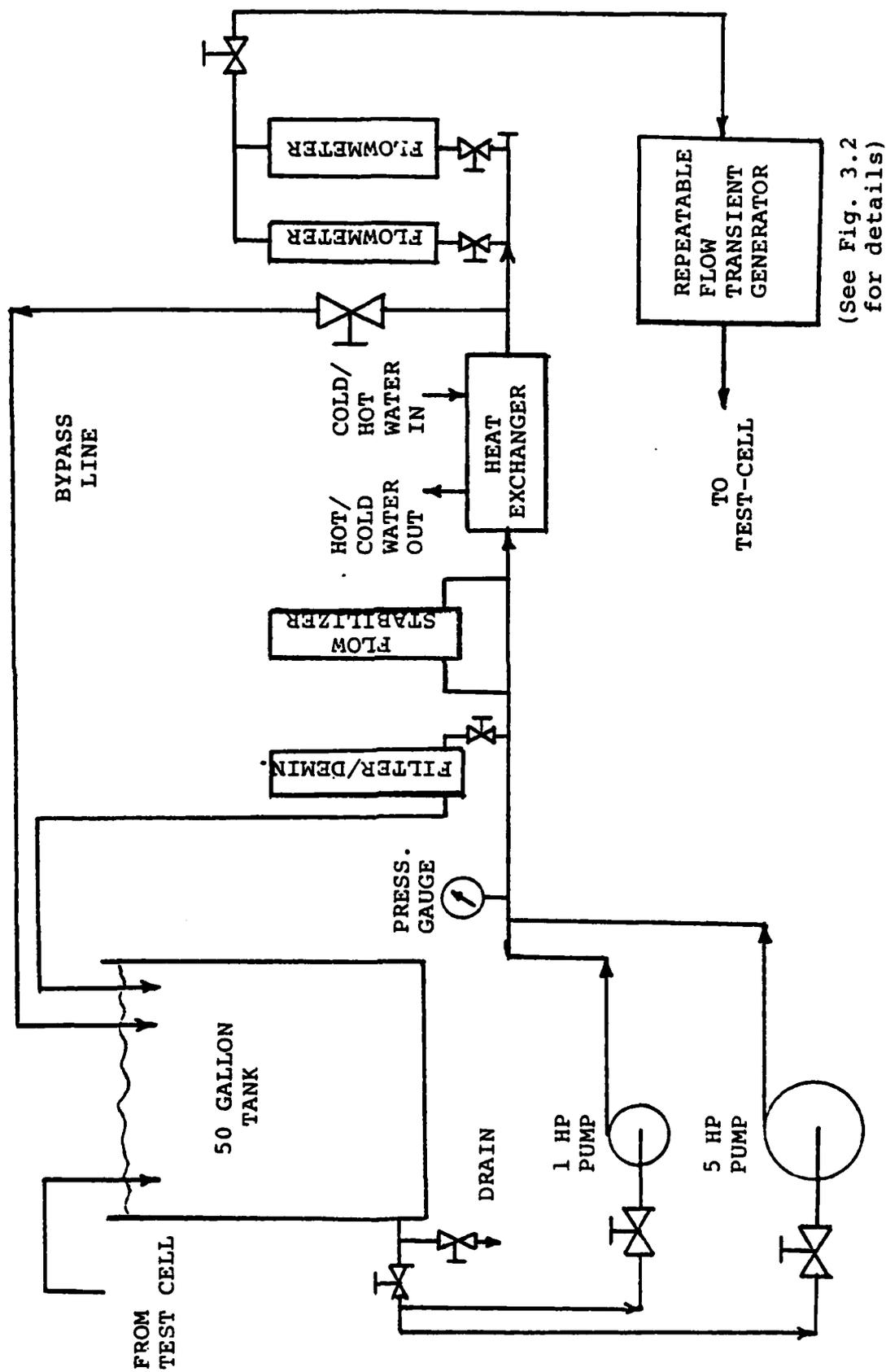
Fig. 3.1 HYDRAULIC LOOP
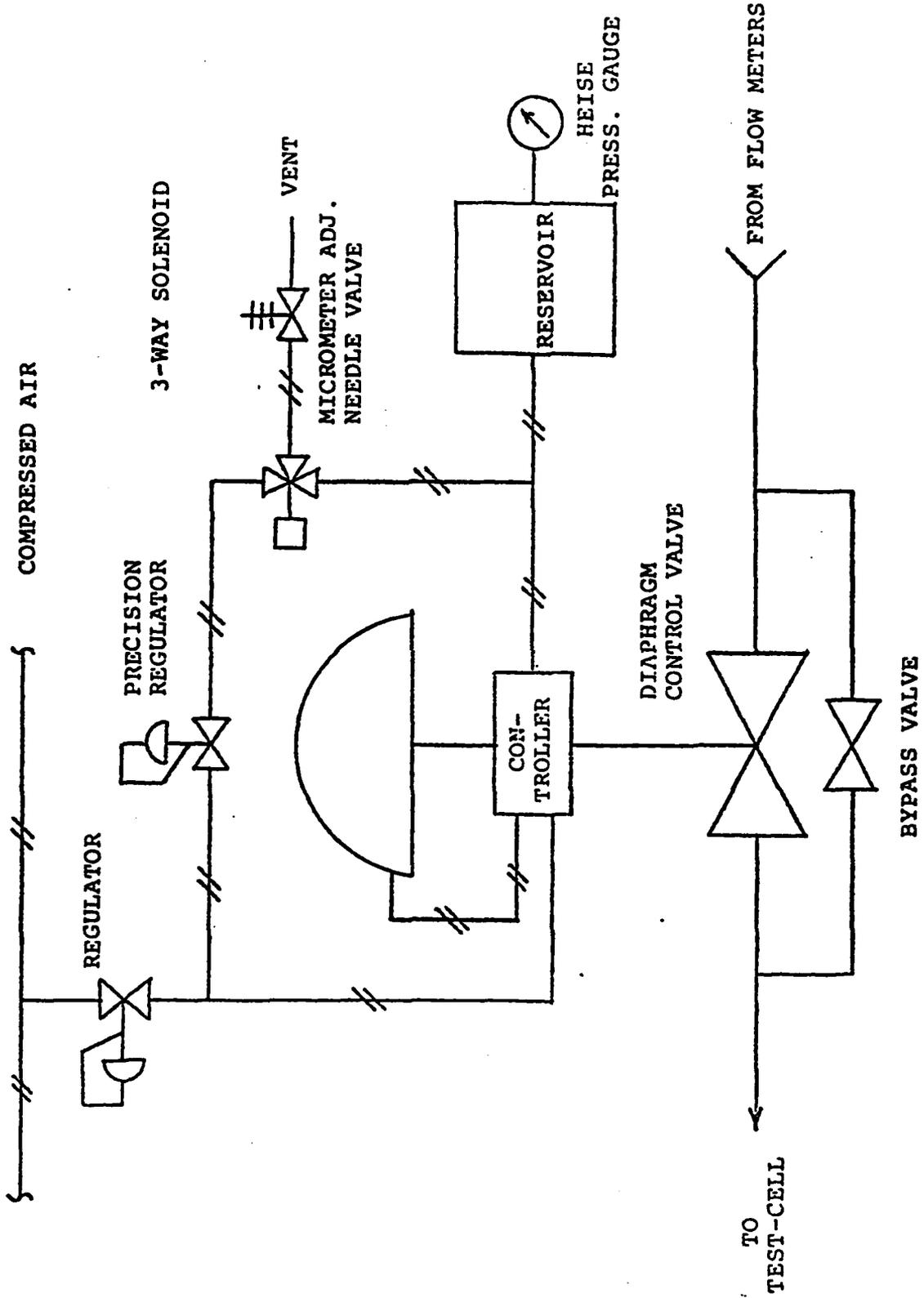
Fig. 3.2 REPEATABLE FLOW TRANSIENT GENERATOR

Fig. 3.3 FFTF TEST-CELL

59
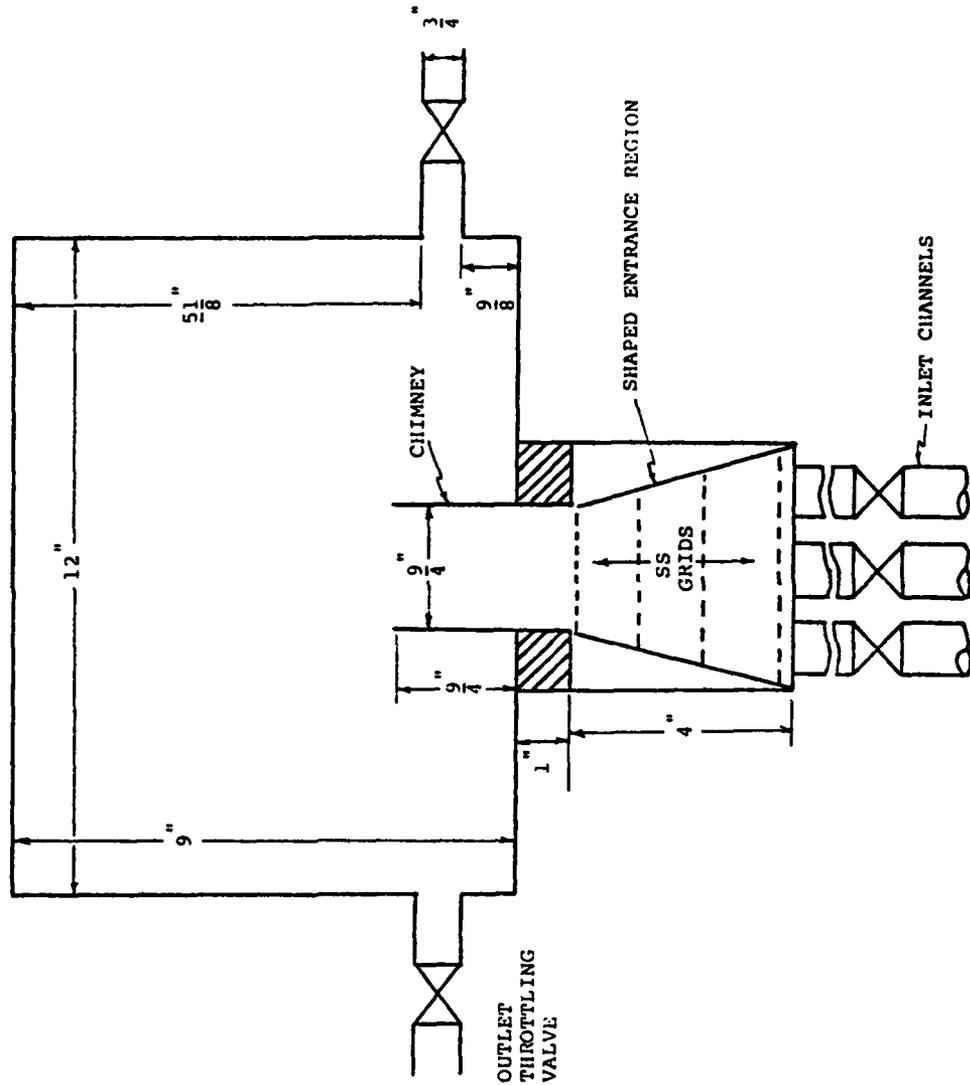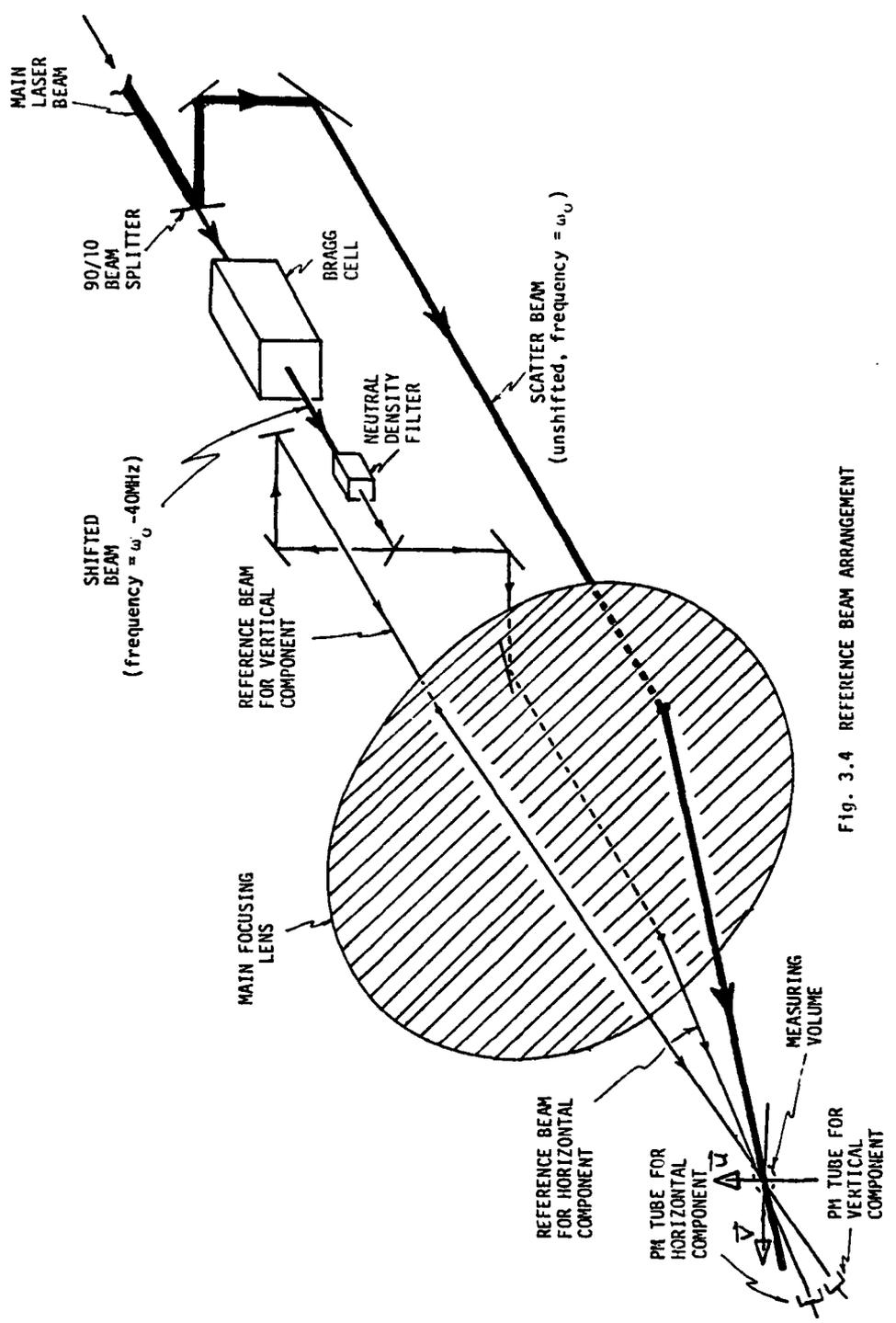
Fig. 3.4 REFERENCE BEAM ARRANGEMENT
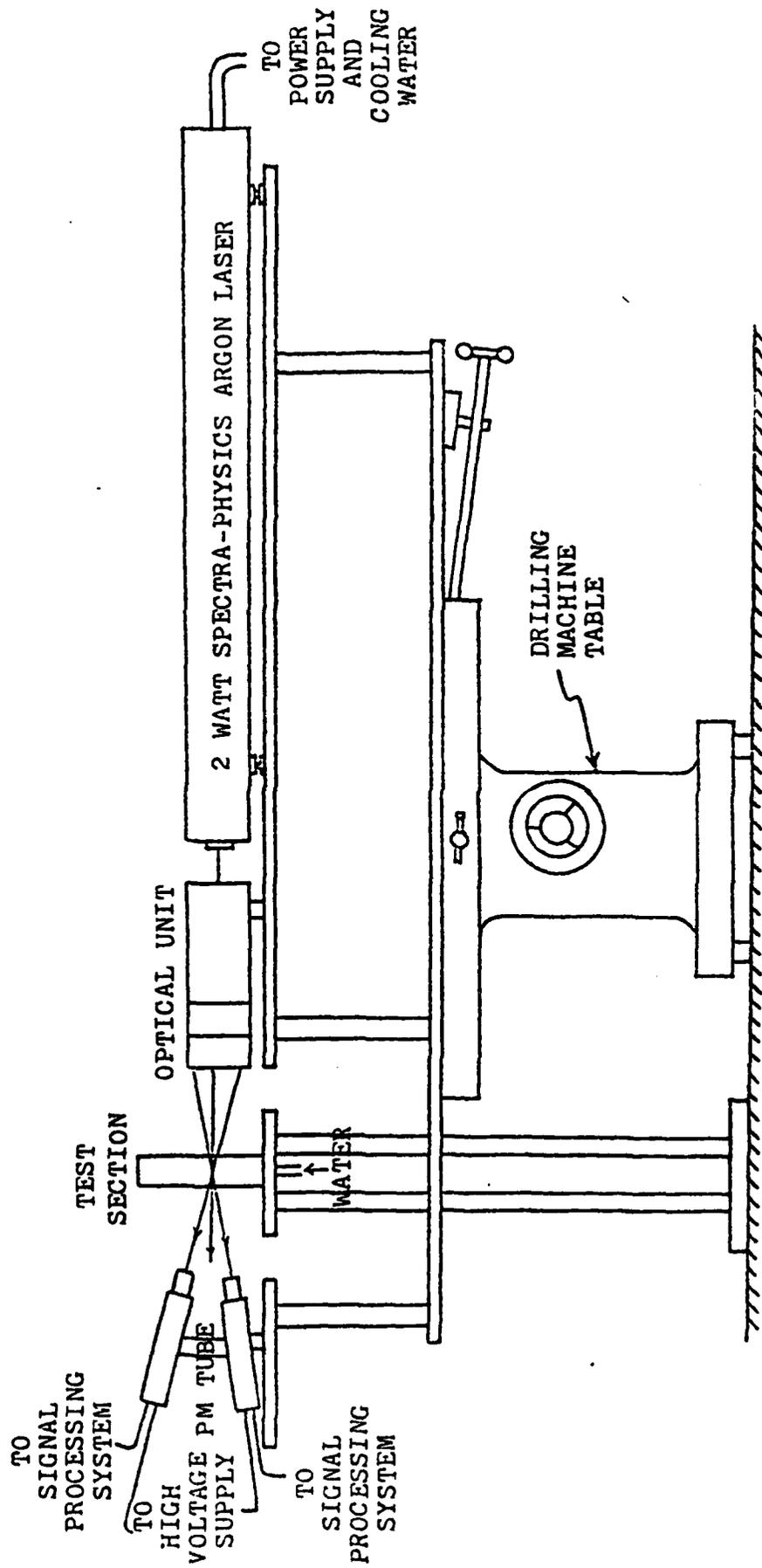
Fig. 3.5 TRANSLATION METHOD
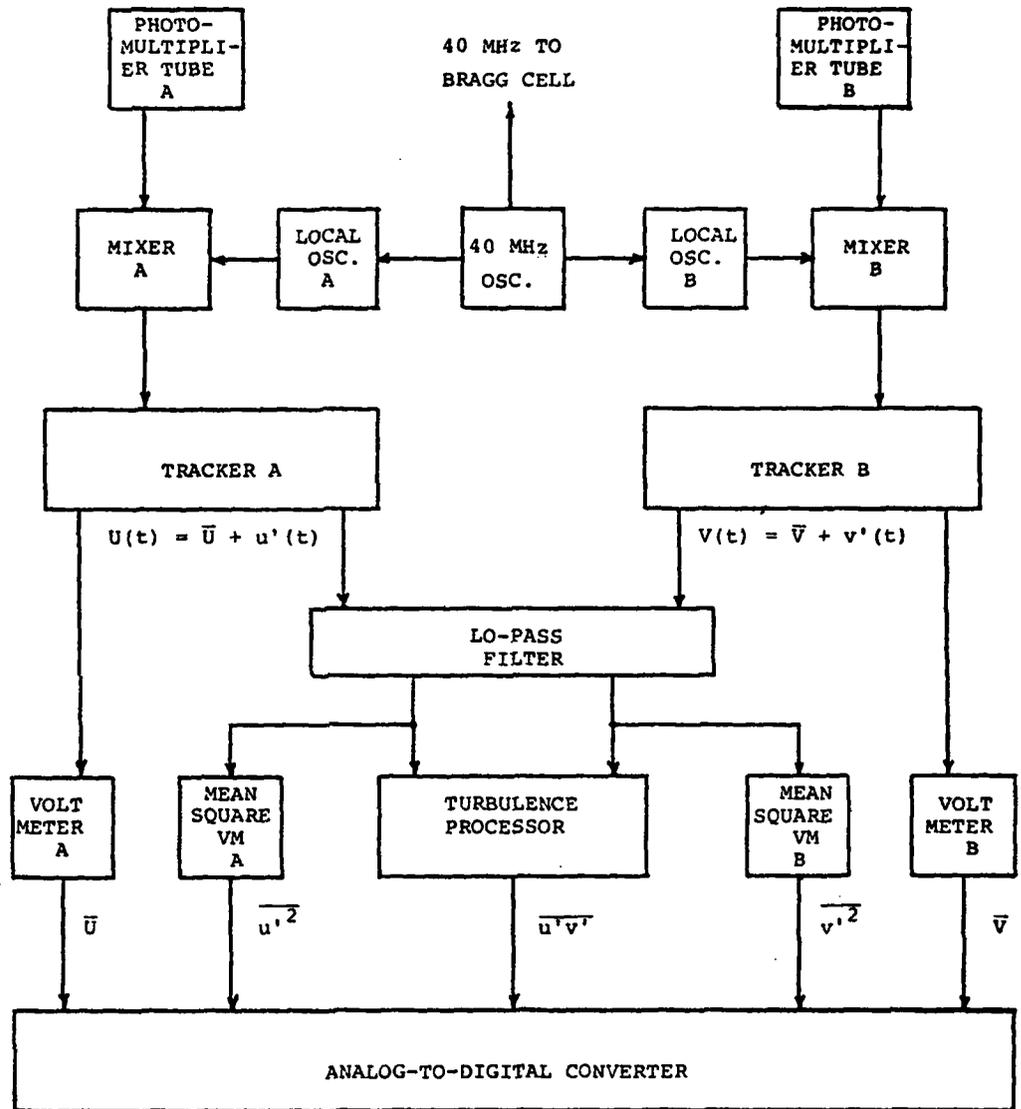
Fig. 3.6   ELECTRONIC LAYOUT

Typical instantaneous output of LDA for one velocity component during a single transient of length t_{fin}.

LDA

$U(t)$

t_{fin}

Output of time-averaging device. Note decreased amplitude and frequency; also time lag = τ.

TIME AVERAGE

$\overline{U}_t(t)$

$t_{fin} + \tau$

A-TO-D and DATA RECORDER

Final output is result of ensemble averaging the digitized and recorded $\overline{U}_t(t)$'s.

MINI COMPUTER

$\overline{U}_e(t)$

1σ

$t_{fin} + \tau$

$$\frac{\sum\limits_{i=1}^{N} \left[\overline{U}_t(t) \right]_i}{N}$$
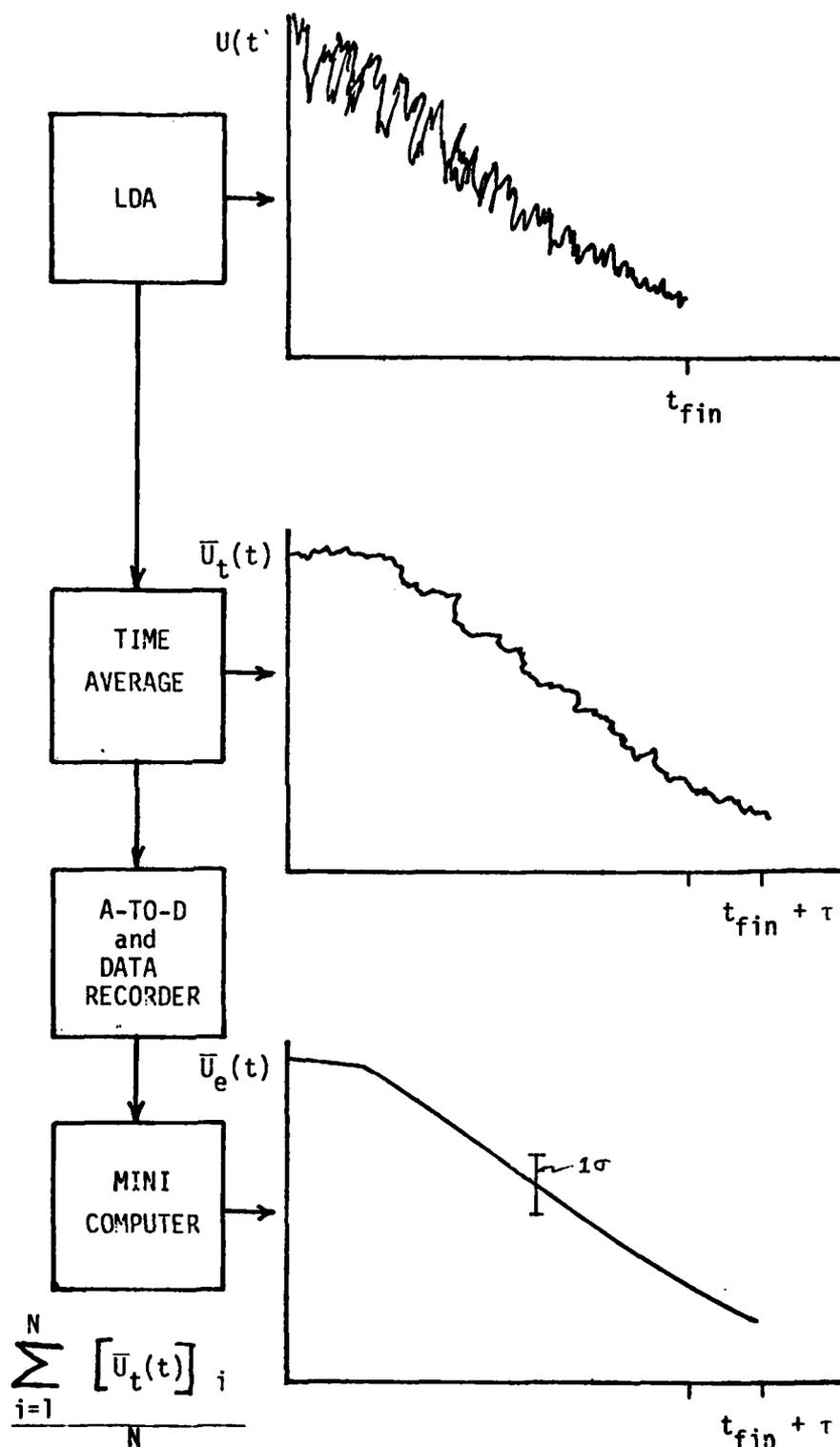
Fig. 3.7 Averaging Method

Table 3.1

Cell-Scale Mass Balances

I-coordinate * vertical position	Area Weighted Average Vertical Flow Rate		% Mass Defect $\equiv$ $\dfrac{(Downflow-Upflow)}{Upflow} \times 100$
	Upflow	Downflow	
8	1.22	1.21	-0.5
10	1.20	1.17	-2.5
12	1.16	1.25	7.7
14	1.14	1.21	6.1
16	1.12	1.21	8.0
18	1.07	1.14	6.5
20	1.08	.95	-12
22	1.12	.64	-43

* see Fig. C.1 in Appendix C

Table 3.2

Equipment List

Unit	Manufacturer	Model No.
Argon Laser	Spectra-Physics	164
Laser Exciter	Spectra-Physics	265
Optical Unit	DISA	55L88
Photomultipliers (2)	DISA	55L12
High Voltage Supplies (2)	Baird-Atomic	312A
Anode Current Meters (2)	Simpson	N/A
LDA Control Unit	DISA	55L70
LDA Frequency Shifter	TSI	985
Doppler Signal Processor	DISA	55L22
Doppler Signal Processor	TSI	1090
Turbulence Processor	DISA	52B25
Averaging Digital Voltmeter	TSI	1076
Integrator	In-House	N/A
Digital Voltmeter	Hewlett-Packard	3456A
RMS/MSQ Voltmeters (2)	DISA	55D35
Oscilloscope	Hewlett-Packard	141B
Low-Pass Filter	In-House	N/A
Analog-to-Digital Converter	In-House	DBC Mark II
Digital Tape Recorder	Tektronix	4924

CHAPTER IV

COMPUTER PROGRAM AND MODELS USED IN THE WORK

4.0 Introduction

VARR-II is a two-dimensional time-dependent thermal-hydraulics code developed by Science Applications, Inc. for the Westinghouse Advanced Reactor Division to aid in the design of the LMFBR outlet plenum. This code uses the two-equation (K-σ) turbulence model developed by Stuhmiller [37]. A modified version of VARR-II was used for all computer predictions in this work, and a number of user-set parameters in the code, primarily affecting boundary treatment, were exercised. These parameters, mesh size considerations, and the important modifications of VARR-II and their rationale are discussed in this chapter.

4.1 VARR-II

The details of the VARR-II structure and operational information are found in the user's manual [38]. Chen [39] also provides a description of VARR-II, a complete list of the partial differential equations involved, and a concise explanation of the solution algorithm. Accordingly, this section discusses only the basic physical principles and special numerical features of the code.

4.1.1 General Principles

VARR-II solves six simultaneous partial differential equations:
one continuity, two momentum, one energy, and two turbulence transport
equations. Although strictly two-dimensional, the code can handle, as an
option, a cylindrical axisymmetric geometry in r-z coordinates. The
momentum equations, differenced in their conservative form, include the
effects of buoyancy through density variations in the gravity term and
contain optional resistance factors that can be used to model the effects
of mechanical structure within a mesh cell. The two turbulence model
equations are described in Sec. 4.3.

4.1.2 Donor Cell Differencing

An interpolated donor cell treatment is applied to the advective
terms in all the transport equations. The user may select, through a
donor cell coefficient (α), center differencing, interpolated donor cell,
or full donor cell differencing. Center differencing provides higher
numerical accuracy at the expense of a more restrictive stability
criterion. Full donor cell differencing gives the greatest numerical
stability, but is less accurate than center differencing; the numerical
inaccuracies manifest themselves as an artificially enhanced viscosity
that makes the flow more diffusive than the center differencing technique.
Interpolated donor cell, as the name implies, is a hybrid combination of
the two extremes just discussed.

In this work, for the mesh sizes, time steps, and flow rates
examined, full donor cell differencing ($\alpha_x = \alpha_z = 1.0$) is always used to
preserve numerical stability. A test case, using the coarse mesh described

in the next section, showed that interpolated donor cell differencing
($\alpha_x = \alpha_z = .5$) results in essentially identical mean velocity predictions,
and slightly higher estimates of TKE than obtained with full donor cell.
However, the proportional increase in calculated TKE throughout the cell
is roughly equal to the artificial increase in the code-specified inlet
TKE that results from using a donor cell coefficient not equal to one.
Accordingly, the use of full donor cell differencing is not judged to
cause significant numerical inaccuracies. Attempts to use a donor cell
coefficient less than 0.5 resulted in numerical instabilities for feasibly-
sized time steps.

4.1.3 Solution Procedure

The solution procedure applied in VARR-II is the Simplified Marker
and Cell (SMAC) method developed by Amsden and Harlow [40] and described
in detail in their report. The basic procedure starts with an explicit
computation of an interim velocity field that, in general, does not
satisfy the continuity equation. Boundary conditions are set, and then
cell pressures are adjusted to satisfy continuity at each mesh cell.
The pressure adjustments update the entire velocity field so that this
step must be performed iteratively. The pressure iteration contains a
user-adjustable relaxation factor (β_0) that, when selected properly, can
improve the convergence rate. For stability reasons, β_0 is usually bounded
between 1.2 and 2.0. In this work the value β_0 = 1.85 was used for all
computations.

4.2 Geometry and Mesh Size

VARR-II permits the use of either cartesian or axisymmetric cylindrical coordinates. Since the experiment was performed in a rectangular test cell (see Sec. 3.1.3), the cartesian system is selected. The calculations as well as the measurements are performed on one half of the symmetric plenum model, as shown in Fig. 4.1.

Two mesh sizes are used in the computational experiments: a 10x12 "coarse" mesh and a 16x24 "fine" mesh. The coarse mesh requires far less computer time and is used for the extensive parametric analysis that examines the effects of changing boundary and inlet conditions, turbulence model constants, and other user-adjustable features in VARR-II. The coarse mesh is depicted in Fig. 4.2. Note that this mesh does not represent the the experimental test-cell exactly, especially at the outlet region. However, comparison of the computed results using both mesh sizes shows that the coarse mesh is adequate for preliminary estimates, and is significantly less expensive. The 16x24 fine mesh, Fig. 4.1, is used for the final parameter studies and transient runs.

4.3 Modifications

4.3.1 Turbulence Model

In Sec. 2.1.2 the rationale for using the more complex two-equation turbulence models (cf. one-equation or Mixing Length models) in predictions of recirculating flows is addressed. One should recall that the two quantities needed to determine the turbulent viscosity are a turbulent

velocity scale and a turbulent length scale. In the two-equation model, the velocity scale is found from a transport equation for K, the turbulent kinetic energy. Attempts to write a second transport equation directly for the length scale, ℓ, have not been fruitful. Instead, workers in the field have developed a second transport equation for some other turbulence quantity that can be related either to ℓ or to the turbulent viscosity directly.

The approach adopted in VARR-II (and discussed in Sec. 2.1) is due to Stuhmiller, who writes the second equation directly in terms of σ, the turbulent viscosity, yielding the K-σ model. His method is unique; the more widely used two-equation model is some form of the K-ε model, where the second equation is written for ε, the turbulence energy dissipation rate, and σ is ultimately found as a function of K and ε. It should be pointed out again that the two partial differential equations that comprise the two-equation turbulence models are merely heuristic approximations to the unsolvable exact equations that truly describe the physics of the flow. In this sense, the "correctness" of a particular model is difficult to define. The final assessment is probably best made by asking which model, for a given amount of computational effort, gives results that are closest to valid experimental data.

The thermal-hydraulics code, TEACH-T [41] , uses the K-ε model developed by the staff in the Mechanical Engineering Department at the Imperial College of Science and Technology in England. However, since this code cannot calculate transient flows, the K-ε model in TEACH-T is transformed into a mathematically equivalent K-σ model and included in VARR-II as an option. In addition to allowing direct comparison of

the results from both models, this exercise gives some insight into the modelling process itself.

4.3.1.1 K-ε to K-σ Transformation

The two-equation K-σ model used in VARR-II is represented by two transport equations for K and σ:

VARR-II K-transport Equation

$$\frac{\partial K}{\partial t} + U_j \frac{\partial K}{\partial X_j} = \frac{\sigma}{2} \left[\frac{\partial U_i}{\partial X_j} + \frac{\partial U_j}{\partial X_i} \right]^2 + \frac{\partial}{\partial X_j} \left[\Gamma \sigma \frac{\partial K}{\partial X_j} \right] - 4\alpha \frac{K^2}{\sigma} \tag{4.1}$$

VARR-II σ-transport Equation

$$\frac{\partial \sigma}{\partial t} + U_j \frac{\partial \sigma}{\partial X_j} = \frac{\sigma^2}{4K} \left[\frac{\partial U_i}{\partial X_j} + \frac{\partial U_j}{\partial X_i} \right]^2 + \frac{\sigma}{K} \frac{\partial}{\partial X_j} \left[\Gamma \sigma \frac{\partial K}{\partial X_j} \right]$$

$$- \frac{\sigma^3}{K^2} \frac{\partial}{\partial X_j} \left[\Gamma_1 K \frac{\partial}{\partial X_j} \left(\frac{K}{\sigma} \right) \right] - 4\alpha_1 K \quad . \tag{4.2}$$

Here, Γ, α, Γ_1, and α_1 are the model free parameters.

The two equation K-ε model used in TEACH-T is represented by two transport equations for K and ε:

TEACH-T K-transport Equation

$$\frac{\partial K}{\partial t} + U_j \frac{\partial K}{\partial X_j} = \sigma \left(\frac{\partial U_i}{\partial X_j} + \frac{\partial U_j}{\partial X_i} \right) \frac{\partial U_i}{\partial X_j} + \frac{\partial}{\partial X_j} \left(\frac{\sigma}{\sigma_K} \frac{\partial K}{\partial X_j} \right) - \varepsilon \tag{4.3}$$

TEACH-T ε-transport Equation

$$\frac{\partial \varepsilon}{\partial t} + U_j \frac{\partial \varepsilon}{\partial X_j} = \frac{C_1 \sigma \varepsilon}{K} \left[\frac{\partial U_i}{\partial X_j} + \frac{\partial U_j}{\partial X_i} \right] \frac{\partial U_i}{\partial X_j} + \frac{\partial}{\partial X_j} \left(\frac{\sigma}{\sigma_\varepsilon} \frac{\partial \varepsilon}{\partial X_j} \right) - C_2 \frac{\varepsilon^2}{K} \quad . \quad (4.4)$$

Also, since σ as a function of time and space is the quantity of primary interest, this model requires the additional relation:

$$\sigma = \frac{C_\mu K^2}{\varepsilon} \quad . \quad (4.5)$$

Here, σ_K, C_1, σ_ε, C_2, and C_μ are the model free parameters.

The desired transformation is obtained by using Eq. 4.5 to eliminate ε wherever it appears in Eqs. 4.3 and 4.4. Equation 4.3 becomes

$$\frac{\partial K}{\partial t} + U_j \frac{\partial K}{\partial X_j} = \frac{\sigma}{2} \left(\frac{\partial U_i}{\partial X_j} + \frac{\partial U_j}{\partial X_i} \right)^2 + \frac{\partial}{\partial X_j} \left(\frac{\sigma}{\sigma_K} \frac{\partial K}{\partial X_j} \right) - C_\mu \frac{K^2}{\sigma} \quad . \quad (4.6)$$

Equation 4.4 (after some involved rearrangement) becomes

$$\frac{\partial \sigma}{\partial t} + U_j \frac{\partial \sigma}{\partial X_j} = \frac{\sigma^2}{K} \left(1 - \frac{C_1}{2} \right) \left(\frac{\partial U_i}{\partial X_j} + \frac{\partial U_j}{\partial X_i} \right)^2 + \frac{2\sigma}{K} \frac{\partial}{\partial X_j} \left(\frac{\sigma}{\sigma_K} \frac{\partial K}{\partial X_j} \right)$$

$$- \frac{\sigma^3}{K^2} \frac{\partial}{\partial X_j} \left(\frac{2K}{\sigma_\varepsilon} \right) \frac{\partial}{\partial X_j} \left(\frac{K}{\sigma} \right) - \underbrace{\frac{1}{\sigma_\varepsilon} \left(\frac{\sigma}{K} \right)^4 \frac{\partial}{\partial X_j} \left(\frac{K^4}{\sigma^3} \frac{\partial \sigma}{\partial X_j} \right)}_{*}$$

$$- C_\mu (2 - C_2) K \quad . \quad (4.7)$$

Equations 4.6 and 4.7 are simply re-ordered forms of Eqs. 4.3, 4.4, and 4.5. In theory, with the exception of errors introduced by the finite difference approximations, use of Eqs. 4.6 and 4.7 in a fluid dynamics code should produce the same results as use of Eqs. 4.3, 4.4, and 4.5. In practice, truncation errors and differences in the treatment of boundary conditions can be expected to make the comparison less exact.

It is interesting to see that two independent modellers, applying physical reasoning and judicious approximation along two entirely different theoretical pathways, have arrived at strikingly similar forms for their respective models. The two TKE equations (4.1 and 4.6) are term-by-term identical, differing only in the values of the model free parameters. Even the more complex σ-transport equations (4.2 and 4.7) share identical terms with the only difference being an extra diffusion-like term, marked with an asterisk, in Eq. 4.7.

Although the structural similarity of the two models is made apparent by this juxtaposition, some specific differences are also emphasized, such as the enhanced diffusion effects mentioned above. Another example is demonstrated by considering the decay of TKE in a homogeneous flow. The two "identical" K-equations, using recommended values of the model constants, predict turbulent energy decay rates that differ by a factor of two. This discrepancy is a reminder of the arbitrariness of the modelling process and the variation in the available data base from which the model constants are obtained.

The programming changes in VARR-II required to use the K-σ version of the K-ϵ model are minimized by writing a generalized pair of transport equations that represents both the original and new K-σ models. Equations

4.1 and 4.6 are contained in this

Generalized K-transport Equation:

$$
\frac{\partial K}{\partial t} + U_j \frac{\partial K}{\partial X_j} = \frac{\sigma}{2}\left(\frac{\partial U_i}{\partial X_j} + \frac{\partial U_j}{\partial X_i}\right)^2 + \frac{\partial}{\partial X_j}\left(k_3 \, \sigma \, \frac{\partial K}{\partial X_j}\right) - 4k_7 \frac{K^2}{\sigma} \quad . \tag{4.8}
$$

Likewise, Eqs. 4.2 and 4.7 are contained in this

Generalized σ-transport Equation:

$$
\frac{\partial \sigma}{\partial t} + U_j \frac{\partial \sigma}{\partial X_j} = k_1 \frac{\sigma^2}{K}\left(\frac{\partial U_i}{\partial X_j} + \frac{\partial U_j}{\partial X_i}\right)^2 + k_2 \frac{\sigma}{K}\frac{\partial}{\partial X_j}\left(k_3 \sigma \frac{\partial K}{\partial X_j}\right)
$$

$$
- k_4 \frac{\sigma^3}{K^2}\frac{\partial}{\partial X_j} K \frac{\partial}{\partial X_j}\left(\frac{K}{\sigma}\right) - \frac{k_5}{\sigma_\epsilon}\left(\frac{\sigma}{K}\right)^4 \frac{\partial}{\partial X_j}\left(\frac{K^4}{\sigma^3}\frac{\partial \sigma}{\partial X_j}\right) - 4\, k_6 \, K \quad .
$$

$$
\tag{4.9}
$$

Equations 4.8 and 4.9 represent either the VARR-II K-σ model or the TEACH-T K-ε model, depending on the values of the k_i. The k_i are functions of the original turbulence model constants and are defined in Table 4.1.

4.3.2 Inlet Conditions

VARR-II provides for a user-specified inlet flow that can be stated in terms of velocity or volumetric flowrate. For time-dependent calculations, a table of inlet velocities is prescribed and the code performs a linear interpolation for time values not in the table. Although this technique permits accurate modelling of the experimentally determined

inlet velocities, the important turbulence quantities, K and σ, are not readily controlled. In a previous work, Chen and Golay [42] showed that VARR-II steady-state predictions are sensitive to the specified levels of inlet K and σ. Accordingly, the code has been modified to permit the following user-specified inlet turbulent conditions:

(1) <u>Normal Treatment</u> - K_{inlet} and σ_{inlet} are calculated by the code as a function of the inlet velocity, mesh size, and TQJET and TSJET (where TQJET and TSJET are given, recommended constants based on experiment).

(2) <u>Steady-State Matching Treatment</u> - K_{inlet} is user-specified at each inlet cell; σ_{inlet} is either ratioed to K_{inlet} in a manner consistent with the normal treatment, or specified as a constant multiple of the normal inlet treatment value.

(3) <u>Transient Matching Treatment</u> - K_{inlet} is user-specified at each inlet cell as a function of time (limited to a maximum of three inlet cells); σ_{inlet} is treated as in (2) above.

4.4 Boundary Conditions

At a solid wall, VARR-II sets perpendicular velocities to zero and provides three options for the parallel velocity: free-slip, no-slip, and derived boundary conditions. The first two are self-explanatory; the derived boundary condition analytically prescribes a logarithmic velocity profile between the computational cell next to the wall and the

wall itself. The purpose of this boundary condition is to provide the correct shear stress at the wall when the mesh size is too large to resolve properly the velocity distribution near the wall.

4.5 Summary

The boundary conditions, special numerical features, and modifications have been extensively exercised in this work while constructing the steady-state flow field from which the computational transient is begun. Proper selection of these parameters and options is important because they often have a more significant impact on calculational results than the turbulence model itself. The outcome of these numerical experiments performed on the steady-state flow field is covered in Chapter Five.
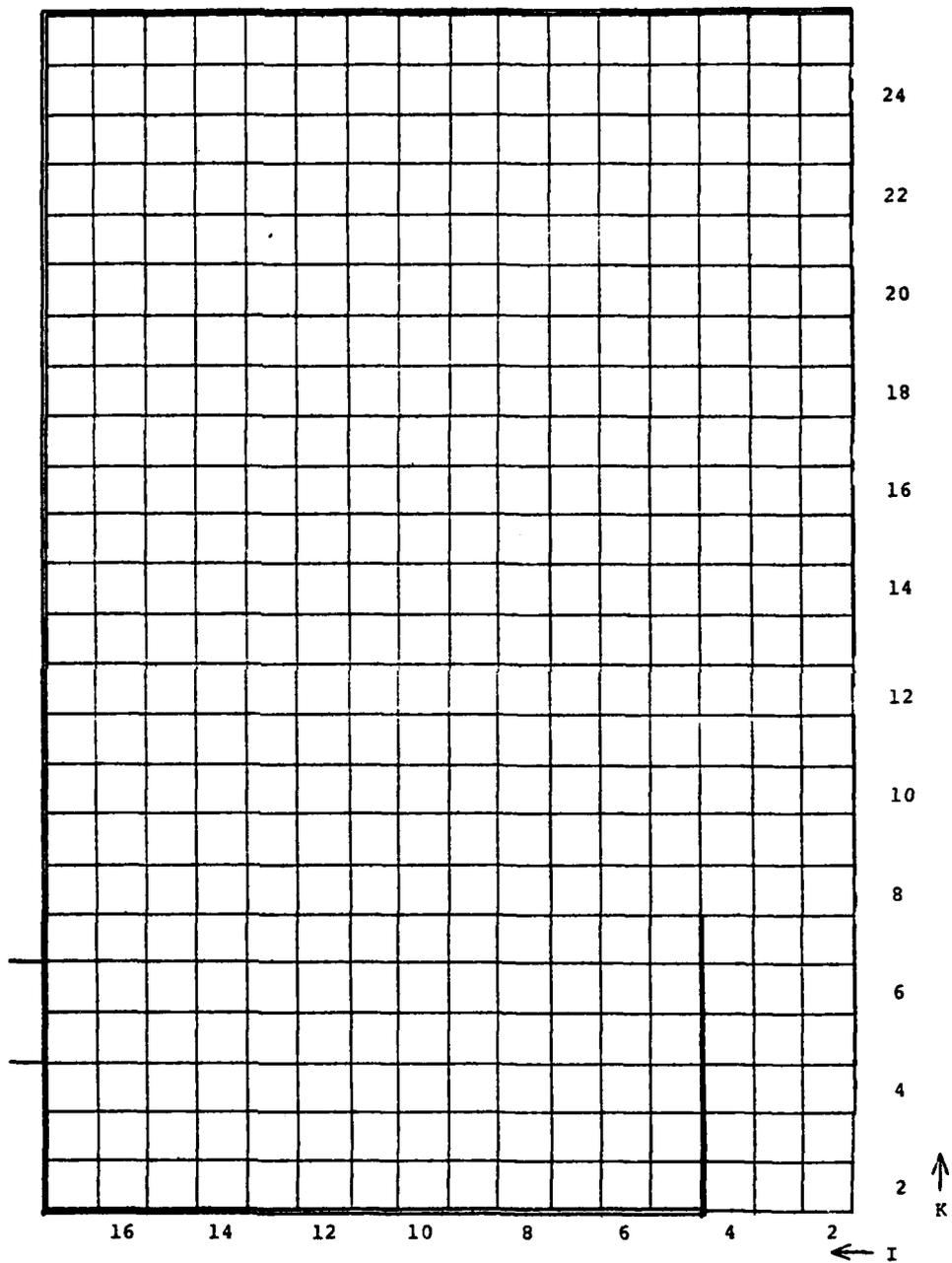
Fig. 4.1   16x24 COMPUTATIONAL MESH
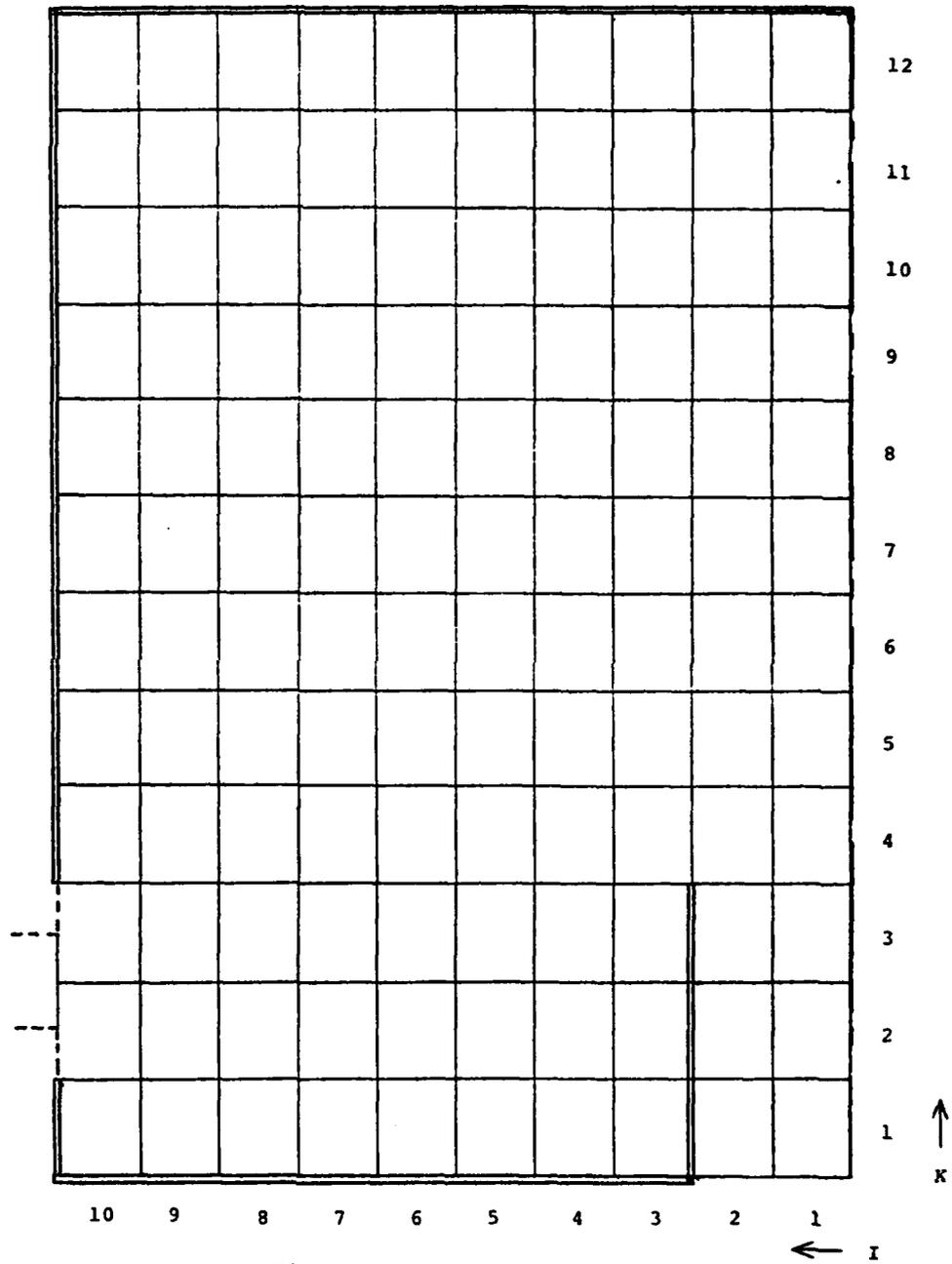
Fig. 4.2   10x12 COMPUTATIONAL MESH

Table 4.1

Generalized Turbulence Model Constants

Generalized Constant	K-σ Model		K-ε Model	
	Original Symbol	Value	Original Symbol	Value
k_1	--	.25	$(1-\frac{c_1}{2}) = 1-\frac{1.44}{2}$	.28
k_2	--	1.0	--	2.0
k_3	Γ	1.5	$\frac{1}{\sigma_K} = \frac{1}{1.0}$	1.0
k_4	Γ_1	.75	$\frac{2}{\sigma_\epsilon} = \frac{2}{1.3}$	1.54
k_5	--	0	--	1.0
k_6	$\alpha_1 = \alpha_0$	.01125	$\frac{c_\mu(2-c_2)}{4} = \frac{(.09)(2-1.92)}{4}$	.0018
k_7	α	.045	$\frac{c_\mu}{4}$	.0225
	from VARR-II		from TEACH-T	

CHAPTER V

DISCUSSION OF EXPERIMENTAL RESULTS AND COMPUTER PREDICTIONS

5.0 Introduction

In this chapter the experimental measurements and the computational predictions are presented and discussed. Since the primary objective of determining transient effects is most conclusively achieved when the initial predicted and experimental steady-state flow fields agree well, understanding this facet of the problem is a necessary first step. It is noted in Chapter Three and Appendix B that experimental error in a previous work (Chen [43]), incurred while measuring the steady-state turbulence field in the same apparatus, may be responsible for some of the discrepancy between experiment and prediction noted in that study. Therefore, new steady-state measurements are performed in this work, and the data reported herein supersede the data of Chen. Moreover, in an effort to obtain the best match between the new experimental data and the computational prediction of the steady-state full-flow condition from which the coast-down transient begins, a substantial number of steady-state numerical experiments are performed. As a result, a significant portion of the computational effort in this work is concerned with the steady-state prediction.

5.1 Steady-State or Full-Flow Condition

5.1.1 Experimental Data

The measured steady-state values of $\bar{U}$, $\bar{V}$, $\overline{u'^2}$, $\overline{v'^2}$, K (TKE), and $\overline{u'v'}$ are listed in Appendix C, Table C.1. Estimated experimental errors are typically on the order of 4% for the mean velocity, 8% for K and 25% for the Reynolds Stress. Appendix B contains the details of the experimental error analysis. All steady-state full-flow conditions referred to in this analysis are for an inlet Reynolds number of 70,000 as calculated in Appendix A.

The measured mean.velocity vectors are plotted in Fig. 5.1 over one half of the symmetrical tes: cell. They exhibit the expected recirculating flow pattern over the .ain body of the flow. In Sec. 3.1.3, a measured defect in the mass-flow balance occurring at the top of the cell is described; this discrepancy is readily observed in the velocity plot. However, over the major part of the vortex region, a good mass-flow balance obtains, which reflects the improved flow symmetry in the modified test-cell.

In addition to being listed in Table C.1, the steady-state measured K and Reynolds Stress are directly compared to calculated values in Figs. 5.2 and 5.3. Since the scalar quantity K is accurately measured and exhibits a distinct spatial structure that should be reproduced by an accurate turbulence model, it is considered a useful measure of turbulence model effectiveness. Consequently, spatial distributions of K, in addition to mean velocity and Reynolds Stress comparisons, are analyzed in the following section.

5.1.2 Comparison of Experiment with Calculation (Standard K-σ and K-ε Models)

5.1.2.1. Mean Velocity Plots

Figures 5.4 and 5.5 are the calculated mean flow vector plots for the K-σ and K-ε models respectively. These predictions of the initial steady-state flow field result from using the VARR-II code on the 16 x 24 fine mesh with the standard K-σ turbulence model and the transformed K-ε model described in Sec. 4.3.1. In addition, the following code variables are used and referred to in the future as "standard" settings:

(1) inlet velocities--matched to experiment;

(2) inlet turbulence quantities (K_{in} and σ_{in})--set by code;

(3) turbulence model free parameters--recommended values;

(4) boundary conditions--free slip.

In order to enhance the comparison of the experimental and computed flow fields, the normal technique of printing an averaged velocity vector at each computational mesh cell is not used. Instead, only velocities at those cells for which a measured velocity exists (approximately every other one) are depicted.

The K-σ and K-ε models are seen to produce basically identical mean flow fields. Comparison of these calculated fields with the experimental data (Fig. 5.1) shows generally good qualitative and quantitative agreement. Discounting the top row for 3-D effects in the experiment, the vortex center location is predicted well. The calculated vortex is elongated, as in the experiment, but with a visibly milder vertical gradient of horizontal velocity near the top. This difference may be an important reason for observed discrepancies in the spatial distribution

of K that are discussed in Sec. 5.1.2.2.

The calculated upflow between the chimney entrance and the top boundary of the test cell overlies almost perfectly the experimental data, suggesting that good flow symmetry is obtained in the experiment. The steepest velocity gradients are found, in both the experiment and calculation, on the right side of the vortex adjacent to the inlet jet; however, the experimental results show a somewhat sharper gradient that persists over the top of the vortex which is not predicted by the code. The gradient discrepancies are noted because they drive production of the turbulence parameters K and σ, and may explain the differences observed between the calculated and measured values of these quantities.

The calculated velocity field also shows slightly less downflow than is observed experimentally on the left-most line of vertical measurements. This is not surprising since the free-slip boundary condition in the calculation permits a higher than normal average fluid velocity in those cells adjacent to the wall, thereby causing a slightly lower than normal velocity to be developed in the next column of interior cells.

Overall, especially in the main recirculating zone away from the region of three-dimensional effects on the data, the mean velocity field prediction is considered good. This judgement holds for both models and, significantly, for the standard code variables that include the somewhat unphysical free-slip boundary condition and the unmatched inlet turbulence quantities.

5.1.2.2 Turbulence Kinetic Energy (K)

It is pointed out in Appendix B that calculated and measured values of K do not represent the exact same quantity, and this must be understood before the predicted and experimental values are compared. Even though VARR-II is a two-dimensional code, it is clear from the theoretical development of Stuhmiller's turbulence model that the scalar quantity K, calculated in the code, is defined by

$$K_{calc.} = \frac{\overline{u'^2} + \overline{v'^2} + \overline{w'^2}}{2} \quad ,$$

where u', v', and w' are the fluctuating components of velocity in all three coordinate directions. The two-channel experimental set-up used in this work permits measurements in only two dimensions so that

$$K_{meas.} = \frac{\overline{u'^2} + \overline{v'^2}}{2} \quad .$$

In the code, consideration of the third dimension momentum equation for $\overline{W}$ is eliminated by assuming that all derivatives with respect to this dimension are identically zero. This assumption represents genuine two-dimensionality, and the resulting equations apply exactly. Likewise, the experiment is designed so that $\overline{W}$ and derivatives in the $\overline{W}$ direction are zero or as small as possible. However, $\overline{w'^2}$ is not zero, since turbulence is necessarily three dimensional. Therefore, one must account for the absence of $\overline{w'^2}$ in the reported values of $K_{meas.}$

If the turbulence is isotropic, then $\overline{w'^2} = \overline{u'^2} = \overline{v'^2}$. Reference to the measured data in Table C.1 show that $\overline{u'^2}$ and $\overline{v'^2}$ are roughly

equal throughout the test-cell. Since mean velocities and gradients in the third coordinate direction are small or non-existent on the plane of the two-dimensional measurements, one would not expect $\overline{w'^2}$ to differ significantly from its isotropic turbulence level. In that case,

$$\overline{w'^2} \cong \frac{\overline{u'^2} + \overline{v'^2}}{2} \quad .$$

Adding this additional component of K onto the measured values yields

$$K_{calc.} \cong 1.5 \; (K_{meas.}) \quad .$$

This approximate relationship should be kept in mind when comparing measured and calculated values of turbulence kinetic energy.

Figure 5.2 compares measured and calculated K throughout the cell for both models using the standard code parameters. Significant differences are observed, even between the two calculations. A clearer picture is obtained by plotting K as a function of horizontal position at a number of vertical planes in the cell. This is done at three representative locations in Fig. 5.6 for the data and both turbulence model predictions.

Throughout the main recirculation zone, the data consistently show two characteristic peaks of K on either side of the vortex. The peaks occur in the regions where the velocity gradients are steepest. This is as expected since K can only be produced by velocity gradients. Further, the magnitudes of the measured peaks follow a logical pattern. The peak on the inlet side is seen to increase monotonically as one follows the flow from just above the chimney to the top of the vortex. Remembering that the inlet K level is dramatically lowered by the screens in the

modified inlet, one observes the inlet flow carrying a relatively low K and entering a region of high K production. As the level of K is increased by the strongly positive net production in this area of high velocity shear, the fluid proceeds up along the inlet jet constantly increasing its K level in the same manner. The K built up in this fashion appears to be convected along a streamline (in fact, the two characteristic peaks occur on exactly the same streamline) and contributes to the relatively larger K peak observed on the downflow side of the vortex. Here the velocity distribution shows a markedly reduced velocity gradient, and one would expect the production of K to fall off. The data are consistent: they show the initially high K level at the top of the vortex decreasing monotonically along the downflow streamline, indicating that *the dissipation rate of K in this region has risen to the point where net production is negative.*

The calculated and measured K-distributions are compared in Fig. 5.6. The location of the K peak on the upflow side of the vortex is predicted reliably by both models while the magnitude is overestimated somewhat. The K-σ and K-ϵ distributions are similar, but the K-ϵ model is seen to have a higher overestimate of magnitude and an apparent greater ability to convect K over the top of the vortex to the downflow side. The most striking disagreement between calculation and measurement is the absence of a predicted K peak on the downflow side of the vortex. A perceptible rise in K close to the wall, however, is observed in the calculations, and in fact decays along the downflow streamline in the same fashion as the data. Possible reasons for these differences are discussed in Sec. 5.1.3 where attempts are made to improve the numerical prediction.

Although it is true that correct prediction of the Reynolds Stress field is all that is required to achieve an accurate calculated velocity field, the importance of correctly predicting K, as well as σ and the Reynolds Stress, should not be overlooked. Since the calculated magnitude and spatial distribution of K play an integral role in the resulting σ-field, accurate Reynolds Stress predictions without accurate K predictions are fortuitous, but not useful determinants of turbulence model performance. If one hopes to develop confidence in the generality of a particular turbulence model, and improved generality is the rationale for these more complex transport-type models, then the ability to predict K-distributions is required. Accordingly, the spatial variation of K across the main recirculating zone is examined frequently in this work as a useful measure of turbulence model performance.

5.1.2.3 Reynolds Stress

Figure 5.3 is a comparison of steady-state measured and calculated Reynolds Stress throughout the cell for both models using the standard code parameters. Physical interpretation of the Reynolds Stress distribution is necessarily less direct than were the K-field comparisons. This is so because of the larger experimental error involved in measuring the velocity cross correlation, and because the turbulent viscosity, σ, which is transported in the computation and reported directly by the code, can only be inferred from experiment. Nevertheless, since the calculated and measured mean velocity fields (and hence mean velocity gradients) are essentially congruent, Reynolds Stress comparison can give useful qualitative information regarding the real and predicted transport of

the important turbulence quantity σ.

Comparison of the K-σ and K-ϵ model estimates of Reynolds Stress indicates qualitatively similar spatial distributions, with generally higher magnitudes in the K-ϵ case. Since calculated velocity gradients are approximately identical in both cases, one expects the calculated σ to be the main contributor to the differences, and this is in fact the case over most of the flow field. Reference to the generalized K-transport equation (Eq. 4.8) used by both models shows that, all other factors being equal, a higher value of σ will result in a net increase in the production rate of K. This is consistent with the overall higher levels of K obtained with the K-ϵ model and discussed in the previous section. Moreover, these findings compare well with the results of TEACH-T and VARR-II calculations performed previously on the same geometry [44]. Whether used in its original form in the TEACH-T code or in the K-σ-equivalent form in the modified VARR-II, the K-ϵ model consistently produces turbulence quantities that are higher than those predicted by Stuhmiller's K-σ model.

Comparison of the K-σ Reynolds Stress prediction with the data are generally poor over most of the main recirculating region with the notable exception of the downflow side of the vortex. Here data and prediction are in very good qualtitative as well as quantitative agreement. To emphasize the importance of correctly predicting σ and the Reynolds Stress, it is noted that, with the exception of the top part of the test-cell where three-dimensional flow effects are important, the major mean flow discrepancies always correspond to points of significant disagreement between measured and calculated Reynolds Stress.

Since the calculated inlet turbulence quantities that feed directly into the upflow side of the vortex are not matched to the experimental values, this discrepancy may cause the significant Reynolds Stress mis-match observed in the high-shear region on the upflow side of the vortex. Such a possibility is examined in the following section where improvements in the steady-state prediction are sought.

5.1.3   Parametric Analysis to Improve Steady-State Prediction

5.1.3.1   Rationale, Method, and Scope

Before the transient calculation was performed, an attempt was made to improve the correspondence between the numerical prediction and the measurement for the initial steady-state full-flow condition. The experimental and calculated mean velocities are shown to be in relatively close agreement in Sec. 5.1.2.1, so efforts are concentrated on improving the K and Reynolds Stress spatial distributions where significant differences between prediction and measurement have been identified.

The user-adjustable parameters that have the potential to change the calculated turbulence field for a given steady-state inlet flow rate are listed and defined below as the following:

(1) $\alpha_x = \alpha_z$ -- donor cell coefficients;

(2) boundary conditions;

(3) inlet turbulence levels -- the values of K and σ ascribed to the inlet flow cells;

(4) turbulence model free parameters:

α -- dissipation coefficient for K.

Γ -- relative diffusivity coefficient for K,

α_0 -- dissipation coefficient for σ,

Γ_1 -- relative diffusivity coefficient for σ.

Based on physical interpretation of the data and comparison with the
original calculated predictions, variations are made in all of the above
parameters in a systematic way to determine if the steady-state numerical
prediction can be improved.

Because VARR-II runs are expensive in computer time, the faster-
running 10 x 12, cell coarse-mesh, described and depicted in Sec. 4.2,
is used for this parametric analysis. The relative accuracy of the
coarse mesh can be evaluated by comparing the results of a fine mesh
calculation to a coarse mesh calculation when all other parameters are
held equal. Figure 5.7 is the mean velocity field for a coarse mesh
calculation using the K-σ model and standard settings on the code para-
meters. The general features of this prediction compare well with
Fig. 5.4, its fine mesh analog. More importantly for our purposes,
spatial distributions of K and σ are essentially equivalent for the coarse
and the fine mesh prediction over the entire recirculating zone.
Significant differences are observed at the level of the plenum outlet
because the coarsh mesh outlet is twice as large as that of the fine
mesh. Therefore, predicted turbulence quantities in this region are not
used in the evaluation.

Approximately one hundred different combinations of the above
listed variables were calculated on the 10 x 12 coarse mesh and the results
compared to the standard code prediction and the data. Table 5.1 depicts
the values assumed by these variables during the course of the study.
In order to further limit the cost, only the K-σ model is used in the

parametric analysis.

The main features of the experimental data that the standard code settings failed to predict, as discussed throughout Sec. 5.1, are:

    (1) magnitudes of K and Reynolds Stress, especially along the upflow side of the vortex;

    (2) spatial distribution of K and Reynolds Stress across the recirculation zone (most notably the absence of a second K-peak on the down-flow side of the vortex);

    (3) the decay rate of K along the upflow side of the vortex.

New predictions are judged to be "improvements" over the standard code settings when they display a better overall fit to the data with respect to the above criteria. In addition, the basically good agreement achieved between predicted and measured mean flow speeds must be maintained.

The major findings of this exercise are discussed individually in the sections that follow. Although they are treated separately in the text, various combinations of the parameter changes are also accomplished. Where these combined effects produce unique results, they are identified.

5.1.3.2 Donor Cell Coefficient

The effect of varying the donor cell coefficient is described in Sec. 4.1.2. There it is shown that full donor cell differencing ($\alpha_x = \alpha_z = 1$) is desirable in terms of numerical stability, and that little change in the prediction is observed for values of $\alpha_x = \alpha_z$ as low as 0.5. In all the following analyses, the full donor cell treatment is applied.

5.1.3.3 Boundary Conditions

The alternative boundary conditions available to the VARR-II user are described in Sec. 4.4. An improvement in the K-distribution, specifically the generation of a second K-peak on the downflow side of the vortex, is possible with a change of the boundary condition. The standard free-slip condition, which is generally adequate for turbulent flow away from the walls, under-estimates the wall shear stress and causes a corresponding underestimate in the production of K near the wall. However, if additional K were produced along the top wall by a change in the boundary condition, it might be convected down into the region of K-deficiency on the left side of the vortex.

A series of numerical experiments was conducted in which no-slip, as well as partial-slip, wall boundary conditions were applied. The production of K near the wall was greatly enhanced by the no-slip option and reduced somewhat in the partial-slip case. However, the substantial levels of additional K generated by the revised boundary condition remained near the wall and were not convected or diffused into the interior region to produce the second K-peak observed in the data. The fact that this second K-peak is not created in the computation by diffusion of K from near the wall is consistent with the data. There it is seen that K levels near the wall are lower than those at the peak on the down-flow side of the vortex, indicating that K is actually diffusing towards the wall. On the other hand, the failure of the turbulence model to convect K produced at the top wall into the downflow side of the vortex is not consistent with the data. This behavior appears to be the result of higher than desired K-dissipation rates in the model, and is addressed further in Sec. 5.1.3.5.

Finally, the mean velocity field was significantly distorted in the no-slip case, and the overall magnitudes of K throughout the cell were increased markedly above the data values.

The use of the derived boundary condition, or wall function treatment, is sometimes recommended for these cases where the mesh size is too large to describe adequately the velocity profile near the wall. But this boundary condition exacts a significant penalty in computer run time [45] and was not attempted. The results of the no-slip case, however, suggest that the derived boundary condition could not have offered substantial improvement since, as noted above, it is seen in the no-slip numerical experiments, and in the data, that diffusion of K from enhanced production near the wall cannot be the source of the second K-peak. As a result, the free-slip boundary condition is seen to give the most accurate mean flow prediction for the lowest computer cost and is apparently not responsible for the observed maldistribution of the turbulence quantity, K. Therefore, the free slip boundary condition is used for the transient computation.

5.1.3.4 Inlet Turbulence Levels

In addition to the inlet mass flow rate, values of the turbulence quantities K and σ in the inlet flow must be specified before the numerical solution can proceed. With the standard code parameters, these values are established as a function of inlet flow velocity, the donor cell coefficient, and two input variables, TQJET and TSJET. For the case where $\alpha_x = \alpha_z = 1$, the relation is

$$K_{in} = TQJET \ (U_{in})^2, \tag{5.1}$$

and

$$\sigma_{in} = \text{TSJET } (U_{in}) \; (\delta X), \tag{5.2}$$

where

U_{in} = average inlet velocity,

δX = cell width.

TQJET and TSJET are obtained from experiments in turbulent jets, and recommended values are given in the VARR User's Manual.

It has been noted, Chen and Golay [46], that the values of the inlet turbulence quantities can have a substantial effect on the predicted mean flow velocity distribution and that attention to these quantities may be as important as attention to the turbulence model itself. In this experiment the measured values of inlet K are approximately two orders of magnitude lower than the values set by the code for the same inlet flow rate; this small measured value is a result of the turbulence-suppressing effect of the inlet grids.

It is somewhat encouraging to note that, even with this large disparity of K at the inlet, the turbulence model brings the overall K-levels into rough agreement a short distance away from the inlet. However, in order to achieve this agreement, the computed levels of K are required to decay along the upflow side of the vortex in contradistinction to the slight, but monotonic build-up observed in the data. Therefore, a series of numerical experiments was performed to determine the effect of matching the inlet turbulence levels to the experiment.

The measured inlet K-levels are known well and, with the code modifications described in Sec. 4.3.2, can be directly applied at the

three inlet mesh cells. However, inlet levels of σ are not readily measured in this region where mean velocity gradients are small and the nearly isotropic turbulence yields a Reynolds Stress that is close to zero. When the inlet K alone is matched to experiment, and inlet σ is calculated by the code with Eq. 5.2, the resulting prediction is severely distorted by the generation of excessively high values of σ throughout the solution space; therefore, some method of "matching" σ_{in} is required. The turbulent jet experiments used to obtain Eqs. 5.1 and 5.2 indicate that the levels of inlet K and σ are related, and matching only K_{in} to the experiment destroys this relationship. Therefore, in cases where σ_{in} is not known, and K_{in} is specified from experiment, an estimated value for σ_{in} is found from the combination of Eqs. 5.1 and 5.2 to be

$$\sigma_{in} = (K_{in}) \left(\frac{TSJET}{TQJET}\right) \left(\frac{\delta X}{U_{in}}\right) \quad . \tag{5.3}$$

When this value of σ_{in} is used, the mean field velocity predictions return to their normal acceptable fit that was observed in the unmatched case. However, there is no improvement in the distribution of turbulence quantities. In fact, both the upflow K decay rate and the spatial distribution of K across the cell are more poorly predicted than in the unmatched case.

This is a surprising result: a somewhat better overall numerical prediction is obtained in the unmatched case where less information about the actual flow is used. This anomaly is thought to be related to the numerical method and the turbulence model formulation. Reference to Eqs. 4.8 and 4.9, the generalized transport model equations for K and σ, show their dependence on the ratio of σ/K. When the very low values of
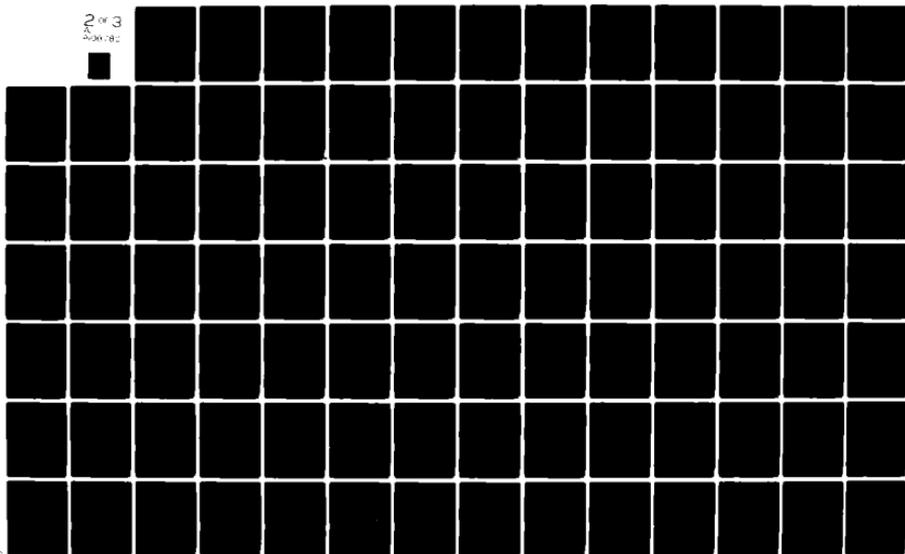
K_{in} and σ_{in} associated with this experiment are used as matched inlet conditions, large spatial gradients in both K and σ are established above the inlet cells. Since the full donor cell treatment computes derivatives to only first order accuracy, truncation errors in the largest gradient approximations could be causing the unrealistic buildup of σ that is observed.

While it is certainly true that the code mean flow and turbulence field predictions are highly sensitive to the values of the inlet turbulence quantities, improved predictions may not always result from matching these quantities to known experimental values. As observed above, the matching of K alone produced extremely degraded results. Therefore, it is recommended that any matching of inlet parameters that is attempted should roughly maintain the $(\sigma/K)_{in}$ ratio that is established by Eq. 5.3 unless specific experimental values of both K and σ are known with certainty.

Numerous combinations of boundary conditions and turbulence model free parameters were tried with the matched inlet conditions. In all cases, the new predictions, considered on the basis of the evaluation criteria listed in Sec. 5.1.3.1, are judged to be inferior to results obtained with the standard code parameters and unmatched inlet conditions. As a result, unmatched inlet turbulence values are chosen for the transient computation.

5.1.3.5 Turbulence Model Free Parameters

Once the boundary and inlet conditions are fixed, the remaining variables that can be used to improve the quality of the steady-state

numerical prediction are the turbulence model free parameters themselves.
The four free parameters used in the K-σ model are listed and defined in
Sec. 5.1.3.1. Guidance as to the specific parameter and the direction of
variation that is most likely to improve the prediction can be sought from
the analysis of the experimental data. For example, the experimental data
in Fig. 5.6 show clearly that the magnitude of the K-peak on the upflow
side of the vortex increases as one proceeds from lower to higher levels
in the test-cell. However, both numerical predictions exhibit the opposite
behavior, suggesting the need for an adjustment to the turbulence model to
reduce the dissipation rate of K. Additional analyses of this nature
were made based on other differences between the measured and calculated
turbulence fields, and the suggested changes to the free parameters were
tested. A partial list of the test runs accomplished and a qualitative
evaluation of their outcome is given in Table 5.2.

These results show that the turbulence field and mean velocities are
highly sensitive to relatively small changes in the turbulence parameters.
In addition, the complex coupling of the model transport equations is
reflected in the somewhat unpredictable response of the turbulence variables
to perturbations in the free parameters. For example, increasing α, the
K dissipation coefficient, results in higher values of K throughout the
cell; decreasing α produces the opposite behavior. On the other hand,
increasing α_0, the σ dissipation coefficient, decreases both σ and K;
decreasing α_0 yields the opposite behavior.

Moderate adjustments to the relative diffusivity coefficients
(Γ and Γ_1) produce relatively small changes, in the expected direction,
in the spatial distribution of the scalars K and σ. In the development of

the K-σ turbulence model, Γ and Γ_1 are shown to be connected by a fixed ratio. Significant changes in the two coefficients can be made as long as this original ratio is maintained. When one or the other coefficient is changed enough to substantially alter their ratio, numerical instabilities result.

Although adjustment of the turbulence parameters can slightly improve the agreement between certain localized features of the experimental data and the computed prediction, such changes always result in deterioration at other points of comparison. No combination of changed turbulence parameters has been identified that can produce a demonstrably better numerical prediction of the measured turbulence field than is obtained using the standard recommended values. This statement applies only to the K-σ turbulence model because funds were not available to exercise the K-ε model in the same way.

An order-of-magnitude analysis of the terms in the K-transport turbulence model equation show that production and dissipation dominate over diffusion and advection throughout most of the flow. Further, although the data show a slight but persistent build-up of K with height above the chimney on the upflow side of the vortex, the model consistently shows decay. Even when inlet K is matched to the relatively low experimental values, the model quickly builds up a high value of K and then begins to decay with height. This behavior may also be related to the aforementioned failure of the model to convect K over the top of the vortex and into the downflow region. Although it appears from the above that K-dissipation is being over-estimated by the model, no tested change to the K-dissipation coefficient was able to correct this behavior. This suggests that a change in the form of the K-dissipation term may be needed

to improve the predictions.

5.2 Transient Comparison and Analysis

5.2.1 General

In order to determine with certainty whether the use of constant turbulence model free parameters, which are derived with steady-state assumptions and obtained from steady-state experiments, adversely affects the computational prediction of flows in the presence of a momentum transient, it is first necessary to minimize the differences between the initial steady-state prediction and the corresponding measured steady field. If this is successfully accomplished, differences observed between computed and measured transient flow behavior can, in most cases, be reliably ascribed to the transient effect. The two-equation turbulence models examined in this work provide steady-state mean velocity field predictions that generally match well the experimental data in regions of the test-cell where two dimensionality is maintained. Unfortunately, the analysis of Secs. 5.1 and 5.2 have shown that the calculated scalar turbulence quantities exhibit significant departures from the measured values at a number of locations. Further, the numerical experiments indicate that no combination of revised boundary conditions, inlet turbulence levels, or turbulence model constants can genuinly improve the initial steady-state match between data and computation.

Concern for the adequacy of the steady-state match of the computed and measured turbulence scalars K and Reynolds Stress stems from two sources. First, there is the notion expressed earlier that the reliable

prediction of such accurately measured and spatially structured turbulence quantities as K is needed before genuine confidence in the generality of the model can be developed. Second, any transient effects that are related to the turbulence model constants should be most directly observable in those dependent variables whose calculation is most closely linked to the values of the constants. The turbulence kinetic energy, K, is the only directly measured quantity that is dependent, in a first-order sense, on the turbulence model free parameters. Here it is recalled from the parametric analysis of Sec. 5.1.3 that relatively small changes in the values of the individual turbulence model constants can markedly affect the predicted K and σ spatial distributions and absolute magnitudes. This fact suggests that the potential for a significant transient effect, that is associated with the model constants, does exist. Moreover, if steady-state distributions of K were accurately predicted by the model, such transient effects could be directly evaluated by observation of the time-varying K-field.

The predicted and measured steady-state fields can be brought into initial agreement by a straightforward normalization at each point in the cell, and the computational transient calculated and compared with the data in this fashion. This is the procedure used in the analysis that follows. However, the non-linear nature of the problem makes it impossible to assure that this initial normalization will compensate throughout the entire transient for the apparently fundamental inability of the model to make accurate steady-state predictions. Therefore, one cannot be certain that differences observed in comparing the time-varying value of a given measured and calculated quantity are the sole result of

transient effects associated with the use of the constant turbulence model parameters. This fact is noted here as a limitation on the analysis of the data that follow.

5.2.2 Description of Computational Transient

The transient calculation was performed by first establishing an initial steady-state flow pattern in the solution space using measured values of the inlet flow speeds as inlet velocities in the code. Once the steady field was developed, the inlet velocities used by the code were matched to the measured inlet velocities as they decreased during the approximately 120 second coastdown transient. The general shape of the coastdown as a function of time is similar to that shown in the $\bar{U}$ plot in Appendix F for the position $I = 10$, $J = 2$, just above the chimney. The flowrate-versus-time table used by the code was generated from the experimental data and is reproduced in Table 5.3.

In accordance with the findings of the previous section, the transient calculation is performed with VARR-II variables set as follows:

- 16 x 24 fine mesh
- free slip boundary conditions
- inlet turbulence parameters set by code (i.e. not matched to experiment)
- K-σ turbulence model with standard free parameter values.

To save funds, the calculation was stopped at eighty seconds into the transient since all observable trends in the calculation were firmly established at this point in problem-time. This observation is readily verified by considering the plots of turbulence field parameters versus time in Appendix F.

During the computed transient, all of the turbulence field parameters were printed after each ten seconds of problem-time. This interval corresponds to points in the experiment where data were digitized and recorded for the ensemble average. Comparison of the computed and measured quantities during the transient is presented in the following sections.

5.2.3 Mean Velocity Plots

The comparison of the calculated and the measured mean velocity fields is presented in Figs. 5.8 through 5.13. Because differences between calculation and measurement are small and difficult to see, only three sets of mean velocity plots are included. The plots correspond to times that span the length of the calculated transient. Note also that transient measurements are made at only 42 of the 79 I-J coordinate positions that are used to describe the steady-state flow pattern, so the vector plots in these cases are less full.

The steady-state mean velocity field was shown to be predicted well in Sec. 5.1, and this observation generally holds for the transient case also. However, when the transient plots are carefully overlaid in sequence, some differences in the computed and measured time behavior can be discerned. The effect is slight, but a definite trend is observed wherein the calculated result moves more than the measured amount of flow to the outside of the vortex as the transient proceeds. A corresponding deficit in down-flow velocity is observed to be growing with time near the center of the vortex. This behavior is related to observed trends in the difference between the calculated scalar turbulence quantities and their measured counterparts in the next section.

5.2.4 Turbulence Field Parameters Versus Time

Plots of the turbulence field parameters, $\overline{U}(t)$, $\overline{V}(t)$, $K(t)$, and $-\rho\,\overline{u'v'}(t)$, as functions of time during the transient, are provided in Appendix F for each of the I-J coordinate locations where transient measurements were made. On a single page, for a specific I-J coordinate position, four plots compare the data (+'s) and corresponding calculated values (solid lines) throughout the transient. At those measurement points where a specific averaged quantity is very small and the statistics are poor, a large normalization factor is used to keep the data scatter from obscuring adjacent charts. This accounts for the occasional plot in which all the data seem to fall on the abscissa.

The plots in Appendix F show that in most cases, the normalized data and calculations appear to follow the shape of the general inlet flow-versus-time curve defined by the inlet flow rate function of Table 5.3 (the scalar quantities seem to vary as the square of the flow rate fractions in Table 5.3). However, a close inspection of all the curves reveals significant departures by the data and the calculation from the general shape of the inlet flow rate curve. The magnitude and sign of these departures is seen to vary considerably throughout the flow region, and this spatial "scatter" of transient-related differences virtually eliminates the possibility that a systematic error in the measurement technique is responsible for the observed departures.

The plots in Appendix F generally show, in cases where the data statistics are good, that the discrepancies between measured and calculated transient behavior are not large. For the flow speed, geometry, and transient rate used in this experiment, the existence of a momentum

transient does not cause differences between the time-dependent measured and calculated normalized turbulence field quantities that are large compared to those observed initially between the two unnormalized steady-state fields.

A qualitative connection between the time-varying mean velocity differences discussed in the previous section and the plots in Appendix F may be drawn by considering the spatial distribution of the time-dependent difference between measurement and calculation. In general, when the calculated and measured values of a particular parameter do not coincide during the transient, they tend to diverge from the point of initial steady-state agreement, with one or the other taking on higher values through time. The value which stays high in these cases is said to "lead"; that which takes on lower values is said to "lag." With this definition, the spatial distributions of lead/lag characteristics are plotted in Figs. 5.14 through 5.17.

In Figs. 5.14 and 5.15 the previously-mentioned tendency to over-estimate the amount of flow along the outside wall during the transient is seen again. Near the center of the vortex on the downflow side, predicted downflow ($\overline{U}$) decreases more rapidly than the data, and predicted crossflow ($\overline{V}$) towards the wall decreases less rapidly than the data. The net result of these two effects is a tendency to show more than the measured amount of fluid along the outside of the vortex, which trend continues and grows as the transient proceeds. Calculated upflow along the outside of the chimney is also seen to decrease less rapidly during the transient than the data, which corresponds again to the notion of predicting more than measured flow at the outside of the vortex.

These subtle departures from the data of the behavior of the
calculated mean velocities is likely due to the transient Reynolds
Stress differences mapped in Fig. 5.17. Though the experimental errors
are largest for the Reynolds Stress measurements, a definite pattern of
the prediction decreasing in-time less rapidly than the data is developed
at most locations in the vortex center and near the cell exit. Differ-
ences in the transient behavior of the mean flow occurring in the vortex
center are more difficult to detect because of the poor statistics of the
data when average magnitudes are near zero. However, when the velocity
field is distorted at such points, the effect is transmitted throughout
the cell and observed more easily in the regions where average velocities
are higher.

Anomalies in the K-versus-time comparison are generally distributed
around the outside of the region of Reynold Stress discrepancy. An area
of strong disagremeent is observed in the downflow region just inside
the vertical wall. Here the predicted K shows a more rapid than measured
rate of decrease in time that grows during the transient. Since this region
receives fluid from that part of the cell where three-dimensional effects
have been observed, it is possible that this discrepancy is caused by
these effects.

5.3 Transient Effects

The above comparison of data and calculation shows that the
transient measurements are generally well-predicted after the initial
steady-state differences are normalized out. In most cases, the
calculated curves follow the data exactly. However, at a number of

locations (shaded areas in Figs. 5.14 - 5.17) small but measureable differences in the transient behavior of specific turbulence quantities are observed. Such small differences become even less significant when the initial normalization factors applied to the data and calculation are compared. The normalization factors account for the difference between the measured and calculated steady-state values of each quantity and differ in some cases by as much as an order of magnitude, and with more frequency, by factors of two to five. With disparities of this order between data and the turbulence model prediction for steady-state conditions, the 10 - 20 percent difference in the transient comparisons, as is observed in the cases of worst agreement, cannot be reliably ascribed to transient effects alone.

An additional reason to suspect that the differences seen between data and calculation in the plots of Appendix F do not indicate a strong transient effect is their spatial irregularity. If the model closure assumptions are deficient in the presence of a momentum transient, then one would expect this deficiency to be expressed throughout the entire flow area, albeit to varying degrees. The fact that most of the calculated quantities are seen to follow the data closely during the transient suggests that such a general transient effect is absent. Further, it is shown in the steady-state parametric analysis (Sec. 5.1.3) that small variations in the turbulence model free parameters have a significant effect on the entire turbulence field; this also suggests that a significant transient effect associated with the turbulence model closure would be more pervasive than is observed in this experiment.

Chapter 1 questions the use of turbulence models, developed from steady-state closure assumption and tested in essentially steady

experiments, in the analysis of transient flows. From the above discussion, for the flow speeds, geometry, and transient rate used in this experiment, it is concluded that the steady-state closure is adequate under the influence of a momentum transient.

5.3.1 Characteristic Time Estimates

The question of the applicability of the above result to flow transients with a shutdown rate different from that used in this experiment, in particular faster rates, can be addressed with a time-scale analysis. This exercise also provides some physical insight to the time-scale over which each term in the turbulence model acts. The technique is illustrated for the turbulent kinetic energy transport equation (Eq. 4.8) which is shown to be shared by both the K-σ and K-ϵ models in Sec. 4.3.1.1.

For example, to estimate the characteristic time for diffusion of K, select the diffusion term in Eq. 4.8 and let

$$\frac{\partial K}{\partial t} \cong \Gamma\sigma \frac{\partial^2 K}{\partial X^2} \quad , \tag{5.4}$$

where σ is assumed approximately constant. Assume an exponential form for K(t),

$$K(t) \cong K_0 \exp [t/\tau_D], \tag{5.5}$$

where $\tau_D \equiv$ characteristic time for diffusion; then approximate

$$\frac{\partial}{\partial X} \sim \frac{1}{L_c} \quad , \tag{5.6}$$

where L_c = characteristic length $\cong$ 1 ft. for this experiment. Substituting Eqs 5.6 and 5.5 into Eq. 5.4 gives

$$\tau_D \cong \frac{L_c^2}{\Gamma\sigma} \quad .$$

A similar procedure can be applied to each term in Eq. 4.8 to produce the characteristic times for advection (τ_A), production (τ_p), and dissipation (τ_ϵ). With the additional approximations (based on the experimental design and a typical VARR-II run)

$$U_c \cong 2 \text{ ft/sec} \quad ,$$

$$\sigma \cong 10^{-3} \frac{\text{ft}^2}{\text{sec}} \quad ,$$

$$\frac{K}{\sigma} \cong 10 \quad ,$$

Table 5.4, showing the form and estimated value for each of the character-istic times discussed above, can be produced. Roughly speaking, 2.3 characteristic times must pass before the specific term of interest can change by an order of magnitude; therefore, the τ's are a measure of relative response time.

It is seen from Table 5.4 that all terms, with the exception of diffusion, are much faster than the characteristic time of the imposed momentum transient, τ_T, which is on the order of 100 seconds. The diffusion time, τ_D, is of the same order as τ_T; however, the magnitude of the diffusion term itself is generally small in comparison to production and diffusion (Sec. 5.1.3.5). As a result, three of the four terms in the

K-equation are faster, by at least an order of magnitude, than the characteristic time of the transient, and if the model closure assumptions are valid, can be expected to readily follow a transient of the order imposed in this experiment. The slower fourth is relatively small in magnitude, so if the assumed form and turbulence model constant in the diffusion term are not valid in the transient, the effect is not readily detected.

From this analysis, one can estimate the fastest transient rates for which the findings of this chapter are applicable. For flows where diffusion is not important, transient rates slower by an order of magnitude than the longest of τ_A, τ_p, or τ_ε should produce equivalent results.

It would be interesting to stress the turbulence model by examining transient effects in a time-scale regime on the order of 1 to 5 seconds. Unfortunately, the experimental hardware required for such an investigation (primarily the fast A-to-D and a much larger data storage and analysis capability) is beyond the financial scope of this effort. However, numerical experiments regarding this phenomena are feasible and included in the recommendations.

.823

$\dfrac{m}{sec.}$

Fig. 5.1 MEASURED MEAN VELOCITY FIELD; STEADY-STATE,
FULL-FLOW CONDITIONS

K-ε
K-σ $\times 10^{-3}(\frac{m}{sec})^2$
DATA

I (vertical axis): 22, 20, 18, 16, 14, 12, 10, 8, 6, 5, 4

J (horizontal axis): 16, 14, 12, 10, 8, 6, 4, 3, 2

Row I = 22:
J=16	J=14	J=12	J=10	J=8	J=6	J=4	J=2
18	8.3	7.3	8.1	9.3	9.7	8.1	6.5
4.5	2.3	2.2	2.6	3.1	3.3	2.5	2.1
•	+	•	+	•	+	•	+
2.9	5.6	7.8	4.9	4.7	1.2	.44	.30

Row I = 20:
J=16	J=14	J=12	J=10	J=8	J=6	J=4	J=2
16	8.3	8.5	11	13	14	9.8	6.8
4.0	2.4	2.8	3.9	5.1	5.5	3.1	2.3
+	•	+	•	+	•	+	•
3.0	9.3	11.2	3.1	2.8	6.6	.50	.26

Row I = 18:
J=16	J=14	J=12	J=10	J=8	J=6	J=4	J=2
15	8.4	9.7	13	17	20	12	7.9
3.6	2.5	3.4	5.2	7.3	8.0	4.2	2.8
•	+	•	+	•	+	•	+
5.0	10.1	.9.0	1.5	1.5	6.4	1.1	.27

Row I = 16:
J=16	J=14	J=12	J=10	J=8	J=6	J=4	J=2
14	8.8	11	16	21	26	15	9.6
3.3	2.8	4.4	6.9	9.5	12	5.6	3.6
+	•	+	•	+	•	•	+
4.6	9.5	7.4	1.4	1.4	3.5	1.5	.31

Row I = 14:
J=16	J=14	J=12	J=10	J=8	J=6	J=4	J=2
13	9.8	14	19	23	30	18	12
3.1	3.2	6.2	9.4	12	15	7.2	5.1
+	•	+	•	+	•	+	•
5.2	8.8	6.0	1.3	1.6	2.5	1.6	.31

Row I = 12:
J=16	J=14	J=12	J=10	J=8	J=6	J=4	J=2
13	12	15	23	26	32	21	16
3.1	4.1	8.7	12	13	17	9.5	7.9
+	+	•	+	•	+	•	+
5.4	8.0	6.5	1.9	2.3	2.5	1.7	.36

Row I = 10:
J=16	J=14	J=12	J=10	J=8	J=6	J=4	J=2
13	15	23	27	28	35	26	24
3.2	6.0	12	14	15	20	14	14
•	+	•	•	+	•	+	+
5.0	7.5	5.0	2.6	3.0	2.9	1.7	.38

Row I = 8:
J=16	J=14	J=12	J=10	J=8	J=6	J=4	J=3	J=2
18	25	31	31	30	37	56	63	61
6.9	12	17	17	18	23	56	63	61
+	•	+	+	•	+	+	+	+
5.6	8.3	5.2	4.1	4.0	3.4	2.3	.67	.43

Row I = 6:
J=16	J=14	J=12	J=10	J=8	J=6
103	52	40	34	32	37
104	40	27	22	21	24
•+	•	+	•	+	•
9.4	9.2	7.2	5.7	4.3	3.0

Row I = 5:
J=16	J=14	J=12	J=10	J=8	J=6	J=4
+	•	+	•	+	•	+

Fig. 5.2 COMPARED TURBULENT KINETIC ENERGY FIELD;

STEADY-STATE, FULL-FLOW CONDITIONS

|	16	14	12	10	8	6	4	3	2	
-.65	-0.12	+0.14	+0.21	-0.02	-0.52	-0.42		+0.06		
-.31	-0.04	+0.06	+0.09	-0.18	-0.26	-0.15		+0.05		22
+.38	+0.39	-0.0	-0.0	-0.72	+0.09	+0.03		+0.01		
-1.16	-.715	-0.45	-0.30	-0.63	-1.59	-0.92		+0.08		
-.49	-0.29	-0.20	-0.09	-0.26	-0.85	-0.34		+0.06		20
0.0	-0.37	+0.10	-0.22	-0.43	-2.54	+.015		+0.02		
-1.61	-1.52	-1.61	-1.59	-1.91	-3.48	-1.63		+0.08		
-0.66	-0.67	-0.86	-0.88	-0.99	-2.12	-0.66		+0.06		18
-.735	-0.41	-1.41	-0.33	-0.18	-2.78	-0.18		+.002		
-2.02	-2.50	-3.33	-3.70	-3.81	-5.85	-2.40		+0.08		
-0.82	-1.16	-2.04	-2.53	-2.40	-3.91	-1.07		+0.06		16
-1.07	-1.38	-1.95	-0.27	-0.12	-0.95	-0.41		+.003		
-2.41	-3.66	-5.53	-6.12	-5.62	-7.73	-2.92		+0.08		
-0.97	-1.74	-3.60	-4.38	-3.78	-5.31	-1.42		+0.06		14
-1.50	-1.92	-1.79	-0.29	-.164	-0.49	-0.46		0.00		
-2.91	-5.24	-8.11	-8.09	-6.72	-8.52	-3.04		+0.08		
-1.14	-2.52	-5.28	-5.58	-4.52	-5.83	-1.65		+0.06		12
-1.63	-2.52	-1.92	-0.35	-0.26	-0.32	-0.49		+0.02		
-4.10	-8.08	-10.9	-9.20	-6.78	-8.16	-2.94		+0.08		
-1.50	-3.89	-6.96	-6.18	-4.62	-5.69	-1.87		+0.06		10
-1.68	-3.21	-1.57	-0.42	-0.25	-0.50	-0.49		+0.05		
-10.1	-14.5	-13.1	-8.77	-5.99	-6.94					
-4.78	-7.99	-8.72	-6.12	-4.29	-5.14					8
-2.62	-3.66	-1.24	-0.67	-0.42	-.816	-.62	.10	.06		
-36.0	-15.9	-9.39	-5.35	-4.44	-5.75					
-41.0	-1.45	-7.78	-4.18	-4.04	-4.54					6
-4.77	-4.72	-2.64	-0.87	-0.56	-0.57	-0.66				5

K-ε
K-σ   (Kg/M-sec^2)
DATA

↑ I

← J

Fig. 5.3   COMPARED REYNOLDS STRESS FIELD; STEADY-STATE,
FULL-FLOW CONDITIONS

Fig. 5.4 CALCULATED MEAN VELOCITY FIELD; STEADY-STATE,
FULL-FLOW CONDITIONS; K-σ TURBULENCE MODEL;
16x24 MESH

Fig. 5.5 CALCULATED MEAN VELOCITY FIELD; STEADY-STATE,
FULL-FLOW CONDITIONS; K-ε TURBULENCE MODEL;
16x24 MESH

$32.4 \times 10^{-3} \left(\frac{m}{sec}\right)^2$

K-ϵ

CALCULATION

$17 \times 10^{-3} \left(\frac{m}{sec}\right)^2$

K-σ

CALCULATION

$11.2 \times 10^{-3} \left(\frac{m}{sec}\right)^2$

EXPERIMENT

I = 20

I = 16

I = 12

Fig. 5.6

TURBULENT KINETIC ENERGY
SPATIAL DISTRIBUTION AT
THREE REPRESENTATIVE
VERTICAL POSITIONS
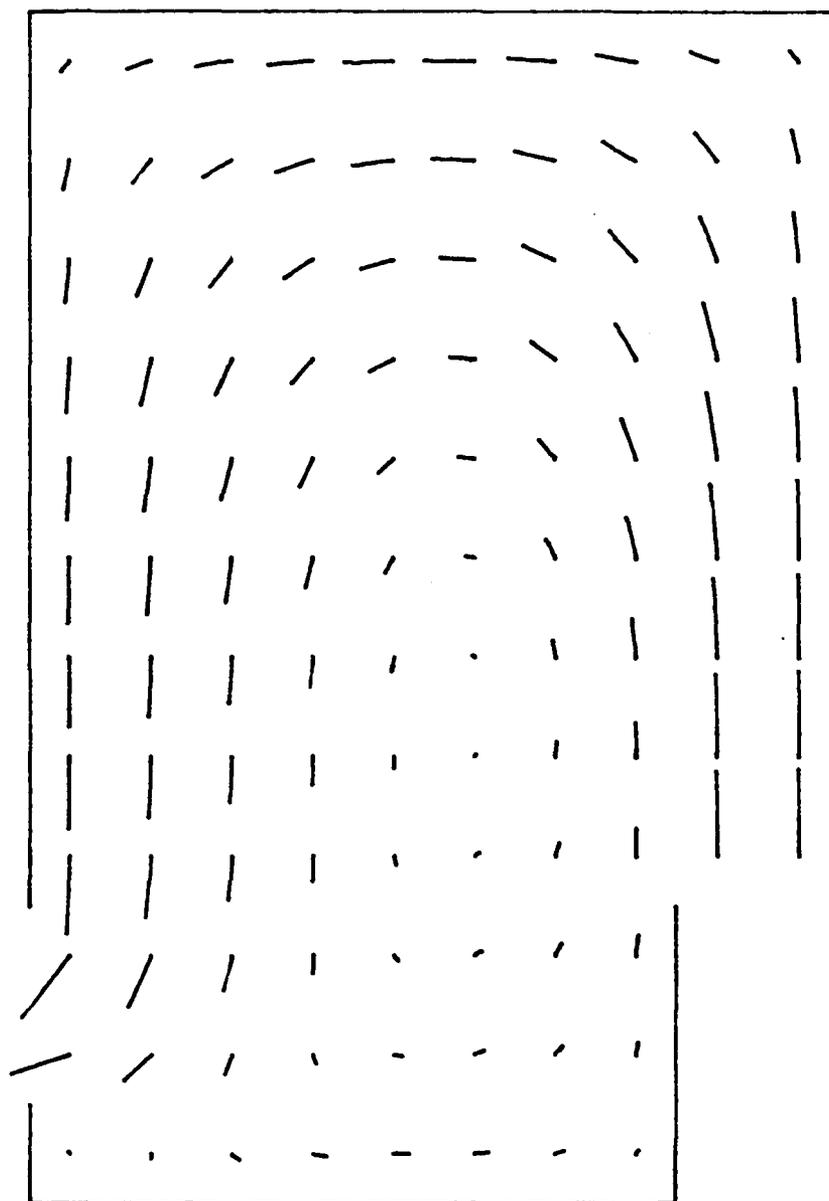
Fig. 5.7 CALCULATED MEAN VELOCITY FIELD; STEADY-STATE
FULL-FLOW CONDITIONS; K-σ TURBULENCE MODEL;
10x12 MESH
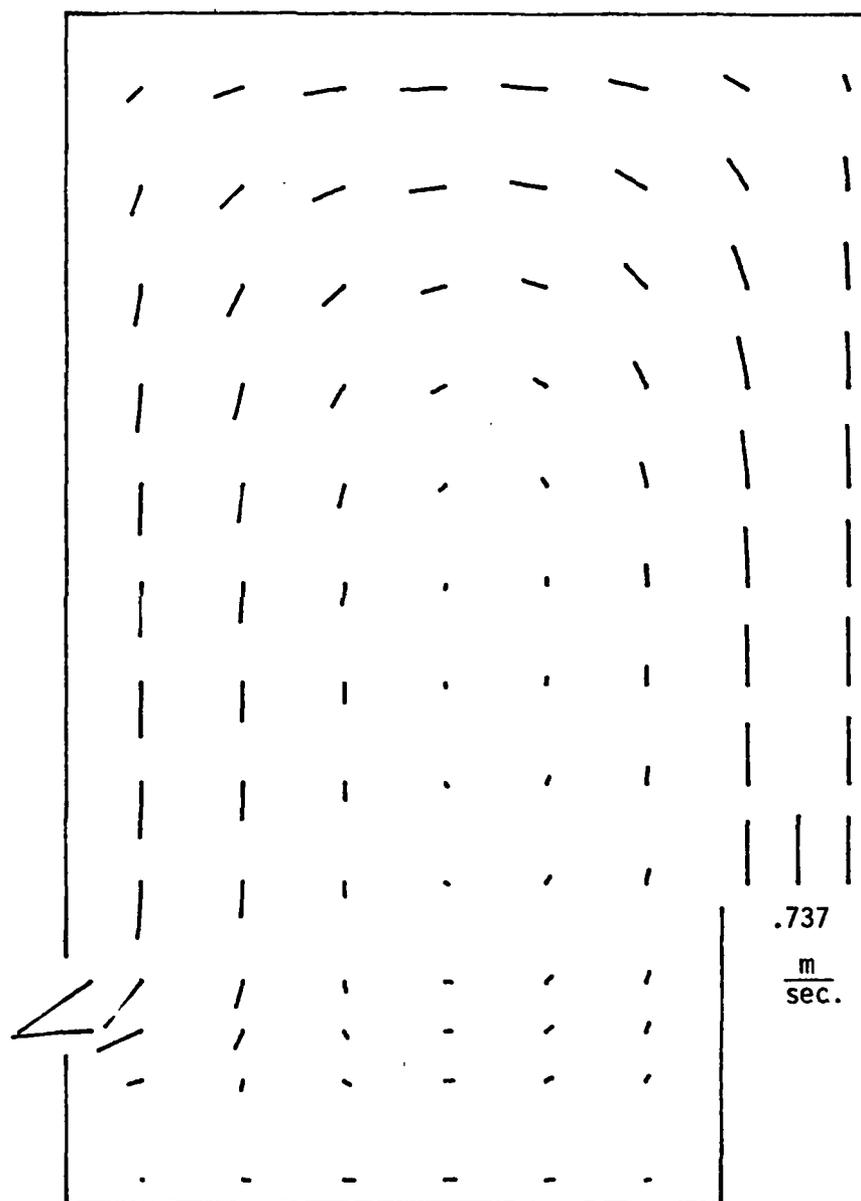
Fig. 5.8 CALCULATED MEAN VELOCITY FIELD

Time = 40 sec.

.737

$\frac{m}{sec.}$
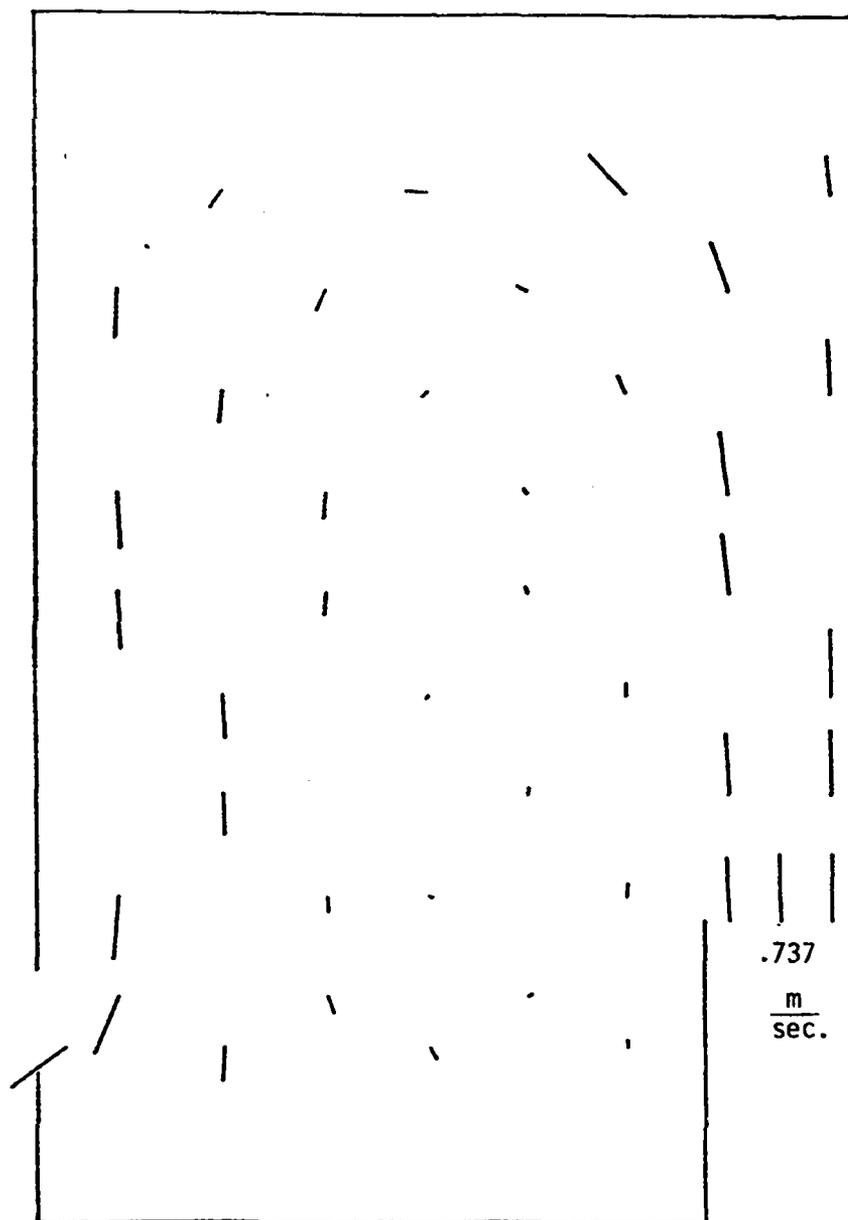
Fig. 5.9 MEASURED MEAN VELOCITY FIELD

Time = 40 sec.
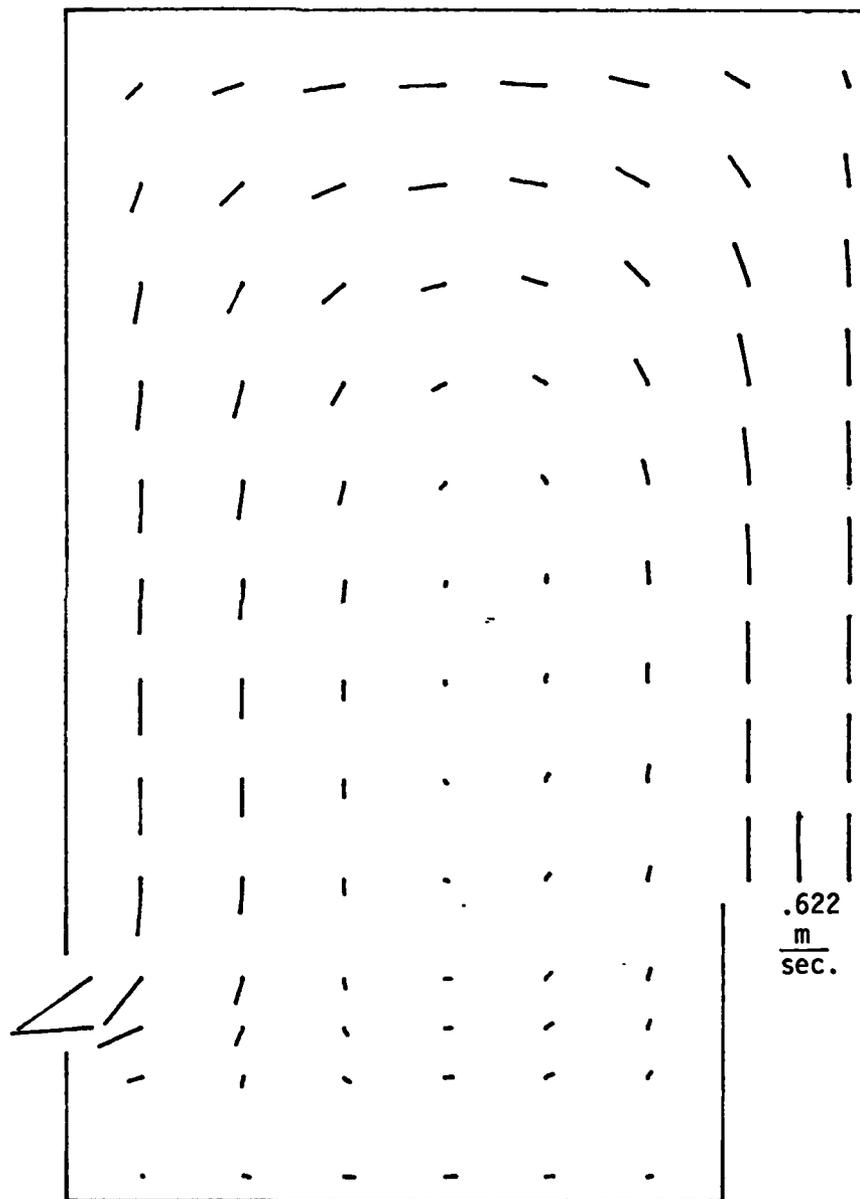
Fig. 5.10   CALCULATED MEAN VELOCITY FIELD

Time = 60 sec.

.622
m
sec.
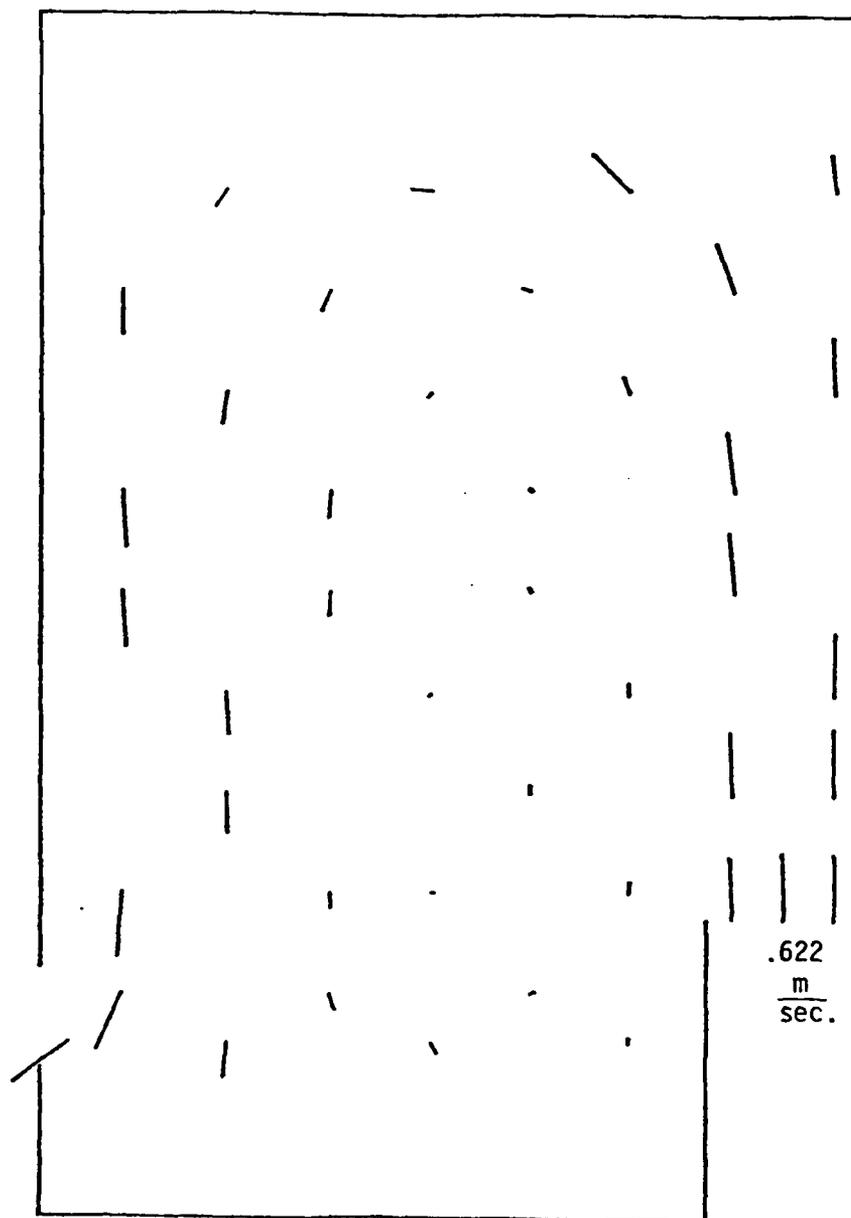
Fig. 5.11 MEASURED MEAN VELOCITY FIELD

Time = 60 sec.
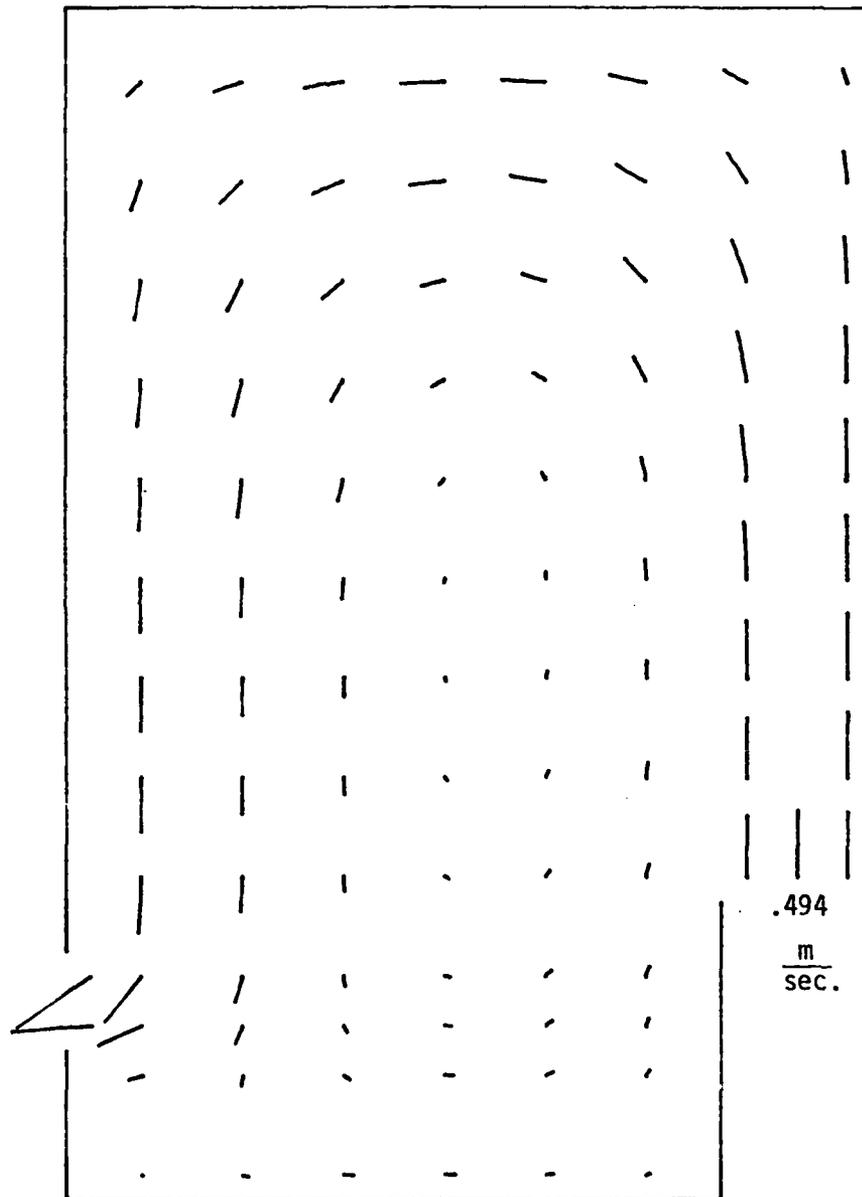
Fig. 5.12 CALCULATED MEAN VELOCITY FIELD

Time = 80 sec.

.494

$\dfrac{m}{sec.}$
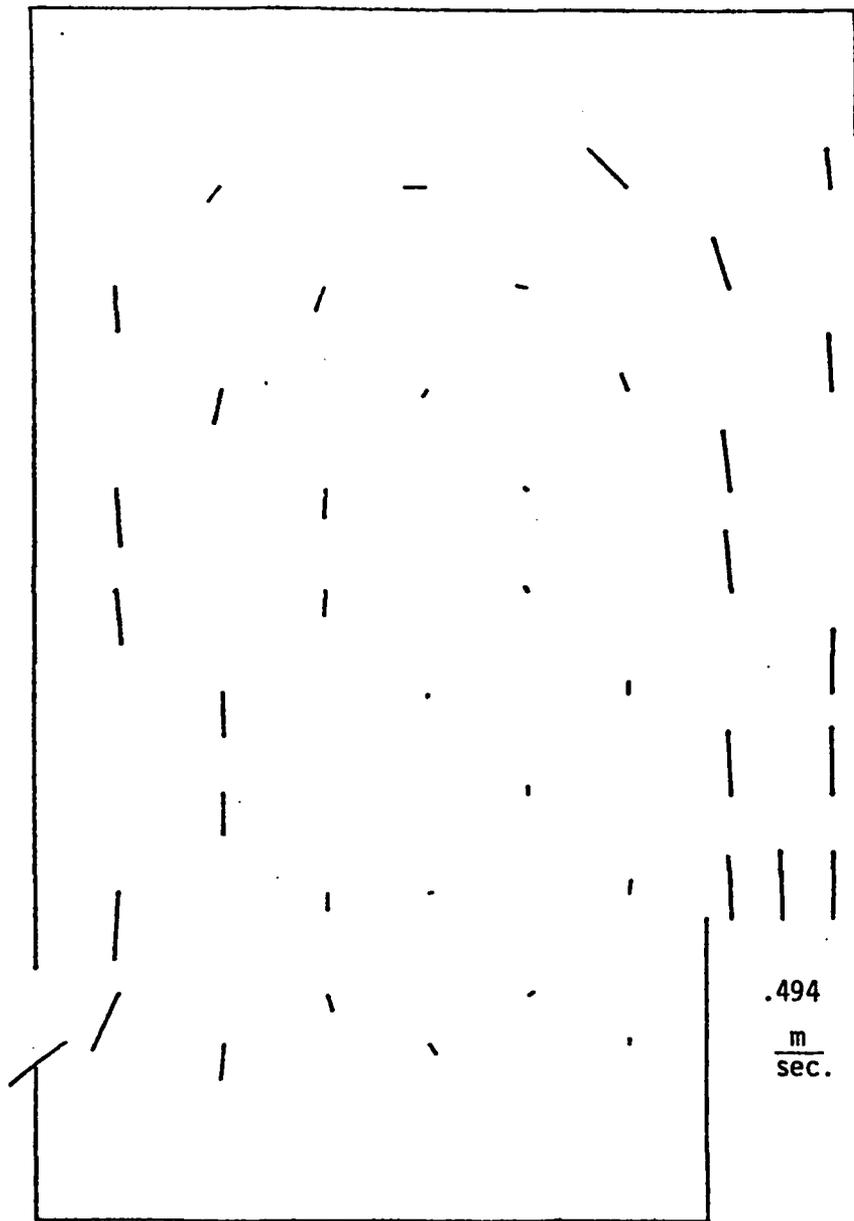
Fig. 513   MEASURED MEAN VELOCITY FIELD

Time = 80 sec.
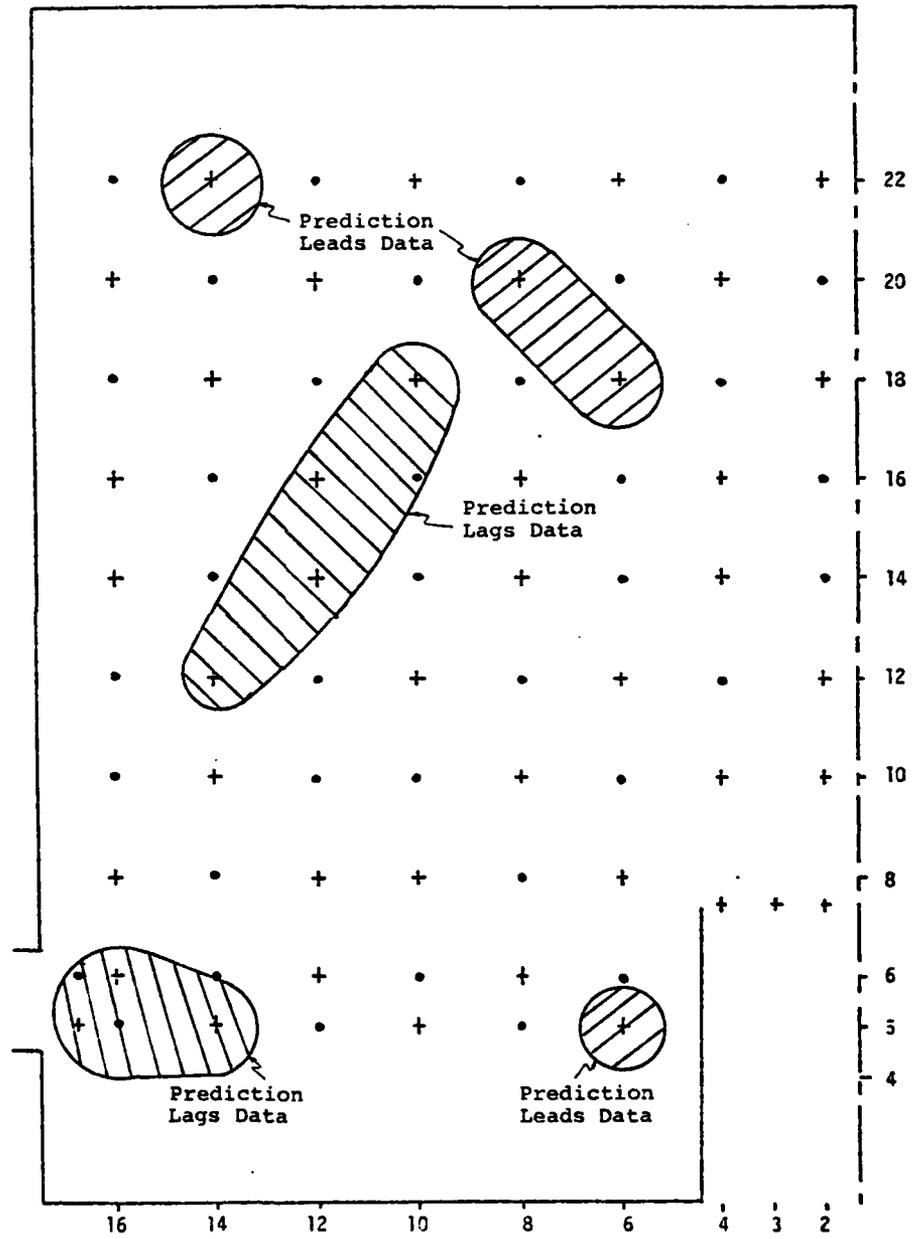
Fig. 5.14   TRANSIENT LEAD/LAG DISTRIBUTION FOR $\overline{U}$
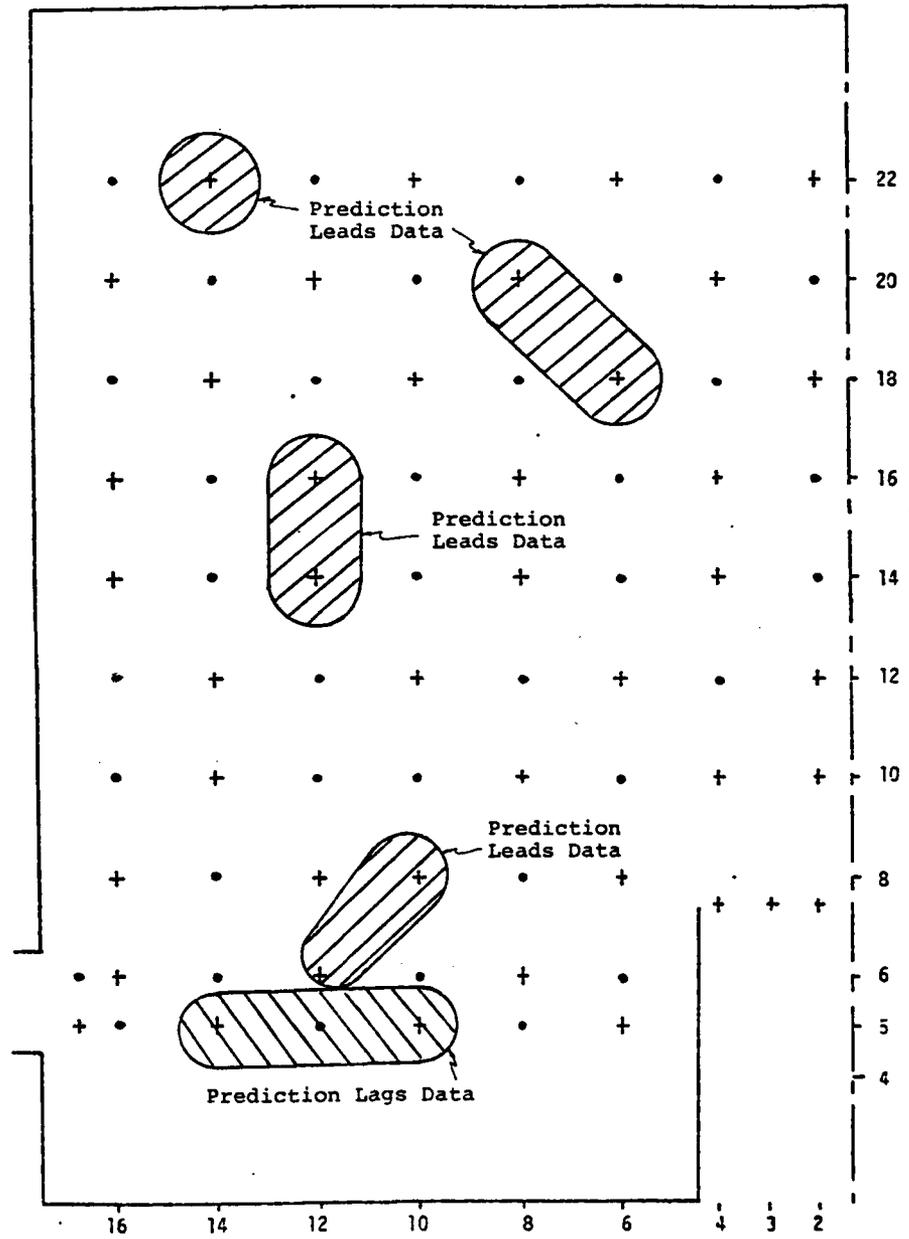
Fig. 5.15 TRANSIENT LEAD/LAG DISTRIBUTION FOR $\overline{V}$
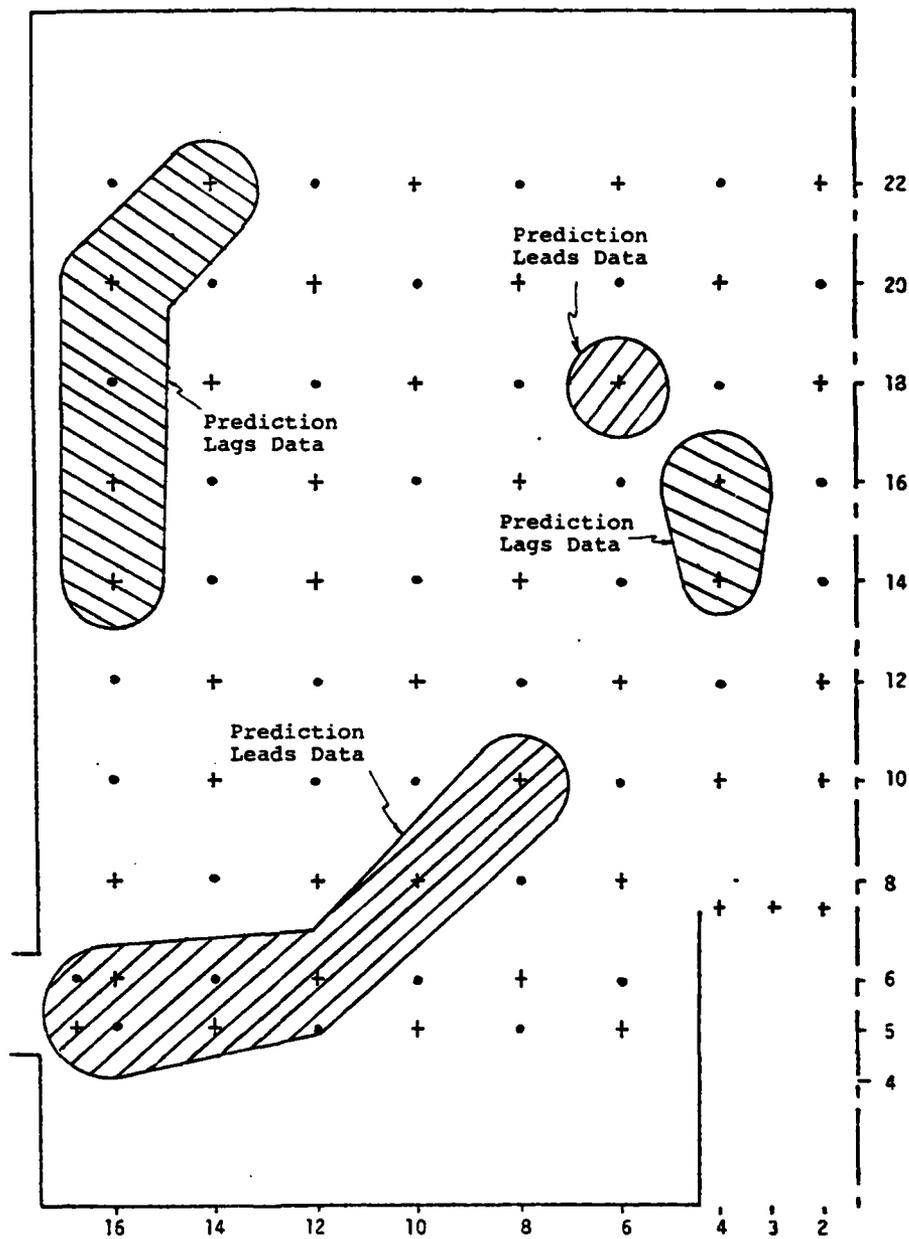
Fig. 5.16   TRANSIENT LEAD/LAG DISTRIBUTION FOR K
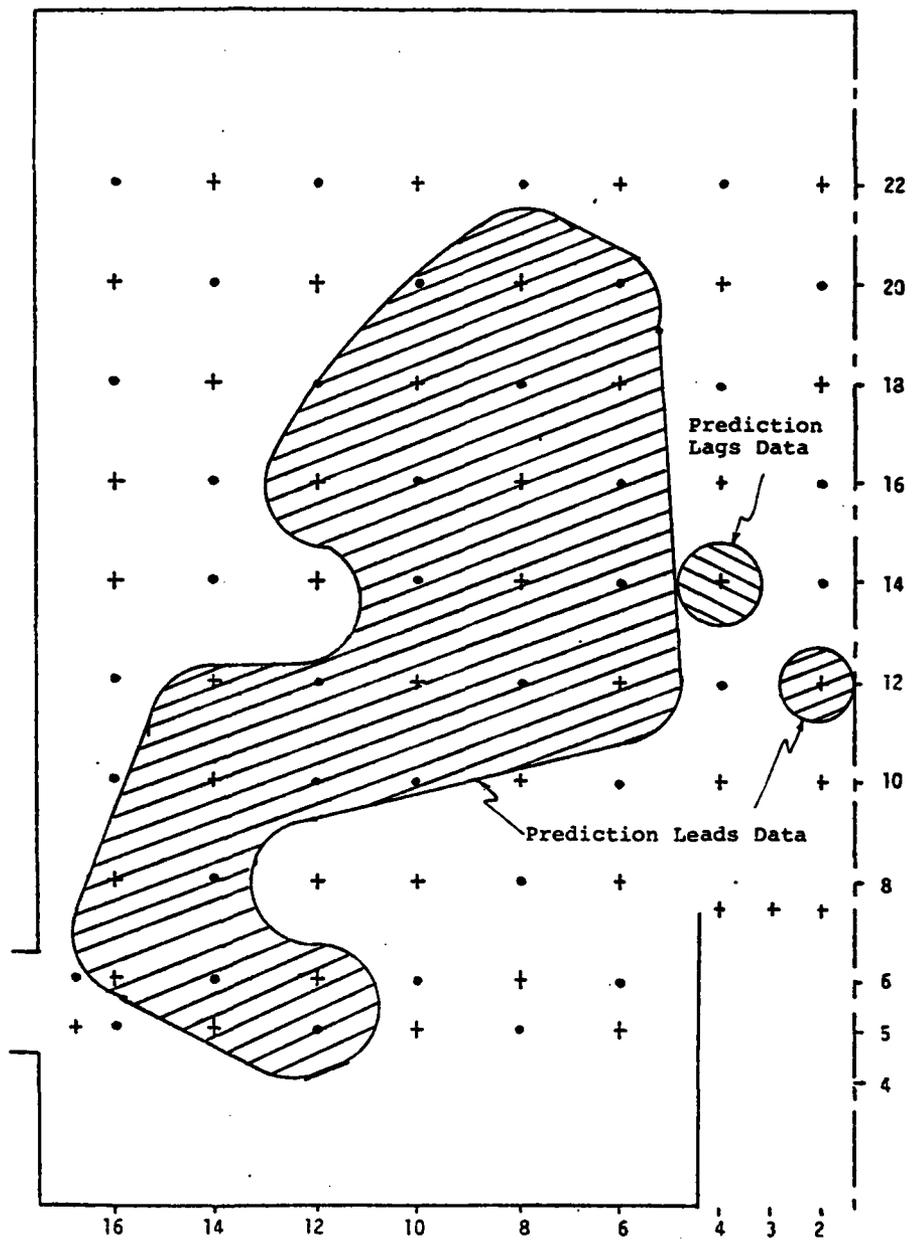
Fig. 5.17 TRANSIENT LEAD/LAG DISTRIBUTION FOR REYNOLDS STRESS

Table 5.1 Values Used in Parametric Analysis

Name/Symbol	Values Tested
Donor Cell Coeficient $\alpha_x = \alpha_z$	1 (full donor cell), .9, .5, .1
Boundary Conditions FSLIP	Free-Slip (FSLIP = 1); No Slip (FSLIP = -1); Partial-Slip (FSLIP = .8, .7, .6, .5, .1)
Inlet Turbulence Levels $K_{in.}, \sigma_{in.}$	Set by Code; Matched to Experiment
Turbulence Free Parameters	
α	.060, .055, .050, .0475, .045*, .040, .035, .030, .020
Γ	5.0, 4.5, 4.0, 3.0, 1.5*, .75, .30, .20
α_o	.06, .0225, .020, .0175, .015, .013, .01238, .012, .01125*, .01012, .009, .00563
Γ_1	2.25, 1.5, .75*, .375, .15, .10

*Values Recommended by Author

Table 5.2 Unmatched Inlet Conditions - Parametric Analysis

10x12 Coarse Mesh
K-σ Model
Inlet K and σ: Not Matched to Experiment

Qualitative Results

TEST CASE No.	α	Γ	α_o	Γ_1	Decay Rate of K in Inlet Jet	Relative Mag. of K at Peak on Upflow Side of Vortex	Convection of K to Downflow Side of Vortex	Comment
Standard	.045	1.5	.01125	.75	baseline	baseline	baseline	--
1	.045	1.5	.00563	.75	worse	worse	slightly better	--
2	.045	1.5	.0225	.75	worse	worse	worse	--
3	.045	.2	.01125	.1	worse	worse	worse	--
4	.045	4	.01125	.75	--	--	same	unstable
5	.045	1.5	.01125	1.5	slightly worse	worse	worse	--
6	.045	3	.01125	1.5	same	better	same	--
7	.045	.75	.01125	.375	worse	worse	worse	Vel. field worse
8	.035	1.5	.01125	.75	slightly better	slightly better	much worse	--
9	.030	1.5	.01125	.75	better	better	slightly better	--
10	.060	1.5	.01125	.75	worse	worse	slightly better	--
11	.050	1.5	.012	.75	slightly worse	slightly worse	slightly better	--
12	.055	1.5	.013	.75	worse	worse	slightly better	--
13	.060	1.5	.015	.75	worse	slightly better	same	--

Table 5.3

Percent Inlet Flow vs. Time

TIME (sec.)	INLET VELOCITY (% of Initial Full-Flow Value)
10	99.4
20	97.6
30	94.3
40	89.5
50	83.1
60	75.6
70	67.7
80	60.0
90	53.2
100	47.1
110	41.8
120	38.1
130	35.6
140	34.7

Table 5.4 Results of Time Scale Analysis

Term:	Advection	Production	Diffusion	Dissipation
Characteristic Time (τ)	$\dfrac{L_c}{U_c}$	$20 \left(\dfrac{L_c}{U_c}\right)^2$	$\dfrac{L_c^2}{\Gamma \sigma}$	$\dfrac{\sigma}{4\,\alpha\,K}$
Order of Magnitude for This Experiment	.5 sec.	5 sec.	670 sec.	.5 sec.

CHAPTER VI

CONCLUSIONS AND RECOMMENDATIONS

6.1 Conclusions

Measurements have been made in an improved experimental apparatus of the mean turbulence field parameters in a recirculating flow under steady-state and transient flow conditions. In Chapter 3 a unique transient measurement technique is developed, and the errors associated with its use are quantified and found to be a function of the transient rate and shape.

In Chapter 4, a two-equation K-ϵ turbulence model is converted to K-σ form for use in the VARR-II fluid dynamics code, and it is found that the two models are nearly identical in mathematical structure. Both models predict well the qualitative and quantitative mean velocity fields under steady-state and transient flow conditions. The K-σ model is found to predict correctly the general magnitudes of the scalar turbulence quantities, K and Reynolds Stress, while these quantities are consistently overestimated by the K-ϵ model. With respect to the spatial distribution of these scalars, both models fail to predict the measured build-up of K above the chimney and on the downflow side of the vortex. Since a local balance of production and dissipation are found to dominate in the K-transport equation, attempts were made to correct the predicted spatial distribution by changing the turbulence model free parameters, in particular, the parameter associated with the dissipation term. The fact that this effort was unsuccessful suggests that the fundamental form of the K-dissipation term needs to be revised

before improvements to the steady-state predictions can be made.

The values of the scalar turbulence quantities at the inlet to the plenum are shown to influence strongly the numerical predictions. Matching the calculation values to the experimental measurements at the inlet produces a poorer overall prediction, which is thought to result from errors in the numerical simulation that are amplified by the large spatial gradients arising in the matched inlet case.

Comparison of transient data and calculation show some small differences in time-behavior that are generally less than 10-20 percent at points of worst agreement. However, these differences are not thought to be attributable solely to transient effects on the turbulence model. Transient effects which occur in the computation as a result of deficient model closure assumptions are expected to manifest themselves, to first order, through the turbulence model constants. The fact that minor adjustments to the turbulence model constants are shown to produce significant variations in computed results suggests that transient effects should produce a noticeable perturbation throughout the solution space; no such effect is seen. More importantly, the failure of the turbulence model to predict accurately the magnitudes of the measured steady-state turbulence scalars results in start-of-transient normalization factors that vary widely throughout the plenum. These normalization factors are likely to be functions of inlet flow rate, as well as position, and therefore can cause differences in the comparison of transient data with calculation that are not true transient effects. Finally, the spatial intermittency of transient discrepancies observed between data and calculation is evidence that the pervasive effects one would expect to be caused by the turbulence

model's failure to handle transients are not present. Therefore, the data indicate that the model's ability to follow a momentum transient of the order used in the experiment is essentially verified, and that improvements of the model's steady-state predictions are required before more comprehensive assessments can be made.

The time-scale analysis in Chapter 5 indicates that the conclusions arrived at regarding transient effects in this experiment can be applied to other transients when the characteristic-times of the new situation meet the criteria of Sec. 5.3.1.

6.2 Recommendations

Two-equation turbulence models are thought to be the simplest type that can successfully predict recirculating flows. Although this experiment shows that some important features of the data, such as the mean velocity fields, are correctly modelled, and that the general magnitudes of the scalar quantities are well-predicted in many cases, it is clear from the analysis of Sec. 5.1 that further effort is required to improve the steady-state predictions of recirculating turbulent flow. The results of the numerical analysis accomplished to date suggest future work as follows: (1) Examine and test alternative forms for the K-dissipation term. The features of the K-distribution that are not predicted well by the current model, and that should be used as a guide in the development of the revised dissipation term, are discussed in detail in Sec. 5.1.2.2. (2) Use a three-dimensional code, ideally with the same turbulence model used here, to account for possible effects from the top part of the cell. (3) Obtain through numerical experiments a better understanding of the problems

experienced in trying to match the inlet turbulence quantities
to the experimental data. Use of a finer mesh to improve the numerical
simulation of the steep gradients that occur in the matched inlet
case is recommended as a first step.

The time-scale analysis showed that faster transients (with
characteristic times on the order of 1-5 seconds), would present a
more severe test of the model closure assumptions. A fluid-flow
experiment similar to the one conducted here but with the faster
coastdown rate would be extremely expensive; however, numerical
experiments examining this aspect of the problem would be worthwhile.

The observed sensitivity of the computational predictions to
small changes in the turbulence model constants is somewhat surprising.
The model constants are generally established in an approximate fashion
from many data sources, and one would not expect the precision
requirements of such constants to be high. It is possible that the
observed sensitivity is problem-dependent, and it would be useful to
know if the same behavior is seen on problems of larger scale. Of
further interest along the same lines, the sensitivity to changes
in the model free parameters of quantities that are of primary
interest to designers (e.g. temperature and mean velocities) should
also be investigated.

REFERENCES

1. Andreychek, T. S., Woods, M. D., "Test Evaluation Report on the CRBRP Outlet Plenum Flow Stratification Study," WARD-D-0125, Vol. 1, 1976, pp. 1-3.

2. Chen, Y. B., Golay, M. W., "Coolant Mixing in the LMFBR Outlet Plenum," ERDA Report, COO-2245-44TR, 1977.

3. Manno, V. P., Golay, M. W., "Measurement of Heat and Momentum Eddy Diffusivities in Recirculating LMFBR Outlet Plenum Flows," ERDA Report, COO-2245-61TR, 1978.

4. Chen, Y. B., Golay, M. W., pp. 43-46.

5. Hirt, C. W., "Computer Studies of Time-Dependent Turbulent Flows," The Physics of Fluids, Supplement II, 1969, p. 220.

6. Hinze, J. O., Turbulence, 2nd ed., McGraw-Hill, New York, 1975, pp. 15-21, p. 197.

7. Reynolds, W. C., "Computation of Turbulent Flows," Annual Review of Fluid Mechanics, Vol. 8, 1976, p. 184.

8. Launder, B. E., Spalding, D. B., Mathematical Models of Turbulence, Academic Press, New York, 1972.

9. Stuhmiller, J. H., "Development and Validation of a Two-Variable Turbulence Model," SAI-74-509-LJ, 1974.

10. Notes on "Turbulent Recirculating Flow-Prediction and Measurement," College of Engineering, The Pennsylvania State University, July 28 - August 1, 1975.

11. Bradshaw, P., Turbulence - Topics in Applied Physics, Vol. 12, 2nd ed., Springer-Verlag, New York, 1978, p. 24.

12. Ibid., p. 27.

13. Reynolds, W. C., Cebeci, T., "Calculation of Turbulent Flows," Topics in Applied Physics, Vol. 12, 2nd Ed., Springer-Verlag, New York, 1978, p. 198.

14. Howard, P. A., Carbajo, J. J., "Experimental Study of SCRAM Transients in Generalized Liquid-Metal Fast Breeder Reactor Outlet Plenums," Nuclear Technology, Vol. 44, July 1979, p. 210.

15. Lorenz, J. J., "MIX, A Computer Code for Transient Thermal Hydraulic Analysis of LMFBR Outlet Plenums," ANL-CT-75-41, May 1975.

16. Howard, P. A., "PLENUM-3: A Lumped Parameter LMFBR Outlet Plenum Mixing Code," ANL-CT-76-32, March 1976.

17. Carbajo, J. J., Howard, P. A., "Experimental and Analytical Study of Transients in LMFBR Outlet Plenums," ANS Transactions, Vol. 28, 1978 (Supplement), p. 434.

18. Markatos, N. C. G., "Transient Flow and Heat Transfer of Liquid Sodium Coolant in the Outlet Plenum of a Fast Nuclear Reactor," Int. J. Heat Mass Transfer, Vol. 21, 1978, pp. 1565-1579.

19. Chen, Y. B., Golay, M. W., p. 22.

20. Ibid., pp. 106-121.

21. Yeh, Y., H. Cummins, "Localized Fluid Flow Measurement with a He-Ne Laser Spectrometer," Appl. Phys. Letters, 4, 176, 1964.

22. Melling, Adrian, "Investigation of Flow in Non-Circular Ducts and Other Configurations by Laser Doppler Anemometry," Ph.D. Thesis, University of London, 1975.

23. Durst, F., Melling, A., Whitelaw, J. H., Principles and Practice of Laser Doppler Anemometry, Academic Press, 1976.

24. Watrasiewicz, B. M., Rudd, M. J., Laser Doppler Measurements, Butterworths & Co., 1976.

25. Chen, Y. B., Golay, M. W., pp. 106-121.

26. Chen, Y. B., Golay, M. W., pp. 23-24.

27. Adrian, R. J., Fingerson, L. M., "Laser Anemometry - Theory, Application, and Techniques," Course Notes, Thermo-Systems Inc., 1978, p. 18/22.

28. Durst, F., Melling, A., Whitelaw, J. H., pp. 272-285.

29. Ibid., p. 3.

30. Watrasiewicz, B. M., Rudd, M. J., p. 42.

31. Deighton, M. O., Sayle, E. A., "An Electronic Tracker for the Continuous Measurement of Doppler Frequency from a Laser Anemometer," DISA Information No. 12, November 1971.

32. Durst, F., Melling, A., Whitelaw, J. H., p. 218.

33. White, F. M., <u>Viscous Fluid Flow</u>, McGraw-Hill Book Company, New York, 1974, p. 454.

34. Murdoch, J. B., <u>Network Theory</u>, McGraw-Hill Book Company, New York, 1970, pp. 398-399.

35. DISA Instruction Manual for Type 55D35 RMS Voltmeter, DISA Electronik A/S. DK-2740 Skovlunde. Denmark, 1973, p. 5.

36. Rice, S. O., "Mathematical Analysis of Random Noise," in <u>Noise and Stochastic Processes</u>, Ed. Nelson Wax, Dover Publications, New York, 1954.

37. Stuhmiller, J. H.

38. Cook, J. L., Nakayama, P. I., "VARRII - A Computer Program for Calculating Time Dependent Turbulent Fluid Flows with Slight Density Variation," WARD-D-0106, 1975.

39. Chen, Y. B., Golay, M. W., Appendix B.

40. Amsden, A. A., Harlow, F. H., "The SMAC Method: A Numerical Technique for Calculating Incompressible Fluid Flows," Los Alamos Sci. Lab. Report LA-4370, May 1970.

41. Notes on "Turbulent Recirculating Flow-Prediction and Measurement."

42. Chen, Y. B., Golay, M. W., "Validation of Turbulence Models for LMFBR Outlet Plenum Flows," AIChE-ASME Heat Transfer Conference, August 15-17, 1977, 77-HT-34, p. 7.

43. Chen, Y. B., Golay, M. W., "Validation of Turbulence Models for LMFBR Outlet Plenum Flows."

44. Ibid.

45. Cook, J. L., Nakayama, P. I., p. 85.

46. Chen, Y. B., Golay, M. W., "Validation of Turbulence Models for LMFBR Outlet Plenum Flows."

47. Chen, Y. B., Golay, M. W., "Coolant Mixing in the LMFBR Outlet Plenum," pp. 122-124.

48. George, W. K., Lumley, J. L., "The Laser-Doppler Velocimeter and its Application to the Measurement of Turbulence," in <u>J. Fluid Mech.</u>, Vol. 60, part 2, 1973, pp. 321-362.

49. Melling, A. and Whitelaw, J. H., "Measurements in Turbulent Water and Two-Phase Flows by Laser Anemometry," <u>Proc. 3rd Symp. on "Turbulence in Fluids</u>," Univ. of Missouri-Rolla, 1973.

50. Chen, Y. B., Golay, M. W., "Coolant Mixing in the LMFBR Outlet Plenum," p. 125.

51. Wilson, E. B. Jr., <u>An Introduction to Scientific Research</u>, McGraw-Hill, New York, 1952.

APPENDIX A

DATA REDUCTION

Since the experiment is similar to that performed by Chen [47],
this appendix closely follows his format. Further, an error in his data
reduction method is noted and quantified in the first section.

1. Average Velocities, Mean Square Amplitudes, and Reynolds Stresses

The theory of Laser Doppler Anemometry shows that, with the reference
beam arrangement, the measured Doppler frequency is linearly related to
the fluid velocity by

$$U = \frac{f_D \lambda}{2\sin\theta} \quad , \tag{A.1}$$

where

U = the component of local flow velocity that is normal to
the bisector of the beam intersection angle, and lies
in the plane formed by the beams;

f_D = Doppler frequency (or shift);

λ = wavelength of laser;

θ = half-angle of the beam intersection.

Care must be taken to account properly for the index of refraction
(n) of the medium in which the measurements are made. The data of Chen
have been called into question in Sec. 3.1.3 because of suspected flow

asymmetry; here it is noted that additional discrepancies exist because of an apparent error involving the index of refraction of water. In Eq. A.1, λ and sin θ are quantities whose values depend on the index of refraction of the medium in which they are observed. Hence,

$$\lambda_{water} = \frac{\lambda_{air}}{\eta_{water}}$$

and

$$(\sin\theta)_{water} = \frac{(\sin\theta)_{air}}{\eta_{water}} \quad . \qquad (A.2)$$

Eqs. A.1 and A.2 taken together show that the index of refraction effects cancel and need not be considered. Chen corrected the angle θ for the index of refraction of water, but did not correct λ; thereby biasing his reported velocities by a factor of 1.33, the index of refraction of water.

In the present experiment,

$$\lambda = 5145 \times 10^{-10} \text{ meters in air;}$$

$$\theta_{vert.} = 5.69° \text{ in air;}$$

$$\theta_{Horiz.} = 5.58° \text{ in air.}$$

Hence,

$$U_{vert.} \left[\frac{m}{sec}\right] = (2.59) \; f_D \; [MHz] \quad ,$$

and

$$U_{Horiz.} \left[\frac{m}{sec}\right] = (2.65) \; f_D \; [MHz] \quad . \qquad (A.3)$$

1.1 Average Velocity

Frequency shifting is employed to remove directional ambiguity. In such a case, when the fluid is at rest, the output voltage from the tracker, call it V_o, corresponds to zero velocity. Since the tracker output voltage minus the V_o offset is proportional to the Doppler frequency, the fluid velocity is (using the vertical component as an example)

$$U \left[\frac{m}{sec}\right] = (2.59) \cdot (\overline{V} - V_o) \cdot K_1 \left[\frac{MHz}{volt}\right] \quad , \qquad (A.4)$$

where

K_1 = a constant that depends on the tracker range setting;

$\overline{V}$ = time averaged value of tracker output voltage.

1.2 Mean Square Amplitude

The output from the tracker is a fluctuating voltage that can be decomposed into its mean and fluctuating components as

$$V(t) = \overline{V} + v'(t) \quad [volts] \quad . \qquad (A.5)$$

The two voltage components on the RHS of Eq. A.5 are proportional, respectively, to the decomposed velocity components:

$$U(t) = \overline{U} + u'(t) \left[\frac{m}{sec}\right] \quad . \qquad (A.6)$$

Therefore, since the proportionality constants are the same, Eq. A.4 shows that the mean square amplitude of the velocity fluctuations is

$$\overline{u'^2} \left[\frac{m}{sec}\right]^2 = (2.59)^2 \cdot (\overline{v'^2}) \cdot K_1^2 \quad . \qquad (A.7)$$

Here, $\overline{v'^2} = \frac{1}{T} \int_0^T v'^2(t)dt$ is the output of a mean square voltmeter.

1.3 Reynolds Stress

The velocity correlation is expressed as

$$\overline{u_1'u_2'} \left[\frac{m}{sec}\right]^2 = \overline{[(2.59(K_1)(v_1')] \cdot [(2.65)(K_2)(v_2')]}$$

$$= 6.86(K_1K_2)\overline{(v_1'v_2')} \quad , \qquad\qquad (A.8)$$

where subscripts one (1) and two (2) represent vertical and horizontal velocity components respectively. The quantity $\overline{v_1' \, v_2'}$ is the output of the DISA Turbulence Processor, an analog correlator.

The Reynolds Stress, in the two-dimensional case, is defined by

$$R.S. \equiv -\rho\overline{u_1' \, u_2'} \quad .$$

2. Cell Reynolds Number

The Reynolds Number is defined by

$$Re \approx \frac{\rho \, \overline{U} \, D}{\mu} \quad ,$$

where:

$\overline{U}$ = average velocity in the chimney;

D = chimney width = .188 ft.

Therefore, at full flow ($\overline{U}$ = 2.64 ft/sec.), with temperature = 110° F, Re = 70,000. During a transient, this value decreases monotonically to Re = 22,750 at the end of the coast-down.

APPENDIX B

ERROR ANALYSIS

The purpose of this appendix is to estimate the errors in the veloci-
ties, mean square velocities, turbulent kinetic energies, and double
velocity correlations from the uncertainties in the LDA measurement tech-
nique and the inaccuracies of the electronic instrumentation.

1. Laser Doppler Anemometer (LDA) Errors

Before demonstrating the mathematical procedure by which the overall
experimental errors are estimated, one must evaluate the source and
magnitude of the individual error contributions associated with LDA opera-
tions. In principle, the output from a perfect (error free) LDA is a
frequency that is proportional, with known proportionality constant, to the
fluid velocity being measured. However, when measuring a steady-state
laminar flow, a real LDA produces an output that is not the single constant
frequency that one expects, but rather it is a Gaussian-shaped band of
frequencies centered about the "true" value. This anomaly arises from
factors associated with the complex light-scattering process in the measur-
ing volume, and its magnitude can be calculated with reasonable precision;
see, e.g., George and Lumley [48].

The various contributions to this error are referred to as Doppler,
or frequency, "broadening" terms. The broadening errors affect turbulence
measurements also. The magnitude of the turbulent velocity fluctuations
is derived from the spectrum of frequency fluctuations about the mean that

are processed by the tracker, and contributions to that spectrum from Doppler broadening may incorrectly be interpreted as local fluid velocity fluctuations.

For a frequency tracker, such as used in the current experiment, the tracked frequency is proportional to the output voltage, $E(t)$, and assuming the probability-density function of $E(t)$ is symmetrical and Gaussian, the mean square turbulence level is given by Melling and Whitelaw [49] as

$$\left(\frac{e^2}{E^2}\right)_t = \left(\frac{e^2}{E^2}\right)_o - \left(\frac{e^2}{E^2}\right)_g + \left(\frac{e^2}{E^2}\right)_f + \left(\frac{e^2}{E^2}\right)_n \qquad (B.1)$$

In this equation:

e = RMS value of the voltage fluctuations;

E = mean value of $E(t)$;

t = true, or correct, value;

o = observed value;

g = gradient broadening;

f = finite transit time broadening;

n = electronic noise broadening.

Equation B.1 shows that if the various broadening contributions in the brackets can be evaluated, the necessary corrections can be made in a straightforward manner.

1.1 Gradient Broadening

If a velocity gradient exists over the finite size of the measuring volume, particles crossing the control volume at different positions will

have different velocities. These velocity differences cannot be distinguished from velocity variations with time, and have to be considered as a broadening contribution. For a frequency tracker, this term is estimated by

$$\left(\frac{e}{E}\right)_g = \frac{\partial U}{\partial X} \cdot \frac{\sigma_x}{U} \ , \qquad (B.2)$$

where σ_x is the dimension of the scattering volume perpendicular to the direction of the velocity gradient measurement [Melling & Whitelaw]. This correction is negligible for the measurements in this report.

1.2 Finite Transit Time Broadening

Due to the finite life-time of the signal associated with each scattering particle passing through the measuring volume, the Doppler spectrum exhibits a finite width over and above that produced by the fluid velocity fluctuations alone. The random arrival and departure of particles to and from the scattering volume causes fluctuations in phase, and hence frequency, of the Doppler signal. The phase fluctuations are correlated only over the transit time of particles across the measuring volume, which depends on the particle velocity and a scattering volume dimension. The broadening contribution that arises from this phenomenon is not consistently reported throughout the literature; therefore, the most conservative expression is used [Melling and Whitelaw]:

$$\left(\frac{e}{E}\right)_f \cong \frac{\sqrt{2}}{\pi N_2} \qquad (B.3)$$

N_2 is the number of fringes in the measuring volume. For this experiment,

N_2 is 47, which gives $\left(\dfrac{e}{E}\right)_f = 9.6 \times 10^{-3}$.

1.3 Electronic Noise Broadening

RMS voltage fluctuations on the LDA output may arise from the noise characteristics of the frequency tracker circuitry. The result is an additional broadening term that Melling and Whitelaw evaluated for a DISA tracker like that used in the current work. They found a worst case value of

$$\left(\frac{e}{E}\right)_n = .002, \tag{B.4}$$

which will be used for both trackers in this analysis.

Referring to Eq. B.1, the effect of the total broadening correction is seen to vary with the value of $\left(\dfrac{e}{E}\right)_t$, the turbulence intensity. For the value of the broadening contributions estimated in this section, Eq. B.1 can be used to show that the error in the measured value of the mean square fluctuation is always less than 1% as long as the turbulence intensity is greater than 3%. Since the experimentally determined turbulence intensity is greater than 3% at all but two locations near the test-cell inlet, a 1% error is assigned to the measurements of mean square fluctuations as the result of Doppler broadening.

2. General Principle of Error Calculation

The current experimental set-up is similar to that used by Chen [50]; therefore, his Error Analysis format is closely followed.

Since the errors come from many sources, the method of compounding errors suggested by Wilson [51] is used.

Suppose that the final result, Y, is related to the components, X_i, by the relation

$$Y = F(X_1, X_2, \ldots X_n)$$

where F is a known functional form. A small variation in the X_i will alter Y by the amount

$$dY = \frac{\partial F}{\partial X_1} dX_1 + \frac{\partial F}{\partial X_2} dX_2 + \ldots + \frac{\partial F}{\partial X_n} dX_n$$

$$= \sum_{i=1}^{n} \frac{\partial F}{\partial X_i} dX_i \quad .$$

The square of the error will be

$$(dY)^2 = \sum_{i,j} \frac{\partial F}{\partial X_j} \frac{\partial F}{\partial X_j} dX_i \; dX_j \quad .$$

If the components dX_1, dX_2, $\ldots$, dX_n are independently distributed and symmetrical with respect to positive and negative values, then the products $dX_i \, dX_j$ $(i \neq j)$, will vanish on the average so that

$$(dY)^2 = \sum_{i=1}^{n} \left(\frac{\partial F}{\partial X_i}\right)^2 (dX_i)^2 \quad .$$

This may also be written in terms of the variance, σ^2, as

$$\sigma^2 = \sum_{i=1}^{n} \left(\frac{\partial F}{\partial X_i}\right)^2 \sigma_i^2 \tag{B.5}$$

3. Calculation of the Error in Velocity

The velocity is calculated by the expression

$$V = \frac{f\lambda}{2\sin\theta} \quad , \tag{B.6}$$

where

      f = the Doppler frequency

      λ = the wavelength of laser light

      θ = the half angle of the beam intersection

Hence, there are three quantities, f, λ, and θ which will make a contribution to the errors. The error in λ is negligibly small. The errors associated with θ and f are discussed below.

3.1 Error Due to the Uncertainty in θ

A nominal value for the angle θ is provided by the optics manufacturer as a function of lens and beam-separation distance. However, since the sine of a small angle is a sensitive function of θ, it is recommended that θ be measured independently for the particular optics arrangement employed. In this case, the intersecting beams were projected onto a flat surface located approximately five meters from their focal point, and the angle θ was determined by trigonometry. This procedure is estimated to result in a 1% error in the value of θ.

In Eq. B.6, differentiate V with respect to θ:

$$\frac{\partial V}{\partial \theta} = -f\ \lambda\cos\theta/2\sin^2\theta \tag{B.7}$$

From Eq. B.5, the error (normalized by the velocity) is

$$\frac{1}{V^2} \left(\frac{\partial V}{\partial \theta}\right)^2 (\Delta\theta)^2 = \left(\frac{\Delta\theta}{\tan\theta}\right)^2$$

$$\approx \left(\frac{\Delta\theta}{\theta}\right)^2 \quad , \tag{B.8}$$

where $\tan\theta \approx \theta$. (In this experiment, $\theta_{vertical} = 5.69°$ and $\theta_{horizontal} = 5.58°$.)

3.2 Error due to the Uncertainty in f

The uncertainty in the frequency comes from the following sources:

1. the accuracy of the frequency tracker

2. the accuracy of the digital voltmeter

3. the accuracy of the frequency shifter

4. the accuracy of the A-to-D converter

5. signal broadening

6. transient data averaging method

Factor one, the overall accuracy of the tracker as specified by the manufacturer is 1% of the full scale deflection. For this experiment, the measured frequency was close to 50% of the full scale reading, hence the accuracy is 2.0%. Factor two, the accuracy of the digital voltmeter is 0.1%. It is small compared to other errors, and thus will be neglected in the calculation. For factor three, the manufacturers do not specify the accuracy of their frequency shifter. It involves both frequency upshifting and downshifting and errors might occur during these processes. The extent of this error is difficult to quantify; however, measurements of the frequency shift observed with no flow indicate that it is generally less than 1%, so this value will be

conservatively assigned to factor three.

Factor four, the accuracy of the A-to-D converter, refers only to the quantization scheme used since linearity errors were negligible over the range of interest, and voltage offset errors were subtracted out during data reduction. For velocity measurements there were two possible digitization modes corresponding to the particular tracker range in use. The worst-case mode will be analyzed to give a conservative estimate. In this case, ten volts were quantized over 255 levels, i.e.,

$$\frac{10 \text{ volts}}{255} = .0392 \frac{\text{volts}}{\text{level}} \quad .$$

Therefore, a sampled voltage could be assigned to a level that is in error by, at most, 0.0392 volts. The accuracy is $\frac{.0392}{10} \sim 0.5\%$.

Factor five, signal broadening, is discussed in Sec. 1 of this Appendix. The broadening correction applies mainly to the mean square value of the frequency fluctuations (i.e. TKE), and has a negligible influence on the average value of the Doppler frequency itself (i.e., $\overline{U}$ and $\overline{V}$).

The accuracy of the transient data averaging method is described in detail in Sec. 3.4.3. It is shown there that the experimental variables were selected to keep each contribution to the error below 1%. Since the errors are time dependent and calculated in an approximate fashion, a conservative estimate of the accuracy assumes that all sources of error add throughout the transient. The accuracy in this case is 2%.

In Eq. B.6 differentiate V with respect to f:

$$\frac{\partial V}{\partial f} = \frac{\lambda}{2 \sin \theta} \quad . \tag{B.9}$$

Hence the error is

$$\sum_i \frac{1}{V^2} \left(\frac{\partial V}{\partial f_i}\right)^2 (\Delta f_i)^2 = \sum_i \left(\frac{\Delta f_i}{f}\right)^2 \qquad (B.10)$$

where i = all six factors discussed above.

3.3 Other Errors

In the above sections, only errors associated with Eq. B.6 were dis-
cussed. The other possible errors are listed here:

1. Position errors, i.e., the measuring points are not
   exactly the desired positions. In this experiment
   the test section is relatively large compared to the
   measuring volume, hence this error is judged to be
   negligibly small.

2. Errors in the measurement angle, i.e., the laser beam
   is not perpendicular to the test section, so that the
   measured velocity component is not the correct one.
   A 1% error in velocity is assigned to this factor.

3.4 Sample Calculation for the Error in the Velocity

The total error for the velocity measurement can be calculated by
combining Eqs. B.5, B.8, B.10, and other errors from the previous
sections:

$$\left(\frac{\Delta V}{V}\right)^2 = \left(\frac{\Delta \theta}{\theta}\right)^2 + \sum_i \left(\frac{\Delta f_i}{f}\right)^2 + \left(\frac{\Delta V_0}{V}\right)^2$$

$$= (0.1)^2 + (0.2)^2 + (.01)^2 + (.005)^2 + (.02)^2 + (.01)^2$$

$$= 0.001125$$

$$\frac{\Delta V}{V} = 3.4\%$$

Hence, the error in the velocity measurement is 3.4%.

4. <u>Calculation of Error in the Turbulent Kinetic Energy (TKE)</u>

The turbulent kinetic energy, K, is calculated from the expression

$$K = \frac{1}{2} \left(\overline{u'^2} + \overline{v'^2} \right) \quad ,$$

where $\overline{u'^2}$ and $\overline{v'^2}$ are the respective mean square amplitudes of the velocity fluctuations.

Since $\overline{u'^2}$ and $\overline{v'^2}$ are measured independently, a conservative estimate of the error in K is calculated by adding the errors from its components, i.e.

$$\left| \frac{\Delta K}{K} \right| = \left| \frac{\overline{\Delta u'^2}}{\overline{u'^2}} \right| + \left| \frac{\overline{\Delta v'^2}}{\overline{v'^2}} \right| \tag{B.11}$$

The mean square amplitude of the velocity fluctations is found from the expression

$$\overline{u'^2} = \overline{f'^2} \left[\frac{\lambda^2}{4\sin^2\theta} \right] \tag{B.12}$$

where f' is the amplitude of the fluctuating component of the Doppler frequency, and $\overline{f'^2} = \frac{1}{T} \int_0^t [f'(t)]^2 dt$, the mean square amplitude. The errors in $\overline{u'^2}$ come from errors in   and $\overline{f'^2}$.

4.1 Error due to the Uncertainty in θ

Using Eq. B.5, the error normalized by $\overline{u'^2}$ is

$$\left[\frac{1}{\overline{u'^2}}\right]^2 \cdot \left[\frac{\partial \overline{u'^2}}{\partial \theta}\right]^2 \cdot (\Delta \theta)^2 \cong 4\left(\frac{\Delta \theta}{\theta}\right)^2 \quad , \tag{B.13}$$

where $\frac{\Delta \theta}{\theta}$ = 1% from Sec. 3.2 in this Appendix.

4.2 Error due to the Uncertainty in $\overline{f'^2}$

The uncertainty comes from the following sources:

1. the accuracy of the frequency tracker

2. the accuracy of the A-to-D converter

3. the accuracy of the transient data averaging method

4. the accuracy of the mean square voltmeter

5. signal broadening

Factor one, two, and three are addressed in Sec. 3 of this Appendix, the values are 2%, 0.5%, and 2% respectively. For factor four, voltmeter accuracy, one need only consider the accuracy of the mean square output voltage since frequency-related errors are a component of factor three. The accuracy for factor four, then, is given by the manufacturer as 1%. Factor five, signal broadening, is estimated in Sec. 1 to be 1%.

Hence, the normalized error from uncertainty in $\overline{f'^2}$ is

$$\sum_i \left(\frac{1}{\overline{u'^2}}\right)^2 \cdot \left(\frac{\partial \overline{u'^2}}{\partial \overline{f'^2}}\right)^2 \cdot \left(\Delta \overline{f'^2}\right)_i^2 = \sum_i \frac{\left[\Delta \overline{f'^2}\right]_i^2}{\left[\overline{f'^2}\right]^2} \tag{B.14}$$

4.3 Sample Calculation for the Error in $\overline{f'^2}$

The total error is calculated by combining Eqs. B.13 and B.14:

$$\left[\frac{\Delta \overline{u'^2}}{\overline{u'^2}}\right]^2 = 4\left(\frac{\Delta\theta}{\theta}\right)^2 + \sum_i \frac{\left(\Delta\overline{f'^2}\right)_i^2}{\left(\overline{f'^2}\right)^2}$$

$$= 4(.01)^2 + (.02)^2 + (.005)^2 + (.02)^2 + (.01)^2 + (.01)^2$$

$$= .001425$$

$$\frac{\Delta\overline{u'^2}}{\overline{u'^2}} = 3.8\%$$

Since the error in $\overline{v'^2}$ comes from the same sources,

$$\frac{\Delta\overline{v'^2}}{\overline{v'^2}} = 3.8\% \quad ,$$

Using these values and Eq. B.11, the estimated error in the measured value of TKE is

$$\frac{\Delta K}{K} = 7.6\% \quad .$$

Note that this error applies to the measured quantity $\frac{\overline{u'^2} + \overline{v'^2}}{2}$, which is defined here as K, the turbulent kinetic energy. This definition is necessarily artificial since it omits $\overline{w'^2}$, the third component of fluctuating velocity, which could not be measured with the two-dimensional LDA system employed. The correct representation of TKE is

$$K = \frac{1}{2} \; (\overline{u'^2} + \overline{v'^2} + \overline{w'^2}).$$

The absence of $\overline{w'^2}$ is not treated as experimental error per se; its probable magnitude is by no means negligible, and its effect on the comparisons is discussed in Sec. 5 of the main report.

5. Calculation of the Error in the Velocity Correlation

The velocity correlation is represented by $\overline{u'v'}$. The error comes from the following four sources:

1. Errors in u' and v'
2. The accuracy of the turbulence processor
3. The accuracy of the A-to-D converter
4. Transient data averaging method

In the first factor, since the errors associated with u' and v' are not expected to be correlated, they will not make a contribution to the error in the velocity correlation measurement. Factor two, the accuracy of the turbulence processor which does the multiplication, is specified by the manufacturer as 2% $\pm$ 10 mV. Since a constant calibration was used, the possible $\pm$ 10 mV electronic drift error was eliminated. Factor three, the accuracy of the A-to-D converter, is negligibly small in this case.

The ten second time constant, τ, used for all five averaging circuits was least satisfactory for the velocity correlation measurements. A precise estimate of factor four is not possible in this case because of a lack of frequency information concerning this signal. An estimate of the upper bound of the error associated with this value can be obtained from the standard deviation of the $\overline{u'v'}$ ensembles at each location. Although these are generally on the order of 10% of the mean, there are numerous

locations where they exceed 25%, especially where the mean value of the correlation is close to zero. For lack of a better measure, the total error in the velocity correlation is estimated to be 25%.

APPENDIX C

TABULATION OF DATA

For ease of interpretation and use, the data in this appendix are compiled in two sections. Section one data are steady-state full-flow values obtained at the X-Y (I-J) coordinate positions listed in Table C.1 and defined over the test cell in Fig. C.1. Section two data are a series of tables, one for each I-J position where a transient was measured, depicting the average value of the turbulence parameters as a function of time during the transient. Also included for each steady-state and transient mean value are the estimated standard deviations arising from the sampling procedure used to record the data.

General Statistics

The mean values and estimated standard deviations of the primary measured quantities were found from

$$\overline{X} = \frac{\sum\limits_{i=1}^{N} X_i}{N} \, ,$$

and

$$S = \sqrt{\frac{1}{N-1} \sum\limits_{i=1}^{N} (X_i - \overline{X})^2} \quad .$$

Here, in the steady-state case, N refers to the number of samples taken while the flowrate is full and constant; in the transient case, N is the

total number of transient runs employed to form the ensemble.

Also, for the indirect quantity

$$TKE = K = \frac{\overline{u'^2} + \overline{v'^2}}{2} \quad ,$$

the estimated standard deviation is found from

$$S = \sqrt{\frac{S_1^2 + S_2^2}{2}} \quad ,$$

where S_1 and S_2 are associated with the two components of K, $\overline{u'^2}$ and $\overline{v'^2}$.
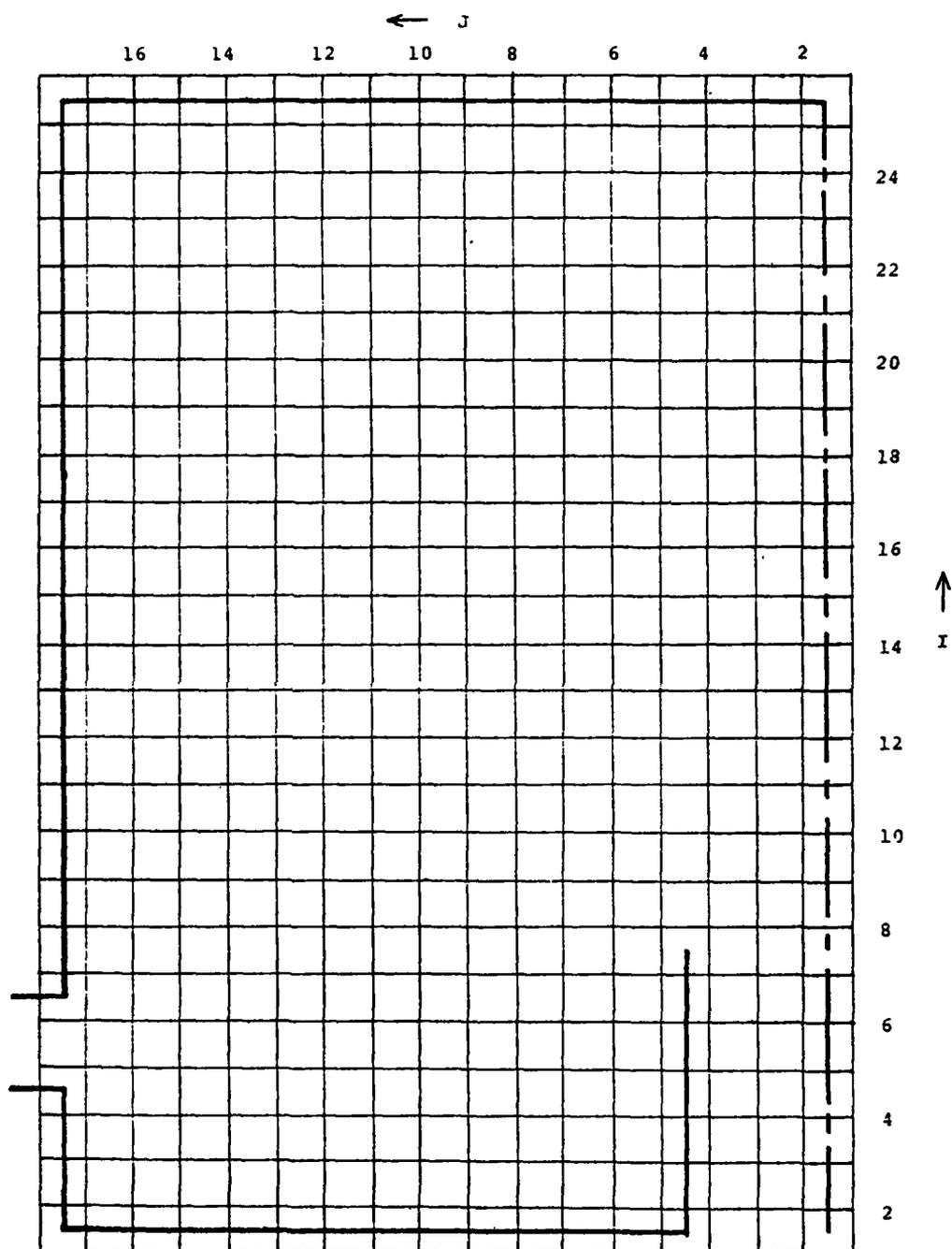
Fig. C.1 EXPERIMENTAL COORDINATE SYSTEM

Table C.1

Full Flow Steady-State Case
(Mean Values)

Position		$\overline{U}$ [m/sec]	$\overline{V}$ [m/sec]	$\overline{u'^2}$ [m/sec]^2 x 10^3	$\overline{v'^2}$ [m/sec]^2 x 10^3	$\overline{u'v'}$ [m/sec]^2 x 10^4	TKE [m/sec]^2 x 10^3
I	J						
5	6	.106	~0	2.34	3.75	7.50	3.04
	8	-.029	-.031	3.41	4.69	5.44	4.05
	10	-.135	-.064	4.34	7.26	4.41	5.80
	12	-.255	-.067	7.83	8.83	12.1	8.33
	14	-.393	.027	11.83	8.90	21.6	10.1
	16	-.538	.304	1.90	6.84	8.61	4.37
	17	-.477	.623	2.03	4.53	7.29	3.28
6	6	.132	~0	1.94	4.01	6.63	2.97
	8	.017	-.028	3.47	5.17	5.76	4.32
	10	-.081	-.079	5.06	6.43	5.67	5.74
	12	-.202	-.066	7.21	7.19	8.75	7.20
	14	-.387	.036	11.1	7.19	26.6	9.15
	16	-.646	.298	12.5	6.26	47.6	9.39
	17	-.864	.655	11.4	5.29	48.1	8.33
7.5	2	.804	-.006	.403	.457	-.588	.430
	3	.823	.015	.485	.449	-.991	.467
	4	.771	.036	2.85	1.70	6.2	2.27
8	6	.160	-.007	2.93	3.77	8.23	3.35
	8	.078	-.028	3.52	4.35	4.26	3.94
	10	~0	-.047	4.26	3.93	6.76	4.09
	12	-.191	-.010	5.39	5.00	12.5	5.20
	14	-.462	.018	9.39	7.29	36.9	8.34
	16	-.759	.072	5.70	5.54	26.4	5.62
10	2	.798	.014	.353	.413	-.510	.383
	4	.762	.042	2.28	1.16	4.98	1.72
	6	.153	.023	2.42	3.27	5.04	2.85
	8	.092	~0	2.32	3.62	2.52	2.97
	10	~0	.010	2.46	2.72	4.19	2.59
	12	-.182	.027	4.52	5.41	15.8	4.97
	14	-.475	-.010	7.75	7.29	32.4	7.52
	16	-.724	-.011	5.19	4.94	16.9	5.06

Table C.1 (cont.)

Full Flow Steady-State Case
(Mean Values)

Position I	J	$\overline{U}$ [m/sec]	$\overline{V}$ [m/sec]	$\overline{u'^2}$ [m/sec]^2 x 10^3	$\overline{v'^2}$ [m/sec]^2 x 10^4	$\overline{u'v'}$ [m/sec]^2 x 10^4	TKE [m/sec]^2 x 10^3
12	2	.779	~0	.344	.381	-.196	.362
	4	.738	.035	2.22	1.26	4.90	1.74
	6	.155	.008	2.33	2.56	3.25	2.45
	8	.090	.008	2.26	2.29	2.64	2.28
	10	.032	.025	2.03	1.71	3.51	1.87
	12	-.251	.015	6.90	6.01	19.40	6.45
	14	-.509	-.021	7.24	8.76	25.4	8.00
	16	-.712	-.028	5.54	5.25	16.4	5.39
14	2	.757	.016	.302	.319	~0	.310
	4	.730	.067	1.90	1.27	4.61	1.59
	6	.164	.024	2.49	2.48	4.94	2.48
	8	.077	.028	1.69	1.59	1.65	1.64
	10	-.029	.038	1.33	1.31	2.90	1.32
	12	-.265	.023	5.83	6.20	18.0	6.02
	14	-.499	-.014	7.81	9.86	19.3	8.84
	16	-.671	-.022	4.96	5.49	15.1	5.23
16	2	.740	.014	.333	.280	~0	.307
	4	.729	.009	1.81	1.25	4.14	1.53
	6	.156	.029	3.77	3.19	9.54	3.48
	8	.055	.030	1.62	1.26	1.25	1.44
	10	-.045	.038	1.50	1.26	2.75	1.38
	12	-.297	.031	6.86	7.95	19.7	7.41
	14	-.471	-.009	7.63	11.3	13.9	9.46
	16	-.674	-.011	4.05	5.12	10.8	4.58
18	2	.664	.032	.320	.219	~0	.270
	4	.670	.153	1.35	.846	1.78	1.10
	6	.235	.103	6.12	6.67	28.0	6.40
	8	.053	.063	1.74	1.27	1.85	1.50
	10	-.064	.058	1.61	1.35	3.30	1.48
	12	-.304	.065	7.08	11.0	14.2	9.03
	14	-.406	.032	7.35	12.9	4.15	10.1
	16	-.617	.025	5.18	4.71	7.41	4.95

Table C.1 (cont.)

Full Flow Steady-State Case
(Mean Values)

Position		$\overline{U}$	$\overline{V}$	$\overline{u'^2}$	$\overline{v'^2}$	$\overline{u'v'}$	TKE
		[m/sec]	[m/sec]	[m/sec]^2 x 10^3	[m/sec]^2 x 10^4	[m/sec]^2 x 10^4	[m/sec]^2 x 10^3
I	J						
20	2	.560	.045	.346	.167	-.203	.256
	4	.603	.204	.703	.452	~0	.577
	6	.376	.268	6.91	6.29	25.6	6.60
	8	.072	.134	2.31	3.34	4.33	2.82
	10	-.081	.095	2.83	3.38	2.25	3.11
	12	-.223	.107	6.57	15.8	~0	11.2
	14	-.295	.060	6.29	12.4	3.75	9.34
	16	-.560	.051	2.41	3.63	~0	3.02
22	2	.449	.048	.459	.138	~0	.298
	4	.478	.233	.665	.220	-.281	.442
	6	.445	.442	1.58	.847	-.905	1.22
	8	.212	.393	3.78	5.66	7.24	4.72
	10	.030	.258	3.14	6.54	~0	4.84
	12	-.084	.199	4.44	11.1	~0	7.77
	14	-.234	.180	4.73	7.16	-3.90	5.94
	16	-.444	.144	1.95	3.83	-3.81	2.89

Table C.1

Full Flow Steady-State Case

(Standard Deviations)

Position I	J	$\overline{U}$ [m/sec]	$\overline{V}$ [m/sec]	$\overline{u'^2}$ [m/sec]^2 x 10^3	$\overline{v'^2}$ [m/sec]^2 x 10^3	$\overline{u'v'}$ [m/sec]^2 x 10^4	TKE [m/sec]^2 x 10^3
5	6	.003	.007	.127	.303	1.59	.232
	8	.008	.011	.181	.377	1.59	.295
	10	.012	.012	.212	.532	2.22	.399
	12	.016	.010	.358	.564	4.40	.473
	14	.015	.005	.591	.647	4.65	.617
	16	.017	.004	.098	.277	1.05	.208
	17	.019	.005	.086	.240	1.26	.180
6	6	.007	--	.135	.421	1.08	.313
	8	.008	.012	.132	.404	1.46	.300
	10	.008	.007	.366	.433	1.78	.401
	12	.014	.006	.416	.696	3.22	.573
	14	.012	.005	.272	.355	.222	.317
	16	.015	.005	.600	.257	3.76	.439
	17	.009	.005	.625	.225	3.41	.470
7.5	2	.002	.003	.008	.006	.057	.006
	3	~0	.002	.010	.009	.079	.010
	4	.002	.002	.075	.028	.398	.054
8	6	.012	.006	.139	.221	1.53	.171
	8	.012	.009	.134	.393	2.25	.293
	10	--	.008	.263	.473	2.47	.371
	12	.015	.008	.328	.333	1.84	.314
	14	.011	.007	.484	.319	4.29	.410
	16	.006	.006	.271	.244	1.91	.258
10	2	.002	.002	.008	.006	.074	.007
	4	.003	.002	.039	.019	.209	.030
	6	.009	.006	.016	.025	1.40	.211
	8	.009	--	.111	.315	1.18	.234
	10	--	.005	.122	.282	1.64	.217
	12	.013	.004	.145	.360	2.47	.274
	14	.009	.005	.292	.418	2.71	.360
	16	.005	.004	.178	.167	1.27	.173

Table C.1 (cont.)

Full Flow Steady-State Case
(Standard Deviations)

Position		$\overline{U}$ [m/sec]	$\overline{V}$ [m/sec]	$\overline{u'^2}$ [m/sec]^2 x 10^3	$\overline{v'^2}$ [m/sec]^2 x 10^3	$\overline{u'v'}$ [m/sec]^2 x 10^4	TKE [m/sec]^2 x 10^3
I	J						
12	2	.002	--	.008	.008	.057	.008
	4	.002	.002	.063	.039	.259	.053
	6	.008	.005	.122	.155	1.01	.129
	8	.009	.003	.105	.253	.759	.193
	10	.008	.005	.098	.197	.761	.155
	12	.011	.003	.418	.399	2.38	.408
	14	.006	.004	.310	.357	2.79	.331
	16	.005	.005	.301	.236	2.21	.270
14	2	.002	.001	.004	.004	--	.004
	4	.002	.005	.055	.063	.471	.058
	6	.004	.003	.183	.245	1.27	.216
	8	.007	.006	.061	.108	.960	.087
	10	.009	.003	.056	.099	1.11	.080
	12	.009	.004	.245	.290	2.22	.250
	14	.004	.005	.275	.387	2.04	.336
	16	.006	.006	.233	.236	1.62	.230
16	2	.002	.001	.004	.007	--	.006
	4	.003	.001	.064	.081	.349	.073
	6	.006	.004	.187	.182	1.27	.184
	8	.008	.004	.093	.105	.552	.099
	10	.005	.003	.082	.155	.450	.124
	12	.008	.006	.287	.385	1.90	.321
	14	.005	.005	.173	.367	2.68	.287
	16	.006	.006	.172	.306	1.76	.235
18	2	.002	.001	.007	.004	--	.006
	4	~0	.001	.026	.041	.213	.035
	6	.008	.003	.363	.363	2.99	.360
	8	.007	.003	.099	.114	.594	.107
	10	.007	.004	.113	.109	.875	.105
	12	.005	.007	.221	.690	1.81	.512
	14	.008	.007	.222	.688	2.92	.492
	16	.005	.004	.341	.340	1.62	.341

Table C.1 (cont.)

Full Flow Steady-State Case
(Standard Deviations)

Position I	J	$\overline{U}$ $[m/sec]^2$	$\overline{V}$ $[m/sec]^2$	$\overline{u'^2}$ $[m/sec]^2$ x 10^3	$\overline{v'^2}$ $[m/sec]^2$ x 10^3	$\overline{u'v'}$ $[m/sec]^2$ x 10^4	TKE $[m/sec]^2$ x 10^3
20	2	.002	.001	.009	.004	.129	.007
	4	.002	.002	.020	.020	--	.020
	5	.005	.003	.336	.250	1.67	.296
	6	.006	.008	.100	.279	1.18	.206
	10	~0	.003	.140	.210	.941	.178
	12	.006	.009	.222	.789	--	.579
	14	.007	.007	.272	.646	2.08	.495
	16	.006	.006	.127	.219	--	.174
22	2	.003	.004	.016	.052	--	.012
	4	.042	.001	.027	.011	.120	.021
	6	.003	.005	.060	.049	.446	.054
	8	.005	.002	.189	.198	1.34	.193
	10	.006	.005	.106	.425	--	.294
	12	.006	.006	.192	.792	--	.533
	14	.009	.009	.223	.566	1.87	.430
	16	.005	.004	.082	.355	1.29	.258

Appendix C   Section 2

Tables of Transient Data

POSITION: I= 5,   J= 6

MEAN VALUES

TIME (SEC)	$\langle U \rangle$ (M/S)	$\langle V \rangle$ (M/S)	$\langle u'^{**}2 \rangle$ (M/S)**2	$\langle v'^{**}2 \rangle$ (M/S)**2	$\langle u'v' \rangle$ (M/S)**2	TKE (M/S)**2
10	1.07E-001	3.12E-003	2.30E-003	3.50E-003	6.23E-004	2.90E-003
20	1.02E-001	-3.12E-003	2.35E-003	3.60E-003	7.23E-004	2.98E-003
30	9.31E-002	-6.24E-003	2.24E-003	3.11E-003	6.12E-004	2.68E-003
40	7.96E-002	-1.56E-003	2.04E-003	2.76E-003	4.95E-004	2.40E-003
50	7.11E-002	-2.08E-003	1.97E-003	2.40E-003	4.78E-004	2.18E-003
60	6.26E-002	3.12E-003	1.65E-003	1.92E-003	3.28E-004	1.79E-003
70	5.25E-002	3.64E-003	1.38E-003	1.42E-003	2.34E-004	1.40E-003
80	4.06E-002	1.04E-003	1.18E-003	1.02E-003	1.33E-004	1.10E-003
90	3.72E-002	1.56E-003	9.99E-004	6.90E-004	8.90E-005	8.44E-004
100	3.05E-002	2.08E-003	9.23E-004	4.77E-004	5.00E-005	7.00E-004
110	2.37E-002	-1.04E-003	8.90E-004	3.59E-004	3.89E-005	6.24E-004
120	2.26E-002	-2.60E-003	8.77E-004	2.61E-004	2.22E-005	5.69E-004
130	2.03E-002	-5.20E-004	8.83E-004	2.26E-004	0.00E+000	5.55E-004
140	2.03E-002	-2.08E-003	8.26E-004	1.99E-004	5.56E-006	5.12E-004

STANDARD DEVIATIONS

TIME (SEC)	$\langle U \rangle$ (M/S)	$\langle V \rangle$ (M/S)	$\langle u'^{**}2 \rangle$ (M/S)**2	$\langle v'^{**}2 \rangle$ (M/S)**2	$\langle u'v' \rangle$ (M/S)**2	TKE (M/S)**2
10	5.56E-003	9.87E-003	8.37E-005	2.56E-004	1.09E-004	1.90E-004
20	1.11E-002	7.90E-003	5.76E-005	4.40E-004	9.59E-005	3.14E-004
30	1.19E-002	7.12E-003	1.01E-004	3.22E-004	1.21E-004	2.38E-004
40	4.15E-003	3.27E-003	1.13E-004	1.61E-004	1.08E-004	1.39E-004
50	9.08E-003	6.14E-003	1.89E-004	2.21E-004	1.41E-004	1.74E-004
60	4.15E-003	6.24E-003	1.17E-004	1.75E-004	1.14E-004	1.49E-004
70	4.15E-003	6.06E-003	8.86E-005	1.42E-004	4.72E-005	1.18E-004
80	6.42E-003	5.81E-003	5.42E-005	1.19E-004	5.97E-005	9.23E-005
90	5.81E-003	4.73E-003	8.91E-005	6.74E-005	2.72E-005	7.90E-005
100	5.24E-003	3.22E-003	8.86E-005	3.35E-005	1.83E-005	6.70E-005
110	5.24E-003	4.26E-003	8.97E-005	2.44E-005	1.36E-005	6.57E-005
120	4.15E-003	4.59E-003	7.87E-005	3.68E-005	1.72E-005	6.15E-005
130	0.00E+000	3.65E-003	7.28E-005	1.57E-005	0.00E+000	5.27E-005
140	0.00E+000	3.22E-003	3.77E-005	2.56E-005	1.36E-005	3.22E-005

POSITION: I = 5, J = 10

TIME (SEC)	⟨U⟩ (M/S)	⟨u'**2⟩ (M/S)**2	⟨v'**2⟩ (M/S)**2	⟨u'v'⟩ (M/S)**2	TKE (M/S)**2
		----MEAN VALUES----			
10	-1.32E-001	-6.04E-002	4.34E-003	6.89E-003	3.48E-004	5.61E-003
20	-1.32E-001	-6.09E-002	4.21E-003	6.67E-003	4.81E-004	5.44E-003
30	-1.27E-001	-6.50E-002	3.91E-003	6.22E-003	5.83E-004	5.06E-003
40	-1.20E-001	-6.56E-002	3.76E-003	5.65E-003	5.32E-004	4.70E-003
50	-1.10E-001	-6.45E-002	3.30E-003	4.66E-003	4.30E-004	3.98E-003
60	-9.82E-002	-6.04E-002	2.98E-003	4.03E-003	3.37E-004	3.51E-003
70	-8.46E-002	-5.41E-002	2.38E-003	2.96E-003	2.45E-004	2.67E-003
80	-6.77E-002	-4.53E-002	1.91E-003	2.18E-003	1.94E-004	2.04E-003
90	-6.09E-002	-3.75E-002	1.47E-003	1.48E-003	1.23E-004	1.48E-003
100	-4.74E-002	-3.43E-002	1.20E-003	1.04E-003	8.18E-005	1.12E-003
110	-4.40E-002	-2.91E-002	1.04E-003	8.35E-004	7.16E-005	9.36E-004
120	-3.72E-002	-2.65E-002	9.59E-004	6.10E-004	6.14E-005	7.84E-004
130	-3.89E-002	-2.13E-002	8.76E-004	4.77E-004	4.09E-005	6.77E-004
140	-3.39E-002	-2.08E-002	8.80E-004	4.51E-004	5.11E-005	6.65E-004
		----STANDARD DEVIATIONS----			
10	1.44E-002	1.24E-002	2.89E-004	2.46E-004	2.97E-004	2.68E-004
20	2.03E-002	1.00E-002	2.90E-004	2.72E-004	1.19E-004	3.34E-004
30	1.54E-002	2.19E-002	2.33E-004	3.77E-004	1.93E-004	3.14E-004
40	2.07E-002	4.41E-003	1.92E-004	3.64E-004	1.89E-004	2.91E-004
50	1.75E-002	8.06E-003	2.89E-004	2.51E-004	2.20E-004	2.70E-004
60	1.39E-002	1.04E-002	1.82E-004	2.27E-004	1.49E-004	2.06E-004
70	1.78E-002	3.78E-003	1.51E-004	1.89E-004	9.51E-005	1.71E-004
80	5.24E-003	4.30E-003	6.65E-005	1.97E-004	9.03E-005	1.47E-004
90	6.42E-003	8.83E-003	1.27E-004	6.96E-005	3.88E-005	1.02E-004
100	1.05E-002	3.42E-003	5.94E-005	4.65E-005	5.01E-005	5.33E-005
110	8.29E-003	8.53E-003	9.98E-005	1.07E-004	4.62E-005	1.03E-004
120	5.24E-003	1.71E-003	5.75E-005	4.11E-005	0.00E+000	5.00E-005
130	4.15E-003	5.00E-003	6.17E-005	6.65E-005	5.01E-005	6.42E-005
140	5.24E-003	4.26E-003	8.66E-005	3.25E-005	2.50E-005	6.54E-005

POSITION: I= 5, J= 14

TIME (SEC)	<U> (M/S)	<V> (M/S)	<u'**2> (M/S)**2	<v'**2> (M/S)**2	<u'v'> (M/S)**2	TKE (M/S)**2
			---MEAN VALUES---			
10	-3.94E-001	2.81E-002	1.10E-002	8.60E-003	1.96E-003	9.82E-003
20	-3.82E-001	3.06E-002	1.07E-002	7.98E-003	1.86E-003	9.36E-003
30	-3.82E-001	2.68E-002	1.01E-002	7.45E-003	1.82E-003	8.75E-003
40	-3.66E-001	2.81E-002	9.19E-003	6.18E-003	1.56E-003	7.69E-003
50	-3.49E-001	2.50E-002	7.85E-003	5.15E-003	1.29E-003	6.50E-003
60	-3.21E-001	2.43E-002	6.58E-003	4.03E-003	1.06E-003	5.30E-003
70	-2.93E-001	2.31E-002	5.01E-003	3.05E-003	8.28E-004	4.03E-003
80	-2.50E-001	2.06E-002	3.56E-003	2.12E-003	5.52E-004	2.84E-003
90	-2.09E-001	1.75E-002	2.88E-003	1.54E-003	3.91E-004	2.21E-003
100	-1.87E-001	1.56E-002	2.25E-003	1.14E-003	2.76E-004	1.69E-003
110	-1.65E-001	1.44E-002	1.80E-003	8.15E-004	2.30E-004	1.31E-003
120	-1.50E-001	1.31E-002	1.55E-003	6.34E-004	1.61E-004	1.09E-003
130	-1.38E-001	1.25E-002	1.41E-003	5.13E-004	1.38E-004	9.60E-004
140	-1.30E-001	1.12E-002	1.38E-003	4.73E-004	1.15E-004	9.27E-004
			---STANDARD DEVIATIONS---			
10	1.51E-002	5.84E-003	5.76E-004	5.95E-004	3.45E-004	5.86E-004
20	1.16E-002	4.63E-003	2.66E-004	4.20E-004	4.34E-004	3.52E-004
30	1.54E-002	7.52E-003	6.41E-004	1.08E-003	9.63E-005	8.91E-004
40	1.90E-002	4.41E-003	4.47E-004	6.48E-004	1.93E-004	5.56E-004
50	1.16E-002	3.82E-003	2.49E-004	3.31E-004	2.49E-004	2.93E-004
60	1.16E-002	4.07E-003	3.63E-004	3.54E-004	2.21E-004	3.59E-004
70	4.54E-003	4.73E-003	2.99E-004	2.86E-004	9.63E-005	2.57E-004
80	1.16E-002	4.19E-003	2.65E-004	6.56E-005	5.15E-005	1.93E-004
90	9.03E-003	2.79E-003	2.05E-004	2.76E-005	1.03E-004	1.46E-004
100	1.16E-002	3.72E-003	1.70E-004	6.75E-005	6.30E-005	1.29E-004
110	8.50E-003	1.71E-003	3.60E-005	5.51E-005	0.00E+000	4.66E-005
120	8.50E-003	2.61E-003	5.88E-005	5.74E-005	6.30E-005	5.81E-005
130	1.16E-002	3.82E-003	9.97E-005	6.56E-005	5.15E-005	5.44E-005
140	8.50E-003	1.71E-003	4.65E-005	2.76E-005	0.00E+000	3.82E-005

POSITION: I= 5, J= 17

TIME (SEC)	$\langle U \rangle$ (M/S)	$\langle V \rangle$ (M/S)	$\langle u'{**}2 \rangle$ (M/S){**}2	$\langle v'{**}2 \rangle$ (M/S){**}2	$\langle u'v' \rangle$ (M/S){**}2	TKE (M/S){**}2
			----MEAN VALUES----			
10	-4.82E-001	6.18E-001	2.00E-003	4.40E-003	7.27E-004	3.20E-003
20	-4.69E-001	6.08E-001	1.94E-003	4.33E-003	6.51E-004	3.13E-003
30	-4.76E-001	5.84E-001	1.70E-003	3.80E-003	6.63E-004	2.75E-003
40	-4.54E-001	5.55E-001	1.55E-003	3.45E-003	5.99E-004	2.50E-003
50	-4.22E-001	5.17E-001	1.33E-003	2.87E-003	5.53E-004	2.10E-003
60	-3.88E-001	4.70E-001	1.08E-003	2.34E-003	4.65E-004	1.71E-003
70	-3.54E-001	4.25E-001	8.16E-004	1.81E-003	3.55E-004	1.31E-003
80	-3.10E-001	3.79E-001	6.44E-004	1.40E-003	2.79E-004	1.02E-003
90	-2.67E-001	3.37E-001	4.89E-004	1.07E-003	2.04E-004	7.78E-004
100	-2.30E-001	3.02E-001	3.83E-004	7.96E-004	1.57E-004	5.89E-004
110	-2.00E-001	2.72E-001	3.05E-004	5.99E-004	1.05E-004	4.52E-004
120	-1.79E-001	2.51E-001	2.69E-004	4.77E-004	7.56E-005	3.73E-004
130	-1.63E-001	2.38E-001	2.40E-004	3.89E-004	6.98E-005	3.15E-004
140	-1.52E-001	2.32E-001	2.38E-004	3.81E-004	6.98E-005	3.09E-004
			----STANDARD DEVIATIONS----			
10	1.07E-002	2.79E-003	8.16E-005	2.00E-004	1.49E-004	1.53E-004
20	1.50E-002	1.61E-003	9.92E-005	2.88E-004	1.05E-004	2.15E-004
30	2.07E-002	5.58E-003	7.81E-005	1.33E-004	7.32E-005	1.09E-004
40	1.39E-002	3.22E-003	4.89E-005	9.34E-005	6.77E-005	7.46E-005
50	1.54E-002	3.22E-003	5.17E-005	9.20E-005	7.78E-005	7.47E-005
60	1.19E-002	2.55E-003	4.11E-005	8.69E-005	6.86E-005	6.80E-005
70	1.50E-002	3.95E-003	6.25E-005	1.17E-004	5.14E-005	9.40E-005
80	1.07E-002	4.26E-003	4.45E-005	6.98E-005	2.21E-005	5.85E-005
90	8.29E-003	2.35E-003	3.47E-005	4.60E-005	2.63E-005	4.07E-005
100	1.05E-002	1.27E-003	1.04E-005	3.95E-005	2.92E-005	2.89E-005
110	5.24E-003	2.79E-003	2.03E-005	5.61E-005	0.00E+000	4.22E-005
120	8.29E-003	3.22E-003	2.25E-005	1.98E-005	1.42E-005	2.12E-005
130	6.42E-003	1.27E-003	9.47E-006	3.07E-005	0.00E+000	2.27E-005
140	6.42E-003	1.61E-003	1.22E-005	2.20E-005	0.00E+000	1.78E-005

POSITION: I= 6, J= 8

TIME (SEC)	<U> (M/S)	<V> (M/S)	<u'**2> (M/S)**2	<v'**2> (M/S)**2	<u'v'> (M/S)**2	TKE (M/S)**2
			---MEAN VALUES---			
10	1.42E-002	-3.18E-002	3.54E-003	5.20E-003	5.66E-004	4.37E-003
20	1.83E-002	-2.93E-002	3.44E-003	5.03E-003	5.35E-004	4.24E-003
30	2.23E-002	-2.87E-002	3.17E-003	4.45E-003	5.76E-004	3.81E-003
40	2.44E-002	-3.87E-002	3.03E-003	4.25E-003	4.73E-004	3.64E-003
50	2.03E-002	-4.25E-002	2.67E-003	3.58E-003	3.60E-004	3.12E-003
60	2.44E-002	-4.74E-002	2.32E-003	2.90E-003	3.60E-004	2.61E-003
70	3.05E-002	-4.00E-002	1.96E-003	2.20E-003	3.09E-004	2.08E-003
80	2.64E-002	-3.25E-002	1.55E-003	1.57E-003	2.26E-004	1.56E-003
90	3.05E-002	-2.12E-002	1.25E-003	1.05E-003	1.44E-004	1.15E-003
100	2.84E-002	-1.94E-002	1.07E-003	7.55E-004	1.03E-004	9.10E-004
110	3.25E-002	-1.75E-002	9.65E-004	5.54E-004	1.13E-004	7.60E-004
120	2.64E-002	-1.25E-002	8.96E-004	4.32E-004	1.03E-004	6.64E-004
130	2.84E-002	-7.49E-003	8.70E-004	3.65E-004	8.23E-005	6.18E-004
140	2.64E-002	-5.62E-003	8.61E-004	3.17E-004	7.20E-005	5.89E-004
			---STANDARD DEVIATIONS---			
10	1.54E-002	1.02E-002	1.59E-004	4.40E-004	2.39E-004	3.31E-004
20	8.50E-003	4.19E-003	3.39E-004	5.83E-004	1.39E-004	4.77E-004
30	8.50E-003	1.40E-003	1.11E-004	3.14E-004	2.80E-004	2.36E-004
40	5.56E-003	8.14E-003	1.19E-004	3.66E-004	1.23E-004	2.72E-004
50	7.18E-003	6.84E-003	1.16E-004	2.52E-004	1.59E-004	1.97E-004
60	5.56E-003	5.13E-003	7.93E-005	1.98E-004	8.91E-005	1.51E-004
70	7.18E-003	2.61E-003	1.05E-004	1.45E-004	6.30E-005	1.27E-004
80	5.56E-003	7.19E-003	7.31E-005	7.64E-005	4.60E-005	7.48E-005
90	7.18E-003	3.42E-003	5.24E-005	7.33E-005	4.30E-005	6.37E-005
100	8.50E-003	4.07E-003	5.54E-005	3.97E-005	3.64E-005	4.82E-005
110	8.50E-003	2.79E-003	6.98E-005	5.44E-005	2.30E-005	6.26E-005
120	9.08E-003	4.94E-003	4.18E-005	5.00E-005	0.00E+000	4.61E-005
130	4.54E-003	4.73E-003	6.34E-005	6.46E-005	2.82E-005	6.40E-005
140	5.56E-003	2.61E-003	6.98E-005	3.47E-005	2.82E-005	5.51E-005

POSITION: I= 6,   J= 12

TIME (SEC)	<U> (M/S)	<V> (M/S)	<u'**2> (M/S)**2	<v'**2> (M/S)**2	<u'v'> (M/S)**2	TKE (M/S)**2
--MEAN VALUES--						
10	-2.05E-001	-6.82E-002	7.17E-003	7.31E-003	7.77E-004	7.24E-003
20	-1.98E-001	-6.56E-002	6.84E-003	6.48E-003	8.73E-004	6.66E-003
30	-1.91E-001	-6.35E-002	6.34E-003	5.57E-003	7.09E-004	5.96E-003
40	-1.78E-001	-5.88E-002	5.86E-003	4.75E-003	6.68E-004	5.31E-003
50	-1.69E-001	-5.41E-002	5.15E-003	3.88E-003	6.14E-004	4.51E-003
60	-1.59E-001	-4.58E-002	4.17E-003	3.02E-003	4.23E-004	3.60E-003
70	-1.39E-001	-4.06E-002	3.30E-003	2.17E-003	3.14E-004	2.74E-003
80	-1.20E-001	-3.54E-002	2.61E-003	1.53E-003	2.59E-004	2.07E-003
90	-9.99E-002	-2.81E-002	2.07E-003	1.13E-003	2.32E-004	1.60E-003
100	-9.31E-002	-2.60E-002	1.66E-003	8.28E-004	1.50E-004	1.24E-004
110	-7.96E-002	-2.39E-002	1.49E-003	6.43E-004	1.23E-004	1.06E-003
120	-6.94E-002	-1.92E-002	1.33E-003	4.90E-004	8.18E-005	9.12E-004
130	-6.60E-002	-1.77E-002	1.23E-003	4.31E-004	8.18E-005	8.29E-004
140	-6.09E-002	-1.40E-002	1.18E-003	3.71E-004	8.18E-005	7.75E-004
--STANDARD DEVIATIONS--						
10	1.35E-002	4.59E-003	3.28E-004	8.04E-004	3.54E-004	6.14E-004
20	1.07E-002	6.55E-003	3.12E-004	4.57E-004	2.91E-004	3.92E-004
30	1.35E-002	8.76E-003	2.64E-004	4.87E-004	2.05E-004	3.92E-004
40	1.54E-002	5.00E-003	3.35E-004	3.40E-004	9.56E-005	3.38E-004
50	1.23E-002	5.10E-003	2.95E-004	4.24E-004	1.00E-004	3.65E-004
60	1.39E-002	5.47E-003	2.09E-004	2.35E-004	9.56E-005	2.22E-004
70	1.05E-002	5.58E-003	2.80E-004	1.83E-004	9.56E-005	2.36E-004
80	9.99E-003	4.26E-003	1.62E-004	1.25E-004	8.04E-005	1.45E-004
90	4.15E-003	2.79E-003	1.08E-004	9.63E-005	6.16E-005	1.02E-004
100	9.99E-003	2.55E-003	9.09E-005	8.50E-005	3.34E-005	8.80E-005
110	9.99E-003	3.22E-003	8.69E-005	6.37E-005	6.84E-005	7.62E-005
120	3.22E-003	4.15E-003	5.75E-005	5.99E-005	0.00E+000	5.87E-005
130	5.56E-003	3.22E-003	7.25E-005	5.85E-005	5.17E-005	6.59E-005
140	6.42E-003	1.71E-003	2.66E-005	4.81E-005	5.17E-005	3.89E-005

POSITION: I= 6, J= 16

TIME (SEC)	<U> (M/S)	<V> (M/S)	<u'**2> (M/S)**2	<v'**2> (M/S)**2	<u'v'> (M/S)**2	TKE (M/S)**2
			---MEAN VALUES---			
10	-6.37E-001	2.95E-001	1.26E-002	6.22E-003	4.82E-003	9.41E-003
20	-6.28E-001	2.88E-001	1.21E-002	6.07E-003	4.60E-003	9.09E-003
30	-6.24E-001	2.74E-001	1.07E-002	5.54E-003	3.96E-003	8.14E-003
40	-6.04E-001	2.58E-001	9.67E-003	4.94E-003	3.51E-003	7.30E-003
50	-5.67E-001	2.40E-001	8.62E-003	4.15E-003	2.99E-003	6.39E-003
60	-5.22E-001	2.19E-001	6.91E-003	3.36E-003	2.35E-003	5.13E-003
70	-4.70E-001	1.98E-001	5.54E-003	2.64E-003	1.86E-003	4.09E-003
80	-4.16E-001	1.75E-001	4.46E-003	2.11E-003	1.46E-003	3.29E-003
90	-3.63E-001	1.55E-001	3.63E-003	1.63E-003	1.11E-003	2.63E-003
100	-3.18E-001	1.40E-001	3.06E-003	1.25E-003	8.77E-004	2.16E-003
110	-2.76E-001	1.28E-001	2.53E-003	9.77E-004	6.43E-004	1.75E-003
120	-2.47E-001	1.17E-001	2.18E-003	7.55E-004	4.97E-004	1.47E-003
130	-2.28E-001	1.10E-001	2.09E-003	6.47E-004	4.24E-004	1.37E-003
140	-2.21E-001	1.09E-001	1.98E-003	5.85E-004	4.09E-004	1.28E-003
			---STANDARD DEVIATIONS---			
10	4.96E-003	3.97E-003	4.10E-004	1.82E-004	3.26E-004	3.17E-004
20	1.37E-002	5.90E-003	6.01E-004	3.76E-004	2.57E-004	5.02E-004
30	5.43E-003	3.34E-003	2.41E-004	2.33E-004	1.84E-004	2.37E-004
40	1.15E-002	5.62E-003	4.46E-004	3.24E-004	1.14E-004	3.90E-004
50	3.84E-003	3.79E-003	3.71E-004	1.80E-004	1.84E-004	2.92E-004
60	5.43E-003	2.36E-003	2.46E-004	1.30E-004	1.18E-004	1.97E-004
70	9.66E-003	3.54E-003	2.68E-004	9.38E-005	1.50E-004	2.01E-004
80	8.29E-003	1.80E-003	2.50E-004	9.02E-005	7.73E-005	1.88E-004
90	7.68E-003	2.36E-003	2.32E-004	5.62E-005	7.06E-005	1.69E-004
100	9.66E-003	2.97E-003	2.24E-004	4.51E-005	8.05E-005	1.62E-004
110	7.01E-003	2.15E-003	1.36E-004	3.88E-005	4.99E-005	1.00E-004
120	4.96E-003	3.54E-003	8.85E-005	3.98E-005	3.87E-005	6.86E-005
130	5.43E-003	1.52E-003	9.08E-005	4.98E-005	3.87E-005	7.32E-005
140	4.96E-003	1.52E-003	1.03E-004	1.94E-005	0.00E+000	7.45E-005

POSITION: I= 75, J= 2

TIME (SEC)	<U> (M/S)	<V> (M/S)	<u'**2> (M/S)**2	<v'**2> (M/S)**2	<u'v'> (M/S)**2	TKE (M/S)**2
			---MEAN VALUES---			
10	7.98E-001	-4.68E-003	4.01E-004	4.49E-004	-5.98E-005	4.25E-004
20	7.85E-001	-5.20E-003	3.85E-004	4.35E-004	-5.69E-005	4.10E-004
30	7.59E-001	-4.68E-003	3.56E-004	4.13E-004	-5.41E-005	3.85E-004
40	7.22E-001	-5.20E-003	3.31E-004	3.75E-004	-5.55E-005	3.53E-004
50	6.72E-001	-5.20E-003	2.94E-004	3.26E-004	-5.55E-005	3.10E-004
60	6.14E-001	-5.20E-003	2.49E-004	2.78E-004	-4.99E-005	2.64E-004
70	5.50E-001	-6.76E-003	2.02E-004	2.26E-004	-4.15E-005	2.14E-004
80	4.88E-001	-6.76E-003	1.58E-004	1.79E-004	-3.30E-005	1.68E-004
90	4.32E-001	-7.80E-003	1.22E-004	1.40E-004	-2.53E-005	1.31E-004
100	3.83E-001	-7.28E-003	9.52E-005	1.10E-004	-1.76E-005	1.02E-004
110	3.41E-001	-6.76E-003	7.73E-005	8.80E-005	-1.48E-005	8.26E-005
120	3.10E-001	-5.72E-003	6.53E-005	7.31E-005	-1.20E-005	6.92E-005
130	2.89E-001	-5.72E-003	5.87E-005	6.56E-005	-1.12E-005	6.21E-005
140	2.34E-001	-5.72E-003	5.70E-005	6.15E-005	-9.84E-006	5.93E-005
			---STANDARD DEVIATIONS---			
10	2.07E-003	1.71E-003	5.99E-006	4.62E-006	6.21E-006	5.35E-006
20	2.78E-003	1.61E-003	8.79E-006	5.03E-006	6.93E-006	7.16E-006
30	2.78E-003	1.71E-003	6.94E-006	6.23E-006	8.19E-006	6.60E-006
40	2.07E-003	1.61E-003	7.27E-006	6.89E-006	3.18E-006	7.09E-006
50	2.62E-003	1.61E-003	7.30E-006	7.30E-006	3.18E-006	7.30E-006
60	0.00E+000	1.61E-003	4.30E-006	5.73E-006	3.18E-006	5.07E-006
70	2.62E-003	1.27E-003	4.65E-006	2.00E-006	1.72E-006	3.58E-006
80	3.82E-003	1.27E-003	2.41E-006	3.58E-006	1.72E-006	3.05E-006
90	3.21E-003	1.71E-003	1.66E-006	3.37E-006	2.67E-006	2.66E-006
100	2.62E-003	1.61E-003	2.64E-006	2.00E-006	1.72E-006	2.34E-006
110	2.07E-003	1.27E-003	8.12E-007	1.15E-006	2.31E-006	9.98E-007
120	0.00E+000	1.27E-003	2.33E-006	2.31E-006	1.72E-006	2.32E-006
130	0.00E+000	1.27E-003	1.66E-006	2.31E-006	2.18E-006	2.01E-006
140	2.07E-003	2.35E-003	1.62E-006	1.22E-006	2.18E-006	1.44E-006

POSITION: I= 75,   J= 3

TIME (SEC)	<U> (M/S)	<V> (M/S)	<u'**2> (M/S)**2	<v'**2> (M/S)**2	<u'v'> (M/S)**2	TKE (M/S)**2
			---MEAN VALUES---			
10	8.18E-001	1.72E-002	4.72E-004	4.46E-004	-8.74E-005	4.59E-004
20	8.02E-001	1.72E-002	4.45E-004	4.30E-004	-8.59E-005	4.37E-004
30	7.77E-001	1.72E-002	4.06E-004	3.98E-004	-7.52E-005	4.02E-004
40	7.36E-001	1.72E-002	3.61E-004	3.56E-004	-6.67E-005	3.59E-004
50	6.86E-001	1.56E-002	3.08E-004	3.08E-004	-5.75E-005	3.09E-004
60	6.25E-001	1.56E-002	2.63E-004	2.57E-004	-4.99E-005	2.60E-004
70	5.61E-001	1.46E-002	2.15E-004	2.10E-004	-3.91E-005	2.13E-004
80	4.97E-001	1.35E-002	1.77E-004	1.66E-004	-3.60E-005	1.72E-004
90	4.41E-001	1.35E-002	1.41E-004	1.33E-004	-2.99E-005	1.37E-004
100	3.90E-001	1.40E-002	1.15E-004	1.06E-004	-2.22E-005	1.11E-004
110	3.43E-001	1.40E-002	9.63E-005	8.65E-005	-1.61E-005	9.14E-005
120	3.14E-001	1.40E-002	7.93E-005	7.34E-005	-1.30E-005	7.64E-005
130	2.94E-001	1.40E-002	7.02E-005	6.60E-005	-9.20E-006	6.81E-005
140	2.84E-001	1.46E-002	6.75E-005	7.42E-005	-9.20E-006	7.08E-005
			---STANDARD DEVIATIONS---			
10	0.00E+000	1.71E-003	6.97E-006	1.07E-005	5.82E-006	9.05E-006
20	0.00E+000	1.71E-003	1.16E-005	9.43E-006	3.76E-006	1.06E-005
30	0.00E+000	2.61E-003	1.05E-005	8.12E-006	6.29E-006	9.36E-006
40	0.00E+000	1.71E-003	1.23E-005	4.40E-006	6.98E-006	9.25E-006
50	2.07E-003	1.97E-003	8.53E-006	4.56E-006	4.83E-006	6.84E-006
60	0.00E+000	1.97E-003	4.59E-006	4.69E-006	4.52E-006	4.64E-006
70	2.78E-003	2.55E-003	2.99E-006	4.47E-006	4.83E-006	3.81E-006
80	2.07E-003	1.61E-003	2.77E-006	6.27E-006	1.88E-006	4.85E-006
90	2.07E-003	1.61E-003	3.87E-006	6.44E-006	2.52E-006	5.31E-006
100	2.07E-003	1.71E-003	4.15E-006	4.18E-006	1.88E-006	4.16E-006
110	0.00E+000	1.71E-003	2.87E-006	2.31E-006	2.52E-006	2.60E-006
120	2.07E-003	1.71E-003	2.48E-006	1.68E-006	1.88E-006	2.12E-006
130	2.07E-003	1.71E-003	1.93E-006	4.18E-006	0.00E+000	3.26E-006
140	2.07E-003	2.55E-003	2.48E-006	3.27E-005	0.00E+000	2.32E-005

POSITION: I = 75,   J = 4

TIME (SEC)	<U> (M/S)	<V> (M/S)	<u'**2> (M/S)**2	<v'**2> (M/S)**2	<u'v'> (M/S)**2	TKE (M/S)**2
			---MEAN VALUES---			
10	7.67E-001	3.62E-002	2.81E-003	1.68E-003	6.28E-004	2.24E-003
20	7.53E-001	3.68E-002	2.74E-003	1.61E-003	6.10E-004	2.17E-003
30	7.26E-001	3.62E-002	2.61E-003	1.50E-003	5.92E-004	2.05E-003
40	6.88E-001	3.37E-002	2.37E-003	1.38E-003	5.60E-004	1.88E-003
50	6.36E-001	3.06E-002	2.09E-003	1.21E-003	5.05E-004	1.65E-003
60	5.75E-001	2.75E-002	1.72E-003	1.01E-003	4.28E-004	1.37E-003
70	5.14E-001	2.50E-002	1.38E-003	8.09E-004	3.46E-004	1.10E-003
80	4.55E-001	2.25E-002	1.10E-003	6.38E-004	2.78E-004	8.66E-004
90	4.02E-001	2.19E-002	8.31E-004	4.86E-004	2.05E-004	6.58E-004
100	3.57E-001	2.00E-002	6.35E-004	3.79E-004	1.73E-004	5.07E-004
110	3.18E-001	1.87E-002	5.02E-004	2.97E-004	1.28E-004	3.99E-004
120	2.89E-001	1.81E-002	4.13E-004	2.45E-004	1.00E-004	3.29E-004
130	2.70E-001	1.81E-002	3.50E-004	2.17E-004	9.11E-005	2.83E-004
140	2.64E-001	1.69E-002	3.32E-004	2.08E-004	8.20E-005	2.70E-004
			---STANDARD DEVIATIONS---			
10	0.00E+000	1.71E-003	6.17E-005	4.34E-005	4.44E-005	5.34E-005
20	2.27E-003	1.40E-003	8.80E-005	2.05E-005	2.97E-005	6.39E-005
30	0.00E+000	1.71E-003	4.27E-005	2.34E-005	1.61E-005	3.45E-005
40	2.78E-003	1.40E-003	2.35E-005	4.78E-006	2.04E-005	1.69E-005
50	2.27E-003	1.40E-003	4.92E-005	2.58E-005	4.07E-005	3.93E-005
60	2.27E-003	1.40E-003	4.33E-005	1.32E-005	1.91E-005	3.20E-005
70	2.27E-003	2.21E-003	2.65E-005	1.17E-005	1.02E-005	2.05E-005
80	2.78E-003	1.40E-003	3.69E-005	8.74E-006	1.02E-005	2.68E-005
90	2.27E-003	2.21E-003	2.78E-005	1.17E-005	1.61E-005	2.13E-005
100	1.71E-003	1.71E-003	1.24E-005	1.46E-005	1.25E-005	1.36E-005
110	1.24E-003	2.78E-003	1.24E-005	6.18E-006	1.25E-005	9.80E-006
120	0.00E+000	0.00E+000	1.24E-005	6.18E-006	1.25E-005	9.80E-006
130	1.40E-003	1.40E-003	8.13E-006	3.91E-006	0.00E+000	6.38E-006
140	1.71E-003	0.00E+000	8.13E-006	7.31E-006	1.25E-005	7.73E-006

POSITION: I= 8, J= 6

TIME (SEC)	<U> (M/S)	<V> (M/S)	<u'**2> (M/S)**2	<v'**2> (M/S)**2	<u'v'> (M/S)**2	TKE (M/S)**2
			--MEAN VALUES---			
10	1.46E-001	-6.24E-003	2.78E-003	3.60E-003	8.82E-004	3.19E-003
20	1.46E-001	-9.36E-003	2.71E-003	3.46E-003	8.67E-004	3.09E-003
30	1.44E-001	-9.36E-003	2.47E-003	3.18E-003	6.98E-004	2.82E-003
40	1.42E-001	-4.99E-003	2.31E-003	2.92E-003	6.37E-004	2.61E-003
50	1.26E-001	-9.36E-003	2.07E-003	2.46E-003	4.99E-004	2.27E-003
60	1.14E-001	-8.12E-003	1.76E-003	1.89E-003	3.30E-004	1.82E-003
70	9.75E-002	-8.74E-003	1.53E-003	1.49E-003	2.76E-004	1.51E-003
80	9.55E-002	-4.99E-003	1.35E-003	1.10E-003	2.07E-004	1.23E-003
90	8.13E-002	-1.25E-003	1.22E-003	7.87E-004	1.53E-004	1.00E-003
100	7.11E-002	6.24E-004	1.13E-003	5.50E-004	1.15E-004	8.41E-004
110	6.30E-002	6.24E-004	1.05E-003	3.94E-004	8.44E-005	7.23E-004
120	5.69E-002	2.50E-003	1.02E-003	2.95E-004	6.90E-005	6.56E-004
130	5.08E-002	0.00E+000	1.01E-003	2.42E-004	6.14E-005	6.27E-004
140	5.08E-002	3.12E-003	1.01E-003	2.33E-004	6.90E-005	6.21E-004
			---STANDARD DEVIATIONS---			
10	9.08E-003	5.84E-003	2.84E-004	2.46E-004	1.05E-004	2.66E-004
20	5.56E-003	5.41E-003	1.97E-004	1.08E-004	6.97E-005	1.59E-004
30	4.54E-003	4.94E-003	1.66E-004	1.47E-004	5.00E-005	1.57E-004
40	0.00E+000	6.47E-003	6.20E-005	2.22E-004	1.00E-004	1.63E-004
50	5.56E-003	2.21E-003	1.56E-004	1.43E-004	5.42E-005	1.49E-004
60	4.54E-003	3.56E-003	8.57E-005	5.15E-005	5.82E-005	7.07E-005
70	5.56E-003	6.00E-003	7.20E-005	8.86E-005	5.00E-005	8.08E-005
80	5.56E-003	2.79E-003	6.88E-005	5.39E-005	5.15E-005	6.18E-005
90	7.18E-003	2.79E-003	5.97E-005	4.30E-005	0.00E+000	5.21E-005
100	7.18E-003	2.61E-003	6.92E-005	2.00E-005	2.71E-005	5.09E-005
110	8.50E-003	2.61E-003	6.58E-005	2.00E-005	1.72E-005	4.86E-005
120	5.56E-003	4.63E-003	7.66E-005	2.92E-005	1.72E-005	5.79E-005
130	0.00E+000	3.12E-003	6.84E-005	1.90E-005	2.10E-005	4.89E-005
140	0.00E+000	3.82E-003	9.12E-005	2.55E-005	1.72E-005	6.70E-005

POSITION: I = 8, J = 10

TIME (SEC)	<U> (M/S)	<V> (M/S)	<u'**2> (M/S)**2	<v'**2> (M/S)**2	<u'v'> (M/S)**2	TKE (M/S)**2
			---MEAN VALUES---			
10	-6.09E-003	-4.37E-002	4.06E-003	3.81E-003	5.52E-004	3.93E-003
20	-4.06E-003	-4.43E-002	3.82E-003	3.25E-003	5.15E-004	3.54E-003
30	-8.13E-003	-4.06E-002	3.61E-003	3.06E-003	4.60E-004	3.34E-003
40	-6.09E-003	-3.68E-002	3.35E-003	2.45E-003	3.96E-004	2.90E-003
50	-6.09E-003	-4.09E-002	2.98E-003	2.07E-003	3.59E-004	2.52E-003
60	0.00E+000	-3.18E-002	2.54E-003	1.50E-003	2.12E-004	2.02E-003
70	8.13E-003	-2.81E-002	2.20E-003	1.08E-003	1.47E-004	1.64E-003
80	-1.02E-002	-2.12E-002	1.87E-003	7.74E-004	1.29E-004	1.32E-003
90	8.13E-003	-1.69E-002	1.70E-003	5.32E-004	1.01E-004	1.11E-003
100	1.02E-002	-1.56E-002	1.55E-003	3.62E-004	7.36E-005	9.55E-004
110	6.09E-003	-1.06E-002	1.47E-003	2.73E-004	5.52E-005	8.73E-004
120	1.22E-002	-5.62E-003	1.44E-003	2.01E-004	4.60E-005	8.23E-004
130	1.42E-002	-6.24E-003	1.45E-003	1.79E-004	4.60E-005	8.16E-004
140	8.13E-003	-6.87E-003	1.43E-003	1.61E-004	4.60E-005	7.96E-004
			---STANDARD DEVIATIONS---			
10	1.54E-002	1.34E-002	2.50E-004	2.22E-004	3.44E-004	2.36E-004
20	1.16E-002	5.13E-003	2.79E-004	1.53E-004	1.36E-004	2.25E-004
30	1.67E-002	3.12E-003	2.14E-004	4.41E-004	1.08E-004	3.47E-004
40	9.08E-003	5.13E-003	1.39E-004	1.32E-004	6.98E-005	1.35E-004
50	1.16E-002	6.40E-003	1.74E-005	2.59E-004	8.23E-005	1.86E-004
60	1.24E-002	6.77E-003	1.78E-004	1.70E-004	4.12E-005	1.74E-004
70	4.54E-003	3.82E-003	1.79E-004	1.60E-004	6.00E-005	1.70E-004
80	7.18E-003	2.61E-003	1.67E-004	7.68E-005	2.06E-005	1.30E-004
90	8.50E-003	4.73E-003	2.44E-004	8.86E-005	2.06E-005	1.84E-004
100	1.02E-002	3.12E-003	2.28E-004	3.67E-005	2.52E-005	1.63E-004
110	5.56E-003	1.71E-003	2.60E-004	2.45E-005	2.06E-005	1.84E-004
120	8.50E-003	2.61E-003	2.70E-004	1.58E-005	0.00E+000	1.92E-004
130	9.08E-003	2.21E-003	2.90E-004	3.16E-005	0.00E+000	2.06E-004
140	1.32E-002	2.61E-003	2.60E-004	2.92E-005	0.00E+000	1.85E-004

POSITION: I= 8, J= 12

---MEAN VALUES---

TIME (SEC)	<U> (M/S)	<V> (M/S)	<u'**2> (M/S)**2	<v'**2> (M/S)**2	<u'v'> (M/S)**2	TKE (M/S)**2
10	-1.81E-001	-8.74E-003	5.56E-003	4.76E-003	1.42E-003	5.16E-003
20	-1.83E-001	-1.31E-002	5.32E-003	4.45E-003	1.31E-003	4.88E-003
30	-1.81E-001	-1.19E-002	4.96E-003	4.17E-003	1.33E-003	4.57E-003
40	-1.73E-001	-1.12E-002	4.69E-003	3.70E-003	1.18E-003	4.19E-003
50	-1.67E-001	-1.06E-002	4.15E-003	3.02E-003	9.18E-004	3.58E-003
60	-1.46E-001	-5.62E-003	3.40E-003	2.37E-003	7.56E-004	2.88E-003
70	-1.34E-001	-3.75E-003	2.78E-003	1.81E-003	5.40E-004	2.29E-003
80	-1.22E-001	-2.50E-001	2.39E-003	1.46E-003	4.43E-004	1.93E-003
90	-1.08E-001	0.00E+000	1.98E-003	1.06E-003	3.56E-004	1.52E-003
100	-8.13E-002	3.75E-003	1.66E-003	7.51E-004	2.70E-004	1.21E-003
110	-7.31E-002	5.62E-003	1.47E-003	5.56E-004	2.16E-004	1.01E-003
120	-6.91E-002	5.62E-003	1.38E-003	4.51E-004	1.73E-004	9.15E-004
130	-6.30E-002	6.24E-003	1.32E-003	3.88E-004	1.62E-004	8.53E-004
140	-6.09E-002	6.24E-003	1.31E-003	3.46E-004	1.51E-004	8.29E-004

---STANDARD DEVIATIONS---

TIME (SEC)	<U> (M/S)	<V> (M/S)	<u'**2> (M/S)**2	<v'**2> (M/S)**2	<u'v'> (M/S)**2	TKE (M/S)**2
10	1.32E-002	5.58E-003	1.72E-004	3.61E-004	2.79E-004	2.83E-004
20	1.90E-002	4.07E-003	1.93E-004	2.94E-004	8.87E-005	2.49E-004
30	1.51E-002	6.77E-003	2.73E-004	1.96E-004	1.82E-004	2.37E-004
40	1.61E-002	1.71E-003	2.96E-004	1.62E-004	7.04E-005	2.38E-004
50	1.54E-002	3.56E-003	2.39E-004	1.92E-004	1.38E-004	2.17E-004
60	1.16E-002	4.07E-003	1.37E-004	6.84E-005	7.64E-005	1.08E-004
70	1.51E-002	3.42E-003	1.20E-004	1.18E-004	3.82E-005	1.19E-004
80	1.24E-002	4.07E-003	1.20E-004	8.38E-005	2.42E-005	1.03E-004
90	5.56E-003	3.12E-003	1.79E-004	8.78E-005	4.83E-005	1.41E-004
100	1.24E-002	4.07E-003	1.41E-004	8.63E-005	7.64E-005	1.17E-004
110	1.11E-002	3.42E-003	1.45E-004	5.98E-005	3.82E-005	1.11E-004
120	1.11E-002	1.40E-003	1.63E-004	1.17E-005	2.42E-005	1.15E-004
130	1.32E-002	3.82E-003	1.17E-004	2.20E-005	0.00E+000	8.43E-005
140	1.24E-002	2.21E-003	1.10E-004	2.20E-005	2.42E-005	7.94E-005

POSITION: I= 8, J= 16

---MEAN VALUES---

TIME (SEC)	<U> (M/S)	<V> (M/S)	<u'**2> (M/S)**2	<v'**2> (M/S)**2	<u'v'> (M/S)**2	TKE (M/S)**2
10	-7.54E-001	7.37E-002	5.69E-003	5.54E-003	2.53E-003	5.62E-003
20	-7.41E-001	7.18E-002	5.48E-003	5.32E-003	2.44E-003	5.40E-003
30	-7.21E-001	6.12E-002	4.98E-003	4.85E-003	2.16E-003	4.92E-003
40	-6.91E-001	5.24E-002	4.46E-003	4.39E-003	1.96E-003	4.42E-003
50	-6.44E-001	4.62E-002	3.89E-003	3.97E-003	1.71E-003	3.93E-003
60	-5.89E-001	4.12E-002	3.29E-003	3.39E-003	1.39E-003	3.34E-003
70	-5.32E-001	3.93E-002	2.71E-003	2.78E-003	1.12E-003	2.74E-003
80	-4.75E-001	3.25E-002	2.13E-003	2.22E-003	8.38E-004	2.17E-003
90	-4.16E-001	3.50E-002	1.68E-003	1.75E-003	6.31E-004	1.72E-003
100	-3.68E-001	3.31E-002	1.41E-003	1.40E-003	5.03E-004	1.41E-003
110	-3.23E-001	3.18E-002	1.20E-003	1.10E-003	4.12E-004	1.15E-003
120	-2.88E-001	3.43E-002	1.06E-003	9.01E-004	3.48E-004	9.79E-004
130	-2.68E-001	3.62E-002	9.89E-004	7.85E-004	2.83E-004	8.87E-004
140	-2.62E-001	3.50E-002	9.61E-004	7.43E-004	2.83E-004	8.52E-004

---STANDARD DEVIATIONS---

TIME (SEC)	<U> (M/S)	<V> (M/S)	<u'**2> (M/S)**2	<v'**2> (M/S)**2	<u'v'> (M/S)**2	TKE (M/S)**2
10	4.54E-003	5.67E-003	2.24E-004	1.65E-004	8.40E-005	1.97E-004
20	7.18E-003	5.84E-003	2.93E-004	2.52E-004	8.40E-005	2.73E-004
30	0.00E+000	2.79E-003	1.24E-004	2.63E-004	1.62E-004	2.06E-004
40	7.18E-003	3.42E-003	1.98E-004	2.44E-004	1.91E-004	2.22E-004
50	5.56E-003	5.58E-003	2.55E-004	1.90E-004	1.26E-004	2.25E-004
60	0.00E+000	2.61E-003	1.01E-004	1.76E-004	5.76E-005	1.43E-004
70	5.56E-003	5.22E-003	1.29E-004	1.74E-004	5.76E-005	1.53E-004
80	4.54E-003	4.19E-003	6.19E-005	1.04E-004	6.44E-005	8.57E-005
90	7.18E-003	2.61E-003	8.82E-005	5.89E-005	5.39E-005	7.20E-005
100	2.61E-003	1.71E-003	7.07E-005	4.30E-005	2.88E-005	5.85E-005
110	1.71E-003	2.61E-003	4.45E-005	2.55E-005	3.53E-005	3.62E-005
120	2.61E-003	0.00E+000	3.41E-005	1.67E-005	3.53E-005	2.68E-005
130	5.56E-003	1.71E-003	4.18E-005	2.55E-005	3.53E-005	3.46E-005
140	4.54E-003	1.40E-003	2.85E-005	3.47E-005	3.53E-005	3.18E-005

POSITION: I= 10,   J= 2

TIME (SEC)	<U> (M/S)	<V> (M/S)	<u'**2> (M/S)**2	<v'**2> (M/S)**2	<u'v'> (M/S)**2	TKE (M/S)**2
			---MEAN VALUES---			
10	7.92E-001	1.14E-002	3.44E-004	4.06E-004	-4.43E-005	3.75E-004
20	7.79E-001	1.14E-002	3.32E-004	3.93E-004	-4.36E-005	3.62E-004
30	7.53E-001	1.14E-002	3.06E-004	3.67E-004	-4.15E-005	3.36E-004
40	7.18E-001	1.04E-002	2.76E-004	3.29E-004	-3.66E-005	3.02E-004
50	6.66E-001	1.04E-002	2.33E-004	2.85E-004	-3.16E-005	2.59E-004
60	6.10E-001	8.32E-003	1.91E-004	2.34E-004	-2.60E-005	2.13E-004
70	5.45E-001	4.68E-003	1.52E-004	1.87E-004	-1.83E-005	1.69E-004
80	4.83E-001	6.24E-003	1.16E-004	1.46E-004	-1.69E-005	1.31E-004
90	4.26E-001	5.72E-003	8.99E-005	1.14E-004	-1.20E-005	1.02E-004
100	3.76E-001	5.72E-003	7.00E-005	8.95E-005	-8.44E-006	7.97E-005
110	3.33E-001	5.72E-003	5.74E-005	7.23E-005	-7.03E-006	6.48E-005
120	3.01E-001	6.76E-003	4.87E-005	6.06E-005	-4.22E-006	5.47E-005
130	2.84E-001	6.24E-003	4.38E-005	5.52E-005	-4.22E-006	4.95E-005
140	2.74E-001	6.76E-003	4.21E-005	5.22E-005	-4.22E-006	4.71E-005
			---STANDARD DEVIATIONS---			
10	0.00E+000	1.61E-003	3.86E-006	8.33E-006	7.89E-006	6.49E-006
20	2.62E-003	2.55E-003	4.82E-006	5.60E-006	7.85E-006	5.22E-006
30	2.62E-003	1.61E-003	4.82E-006	6.63E-006	8.19E-006	7.25E-006
40	2.62E-003	1.61E-003	7.82E-006	5.83E-006	3.44E-006	6.49E-006
50	2.07E-003	1.61E-003	7.08E-006	3.92E-006	5.17E-006	5.72E-006
60	2.07E-003	1.61E-003	7.08E-006	3.85E-006	4.15E-006	3.96E-006
70	2.62E-003	1.71E-003	4.06E-006	4.83E-006	3.44E-006	4.02E-006
80	2.07E-003	1.97E-003	3.00E-006	4.42E-006	2.67E-006	3.45E-006
90	3.82E-003	1.27E-003	2.09E-006	2.20E-006	3.18E-006	2.26E-006
100	3.21E-003	1.27E-003	2.33E-006	2.00E-006	2.67E-006	1.77E-006
110	2.62E-003	1.27E-003	1.50E-007	1.15E-006	2.18E-006	9.98E-007
120	2.62E-003	1.27E-003	8.12E-007	1.68E-006	2.67E-006	1.42E-006
130	0.00E+000	0.00E+000	2.52E-006	1.83E-006	2.67E-006	2.20E-006
140	0.00E+000	1.27E-003	8.12E-007	1.83E-006	0.00E+000	1.41E-006

POSITION: I = 10, J = 4

TIME (SEC)	⟨U⟩ (M/S)	⟨V⟩ (M/S)	⟨u'**2⟩ (M/S)**2	⟨v'**2⟩ (M/S)**2	⟨u'v'⟩ (M/S)**2	TKE (M/S)**2
			----MEAN VALUES----			
10	7.55E-001	4.01E-002	2.28E-003	1.16E-003	4.92E-004	1.72E-003
20	7.41E-001	3.95E-002	2.20E-003	1.11E-003	4.78E-004	1.65E-003
30	7.16E-001	3.80E-002	2.07E-003	1.05E-003	4.53E-004	1.56E-003
40	6.80E-001	3.59E-002	1.87E-003	9.54E-004	4.07E-004	1.41E-003
50	6.32E-001	3.12E-002	1.61E-003	8.25E-004	3.57E-004	1.22E-003
60	5.75E-001	2.86E-002	1.31E-003	7.08E-004	3.03E-004	1.01E-003
70	5.14E-001	2.45E-002	1.05E-003	5.76E-004	2.38E-004	8.15E-004
80	4.55E-001	2.19E-002	8.18E-004	4.58E-004	1.87E-004	6.38E-004
90	4.03E-001	2.03E-002	6.34E-004	3.65E-004	1.47E-004	5.00E-004
100	3.55E-001	1.87E-002	4.97E-004	2.92E-004	1.16E-004	3.94E-004
110	3.17E-001	1.82E-002	3.89E-004	2.35E-004	9.34E-005	3.12E-004
120	2.89E-001	1.66E-002	3.11E-004	1.94E-004	7.36E-005	2.52E-004
130	2.70E-001	1.61E-002	2.71E-004	1.74E-004	6.23E-005	2.22E-004
140	2.60E-001	1.66E-002	2.55E-004	1.65E-004	5.94E-005	2.10E-004
			---STANDARD DEVIATIONS---			
10	2.62E-003	1.27E-003	4.62E-005	3.15E-005	4.02E-005	3.96E-005
20	3.21E-003	1.61E-003	6.67E-005	1.16E-005	2.50E-005	4.79E-005
30	3.21E-003	1.27E-003	3.79E-005	1.84E-005	8.77E-006	2.98E-005
40	2.07E-003	1.71E-003	4.24E-005	2.96E-005	1.86E-005	3.66E-005
50	2.78E-003	0.00E+000	4.40E-005	1.78E-005	1.52E-005	3.36E-005
60	2.07E-003	1.27E-003	2.69E-005	1.47E-005	1.28E-005	2.17E-005
70	2.07E-003	0.00E+000	1.76E-005	1.79E-005	1.07E-005	2.34E-005
80	2.78E-003	1.71E-003	1.79E-005	7.52E-006	1.07E-005	1.35E-005
90	2.62E-003	1.97E-003	2.03E-005	1.14E-005	1.39E-005	1.65E-005
100	3.21E-003	1.27E-003	1.36E-005	9.62E-006	1.28E-005	1.18E-005
110	2.62E-003	1.61E-003	6.35E-006	2.54E-006	9.30E-006	4.84E-006
120	2.07E-003	1.27E-003	1.14E-005	9.14E-006	8.77E-006	1.03E-005
130	2.07E-003	1.27E-003	9.47E-006	3.93E-006	8.77E-006	7.25E-006
140	2.07E-003	1.61E-003	1.27E-005	3.40E-006	9.30E-006	9.30E-006

POSITION: I= 10, J= 8

TIME (SEC)	<U> (M/S)	<V> (M/S)	<u'**2> (M/S)**2	<v'**2> (M/S)**2	<u'v'> (M/S)**2	TKE (M/S)**2
			---MEAN VALUES---			
10	8.73E-002	6.24E-003	2.25E-003	3.69E-003	3.45E-004	2.97E-003
20	8.94E-002	3.75E-003	2.14E-003	3.31E-003	3.11E-004	2.72E-003
30	8.94E-002	4.37E-003	1.93E-003	2.95E-003	2.55E-004	2.44E-003
40	8.94E-002	0.00E+000	1.85E-003	2.79E-003	2.07E-004	2.32E-003
50	8.94E-002	2.50E-003	1.61E-003	2.20E-003	1.86E-004	1.91E-003
60	8.33E-002	0.00E+000	1.36E-003	1.61E-003	1.79E-004	1.49E-003
70	7.11E-002	3.12E-003	1.09E-003	1.17E-003	1.24E-004	1.13E-003
80	6.30E-002	4.37E-003	9.03E-004	8.77E-004	1.04E-004	8.90E-004
90	5.89E-002	4.99E-003	7.62E-004	6.13E-004	6.21E-005	6.87E-004
100	9.41E-002	-2.08E-003	2.29E-003	3.51E-003	2.85E-004	2.86E-003
110	-1.99E-001	3.12E-003	4.39E-004	5.59E-004	1.16E-004	4.99E-004
120	-1.81E-001	4.37E-003	3.81E-004	4.43E-004	1.04E-004	4.12E-004
130	-1.69E-001	4.37E-003	3.49E-004	3.71E-004	7.59E-005	3.60E-004
140	-1.63E-001	3.75E-003	3.49E-004	3.31E-004	8.28E-005	3.40E-004
			---STANDARD DEVIATIONS---			
10	9.03E-003	7.96E-003	4.89E-005	3.34E-004	1.36E-004	2.38E-004
20	8.50E-003	3.42E-003	1.81E-004	6.15E-004	1.48E-004	4.53E-004
30	4.54E-003	4.73E-003	1.15E-004	2.05E-004	1.46E-004	1.66E-004
40	8.50E-003	3.82E-003	3.32E-005	1.34E-004	8.80E-005	9.75E-005
50	1.11E-002	4.07E-003	9.83E-005	1.40E-004	1.02E-004	1.21E-004
60	1.11E-002	4.41E-003	9.58E-005	2.92E-005	4.50E-005	7.08E-005
70	7.18E-003	2.21E-003	8.68E-005	7.52E-005	3.09E-005	8.12E-005
80	4.54E-003	2.79E-003	4.56E-005	7.32E-005	2.44E-005	6.09E-005
90	4.54E-003	3.56E-003	7.84E-005	4.06E-005	4.50E-005	6.25E-005
100	1.12E-002	0.00E+000	9.22E-005	2.65E-004	1.09E-004	1.99E-004
110	9.08E-003	1.71E-003	8.83E-005	1.58E-005	1.54E-005	6.35E-005
120	1.11E-002	1.21E-003	7.51E-005	3.32E-005	2.44E-005	5.81E-005
130	1.16E-002	1.21E-003	7.50E-005	2.00E-005	1.54E-005	5.49E-005
140	1.24E-002	1.40E-003	7.96E-005	1.00E-005	1.89E-005	5.67E-005

POSITION: I = 10, J = 14

TIME (SEC)	<U> (M/S)	<V> (M/S)	<u'**2> (M/S)**2	<v'**2> (M/S)**2	<u'v'> (M/S)**2	TKE (M/S)**2
			---MEAN VALUES---			
10	-4.77E-001	-1.12E-002	7.69E-003	7.16E-003	3.13E-003	7.42E-003
20	-4.71E-001	-9.36E-003	7.26E-003	6.85E-003	2.95E-003	7.06E-003
30	-4.65E-001	-1.37E-002	6.68E-003	6.17E-003	2.57E-003	6.42E-003
40	-4.39E-001	-1.06E-002	5.88E-003	5.61E-003	2.23E-003	5.74E-003
50	-4.18E-001	-1.25E-002	5.07E-003	5.07E-003	1.87E-003	5.07E-003
60	-3.82E-001	-8.12E-003	4.22E-003	4.03E-003	1.49E-003	4.12E-003
70	-3.47E-001	-3.75E-003	3.37E-003	3.26E-003	1.10E-003	3.31E-003
80	-3.09E-001	0.00E+000	2.64E-003	2.43E-003	7.53E-004	2.53E-003
90	-2.68E-001	4.37E-003	2.10E-003	1.84E-003	5.56E-004	1.97E-003
100	-2.32E-001	5.62E-003	1.73E-003	1.37E-003	4.25E-004	1.55E-003
110	-1.99E-001	6.24E-003	1.39E-003	9.94E-004	2.62E-004	1.19E-003
120	-1.81E-001	7.49E-003	1.20E-003	7.87E-004	2.45E-004	9.95E-004
130	-1.69E-001	7.49E-003	1.10E-003	6.60E-004	1.80E-004	8.81E-004
140	-1.63E-001	6.87E-003	1.10E-003	5.88E-004	1.96E-004	8.46E-004
			---STANDARD DEVIATIONS---			
10	7.18E-003	5.22E-003	3.17E-004	3.72E-004	4.27E-004	3.46E-004
20	5.56E-003	3.82E-003	4.88E-004	2.13E-004	4.13E-004	3.76E-004
30	1.32E-002	6.47E-003	2.82E-004	1.67E-004	2.28E-004	2.32E-004
40	8.50E-003	3.56E-003	2.89E-004	2.12E-004	1.07E-004	2.54E-004
50	8.50E-003	3.82E-003	2.57E-004	1.79E-004	1.57E-004	2.22E-004
60	5.56E-003	3.56E-003	2.03E-004	2.02E-004	1.77E-004	2.02E-004
70	8.50E-003	3.42E-003	8.93E-005	1.51E-004	1.10E-004	1.24E-004
80	5.56E-003	3.82E-003	2.05E-004	1.41E-004	6.84E-005	1.76E-004
90	5.56E-003	4.73E-003	2.37E-004	9.98E-005	3.66E-005	1.82E-004
100	8.50E-003	3.42E-003	3.11E-004	6.65E-005	3.66E-005	2.25E-004
110	9.08E-003	0.00E+000	2.79E-004	2.81E-005	3.66E-005	1.98E-004
120	1.11E-002	1.71E-003	2.37E-004	5.90E-005	5.79E-005	1.73E-004
130	1.16E-002	1.71E-003	2.37E-004	3.56E-005	3.66E-005	1.69E-004
140	1.24E-002	1.40E-003	2.51E-004	1.78E-005	4.48E-005	1.78E-004

POSITION: I = 12, J = 2

MEAN VALUES

TIME (SEC)	⟨U⟩ (M/S)	⟨V⟩ (M/S)	⟨u'**2⟩ (M/S)**2	⟨v'**2⟩ (M/S)**2	⟨u'v'⟩ (M/S)**2	TKE (M/S)**2
10	7.76E-001	-2.60E-003	3.44E-004	3.78E-004	-2.28E-005	3.61E-004
20	7.61E-001	-3.12E-003	3.23E-004	3.62E-004	-1.97E-005	3.42E-004
30	7.36E-001	-3.12E-003	2.99E-004	3.36E-004	-1.72E-005	3.18E-004
40	7.03E-001	-3.12E-003	2.70E-004	3.03E-004	-1.29E-005	2.87E-004
50	6.54E-001	-3.12E-003	2.31E-004	2.62E-004	-1.23E-005	2.46E-004
60	5.98E-001	-4.16E-003	1.89E-004	2.18E-004	-7.38E-006	2.04E-004
70	5.37E-001	-6.24E-003	1.49E-004	1.74E-004	-1.85E-006	1.62E-004
80	4.73E-001	-5.20E-003	1.18E-004	1.33E-004	-1.23E-006	1.25E-004
90	4.19E-001	-5.20E-003	9.18E-005	1.04E-004	-6.15E-007	9.79E-005
100	3.71E-001	-5.20E-003	7.31E-005	8.08E-005	6.15E-007	7.70E-005
110	3.30E-001	-5.72E-003	6.01E-005	6.39E-005	0.00E+000	6.20E-005
120	3.00E-001	-5.20E-003	5.23E-005	5.39E-005	-6.15E-007	5.31E-005
130	2.84E-001	-5.20E-003	4.77E-005	4.89E-005	-6.15E-007	4.83E-005
140	2.77E-001	-5.20E-003	4.62E-005	4.67E-005	0.00E+000	4.64E-005

STANDARD DEVIATIONS

TIME (SEC)	⟨U⟩ (M/S)	⟨V⟩ (M/S)	⟨u'**2⟩ (M/S)**2	⟨v'**2⟩ (M/S)**2	⟨u'v'⟩ (M/S)**2	TKE (M/S)**2
10	2.07E-003	1.27E-003	4.82E-006	5.40E-006	6.36E-006	5.12E-006
20	2.07E-003	1.97E-003	4.78E-006	3.90E-006	6.87E-006	4.36E-006
30	0.00E+000	0.00E+000	5.85E-006	5.50E-006	3.01E-006	5.68E-006
40	2.62E-003	0.00E+000	4.29E-006	5.13E-006	3.87E-006	4.73E-006
50	2.07E-003	1.61E-003	7.20E-006	3.09E-006	4.67E-006	5.54E-006
60	2.62E-003	0.00E+000	2.50E-006	3.45E-006	2.02E-006	3.01E-006
70	2.07E-003	1.61E-003	2.67E-006	3.88E-006	1.91E-006	3.33E-006
80	2.07E-003	1.61E-003	2.67E-006	2.20E-006	1.51E-006	2.44E-006
90	2.78E-003	1.61E-003	1.48E-006	3.88E-006	1.51E-006	2.94E-006
100	0.00E+000	1.61E-003	1.87E-006	2.38E-006	0.00E+000	2.14E-006
110	0.00E+000	1.27E-003	3.12E-006	1.19E-006	1.51E-006	2.36E-006
120	0.00E+000	1.61E-003	1.78E-006	1.53E-006	1.51E-006	1.66E-006
130	0.00E+000	1.61E-003	1.87E-006	2.38E-006	0.00E+000	2.14E-006
140	2.78E-003	1.61E-003	1.52E-006	2.20E-006	0.00E+000	1.89E-006

POSITION: I= 12, J= 6

----MEAN VALUES----

TIME <SEC>	<U> (M/S)	<V> (M/S)	<u'**2> (M/S)**2	<v'**2> (M/S)**2	<u'v'> (M/S)**2	TKE (M/S)**2
10	1.49E-001	7.58E-003	2.44E-003	2.53E-003	3.22E-004	2.48E-003
20	1.47E-001	7.14E-003	2.31E-003	2.40E-003	2.51E-004	2.35E-003
30	1.41E-001	6.24E-003	2.20E-003	2.19E-003	2.18E-004	2.20E-003
40	1.38E-001	4.91E-003	2.05E-003	1.90E-003	1.78E-004	1.98E-003
50	1.26E-001	2.68E-003	1.90E-003	1.63E-003	1.59E-004	1.76E-003
60	1.16E-001	4.01E-003	1.71E-003	1.25E-003	1.33E-004	1.48E-003
70	1.02E-001	1.78E-003	1.50E-003	9.38E-004	8.51E-005	1.22E-003
80	9.14E-002	0.00E+000	1.30E-003	6.76E-004	5.92E-005	9.88E-004
90	7.69E-002	-1.34E-003	1.15E-003	4.73E-004	3.33E-005	8.12E-004
100	6.53E-002	-1.78E-003	1.07E-003	3.47E-004	3.33E-005	7.06E-004
110	5.66E-002	-2.68E-003	1.01E-003	2.53E-004	1.85E-005	6.34E-004
120	4.79E-002	-3.12E-003	9.78E-004	1.98E-004	2.22E-005	5.88E-004
130	4.50E-002	-2.68E-003	9.55E-004	1.62E-004	1.11E-005	5.58E-004
140	4.06E-002	-4.46E-003	9.55E-004	1.51E-004	1.85E-005	5.53E-004

----STANDARD DEVIATIONS----

TIME <SEC>	<U> (M/S)	<V> (M/S)	<u'**2> (M/S)**2	<v'**2> (M/S)**2	<u'v'> (M/S)**2	TKE (M/S)**2
10	4.96E-003	6.95E-003	1.41E-004	2.11E-004	1.68E-004	1.80E-004
20	5.43E-003	5.01E-003	1.12E-004	1.02E-004	6.96E-005	1.07E-004
30	9.14E-003	4.41E-003	9.66E-005	1.42E-004	7.15E-005	1.22E-004
40	9.91E-003	3.97E-003	1.38E-004	1.03E-004	8.24E-005	1.22E-004
50	5.43E-003	4.20E-003	1.56E-004	1.08E-004	5.05E-005	1.34E-004
60	5.43E-003	3.91E-003	1.42E-004	8.21E-005	5.05E-005	1.16E-004
70	5.86E-003	2.46E-003	1.32E-004	5.02E-005	1.96E-005	1.00E-004
80	0.00E+000	2.55E-003	7.61E-005	3.96E-005	1.96E-005	6.06E-005
90	5.43E-003	2.46E-003	5.48E-005	2.70E-005	1.26E-005	4.32E-005
100	1.67E-003	1.67E-003	5.16E-005	1.90E-005	1.26E-005	3.89E-005
110	5.43E-003	2.15E-003	4.89E-005	8.68E-006	1.26E-005	3.51E-005
120	4.96E-003	1.80E-003	5.48E-005	1.58E-005	9.78E-006	4.03E-005
130	5.43E-003	2.15E-003	4.97E-005	1.53E-005	1.38E-005	3.67E-005
140	0.00E+000	1.67E-003	4.91E-005	1.62E-005	1.26E-005	3.65E-005

POSITION: I= 12,   J= 10

TIME (SEC)	<U> (M/S)	<U> (M/S)	<u'**2> (M/S)**2	<v'**2> (M/S)**2	<u'v'> (M/S)**2	TKE (M/S)**2
			----MEAN VALUES----			
10	-3.19E-002	2.23E-002	1.97E-003	1.68E-003	3.57E-004	1.82E-003
20	-3.05E-002	2.41E-002	1.94E-003	1.56E-003	3.57E-004	1.75E-003
30	-3.48E-002	2.01E-002	1.76E-003	1.45E-003	2.92E-004	1.61E-003
40	-3.05E-002	2.23E-002	1.67E-003	1.20E-003	2.48E-004	1.43E-003
50	-3.48E-002	1.61E-002	1.51E-003	1.00E-003	1.99E-004	1.26E-003
60	-2.90E-002	1.52E-002	1.37E-003	8.46E-004	1.74E-004	1.11E-003
70	-2.76E-002	1.16E-002	1.17E-003	5.75E-004	1.12E-004	8.75E-004
80	-2.47E-002	8.03E-003	1.06E-003	3.86E-004	6.83E-005	7.21E-004
90	-2.32E-002	7.58E-003	9.70E-004	2.66E-004	4.04E-005	6.18E-004
100	-2.18E-002	6.69E-003	9.26E-004	1.81E-004	3.41E-005	5.54E-004
110	-2.47E-002	5.80E-003	9.12E-004	1.39E-004	2.79E-005	5.26E-004
120	-2.32E-002	3.57E-003	8.96E-004	1.15E-004	2.17E-005	5.06E-004
130	-1.89E-002	3.12E-003	8.81E-004	9.30E-005	1.86E-005	4.87E-004
140	-2.03E-002		8.78E-004	8.50E-005	2.17E-005	4.81E-004
			---STANDARD DEVIATIONS---			
10	7.01E-003	4.20E-003	1.03E-004	1.73E-004	3.29E-005	1.42E-004
20	5.86E-003	6.91E-003	1.20E-004	1.58E-004	1.06E-004	1.40E-004
30	5.43E-003	4.72E-003	7.26E-005	1.29E-004	6.13E-005	1.05E-004
40	8.29E-003	6.09E-003	4.37E-005	7.28E-005	8.86E-005	6.01E-005
50	9.91E-003	4.91E-003	8.43E-005	8.88E-005	5.24E-005	8.66E-005
60	3.84E-003	5.82E-003	9.86E-005	1.14E-004	6.02E-005	1.06E-004
70	4.96E-003	3.47E-003	8.55E-005	4.75E-005	1.50E-005	6.91E-005
80	5.43E-003	4.36E-003	5.94E-005	5.22E-005	2.32E-005	5.59E-005
90	4.96E-003	3.05E-003	7.33E-005	4.13E-005	1.50E-005	5.95E-005
100	7.01E-003	1.67E-003	7.29E-005	2.28E-005	1.71E-005	5.40E-005
110	5.43E-003	3.34E-003	8.03E-005	2.66E-005	1.06E-005	5.98E-005
120	4.96E-003	2.81E-003	6.99E-005	1.91E-005	0.00E+000	5.13E-005
130	3.84E-003	3.79E-003	6.07E-005	5.47E-006	8.21E-006	4.31E-005
140	5.86E-003	2.55E-003	4.46E-005	1.09E-005	0.00E+000	3.25E-005

POSITION: I = 12, J = 14

TIME (SEC)	<U> (M/S)	<V> (M/S)	<u'**2> (M/S)**2	<v'**2> (M/S)**2	<u'v'> (M/S)**2	TKE (M/S)**2
			---MEAN VALUES---			
10	-5.08E-001	-1.98E-002	7.00E-003	8.37E-003	2.49E-003	7.69E-003
20	-5.01E-001	-2.08E-002	6.78E-003	7.96E-003	2.36E-003	7.37E-003
30	-4.88E-001	-2.08E-002	6.38E-003	7.37E-003	2.05E-003	6.87E-003
40	-4.69E-001	-1.82E-002	5.79E-003	6.55E-003	1.71E-003	6.17E-003
50	-4.40E-001	-1.61E-002	5.12E-003	5.52E-003	1.38E-003	5.32E-003
60	-4.05E-001	-1.35E-002	4.32E-003	4.50E-003	1.07E-003	4.41E-003
70	-3.64E-001	-1.04E-002	3.46E-003	3.54E-003	8.18E-004	3.50E-003
80	-3.27E-001	-5.72E-003	2.64E-003	2.56E-003	5.11E-004	2.60E-003
90	-2.89E-001	-3.64E-003	2.07E-003	1.95E-003	3.58E-004	2.01E-003
100	-2.56E-001	-3.12E-003	1.66E-003	1.47E-003	2.81E-004	1.57E-003
110	-2.32E-001	-2.60E-003	1.39E-003	1.13E-003	2.17E-004	1.26E-003
120	-2.12E-001	-1.56E-003	1.21E-003	9.08E-004	1.53E-004	1.06E-003
130	-2.01E-001	-1.56E-003	1.11E-003	7.55E-004	1.41E-004	9.33E-004
140	-1.98E-001	-2.08E-003	1.07E-003	7.09E-004	1.15E-004	8.88E-004
			---STANDARD DEVIATIONS---			
10	0.00E+000	2.55E-003	2.36E-004	3.41E-004	2.60E-004	2.93E-004
20	5.24E-003	1.61E-003	2.58E-004	3.77E-004	2.24E-004	3.23E-004
30	0.00E+000	3.78E-003	2.38E-004	5.08E-004	2.10E-004	3.97E-004
40	4.15E-003	5.38E-003	1.79E-004	3.40E-004	2.31E-004	2.72E-004
50	8.29E-003	3.65E-003	1.42E-004	1.58E-004	1.46E-004	1.50E-004
60	4.15E-003	5.10E-003	1.16E-004	1.71E-004	8.40E-005	1.46E-004
70	4.15E-003	1.61E-003	1.21E-004	1.28E-004	9.29E-005	1.25E-004
80	4.15E-003	2.35E-003	1.25E-004	1.28E-004	6.26E-005	1.26E-004
90	5.56E-003	3.07E-003	8.24E-005	8.50E-005	9.29E-005	8.37E-005
100	4.15E-003	3.42E-003	6.19E-005	5.03E-005	3.96E-005	5.64E-005
110	4.15E-003	2.35E-003	5.57E-005	6.49E-005	3.13E-005	6.05E-005
120	2.61E-003	2.61E-003	6.89E-005	2.99E-005	0.00E+000	5.31E-005
130	4.15E-003	2.61E-003	7.40E-005	3.56E-005	3.13E-005	5.80E-005
140	5.56E-003	1.61E-003	8.88E-005	3.91E-005	4.20E-005	6.86E-005

POSITION: I= 14, J= 4

TIME (SEC)	<U> (M/S)	<V> (M/S)	<u'**2> (M/S)**2	<v'**2> (M/S)**2	<u'v'> (M/S)**2	TKE (M/S)**2
			---MEAN VALUES---			
10	7.26E-001	6.56E-002	1.90E-003	1.28E-003	4.83E-004	1.59E-003
20	7.15E-001	6.47E-002	1.84E-003	1.27E-003	4.70E-004	1.55E-003
30	6.90E-001	6.20E-002	1.76E-003	1.20E-003	4.44E-004	1.48E-003
40	6.58E-001	5.89E-002	1.60E-003	1.10E-003	4.05E-004	1.35E-003
50	6.13E-001	5.49E-002	1.43E-003	9.79E-004	3.66E-004	1.20E-003
60	5.59E-001	4.86E-002	1.20E-003	8.37E-004	3.25E-004	1.02E-003
70	5.01E-001	4.24E-002	1.02E-003	7.24E-004	2.84E-004	8.72E-004
80	4.43E-001	3.75E-002	8.22E-004	5.81E-004	2.40E-004	7.02E-004
90	3.94E-001	3.39E-002	6.45E-004	4.59E-004	1.91E-004	5.52E-004
100	3.50E-001	3.03E-002	5.22E-004	3.85E-004	1.60E-004	4.53E-004
110	3.13E-001	2.90E-002	4.12E-004	2.97E-004	1.13E-004	3.55E-004
120	2.85E-001	2.59E-002	3.51E-004	2.52E-004	9.75E-005	3.02E-004
130	2.69E-001	2.54E-002	3.07E-004	2.31E-004	9.10E-005	2.69E-004
140	2.63E-001	2.54E-002	2.76E-004	2.09E-004	7.58E-005	2.42E-004
			---STANDARD DEVIATIONS---			
10	0.00E+000	4.03E-003	2.92E-005	7.14E-005	4.75E-005	5.45E-005
20	1.92E-003	4.31E-003	5.64E-005	8.09E-005	5.03E-005	6.97E-005
30	1.92E-003	3.79E-003	6.17E-005	7.93E-005	3.89E-005	7.11E-005
40	2.71E-003	3.79E-003	6.94E-005	5.59E-005	4.08E-005	6.30E-005
50	2.48E-003	5.05E-003	4.64E-005	5.84E-005	3.65E-005	5.27E-005
60	0.00E+000	5.05E-003	4.77E-005	3.94E-005	3.49E-005	4.37E-005
70	2.71E-003	5.05E-003	5.89E-005	5.65E-005	2.09E-005	5.77E-005
80	2.48E-003	4.03E-003	7.37E-005	6.59E-005	4.14E-005	6.99E-005
90	2.71E-003	3.79E-003	3.53E-005	2.72E-005	2.29E-005	3.15E-005
100	1.92E-003	4.67E-003	3.29E-005	2.46E-005	1.93E-005	2.90E-005
110	2.71E-003	3.91E-003	3.20E-005	1.66E-005	1.48E-005	2.55E-005
120	1.92E-003	3.91E-003	1.19E-005	1.52E-005	8.10E-006	1.36E-005
130	0.66E+000	4.57E-003	2.41E-005	1.70E-005	1.24E-005	2.09E-005
140	1.92E-003	4.57E-003	2.23E-005	1.60E-005	8.75E-006	1.94E-005

POSITION: I= 14, J= 8

TIME (SEC)	<U> (M/S)	<V> (M/S)	<u'**2> (M/S)**2	<v'**2> (M/S)**2	<u'v'> (M/S)**2	TKE (M/S)**2
			---MEAN VALUES---			
10	7.72E-002	3.00E-002	1.74E-003	1.62E-003	1.51E-004	1.68E-003
20	7.31E-002	2.75E-002	1.70E-003	1.55E-003	1.27E-004	1.62E-003
30	7.31E-002	2.50E-002	1.58E-003	1.40E-003	1.60E-004	1.49E-003
40	7.11E-002	2.43E-002	1.50E-003	1.21E-003	1.15E-004	1.35E-003
50	6.30E-002	2.62E-002	1.29E-003	9.86E-004	1.19E-004	1.10E-003
60	5.28E-002	2.31E-002	1.11E-003	6.66E-004	8.59E-005	8.89E-004
70	5.49E-002	2.19E-002	9.87E-004	5.21E-004	5.73E-005	7.54E-004
80	4.47E-002	2.06E-002	9.13E-004	3.66E-004	5.32E-005	6.40E-004
90	3.25E-002	1.81E-002	8.10E-004	2.80E-004	3.68E-005	5.45E-004
100	3.05E-002	1.62E-002	7.51E-004	2.01E-004	2.86E-005	4.76E-004
110	2.23E-002	1.37E-002	7.11E-004	1.51E-004	2.86E-005	4.31E-004
120	1.63E-002	1.06E-002	6.76E-004	1.19E-004	1.64E-005	3.97E-004
130	1.63E-002	9.99E-003	6.71E-004	9.94E-005	1.64E-005	3.85E-004
140	1.42E-002	9.99E-003	6.57E-004	9.54E-005	1.64E-005	3.76E-004
			---STANDARD DEVIATIONS---			
10	5.56E-003	3.56E-003	4.74E-005	1.15E-004	8.63E-005	8.81E-005
20	4.54E-003	4.63E-003	6.60E-005	8.97E-005	7.00E-005	7.87E-005
30	8.50E-003	6.62E-003	1.57E-004	1.28E-004	5.49E-005	1.44E-004
40	7.18E-003	7.12E-003	1.33E-004	1.62E-004	8.26E-005	1.48E-004
50	1.11E-002	7.19E-003	3.01E-005	7.78E-005	3.93E-005	5.90E-005
60	4.54E-003	2.79E-003	4.62E-005	3.30E-005	1.71E-005	4.01E-005
70	5.56E-003	2.21E-003	4.73E-005	3.19E-005	2.67E-005	4.03E-005
80	5.56E-003	2.79E-003	3.89E-005	2.27E-005	1.83E-005	3.19E-005
90	4.54E-003	1.40E-003	3.57E-005	3.10E-005	1.71E-005	3.34E-005
100	0.00E+000	1.40E-003	2.84E-005	1.63E-005	1.12E-005	2.32E-005
110	4.54E-003	1.71E-003	2.64E-005	1.30E-005	1.12E-005	2.08E-005
120	9.08E-003	4.19E-003	4.10E-005	1.22E-005	9.15E-006	3.03E-005
130	3.42E-003	3.42E-003	3.75E-005	9.94E-006	9.15E-006	2.74E-005
140	5.56E-003	1.40E-003	4.38E-005	8.89E-006	9.15E-006	3.16E-005

POSITION: I= 14,   J= 12

TIME (SEC)	$\langle U \rangle$ (M/S)	$\langle V \rangle$ (M/S)	$\langle u'{*}{*}2 \rangle$ (M/S)**2	$\langle v'{*}{*}2 \rangle$ (M/S)**2	$\langle u'v' \rangle$ (M/S)**2	TKE (M/S)**2
			---MEAN VALUES---			
10	-2.67E-001	2.01E-002	5.80E-003	6.02E-003	1.76E-003	5.91E-003
20	-2.66E-001	2.05E-002	5.62E-003	5.94E-003	1.72E-003	5.78E-003
30	-2.67E-001	1.65E-002	5.27E-003	5.30E-003	1.51E-003	5.29E-003
40	-2.52E-001	1.78E-002	4.73E-003	5.02E-003	1.48E-003	4.87E-003
50	-2.47E-001	1.11E-002	4.31E-003	4.18E-003	1.30E-003	4.25E-003
60	-2.28E-001	9.81E-003	3.52E-003	3.28E-003	1.02E-003	3.40E-003
70	-2.10E-001	8.03E-003	2.96E-003	2.58E-003	8.34E-004	2.77E-003
80	-1.96E-001	7.58E-003	2.33E-003	1.90E-003	6.42E-004	2.12E-003
90	-1.67E-001	7.14E-003	1.83E-003	1.37E-003	4.89E-004	1.60E-003
100	-1.51E-001	7.14E-003	1.45E-003	1.03E-003	3.36E-004	1.24E-003
110	-1.36E-001	6.24E-003	1.22E-003	8.14E-004	2.97E-004	1.02E-003
120	-1.22E-001	7.14E-003	1.04E-003	5.99E-004	2.21E-004	8.17E-004
130	-1.16E-001	7.58E-003	9.48E-004	4.94E-004	2.01E-004	7.21E-004
140	-1.07E-001	5.80E-003	9.11E-004	4.44E-004	1.92E-004	6.78E-004
			---STANDARD DEVIATIONS---			
10	9.66E-003	1.67E-003	1.94E-004	2.07E-004	1.96E-004	2.01E-004
20	7.01E-003	3.54E-003	1.10E-004	2.80E-004	2.25E-004	2.13E-004
30	9.66E-003	3.47E-003	2.22E-004	1.89E-004	2.15E-004	2.66E-004
40	1.60E-002	7.80E-003	3.02E-004	3.07E-004	1.94E-004	3.05E-004
50	9.66E-003	3.97E-003	2.24E-004	1.89E-004	1.77E-004	2.07E-004
60	5.43E-003	2.15E-003	1.75E-004	1.37E-004	1.25E-004	1.57E-004
70	7.68E-003	3.54E-003	1.45E-004	9.18E-005	1.01E-004	1.21E-004
80	7.68E-003	1.67E-003	1.53E-004	1.32E-004	5.28E-005	1.43E-004
90	5.43E-003	2.36E-003	1.59E-004	9.18E-005	5.07E-005	1.30E-004
100	3.84E-003	2.36E-003	9.49E-005	3.41E-005	5.48E-005	7.13E-005
110	5.43E-003	3.12E-003	6.82E-005	3.32E-005	3.59E-005	5.36E-005
120	5.86E-003	2.36E-003	6.82E-005	4.25E-005	3.27E-005	5.68E-005
130	5.43E-003	2.46E-003	7.86E-005	4.25E-005	3.87E-005	6.32E-005
140	5.43E-003	2.15E-003	6.63E-005	3.89E-005	2.54E-005	5.44E-005

POSITION: I= 14, J= 16
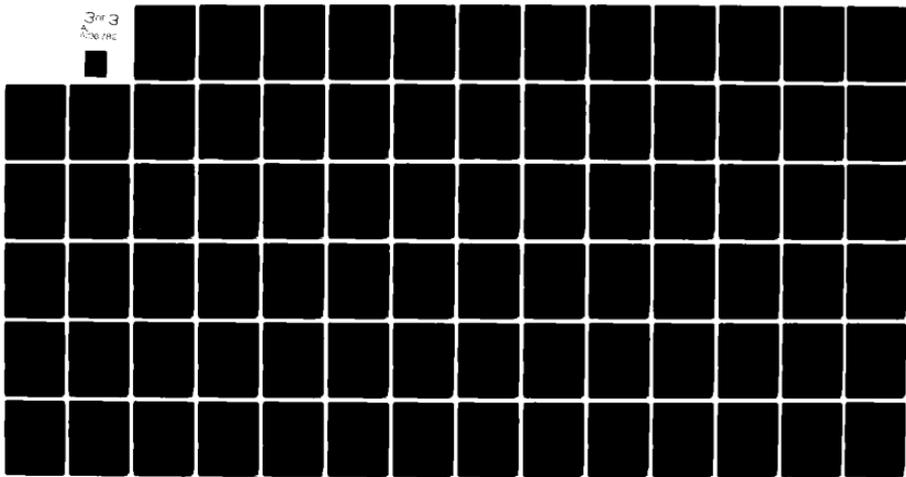
TIME (SEC)	<U> (M/S)	<U> (M/S)	<u'**2> (M/S)**2	<v'**2> (M/S)**2	<u'v'> (M/S)**2	TKE (M/S)**2
			---MEAN VALUES---			
10	-6.69E-001	-2.03E-002	4.68E-003	5.39E-003	1.47E-003	5.03E-003
20	-6.55E-001	-2.19E-002	4.59E-003	5.08E-003	1.39E-003	4.84E-003
30	-6.35E-001	-2.76E-002	4.41E-003	4.88E-003	1.35E-003	4.65E-003
40	-6.08E-001	-3.38E-002	4.11E-003	4.63E-003	1.20E-003	4.37E-003
50	-5.69E-001	-3.38E-002	3.75E-003	4.19E-003	1.01E-003	3.97E-003
60	-5.18E-001	-3.49E-002	3.41E-003	3.70E-003	9.09E-004	3.55E-003
70	-4.59E-001	-3.02E-002	3.03E-003	3.28E-003	8.01E-004	3.15E-003
80	-4.05E-001	-2.86E-002	2.58E-003	2.74E-003	6.03E-004	2.66E-003
90	-3.54E-001	-2.39E-002	2.25E-003	2.20E-003	4.77E-004	2.22E-003
100	-3.13E-001	-2.19E-002	1.91E-003	1.74E-003	3.42E-004	1.83E-003
110	-2.74E-001	-1.61E-002	1.69E-003	1.45E-003	2.88E-004	1.57E-003
120	-2.44E-001	-1.14E-002	1.54E-003	1.29E-003	2.61E-004	1.41E-003
130	-2.30E-001	-9.88E-003	1.44E-003	1.14E-003	2.16E-004	1.29E-003
140	-2.23E-001	-6.76E-003	1.40E-003	1.06E-003	1.98E-004	1.23E-003
			---STANDARD DEVIATIONS---			
10	4.15E-003	5.84E-003	1.46E-004	3.40E-004	1.79E-004	2.62E-004
20	5.56E-003	7.12E-003	1.75E-004	3.20E-004	1.51E-004	2.58E-004
30	5.56E-003	4.59E-003	2.21E-004	2.91E-004	1.41E-004	2.59E-004
40	4.15E-003	3.07E-003	2.07E-004	3.35E-004	1.25E-004	2.78E-004
50	0.00E+000	6.06E-003	1.58E-004	2.39E-004	1.01E-004	2.02E-004
60	0.00E+000	4.59E-003	1.24E-004	2.86E-004	5.31E-005	2.20E-004
70	4.15E-003	6.14E-003	1.28E-004	2.04E-004	2.20E-005	1.71E-004
80	4.15E-003	5.73E-003	1.04E-004	2.04E-004	5.31E-005	1.14E-004
90	4.15E-003	5.10E-003	7.86E-005	1.24E-004	4.07E-005	7.34E-005
100	4.15E-003	2.79E-003	6.19E-005	6.78E-005	2.79E-005	5.58E-005
110	0.00E+000	3.65E-003	7.03E-005	4.89E-005	2.79E-005	7.39E-005
120	0.00E+000	3.22E-003	6.02E-005	7.73E-005	4.07E-005	5.77E-005
130	5.24E-003	4.15E-003	1.43E-005	5.51E-005	3.42E-005	3.20E-005
140	0.00E+000	3.65E-003	4.57E-005	5.93E-005	2.79E-005	5.29E-005

POSITION: I= 16,   J= 4

TIME (SEC)	⟨U⟩ (M/S)	⟨V⟩ (M/S)	⟨u'**2⟩ (M/S)**2	⟨v'**2⟩ (M/S)**2	⟨u'v'⟩ (M/S)**2	TKE (M/S)**2
--- MEAN VALUES ---						
10	7.28E-001	9.00E-002	1.80E-003	1.25E-003	4.35E-004	1.53E-003
20	7.15E-001	8.88E-002	1.72E-003	1.22E-003	3.94E-004	1.47E-003
30	6.93E-001	8.64E-002	1.62E-003	1.15E-003	3.75E-004	1.38E-003
40	6.59E-001	8.08E-002	1.55E-003	1.12E-003	3.77E-004	1.34E-003
50	6.14E-001	7.38E-002	1.43E-003	1.06E-003	3.94E-004	1.24E-003
60	5.60E-001	6.61E-002	1.21E-003	8.83E-004	3.16E-004	1.05E-003
70	5.01E-001	5.75E-002	1.05E-003	7.92E-004	2.89E-004	9.20E-004
80	4.42E-001	5.03E-002	7.91E-004	6.05E-004	2.04E-004	6.94E-004
90	3.87E-001	4.35E-002	6.43E-004	4.85E-004	1.58E-004	5.64E-004
100	3.38E-001	3.71E-002	5.19E-004	3.93E-004	1.29E-004	4.54E-004
110	3.00E-001	3.24E-002	4.18E-004	3.23E-004	1.87E-004	3.70E-004
120	2.76E-001	3.03E-002	3.25E-004	2.42E-004	7.30E-005	2.83E-004
130	2.62E-001	2.85E-002	2.96E-004	2.20E-004	6.81E-005	2.58E-004
140	2.58E-001	2.82E-002	2.96E-004	2.17E-004	7.30E-005	2.57E-004
--- STANDARD DEVIATIONS ---						
10	2.48E-003	1.45E-003	5.78E-005	6.20E-005	6.43E-005	
20	2.48E-003	1.01E-003	5.88E-005	3.66E-005	3.64E-005	
30	2.71E-003	1.74E-003	6.57E-005	7.67E-005	8.34E-005	
40	3.84E-003	1.67E-003	9.94E-005	1.27E-004	8.96E-005	
50	3.50E-003	8.49E-004	6.64E-005	7.79E-005	1.15E-005	
60	3.84E-003	8.18E-004	6.01E-005	3.79E-005	2.92E-005	
70	2.71E-003	1.16E-003	6.22E-005	4.44E-005	4.81E-005	
80	4.15E-003	1.45E-003	5.13E-005	4.69E-005	2.78E-005	
90	6.83E-003	1.74E-003	6.88E-005	5.95E-005	3.66E-005	
100	4.00E-003	1.55E-003	4.77E-005	5.20E-005	2.75E-005	
110	4.57E-003	1.26E-003	2.25E-005	1.84E-005	1.62E-005	
120	2.71E-003	1.76E-004	1.76E-005	1.28E-005	8.31E-005	
130	2.71E-003	5.55E-004	2.14E-005	1.12E-005	1.39E-005	
140	2.48E-003	7.17E-004	2.68E-005	1.68E-005	1.29E-005	

192

POSITION: I = 16,   J = 8

TIME (SEC)	⟨U⟩ (M/S)	⟨V⟩ (M/S)	⟨u'**2⟩ (M/S)**2	⟨v'**2⟩ (M/S)**2	⟨u'v'⟩ (M/S)**2	TKE (M/S)**2
			---MEAN VALUES---			
10	5.25E-002	3.12E-002	1.54E-003	1.17E-003	8.89E-005	1.36E-003
20	5.59E-002	3.12E-002	1.53E-003	1.13E-003	1.16E-004	1.33E-003
30	5.59E-002	3.23E-002	1.49E-003	1.11E-003	9.70E-005	1.30E-003
40	5.25E-002	3.12E-002	1.30E-003	9.08E-004	9.70E-005	1.16E-003
50	3.89E-002	2.50E-002	1.14E-003	7.28E-004	8.35E-005	9.34E-004
60	3.22E-002	2.13E-002	9.98E-004	5.36E-004	5.66E-005	7.67E-004
70	3.05E-002	1.98E-002	8.72E-004	3.97E-004	4.58E-005	6.34E-004
80	2.03E-002	1.72E-002	7.49E-004	2.66E-004	2.16E-005	5.07E-004
90	1.69E-002	1.25E-002	6.70E-004	1.85E-004	1.35E-005	4.28E-004
100	1.02E-002	8.84E-003	6.26E-004	1.27E-004	1.62E-005	3.77E-004
110	5.08E-003	6.24E-003	6.02E-004	9.42E-005	8.08E-006	3.48E-004
120	6.77E-003	5.72E-003	5.91E-004	7.66E-005	1.08E-005	3.34E-004
130	6.77E-003	4.68E-003	5.86E-004	7.04E-005	1.35E-005	3.28E-004
140	3.39E-003	4.68E-003	5.72E-004	5.90E-005	5.39E-006	3.15E-004
			---STANDARD DEVIATIONS---			
10	9.99E-003	4.84E-003	1.11E-004	9.66E-005	5.48E-005	1.04E-004
20	1.07E-002	5.58E-003	1.61E-004	1.10E-004	8.40E-005	1.38E-004
30	1.07E-002	5.10E-003	1.10E-004	1.08E-004	6.86E-005	8.87E-005
40	7.65E-003	5.22E-003	6.37E-005	5.35E-005	3.54E-005	6.14E-005
50	4.15E-003	4.84E-003	6.84E-005	5.31E-005	4.39E-005	5.61E-005
60	9.99E-003	2.35E-003	5.90E-005	2.14E-005	3.35E-005	4.31E-005
70	6.42E-003	3.78E-003	5.70E-005	4.54E-005	2.79E-005	4.13E-005
80	6.42E-003	3.27E-003	3.67E-005	2.30E-005	1.32E-005	5.03E-005
90	5.24E-003	3.95E-003	6.73E-005	2.27E-005	1.59E-005	5.59E-005
100	0.00E+000	3.07E-003	7.58E-005	1.46E-005	1.02E-005	6.23E-005
110	5.56E-003	1.97E-003	8.70E-005	1.21E-005	1.35E-005	6.08E-005
120	5.24E-003	2.35E-003	8.51E-005	1.09E-005	8.35E-006	6.42E-005
130	5.24E-003	1.71E-003	9.01E-005	6.42E-006	6.60E-006	6.60E-005
140	5.24E-003	3.27E-003	7.13E-005	3.40E-006	1.32E-005	5.04E-005

POSITION: I = 16, J = 12

TIME (SEC)	<U> (M/S)	<V> (M/S)	<u'**2> (M/S)**2	<v'**2> (M/S)**2	<u'v'> (M/S)**2	TKE (M/S)**2
			—MEAN VALUES—			
10	-2.95E-001	2.68E-002	6.89E-003	7.51E-003	2.08E-003	7.20E-003
20	-2.92E-001	2.45E-002	6.61E-003	7.59E-003	2.01E-003	7.10E-003
30	-2.92E-001	1.96E-002	6.08E-003	7.09E-003	1.74E-003	6.59E-003
40	-2.80E-001	2.05E-002	5.60E-003	6.38E-003	1.61E-003	5.99E-003
50	-2.66E-001	1.43E-002	4.70E-003	5.22E-003	1.34E-003	4.96E-003
60	-2.47E-001	1.29E-002	3.73E-003	4.09E-003	9.47E-004	3.91E-003
70	-2.32E-001	8.92E-003	2.93E-003	3.14E-003	7.83E-004	3.04E-003
80	-2.06E-001	8.92E-003	2.24E-003	2.29E-003	5.84E-004	2.26E-003
90	-1.89E-001	8.03E-003	1.68E-003	1.67E-003	3.74E-004	1.68E-003
100	-1.71E-001	6.69E-003	1.32E-003	1.19E-003	2.81E-004	1.25E-003
110	-1.51E-001	6.24E-003	1.06E-003	8.63E-004	2.10E-004	9.64E-004
120	-1.41E-001	6.24E-003	8.78E-004	6.82E-004	1.52E-004	7.80E-004
130	-1.36E-001	4.91E-003	7.76E-004	5.51E-004	1.40E-004	6.63E-004
140	-1.31E-001	6.24E-003	7.58E-004	4.88E-004	1.17E-004	6.23E-004
			—STANDARD DEVIATIONS—			
10	1.02E-002	4.72E-003	2.65E-004	2.39E-004	2.83E-004	2.52E-004
20	1.40E-002	7.94E-003	3.09E-004	3.88E-004	3.23E-004	3.51E-004
30	9.66E-003	4.31E-003	1.90E-004	2.18E-004	1.13E-004	2.04E-004
40	9.91E-003	7.18E-003	1.65E-004	2.21E-004	1.22E-004	1.95E-004
50	9.14E-003	4.72E-003	9.68E-005	1.57E-004	1.63E-004	1.30E-004
60	4.96E-003	4.57E-003	1.21E-004	1.15E-004	1.48E-004	1.18E-004
70	7.01E-003	2.81E-003	1.21E-004	2.15E-004	1.32E-004	1.75E-004
80	7.68E-003	2.15E-003	1.20E-004	1.28E-004	8.75E-005	1.24E-004
90	5.43E-003	1.67E-003	1.06E-004	1.36E-004	6.44E-005	1.22E-004
100	3.84E-003	1.18E-003	1.02E-004	1.01E-004	4.37E-005	1.02E-004
110	3.84E-003	2.55E-003	6.75E-005	6.78E-005	4.37E-005	6.76E-005
120	3.84E-003	2.55E-003	5.66E-005	6.66E-005	3.09E-005	6.18E-005
130	5.43E-003	3.05E-003	4.11E-005	3.58E-005	3.99E-005	3.85E-005
140	7.01E-003	1.80E-003	5.43E-005	1.94E-005	4.37E-005	4.08E-005

POSITION: I = 16,   J = 16

TIME (SEC)	⟨U⟩ (M/S)	⟨V⟩ (M/S)	⟨u'**2⟩ (M/S)**2	⟨v'**2⟩ (M/S)**2	⟨u'v'⟩ (M/S)**2	TKE (M/S)**2
			---MEAN VALUES---			
10	-6.72E-001	-1.38E-002	3.94E-003	5.15E-003	1.07E-003	4.55E-003
20	-6.59E-001	-1.38E-002	3.79E-003	4.95E-003	1.00E-003	4.37E-003
30	-6.37E-001	-1.81E-002	3.60E-003	4.69E-003	9.20E-004	4.14E-003
40	-6.09E-001	-2.59E-002	3.33E-003	4.32E-003	8.44E-004	3.83E-003
50	-5.69E-001	-2.90E-002	3.19E-003	3.93E-003	7.13E-004	3.56E-003
60	-5.17E-001	-2.99E-002	2.90E-003	3.47E-003	6.29E-004	3.18E-003
70	-4.64E-001	-2.90E-002	2.50E-003	2.91E-003	5.14E-004	2.70E-003
80	-4.06E-001	-2.54E-002	2.25E-003	2.57E-003	4.99E-004	2.41E-003
90	-3.53E-001	-2.32E-002	1.93E-003	2.19E-003	3.76E-004	2.06E-003
100	-3.11E-001	-2.19E-002	1.59E-003	1.86E-003	3.22E-004	1.72E-003
110	-2.74E-001	-1.43E-002	1.33E-003	1.53E-003	2.99E-004	1.43E-003
120	-2.44E-001	-1.25E-002	1.17E-003	1.34E-003	2.61E-004	1.26E-003
130	-2.34E-001	-9.81E-003	1.05E-003	1.19E-003	2.22E-004	1.12E-003
140	-2.23E-001	-8.03E-003	9.84E-004	1.07E-003	2.22E-004	1.03E-003
			---STANDARD DEVIATIONS---			
10	3.84E-003	4.36E-003	1.46E-004	3.11E-004	2.07E-004	2.43E-004
20	3.84E-003	3.05E-003	1.88E-004	4.33E-004	1.19E-004	3.34E-004
30	4.96E-003	4.72E-003	1.34E-004	3.48E-004	1.22E-004	2.64E-004
40	0.00E+000	3.47E-003	1.46E-004	3.26E-004	7.41E-005	1.91E-004
50	5.86E-003	3.91E-003	2.11E-004	2.26E-004	1.30E-004	2.24E-004
60	3.84E-003	5.66E-003	9.64E-005	2.36E-004	1.27E-004	1.50E-004
70	4.96E-003	2.97E-003	1.06E-004	1.90E-004	9.73E-005	1.43E-004
80	5.86E-003	3.79E-003	1.06E-004	1.72E-004	9.15E-005	1.17E-004
90	4.96E-003	2.46E-003	8.41E-005	1.26E-004	7.59E-005	9.89E-005
100	5.43E-003	3.60E-003	9.57E-005	1.12E-004	5.37E-005	1.28E-004
110	0.00E+000	3.97E-003	7.97E-005	1.53E-004	2.87E-005	8.36E-005
120	0.00E+000	1.80E-003	7.84E-005	8.74E-005	3.70E-005	6.00E-005
130	0.00E+000	2.81E-003	7.90E-005	3.25E-005	3.70E-005	5.99E-005
140	0.00E+000	3.97E-003	5.94E-005	5.40E-005	2.03E-005	5.67E-005

POSITION: I = 18, J = 2

TIME (SEC)	<U> (M/S)	<U> (M/S)	<U'**2> (M/S)**2	<V'**2> (M/S)**2	<U'V'> (M/S)**2	TKE (M/S)**2
			----MEAN VALUES----			
10	6.59E-001	3.24E-002	3.20E-004	2.17E-004	-8.97E-007	2.68E-004
20	6.43E-001	3.15E-002	3.09E-004	2.12E-004	-3.59E-006	2.60E-004
30	6.27E-001	3.10E-002	2.81E-004	1.97E-004	-4.93E-006	2.39E-004
40	5.98E-001	2.96E-002	2.51E-004	1.75E-004	-5.38E-006	2.13E-004
50	5.58E-001	2.79E-002	2.14E-004	1.53E-004	-3.59E-006	1.84E-004
60	5.10E-001	2.55E-002	1.70E-004	1.26E-004	-5.38E-006	1.48E-004
70	4.60E-001	2.34E-002	1.34E-004	1.01E-004	-5.38E-006	1.18E-004
80	4.06E-001	2.08E-002	1.02E-004	7.69E-005	-3.14E-006	8.96E-005
90	3.60E-001	1.84E-002	7.89E-005	5.91E-005	-3.59E-006	6.90E-005
100	3.16E-001	1.66E-002	6.25E-005	4.53E-005	-2.24E-006	5.39E-005
110	2.83E-001	1.54E-002	5.04E-005	3.54E-005	-1.35E-006	4.29E-005
120	2.59E-001	1.42E-002	4.33E-005	2.92E-005	-8.97E-007	3.62E-005
130	2.42E-001	1.37E-002	3.95E-005	2.53E-005	-1.79E-006	3.24E-005
140	2.34E-001	1.35E-002	3.86E-005	2.33E-005	-8.97E-007	3.10E-005
			---STANDARD DEVIATIONS---			
10	2.07E-003	4.24E-004	1.01E-005	5.37E-006	2.78E-006	8.07E-006
20	2.78E-003	5.37E-004	1.13E-005	5.32E-006	3.26E-006	8.85E-006
30	2.78E-003	4.24E-004	1.12E-005	3.55E-006	3.15E-006	8.31E-006
40	2.62E-003	5.69E-004	7.38E-006	2.87E-006	3.40E-006	5.60E-006
50	2.07E-003	7.82E-004	7.46E-006	2.74E-006	2.20E-006	5.62E-006
60	2.78E-003	5.69E-004	2.88E-006	2.74E-006	3.81E-006	2.81E-006
70	2.78E-003	5.69E-004	3.98E-006	2.28E-006	1.70E-006	3.24E-006
80	3.21E-003	6.57E-004	2.42E-006	2.14E-006	2.03E-006	2.28E-006
90	2.07E-003	5.37E-004	2.08E-006	2.17E-006	1.39E-006	2.12E-006
100	3.82E-003	0.00E+000	1.04E-006	1.29E-006	2.03E-006	1.17E-006
110	2.07E-003	4.24E-004	8.49E-007	4.50E-007	1.47E-006	6.79E-007
120	2.62E-003	5.37E-004	1.34E-006	9.22E-007	1.39E-006	1.15E-006
130	2.62E-003	4.24E-004	1.04E-006	6.97E-007	1.39E-006	8.85E-007
140	2.07E-003	0.00E+000	9.01E-007	4.50E-007	1.39E-006	7.12E-007

POSITION: I = 18,   J = 6

TIME (SEC)	<U> (M/S)	<V> (M/S)	<u'**2> (M/S)**2	<v'**2> (M/S)**2	<u'v'> (M/S)**2	TKE (M/S)**2
			---MEAN VALUES---			
10	2.29E-001	1.02E-001	6.03E-003	6.58E-003	2.78E-003	6.31E-003
20	2.29E-001	1.00E-001	5.81E-003	6.25E-003	2.57E-003	6.03E-003
30	2.23E-001	9.72E-002	5.55E-003	5.95E-003	2.32E-003	5.75E-003
40	1.97E-001	8.78E-002	4.63E-003	5.00E-003	1.92E-003	4.86E-003
50	1.81E-001	7.89E-002	3.84E-003	4.26E-003	1.54E-003	4.05E-003
60	1.60E-001	6.73E-002	3.10E-003	3.45E-003	1.19E-003	3.28E-003
70	1.33E-001	5.80E-002	2.26E-003	2.55E-003	7.81E-004	2.40E-003
80	1.18E-001	4.91E-002	1.74E-003	1.90E-003	5.65E-004	1.82E-003
90	1.02E-001	4.28E-002	1.38E-003	1.42E-003	4.01E-004	1.40E-003
100	8.42E-002	3.75E-002	1.12E-003	1.06E-003	3.08E-004	1.09E-003
110	7.55E-002	3.26E-002	9.51E-004	7.79E-004	2.36E-004	8.65E-004
120	6.67E-002	2.99E-002	8.51E-004	6.09E-004	1.85E-004	7.30E-004
130	6.38E-002	2.94E-002	7.82E-004	5.54E-004	1.54E-004	6.68E-004
140	6.09E-002	2.90E-002	7.82E-004	5.29E-004	1.64E-004	6.56E-004
			---STANDARD DEVIATIONS---			
10	7.99E-003	3.91E-003	5.65E-004	5.84E-004	3.23E-004	5.74E-004
20	7.99E-003	4.20E-003	2.76E-004	3.78E-004	1.59E-004	3.31E-004
30	5.86E-003	3.79E-003	3.39E-004	5.01E-004	2.71E-004	4.28E-004
40	7.99E-003	3.79E-003	1.64E-004	2.31E-004	1.08E-004	2.00E-004
50	7.01E-003	3.91E-003	2.66E-004	2.30E-004	1.65E-004	2.49E-004
60	4.96E-003	3.97E-003	1.50E-004	1.23E-004	8.15E-005	1.13E-004
70	3.84E-003	2.46E-003	1.05E-004	1.84E-004	6.47E-005	1.68E-004
80	5.43E-003	3.47E-003	7.31E-005	1.29E-004	6.47E-005	1.17E-004
90	8.29E-003	3.12E-003	7.22E-005	1.86E-004	5.66E-005	9.13E-005
100	4.96E-003	1.67E-003	4.12E-005	1.86E-004	6.84E-005	9.10E-005
110	5.43E-003	1.67E-003	3.70E-005	5.60E-005	5.44E-005	4.92E-005
120	5.43E-003	1.67E-003	4.98E-005	4.88E-005	3.84E-005	4.34E-005
130	4.96E-003	1.67E-003	4.98E-005	4.70E-005	2.72E-005	4.84E-005
140	0.00E+000	2.36E-003	4.49E-005	3.74E-005	3.51E-005	4.13E-005

POSITION: I= 18,   J= 10

TIME (SEC)	<U> (M/S)	<V> (M/S)	<u'**2> (M/S)**2	<v'**2> (M/S)**2	<u'v'> (M/S)**2	TKE (M/S)**2
			---MEAN VALUES---			
10	-6.30E-002	5.43E-002	1.61E-003	1.38E-003	3.95E-004	1.50E-003
20	-6.30E-002	5.24E-002	1.60E-003	1.33E-003	3.11E-004	1.47E-003
30	-6.09E-002	5.37E-002	1.54E-003	1.26E-003	2.95E-004	1.40E-003
40	-5.89E-002	5.12E-002	1.45E-003	1.11E-003	2.76E-004	1.28E-003
50	-5.89E-002	4.50E-002	1.25E-003	9.14E-004	2.07E-004	1.08E-003
60	-5.28E-002	3.75E-002	1.08E-003	7.08E-004	1.80E-004	8.91E-004
70	-4.88E-002	3.43E-002	8.97E-004	4.86E-004	1.38E-004	6.91E-004
80	-4.67E-002	3.02E-002	7.91E-004	3.65E-004	9.97E-005	5.78E-004
90	-4.47E-002	2.65E-002	7.34E-004	2.67E-004	8.44E-005	5.01E-004
100	-4.27E-002	2.25E-002	6.67E-004	1.83E-004	5.75E-005	4.25E-004
110	-3.86E-002	2.00E-002	6.42E-004	1.29E-004	3.83E-005	3.86E-004
120	-4.06E-002	1.62E-002	6.12E-004	9.96E-005	3.45E-005	3.56E-004
130	-3.86E-002	1.56E-002	5.96E-004	9.26E-005	2.68E-005	3.44E-004
140	-3.25E-002	1.56E-002	5.93E-004	1.08E-004	1.92E-005	3.51E-004
			---STANDARD DEVIATIONS---			
10	4.54E-003	1.71E-003	1.20E-004	1.00E-004	7.98E-005	1.11E-004
20	8.50E-003	2.61E-003	1.03E-004	1.08E-004	5.15E-005	1.06E-004
30	7.18E-003	1.40E-003	8.70E-005	8.50E-005	5.52E-005	8.60E-005
40	4.54E-003	4.19E-003	8.00E-005	1.26E-004	6.30E-005	1.06E-004
50	3.56E-003	3.56E-003	5.01E-005	1.24E-004	4.16E-005	9.47E-005
60	2.21E-003	2.21E-003	4.79E-005	2.90E-005	2.91E-005	3.96E-005
70	2.21E-003	2.21E-003	8.59E-005	4.44E-005	2.84E-005	6.84E-005
80	9.08E-003	2.79E-003	9.68E-005	5.11E-005	1.60E-005	7.74E-005
90	5.56E-003	2.79E-003	8.40E-005	3.30E-005	1.05E-005	6.38E-005
100	4.54E-003	2.61E-003	6.12E-005	1.24E-005	1.36E-005	4.41E-005
110	4.54E-003	2.79E-003	5.91E-005	1.30E-005	0.00E+000	4.28E-005
120	0.00E+000	1.40E-003	7.34E-005	1.17E-005	8.58E-006	5.26E-005
130	4.54E-003	2.21E-003	6.92E-005	9.96E-006	1.05E-005	4.95E-005
140	4.54E-003	2.21E-003	6.84E-005	2.59E-005	0.00E+000	5.15E-005

POSITION: I= 18,   J= 14

TIME (SEC)	<U> (M/S)	<V> (M/S)	<u'**2> (M/S)**2	<v'**2> (M/S)**2	<u'v'> (M/S)**2	TKE (M/S)**2
			---MEAN VALUES---			
10	-4.09E-001	3.39E-002	7.32E-003	1.25E-002	4.24E-004	9.92E-003
20	-3.99E-001	3.48E-002	7.09E-003	1.25E-002	4.53E-004	9.78E-003
30	-3.83E-001	3.70E-002	6.85E-003	1.19E-002	4.09E-004	9.39E-003
40	-3.64E-001	3.88E-002	6.34E-003	1.07E-002	8.77E-005	8.51E-003
50	-3.42E-001	4.73E-002	5.62E-003	9.34E-003	1.75E-004	7.48E-003
60	-3.08E-001	4.86E-002	4.62E-003	7.76E-003	4.38E-005	6.19E-003
70	-2.79E-001	5.04E-002	3.76E-003	6.22E-003	-5.84E-005	4.99E-003
80	-2.48E-001	5.17E-002	2.92E-003	4.77E-003	-7.30E-005	3.85E-003
90	-2.23E-001	5.26E-002	2.39E-003	3.62E-003	-1.61E-004	3.01E-003
100	-2.03E-001	5.31E-002	1.86E-003	2.71E-003	-8.77E-005	2.29E-003
110	-1.86E-001	4.91E-002	1.55E-003	2.08E-003	-2.92E-005	1.81E-003
120	-1.73E-001	4.46E-002	1.32E-003	1.66E-003	-1.46E-005	1.49E-003
130	-1.64E-001	4.37E-002	1.22E-003	1.47E-003	-1.46E-005	1.35E-003
140	-1.63E-001	4.46E-002	1.17E-003	1.38E-003	-4.38E-005	1.28E-003
			---STANDARD DEVIATIONS---			
10	4.96E-003	2.81E-003	2.31E-004	7.56E-004	2.46E-004	5.59E-004
20	4.96E-003	4.57E-003	1.63E-004	3.97E-004	2.28E-004	3.03E-004
30	4.96E-003	6.60E-003	1.20E-004	6.02E-004	1.67E-004	4.34E-004
40	3.84E-003	5.94E-003	1.47E-004	6.61E-004	1.38E-004	4.79E-004
50	4.96E-003	6.60E-003	1.80E-004	3.38E-004	1.84E-004	2.71E-004
60	4.96E-003	9.34E-003	1.32E-004	1.72E-004	1.55E-004	1.53E-004
70	5.43E-003	5.53E-003	1.73E-004	1.91E-004	1.66E-004	1.82E-004
80	5.43E-003	3.54E-003	1.66E-004	7.55E-005	1.14E-004	1.29E-004
90	0.00E+000	6.60E-003	1.78E-004	1.67E-004	1.16E-004	1.72E-004
100	0.00E+000	4.41E-003	1.02E-004	1.23E-004	7.06E-005	1.13E-004
110	4.96E-003	2.97E-003	7.46E-005	1.18E-004	4.99E-005	9.88E-005
120	0.00E+000	3.47E-003	4.11E-005	1.33E-004	3.87E-005	9.83E-005
130	3.84E-003	4.03E-003	5.95E-005	9.29E-005	3.87E-005	7.80E-005
140	0.00E+000	3.47E-003	4.00E-005	4.70E-005	5.47E-005	4.36E-005

POSITION: I= 20, J= 4

---MEAN VALUES---

TIME (SEC)	<U> (M/S)	<V> (M/S)	<u'**2> (M/S)**2	<v'**2> (M/S)**2	<u'v'> (M/S)**2	TKE (M/S)**2
10	5.99E-001	1.99E-001	7.03E-004	4.66E-004	-7.07E-006	5.85E-004
20	5.87E-001	1.97E-001	6.78E-004	4.27E-004	-1.21E-005	5.53E-004
30	5.70E-001	1.88E-001	6.44E-004	4.07E-004	-5.05E-006	5.26E-004
40	5.43E-001	1.79E-001	5.91E-004	3.77E-004	3.03E-006	4.84E-004
50	5.07E-001	1.65E-001	5.22E-004	3.42E-004	2.02E-006	4.32E-004
60	4.65E-001	1.51E-001	4.38E-004	2.87E-004	7.07E-006	3.63E-004
70	4.18E-001	1.33E-001	3.42E-004	2.24E-004	4.04E-006	2.83E-004
80	3.71E-001	1.17E-001	2.66E-004	1.75E-004	4.04E-006	2.20E-004
90	3.29E-001	1.00E-001	2.10E-004	1.38E-004	4.04E-006	1.74E-004
100	2.89E-001	8.83E-002	1.62E-004	1.05E-004	3.03E-006	1.33E-004
110	2.59E-001	7.79E-002	1.27E-004	7.97E-005	3.03E-006	1.03E-004
120	2.35E-001	7.19E-002	1.04E-004	6.36E-005	2.02E-006	8.39E-005
130	2.23E-001	6.75E-002	9.19E-005	5.45E-005	1.01E-006	7.32E-005
140	2.18E-001	6.67E-002	8.76E-005	5.20E-005	2.02E-006	6.98E-005

---STANDARD DEVIATIONS---

TIME (SEC)	<U> (M/S)	<V> (M/S)	<u'**2> (M/S)**2	<v'**2> (M/S)**2	<u'v'> (M/S)**2	TKE (M/S)**2
10	0.00E+000	2.68E-003	2.06E-005	3.64E-005	1.55E-005	2.96E-005
20	2.62E-003	2.12E-003	1.65E-005	1.98E-005	1.88E-005	1.82E-005
30	2.62E-003	2.12E-003	2.00E-005	2.65E-005	1.11E-005	2.35E-005
40	0.00E+000	2.85E-003	1.25E-005	2.45E-005	9.95E-006	1.94E-005
50	2.07E-003	2.12E-003	1.70E-005	1.22E-005	1.56E-005	1.48E-005
60	2.78E-003	0.00E+000	1.88E-005	2.43E-005	5.95E-006	2.17E-005
70	2.62E-003	2.85E-003	1.81E-005	1.35E-005	6.25E-006	1.19E-005
80	0.00E+000	2.68E-003	7.91E-006	6.02E-006	8.27E-006	7.03E-006
90	2.07E-003	0.00E+000	1.36E-005	1.28E-005	9.12E-006	1.32E-005
100	0.00E+000	0.00E+000	1.13E-005	7.25E-006	5.87E-006	9.51E-006
110	0.00E+000	2.12E-003	9.26E-006	9.06E-006	5.07E-006	9.16E-006
120	2.62E-003	0.00E+000	6.37E-006	5.12E-006	3.13E-006	5.78E-006
130	0.00E+000	0.00E+000	3.64E-006	2.72E-006	2.47E-006	3.21E-006
140	2.07E-003	2.12E-003	3.82E-006	3.14E-006	3.13E-006	3.49E-006

POSITION: I = 20, J = 8

---MEAN VALUES---

TIME (SEC)	<U> (M/S)	<V> (M/S)	<u'**2> (M/S)**2	<v'**2> (M/S)**2	<u'v'> (M/S)**2	TKE (M/S)**2
10	6.91E-002	1.31E-001	2.23E-003	3.13E-003	3.48E-004	2.68E-003
20	6.70E-002	1.29E-001	2.21E-003	2.94E-003	3.71E-004	2.58E-003
30	5.89E-002	1.22E-001	2.08E-003	2.81E-003	3.99E-004	2.45E-003
40	4.67E-002	1.11E-001	1.92E-003	2.50E-003	3.31E-004	2.21E-003
50	4.06E-002	1.02E-001	1.72E-003	2.02E-003	2.68E-004	1.87E-003
60	3.25E-002	8.93E-002	1.43E-003	1.58E-003	1.54E-004	1.50E-003
70	2.03E-002	7.80E-002	1.18E-003	1.13E-003	1.20E-004	1.16E-003
80	1.63E-002	6.81E-002	1.01E-003	8.60E-004	9.13E-005	9.33E-004
90	1.02E-002	5.74E-002	8.29E-004	5.86E-004	5.13E-005	7.07E-004
100	4.06E-003	4.99E-002	7.46E-004	4.42E-004	4.56E-005	5.94E-004
110	0.00E+000	4.62E-002	6.79E-004	3.15E-004	3.42E-005	4.97E-004
120	2.03E-003	4.31E-002	6.51E-004	2.64E-004	2.85E-005	4.57E-004
130	0.00E+000	3.93E-002	6.06E-004	2.26E-004	2.85E-005	4.16E-004
140	0.00E+000	3.87E-002	6.01E-004	1.88E-004	1.71E-005	3.95E-004

---STANDARD DEVIATIONS---

TIME (SEC)	<U> (M/S)	<V> (M/S)	<u'**2> (M/S)**2	<v'**2> (M/S)**2	<u'v'> (M/S)**2	TKE (M/S)**2
10	4.54E-003	4.41E-003	1.26E-004	2.41E-004	4.69E-005	1.92E-004
20	5.56E-003	6.77E-003	1.02E-004	1.63E-004	5.70E-005	1.36E-004
30	4.54E-003	4.94E-003	9.38E-005	1.92E-004	1.03E-004	1.51E-004
40	5.56E-003	4.73E-003	6.11E-005	1.72E-004	5.91E-005	1.29E-004
50	0.00E+000	6.00E-003	9.02E-005	1.40E-004	6.57E-005	1.18E-004
60	4.54E-003	4.54E-003	7.16E-005	1.24E-004	3.25E-005	1.03E-004
70	0.00E+000	3.12E-003	7.00E-005	1.28E-004	3.72E-005	1.00E-004
80	5.56E-003	4.63E-003	8.20E-005	5.98E-005	3.72E-005	7.18E-005
90	0.00E+000	3.56E-003	5.98E-005	2.23E-005	2.39E-005	2.55E-005
100	5.56E-003	4.41E-003	2.84E-005	2.84E-005	1.56E-005	3.62E-005
110	0.00E+000	4.07E-003	2.84E-005	4.26E-005	1.28E-005	3.81E-005
120	4.54E-003	2.61E-003	4.23E-005	3.34E-005	0.00E+000	3.02E-005
130	0.00E+000	3.56E-003	3.79E-005	1.95E-005	0.00E+000	2.67E-005
140	0.00E+000	3.56E-003	5.22E-005	2.54E-005	1.56E-005	4.07E-005

POSITION: I = 20,   J = 12

---MEAN VALUES---

TIME (SEC)	$\langle U \rangle$ (M/S)	$\langle V \rangle$ (M/S)	$\langle u'{**}2 \rangle$ (M/S)**2	$\langle v'{**}2 \rangle$ (M/S)**2	$\langle u'v' \rangle$ (M/S)**2	TKE (M/S)**2
10	-2.21E-001	1.07E-001	6.70E-003	1.60E-002	-2.11E-004	1.13E-002
20	-2.22E-001	1.05E-001	6.43E-003	1.54E-002	-1.46E-004	1.09E-002
30	-2.16E-001	1.02E-001	5.98E-003	1.45E-002	-8.12E-005	1.02E-002
40	-2.05E-001	9.59E-002	5.60E-003	1.27E-002	-2.11E-004	9.17E-003
50	-2.03E-001	8.83E-002	4.92E-003	1.09E-002	-3.25E-004	7.93E-003
60	-1.90E-001	8.34E-002	4.15E-003	8.79E-003	-1.95E-004	6.47E-003
70	-1.83E-001	7.18E-002	3.29E-003	6.56E-003	-2.44E-004	4.93E-003
80	-1.65E-001	6.73E-002	2.63E-003	4.99E-003	-1.30E-004	3.81E-003
90	-1.52E-001	5.84E-002	2.07E-003	3.58E-003	-6.50E-005	2.82E-003
100	-1.41E-001	5.35E-002	1.64E-003	2.65E-003	-8.12E-005	2.14E-003
110	-1.31E-001	4.50E-002	1.23E-003	1.93E-003	-3.25E-005	1.58E-003
120	-1.22E-001	4.01E-002	1.07E-003	1.51E-003	-1.62E-005	1.29E-003
130	-1.20E-001	3.48E-002	9.67E-004	1.25E-003	-4.87E-005	1.11E-003
140	-1.18E-001	3.43E-002	9.20E-004	1.14E-003	0.00E+000	1.03E-003

---STANDARD DEVIATIONS---

TIME (SEC)	$\langle U \rangle$ (M/S)	$\langle V \rangle$ (M/S)	$\langle u'{**}2 \rangle$ (M/S)**2	$\langle v'{**}2 \rangle$ (M/S)**2	$\langle u'v' \rangle$ (M/S)**2	TKE (M/S)**2
10	4.96E-003	5.82E-003	1.87E-003	5.43E-004	3.62E-004	4.06E-004
20	3.84E-003	6.91E-003	2.30E-004	6.49E-004	3.13E-004	4.87E-004
30	4.96E-003	8.99E-003	2.25E-004	5.88E-004	3.26E-004	4.45E-004
40	3.84E-003	3.47E-003	1.13E-004	3.37E-004	3.31E-004	2.51E-004
50	0.00E+000	7.59E-003	3.07E-004	5.65E-004	1.66E-004	4.55E-004
60	4.96E-003	6.67E-003	2.87E-004	5.75E-004	1.08E-004	4.54E-004
70	0.00E+000	4.03E-003	1.80E-004	2.92E-004	1.22E-004	2.42E-004
80	4.96E-003	3.05E-003	1.30E-004	1.06E-004	1.02E-004	1.19E-004
90	0.00E+000	5.01E-003	7.53E-005	1.43E-004	6.08E-005	1.14E-004
100	3.84E-003	3.79E-003	5.53E-005	8.31E-005	8.59E-005	7.06E-005
110	3.84E-003	4.36E-003	3.33E-005	1.37E-004	5.55E-005	1.00E-004
120	0.00E+000	4.20E-003	6.90E-005	4.26E-005	4.30E-005	5.73E-005
130	3.84E-003	4.20E-003	7.22E-005	4.26E-005	6.08E-005	5.93E-005
140	5.43E-003	4.41E-003	7.22E-005	7.13E-005	0.00E+000	7.18E-005

POSITION: I = 20, J = 16

TIME (SEC)	<U> (M/S)	<V> (M/S)	<u'**2> (M/S)**2	<v'**2> (M/S)**2	<u'v'> (M/S)**2	TKE (M/S)**2
			—MEAN VALUES—			
10	-5.60E-001	4.55E-002	2.43E-003	3.65E-003	9.86E-006	3.04E-003
20	-5.47E-001	4.33E-002	2.33E-003	3.47E-003	-2.47E-005	2.90E-003
30	-5.30E-001	3.26E-002	2.37E-003	3.55E-003	-4.93E-005	2.96E-003
40	-5.06E-001	2.54E-002	2.29E-003	3.46E-003	-6.41E-005	2.87E-003
50	-4.69E-001	1.69E-002	2.24E-003	3.12E-003	5.42E-005	2.68E-003
60	-4.21E-001	2.68E-003	2.17E-003	2.77E-003	-7.40E-005	2.47E-003
70	-3.70E-001	-3.12E-003	1.98E-003	2.42E-003	-2.47E-005	2.20E-003
80	-3.24E-001	-8.92E-003	1.84E-003	2.17E-003	4.93E-005	2.00E-003
90	-2.81E-001	-1.20E-002	1.59E-003	1.81E-003	7.89E-005	1.70E-003
100	-2.45E-001	-1.43E-002	1.36E-003	1.53E-003	1.23E-004	1.45E-003
110	-2.16E-001	-1.47E-002	1.21E-003	1.25E-003	9.86E-005	1.23E-003
120	-1.94E-001	-1.29E-002	1.11E-003	1.11E-003	9.86E-005	1.11E-003
130	-1.83E-001	-1.38E-002	1.02E-003	9.84E-004	9.86E-005	1.00E-003
140	-1.73E-001	-9.81E-003	9.97E-004	9.84E-004	1.28E-004	9.90E-004
			—STANDARD DEVIATIONS—			
10	3.84E-003	3.05E-003	1.02E-004	2.43E-004	4.76E-005	1.87E-004
20	7.01E-003	5.53E-003	1.97E-004	3.76E-004	1.05E-004	3.00E-004
30	3.84E-003	3.05E-003	1.08E-004	1.99E-004	7.42E-005	1.60E-004
40	3.84E-003	3.79E-003	1.04E-004	3.41E-004	1.78E-004	2.52E-004
50	3.84E-003	5.05E-003	1.38E-004	1.97E-004	1.42E-004	1.70E-004
60	5.43E-003	2.81E-003	5.15E-005	1.13E-004	8.08E-005	8.86E-005
70	5.43E-003	4.20E-003	1.11E-004	1.32E-004	6.82E-005	1.22E-004
80	7.01E-003	4.34E-003	1.24E-004	2.42E-004	8.42E-005	1.92E-004
90	4.96E-003	3.34E-003	5.94E-005	1.21E-004	3.37E-005	9.54E-005
100	3.84E-003	3.05E-003	7.87E-005	1.80E-004	4.33E-005	1.39E-004
110	4.96E-003	5.01E-003	1.02E-004	1.42E-004	3.69E-005	1.23E-004
120	3.84E-003	4.91E-003	8.20E-005	1.02E-004	2.38E-005	9.26E-005
130	0.00E+000	3.05E-003	6.47E-005	7.07E-005	3.11E-005	6.78E-005
140	0.00E+000	2.81E-003	3.30E-005	5.48E-005	2.61E-005	4.52E-005

POSITION: I = 22, J = 2

TIME (SEC)	<U> (M/S)	<V> (M/S)	<u'**2> (M/S)**2	<v'**2> (M/S)**2	<u'v'> (M/S)**2	TKE (M/S)**2
			MEAN VALUES			
10	4.45E-001	4.79E-002	4.59E-004	1.33E-004	-3.13E-006	2.96E-004
20	4.40E-001	4.73E-002	4.44E-004	1.28E-004	-7.61E-006	2.86E-004
30	4.27E-001	4.63E-002	4.06E-004	1.21E-004	-1.34E-005	2.63E-004
40	4.10E-001	4.27E-002	3.64E-004	1.10E-004	-1.39E-005	2.37E-004
50	3.82E-001	3.95E-002	3.16E-004	9.46E-005	-1.57E-005	2.05E-004
60	3.52E-001	3.59E-002	2.55E-004	7.89E-005	-1.34E-005	1.67E-004
70	3.15E-001	3.17E-002	1.96E-004	6.29E-005	-9.40E-006	1.30E-004
80	2.79E-001	2.76E-002	1.47E-004	5.00E-005	-8.05E-006	9.84E-005
90	2.45E-001	2.39E-002	1.10E-004	3.99E-005	-4.47E-006	7.50E-005
100	2.16E-001	2.03E-002	8.13E-005	3.31E-005	-3.58E-006	5.72E-005
110	1.92E-001	1.82E-002	6.59E-005	2.83E-005	-1.79E-006	4.71E-005
120	1.74E-001	1.51E-002	5.52E-005	2.55E-005	-8.95E-007	4.04E-005
130	1.63E-001	1.46E-002	4.97E-005	2.36E-005	-1.34E-006	3.67E-005
140	1.57E-001	1.40E-002	4.81E-005	2.33E-005	-1.34E-006	3.57E-005
			STANDARD DEVIATIONS			
10	2.62E-003	3.78E-003	2.54E-005	4.89E-006	9.21E-006	1.83E-005
20	2.62E-003	3.65E-003	1.02E-005	2.50E-006	1.01E-005	7.45E-006
30	3.82E-003	3.07E-003	1.19E-005	5.50E-006	8.98E-006	9.24E-006
40	2.62E-003	4.26E-003	8.43E-006	3.87E-006	8.39E-006	6.56E-006
50	2.07E-003	3.22E-003	1.71E-005	3.78E-006	5.74E-006	1.23E-005
60	2.62E-003	3.27E-003	1.58E-005	3.93E-006	6.35E-006	1.15E-005
70	0.00E+000	3.07E-003	6.93E-006	1.15E-006	3.29E-006	4.97E-006
80	0.00E+000	2.35E-003	1.18E-005	1.15E-006	2.40E-006	8.38E-006
90	2.62E-003	3.22E-003	6.31E-006	7.98E-007	1.39E-006	4.50E-006
100	2.78E-003	3.27E-003	4.41E-006	7.98E-007	2.19E-006	3.17E-006
110	2.07E-003	2.35E-003	2.33E-006	1.01E-006	2.19E-006	1.79E-006
120	2.62E-003	2.35E-003	1.93E-006	7.98E-007	1.39E-006	1.48E-006
130	0.00E+000	2.55E-003	1.50E-006	1.00E-006	1.47E-006	1.30E-006
140	0.00E+000	3.27E-003	1.22E-006	6.21E-007	1.47E-006	9.70E-007

POSITION: I= 22, J= 6

TIME (SEC)	<U> (M/S)	<V> (M/S)	<u'**2> (M/S)**2	<v'**2> (M/S)**2	<u'v'> (M/S)**2	TKE (M/S)**2
			----MEAN VALUES----			
10	4.42E-001	4.41E-001	1.54E-003	8.19E-004	-5.52E-005	1.18E-003
20	4.35E-001	4.33E-001	1.58E-003	8.53E-004	-1.01E-004	1.22E-003
30	4.22E-001	4.21E-001	1.48E-003	8.01E-004	-7.73E-005	1.14E-003
40	4.03E-001	4.01E-001	1.35E-003	7.83E-004	-4.60E-005	1.07E-003
50	3.77E-001	3.76E-001	1.21E-003	7.14E-004	-3.50E-005	9.62E-004
60	3.45E-001	3.47E-001	1.01E-003	6.05E-004	-2.02E-005	8.06E-004
70	3.08E-001	3.13E-001	8.39E-004	4.97E-004	-7.36E-006	6.68E-004
80	2.72E-001	2.81E-001	6.53E-004	3.85E-004	5.52E-006	5.19E-004
90	2.40E-001	2.51E-001	4.91E-004	3.00E-004	7.36E-006	3.96E-004
100	2.12E-001	2.26E-001	3.73E-004	2.26E-004	7.36E-006	2.99E-004
110	1.89E-001	2.06E-001	2.95E-004	1.83E-004	5.52E-006	2.39E-004
120	1.78E-001	1.91E-001	2.43E-004	1.53E-004	1.10E-005	1.98E-004
130	1.60E-001	1.82E-001	2.03E-004	1.25E-004	5.52E-006	1.64E-004
140	1.57E-001	1.79E-001	1.90E-004	1.15E-004	3.68E-006	1.53E-004
			----STANDARD DEVIATIONS----			
10	4.15E-003	3.47E-003	6.34E-005	4.58E-005	2.65E-005	5.53E-005
20	3.84E-003	3.05E-003	5.67E-005	8.54E-005	1.73E-005	7.25E-005
30	3.50E-003	2.15E-003	6.37E-005	4.92E-005	3.24E-005	5.69E-005
40	2.71E-003	3.54E-003	7.67E-005	6.13E-005	5.76E-005	6.94E-005
50	3.50E-003	3.05E-003	5.46E-005	4.19E-005	3.22E-005	4.87E-005
60	3.50E-003	3.34E-003	4.18E-005	2.56E-005	1.64E-005	3.47E-005
70	2.71E-003	4.21E-003	6.36E-005	4.12E-005	2.67E-005	5.36E-005
80	2.71E-003	2.55E-003	5.94E-005	3.15E-005	2.77E-005	4.75E-005
90	2.48E-003	3.05E-003	3.98E-005	3.30E-005	1.46E-005	3.65E-005
100	2.48E-003	2.36E-003	3.45E-005	2.84E-005	6.89E-006	3.16E-005
110	1.92E-003	2.81E-003	2.95E-005	2.70E-005	1.01E-005	2.83E-005
120	2.71E-003	2.97E-003	1.75E-005	1.38E-005	4.87E-006	1.58E-005
130	2.71E-003	2.36E-003	1.85E-005	9.84E-006	6.89E-006	1.48E-005
140	1.92E-003	2.36E-003	1.18E-005	9.94E-006	9.74E-006	1.09E-005

POSITION: I= 22, J= 10

TIME (SEC)	<U> (M/S)	<V> (M/S)	<u'**2> (M/S)**2	<v'**2> (M/S)**2	<u'v'> (M/S)**2	TKE (M/S)**2
			---MEAN VALUES---			
10	3.05E-002	2.52E-001	3.11E-003	6.55E-003	-1.60E-005	4.83E-003
20	2.88E-002	2.52E-001	3.02E-003	6.26E-003	-1.52E-004	4.64E-003
30	2.88E-002	2.44E-001	2.93E-003	5.95E-003	-5.59E-005	4.44E-003
40	2.20E-002	2.25E-001	2.73E-003	5.44E-003	0.00E+000	4.09E-003
50	2.03E-002	2.10E-001	2.39E-003	4.44E-003	-1.60E-005	3.41E-003
60	1.69E-002	1.91E-001	2.04E-003	3.61E-003	-7.19E-005	2.83E-003
70	1.72E-002	1.72E-001	1.69E-003	2.82E-003	-6.39E-005	2.26E-003
80	3.39E-003	1.51E-001	1.41E-003	2.17E-003	-4.79E-005	1.79E-003
90	0.00E+000	1.36E-001	1.22E-003	1.64E-003	-3.20E-005	1.43E-003
100	0.00E+000	1.22E-001	1.01E-003	1.28E-003	-7.99E-006	1.14E-003
110	-3.39E-003	1.11E-001	8.60E-004	9.90E-004	-7.99E-006	9.25E-004
120	-8.46E-003	1.01E-001	7.70E-004	7.86E-004	-1.60E-005	7.78E-004
130	-1.02E-002	9.78E-002	7.15E-004	6.58E-004	1.60E-005	6.87E-004
140	-1.02E-002	9.99E-002	7.10E-004	6.29E-004	0.00E+000	6.69E-004
			---STANDARD DEVIATIONS---			
10	6.42E-003	2.35E-003	1.45E-004	5.84E-004	1.44E-004	4.26E-004
20	7.65E-003	3.22E-003	9.22E-005	4.73E-004	1.59E-004	3.41E-004
30	4.15E-003	5.73E-003	9.70E-005	3.75E-004	8.80E-005	2.74E-004
40	4.15E-003	3.95E-003	2.16E-004	3.68E-004	9.10E-005	3.01E-004
50	0.00E+000	6.06E-003	1.29E-004	2.51E-004	9.99E-005	1.99E-004
60	5.24E-003	2.35E-003	7.60E-005	2.17E-004	9.47E-005	1.63E-004
70	0.00E+000	3.07E-003	7.78E-005	1.12E-004	7.22E-005	9.64E-005
80	5.24E-003	2.55E-003	1.24E-004	1.27E-004	4.29E-005	1.26E-004
90	0.00E+000	3.95E-003	1.16E-004	9.63E-005	3.91E-005	1.06E-004
100	0.00E+000	2.61E-003	3.81E-005	4.23E-005	3.61E-005	4.03E-005
110	5.24E-003	3.27E-003	2.88E-005	8.46E-005	1.96E-005	6.32E-005
120	4.15E-003	2.55E-003	2.19E-005	6.15E-005	2.48E-005	4.62E-005
130	0.00E+000	0.00E+000	1.72E-005	2.63E-005	2.48E-005	2.22E-005
140	0.00E+000	0.00E+000	3.02E-005	5.85E-005	3.03E-005	4.65E-005

POSITION: I = 22, J = 14

TIME (SEC)	<U> (M/S)	<V> (M/S)	<u'**2> (M/S)**2	<v'**2> (M/S)**2	<u'v'> (M/S)**2	TKE (M/S)**2
			---MEAN VALUES---			
10	-2.31E-001	1.77E-001	4.84E-003	7.33E-003	-3.61E-004	6.09E-003
20	-2.28E-001	1.67E-001	4.61E-003	6.99E-003	-2.56E-004	5.80E-003
30	-2.07E-001	1.53E-001	4.49E-003	7.18E-003	-1.42E-004	5.83E-003
40	-1.86E-001	1.35E-001	4.10E-003	6.72E-003	2.85E-004	5.41E-003
50	-1.64E-001	1.20E-001	3.81E-003	6.03E-003	2.09E-004	4.92E-003
60	-1.42E-001	1.06E-001	3.34E-003	5.45E-003	2.85E-004	4.40E-003
70	-1.22E-001	9.54E-002	2.93E-003	4.70E-003	3.42E-004	3.81E-003
80	-1.04E-001	8.56E-002	2.38E-003	3.85E-003	2.56E-004	3.11E-003
90	-9.00E-002	7.94E-002	2.00E-003	3.20E-003	2.18E-004	2.60E-003
100	-8.13E-002	7.22E-002	1.66E-003	2.57E-003	1.42E-004	2.12E-003
110	-7.11E-002	6.87E-002	1.44E-003	2.04E-003	1.14E-004	1.74E-003
120	-6.53E-002	6.29E-002	1.30E-003	1.70E-003	9.50E-005	1.50E-003
130	-6.24E-002	6.42E-002	1.25E-003	1.57E-003	7.60E-005	1.41E-003
140	-6.09E-002	6.51E-002	1.19E-003	1.41E-003	1.04E-004	1.30E-003
			---STANDARD DEVIATIONS---			
10	1.13E-002	1.33E-002	2.05E-004	7.88E-004	3.10E-004	5.76E-004
20	9.91E-003	7.40E-003	1.16E-004	2.73E-004	2.08E-004	2.10E-004
30	5.43E-003	7.52E-003	2.42E-004	6.14E-004	1.94E-004	4.67E-004
40	7.68E-003	8.78E-003	1.80E-004	5.53E-004	2.17E-004	4.12E-004
50	3.84E-003	9.32E-003	1.13E-004	3.79E-004	1.94E-004	2.80E-004
60	0.00E+000	8.34E-003	1.56E-004	3.18E-004	1.42E-004	2.50E-004
70	5.86E-003	8.95E-003	9.72E-005	2.52E-004	2.28E-004	1.91E-004
80	4.96E-003	5.36E-003	1.45E-004	1.88E-004	8.94E-005	1.68E-004
90	3.84E-003	6.95E-003	9.55E-005	2.70E-004	6.32E-005	2.02E-004
100	0.00E+000	3.79E-003	1.08E-004	1.04E-004	4.59E-005	1.06E-005
110	0.00E+000	5.10E-003	6.94E-005	7.15E-005	6.32E-005	7.05E-005
120	5.43E-003	3.79E-003	7.60E-005	7.15E-005	6.49E-005	7.38E-005
130	3.84E-003	3.05E-003	9.81E-005	1.19E-004	4.59E-005	1.41E-004
140	0.00E+000	7.74E-003	4.07E-005	1.28E-004	5.23E-005	9.46E-005

APPENDIX D

TITLE:	Z80-Based Data Acquisition System
DESIGNED AND IMPLEMENTED BY:	Byron Cheeying Cheung
SUPERVISED BY:	Professor Michael W. Golay
TITLE:	Associate Professor of Nuclear Engineering
DATE:	June 22, 1979

Contents

*Not Included Here

ABSTRACT

This report discusses the realization of a five-channel data acquisition system. The data on these five channels are written on a Tektronix cassette recorder via the Z-80 system.

SYSTEM DBC MARK II

Features:

(1) Digitizing 1 to 5 channels simultaneously

(2) Software selection of 1 to 5 channels

(3) Variable sampling time: 0.1 sec to 25.5 sec

(4) Scattering sampling time capability

(5) Variable header length

(6) System can be expanded very easily: PIO, S10 & RAM,

EPROM can be added with little modifications in memory (EPROM)

(7) System is a talker. It can easily be turned into both
talker and listener; hence it can be a mini 4051 at much

lower cost.

(8) External programming available. There are 128 programming

steps plus two manual interrupts.

1.1   Introduction

The Nuclear Engineering Department currently operates a Tektronix 4051 Graphic Terminal. With the recent acquisition of a Tektronix 4924 Cassette Drive, it is desirable to have a portable system that can communicate with the Cassette Drive since the 4051 is not easily moved around.

Since the main use of the cassette drive is logging data, the desired system must have the capabilities of accepting data from the outside world and the capabilities of interfacing this cassette drive. After some careful considerations, a microprocessor is best fitted for such a system. The advantages of using a microprocessor to implement this particular system are:

(1)   It minimizes hardwares.

(2)   It uses program to control all the activities. A software change is much easier and cheaper than hardware.

(3)   It consumes less power.

(4)   Future expansion is very easy.

There are disadvantages of using microprocessor also. Microprocessor nowaday are still very slow and are quite expensive. However speed is not the main concern for this particular application.

1.2   Basic System Configuration (Please refer to the System Block Diagram)

The microprocessor employed for this application is the Z80 CPU. The system also consists of one K bytes of EPROM, 256 bytes of static RAM, three PIO's (Parallel Input Output Port), and a CTC (Counter Time Control).

Fig. D.1 SYSTEM BLOCK DIAGRAM

There are five analog inputs which will accept from one to five external voltages. These voltages are digitized sequentially through the A/D Circuitry and the A/D Timing Control and Input Channel Multiplexor. The digitized data are transferred to the RAM via PIOA. CTC provides the timings for the A/D. PIOB is used for interfacing the Tecktronix 4924 Cassette Drive. PIOC is used to multiplex the 10 digit displays which indicate current run number, number of sample points collected and the number of sample points wanted.

The EPROM is the brain of the system. It contains all the operational programs. The Z80 CPU executes the instructions supplied by the EPROM. The Data Entry Control Logics serves two important functions. It is a pseudo-DMA (direct memory access) control to the static RAM. It is also maintenance control. This is an extremely helpful function since no logic analyzer is available to debug the system. There are three buses used in the system: A 16-bit Address Bus, an 8-bit Data Bus and a Control Bus.

1.3 System Functions

The system was first designed to perform the exact functions as the Tektronix 4051. However, due to limited space of the EPROM, most of the 4051 statements were not implemented. The system is implemented as a Talker which can execute the FIND, MARK and WBYTE Statements. There is one PIO port open in case the system is needed to be implemented as a Listener. Additional statements can also be implemented when more EPROM is added. The system is designed under the IEEE 488 GPIB standards.

The system essentially is capable of executing the following statements:

```
FIND @ 2:N                  ;N=nth record, 0≤ N < 9999
MARK @ 2:M,X                ;M=# of records, 0<M≤255
                            ;X=# of bytes per record, 0<X≤9999
WBYTE @ 34:63,95            ;this statement terminates the
                            ; handshake operation on unit 2
WBYTE @34,121:data          ;this statement calls for a byte
                            ;by byte transfer operation.  Data
                            ;can be transferred to the unit as
                            ;soon as the statement is executed
WBYTE @ 121:data            ;this statement put the system in a
                            ;continuous data transfer mode
                            ;without terminating and restarting
                            ;the GPIB.
```

The system is designed to be the Talker and any Listener handshake with the system is designated for unit 2. This is a fixed unit number. This number can be changed only by reprogramming the EPROM.

1.4 System Implementation

Since no TTY is connected to the system, the only way to initiate operations are by depressing switches.

When power is applied, the system is put in a known state through the Initialization program. All the PIOS and CTC are provided with the required Control Words and Interrupt Vectors. Once the system is initialized and interrupt mode 2 is enabled, the system is idle and loops in the BCDPLAY subroutine which will scan all ten digits sequentially.

At this point, user can put the system in Local mode by flipping the LOCAL/REMOTE switch. The MEMORY/DATA will indicate whether the content of the memory is being scanned or data is to be written into memory. When MEMORY/DATA is at MEMORY and READ/WRITE is at READ, the content of a specified memory location

is scanned. The first three 7-segment displays indicate the memory location and the remaining two displays indicate its content. The address as well as content are hexidecimally represented. When MEMORY/DATA is at DATA and READ/WRITE is at WRITE, a memory write is to be performed. The basic procedures for doing memory read or memory write are:

    (1)   put system in local

    (2)   key in desired address

    (3)   select read or write operation.

There are three other switches which are associated with this function. The UPCOUNT increments the displayed address by one. The DOWNCOUNT decrements the memory address by one. The MEMORY/DATA CLR will clear the Memory Address register if it is a memory read or the data register if it is memory write. The actual memory write occurs when the second half of the 8-bit byte is entered. The memory address will automatically be incremented by one when the word is written.

The A/D CLR switch clears the analog to digital circuit, unpicks the Solid State relay and clears the CTC. The SYS RESTART switch reinitializes the system. There are five program interrupt switches. They are WRITEHEADER, FIND, USERINTERRUPT1, START and STOP.

The WRITEHEADER switch interrupts the system and writes the necessary header on the cassette tape. It essentially performs the following program in basic:

```
N = 1
FIND @ 2:N
MARK @ 2:1,X              ;X is pre-loaded in memory
FIND @ 2:N
WBYE @ 34,121:header      ;length of header varies
N = N + 1
```

The WRITEHEADER switch also loads the CTC with the correct
time constants such as sampling time and number of channels.
Once the header is written, the system is ready for quantizing
the inputs. The START switch applies an external trigger
pulse to initiate the CTC operation. This trigger pulse also
triggers a 50 microseconds sample and hold pulse. All five
channels are sampled at the same instance. The trailing edge of
and H pulse triggers a 3 microseconds pulse. This pulse
in conjunction with the System Clock, produces the start
signal required to start the A to D. When the conversion is
done, a few operations are performed before the next conversion
can begin. The next analog switch is turned on, supplying the
A to D input with new analog signal to be digitized. A
downcount pulse is generated and applied to the CTC to downcount
the number of channels remaining to be digitized. The previous
digitized signal is written into the scratch pad memory at
location zero. The scratch pad memory is then upcounted by one.

When TO2 of CTC comes on, it indicates that the channel
being quantized is the last channel. As soon as this last
channel is written into the scratch pad memory, a DONE signal
is generated. This DONE signal then interrupts the system.
The system services this interrupt in this manner. It first
checks if the scattering sample operation is selected. If it
has been selected, then the system checks for the number of
STC left and then loads the necessary sampling time for the
next operation. The system then proceeds to read in the
digitized data and store them at memory location starting at
4DA. Once all the data are written into the RAM. The data are
transferred to the GPIB one byte at a time until all digitized
channels are written on the Cassette Drive. A dummy byte is
also written to provide a checking mechanism for the number of
samples collected. The system then increments the sample

points collected register by one. This incremented number is
compared with set number of sample points. If they are equal,
the system will stop by resetting the CTC time constant.
The STOP switch has the identical function as mentioned in
the last sentence. The system then terminates the handshake
operation by sending the EOI (end of information), UNTALK and
UNLISTEN. If the comparison is not equal, the system will remain
in the wait mode for more data. The GPIB is not terminated in
this case.

One thing should be clarified here. In the previous
paragraph, it is mentioned that data are first transferred to the
static RAM, then to the GPIB. This may seem to be a very foolish
idea. There are two reasons for doing it in such a way. From
the maintainence standpoint, it is easier to check the memory
locations to see if the A to D are working correctly than to
carry the Cassette Drive to the 4051 to verify the results.
The second reason is that transferring a group of data at a time
saves more programming steps, hence more EPROM space available
for other programs. The fact that the minimum sample time is
0.1 second provides ample time for time-sharing the CPU.

Chapter 2   SYSTEM OPERATING PROCEDURES

COMMENTS:

To enter information, one needs to do:

(1) MEM/DATA at MEM
(2) READ/WRITE at READ
(3) Press MEM/DATA CLR
(4) Key in Address
(5) MEM/DATA at DATA
(6) READ/WRITE at WRITE
(7) Press MEM/DATACLR
(8) Key in Data
(9) MEM/DATA at MEM
(10) READ/WRITE READ

(A) If the tape is a brand new one, perform Step 1 to 7. If
tape is a used tape, go to Part B.

(1) turn power on both the system and the Cassette drive
(2) press SYSRESTART
(3) press A/DCLR
(4) switch to "LOCAL"
(5) Enter

Address	Content
4F5	00
4F6	00
4E6	00
4E7	10
4E8	00
4E9	01
403	D2 02
406	CD 5E 03
409	CD 7C 03
40C	CD AF 02

(6)   press "USERINTERRUPT1" once. Observe that tape will be marked and then stopped

(7)   go to Part B Step 12.

(B) If tape is used, perform the following steps:

B.1 For the very first run:

(8)   turn power on both the system and the cassette drive

(9)   press SYSRESTART

(10) press A/D CLR

(11) switch to "LOCAL"

(12) enter

Address	Content	Comments
4F5	00	Program FIND
4F6	01	
4D1	# $ TC	
4D2	MSD TC	
4D3	LSD TC	
4D4	MSD $ TC	Duration of $TC
4D5	LSD $ TC	
4E0	# ch. in use	Starts 00 to 04
4E4	MSD # of samples	
4E5	LSD wanted	
4E6	MSD # of bytes in	BYTE # in MARK N,:
4E7	LSD the next run	
4E8	MSD 00	Record # in MARK N,X
4E9	LSD 01	

For the location of Dummy data, it depends on how many channels are in use.

For 1 channel	4DA = Data
	4DB = Dummy data
2 channels	4DA,4DB = Data
	4DC = Dummy data

3 channels	4DA,4DB,4DC = Data
	4DD = Dummy data
4 channels	4DA,4DB,4DC,4DD = Data
	4DE = Dummy data
5 channels	4DA,4DB,4DC,4DD,4DE = Data
	4DF = Dummy data

(13)   enter header starting at 4A∅ for a maximum of
48 bytes

(14)   switch to "REMOTE"

(15)   press "WRHEADER" to start writing the header

(16)   when cassette drive stops, press "START" to start
the current run

(17)   go to Part C Step 24 for next run operating procedures

B.2   If the operation is not the first run, the last run # must
be known. Then proceed as following:

(18)   turn power on both the system and the cassette drive

(19)   press SYSRESTART

(20)   Press A/D CLR

(21)   Switch to "LOCAL"

(22)   enter all required parameters as described in Step 12
except locations 4F5 and 4F6 and enter

4F5   } last run # plus one
4F6

4E1   last run #

(23)   go to Step 13.

(C)   For the next run operation, perform the following:

(24)   DO NOT press SYSRESTART

(25)   press A/D CLR

(26)   if no changes at all, go to Step 15. If there are
changes, do

(27)   switch to "LOCAL"

(28)   make any necessary changes, go to Step 14.

(D) If system hangs, do

    (29) switch to "LOCAL"

    (30) enter

Address	Content
400	FB
401	ED4D

    (31) switch to "REMOTE"

    (32) press SYSRESTART

    (33) go to Part A Step 2

    (34) if Steps 29 to 32 fail, drop power and go to Part A Step 1

3.1 Introduction

Since no logic analyzer is available to debug and troubleshoot the system, it is necessary to have a maintenance panel in the system. One third of the entire system real-estate was devoted to the maintenance panel. There are many built-in maintenance procedures which can be tested in local or remote mode. It is hoped that this panel can be used to help users to narrow down any specific problems, whether they are hardware or software related.

3.2 Maintenance Panel Design

The main concerns in designing the panel are:

(1) What is content of memory?

(2) What is content of address line?

(3) Can we read/write to any writable memory?

(4) Can we program all the PIO's and CTC?

(5) Can we test all the programs locally?

(6) Can we bind individual programs to form a master program?

(7) Can we talk to the outside world?

To satisfy all these concerns, three 7-segment LED's are used to display the address and two 7-segment LEDs are used to indicate the content of memory. A switch is designated to control remote or local mode. There is single-pulse switch to single step the Z80. The memory Write/memory Read switch provides the read or write operation to the static RAM. Memory Address/Data controls what is being entered through the Hex keyboard. There are reset switches to clear the internal register or restart the system. The combination of all these switches provide all the necessary capabilities to test the system locally.

Once the fundamental system is operating, simulated programs can then be initiated and other peripherals can be tested. This is the concept for testing all the PIO's and CTC.

The USERINTERRUPT1 Switch is used to test PIOs and CTC. A test program for a particular PIO or CTC must be generated and written into the memory starts at memory location A03. The length of the program cannot exceed 128 words. The procedures for running this test will be described in the next section.

3.3 Maintenance and Testing Procedures

3.3.1 EPROM Content Check
(1) Power up system.
(2) LOCAL/REMOTE at LOCAL
(3) MEM/DATA at MEM
(4) MW ON/OFF at OFF
(5) IOW ON/OFF at OFF
(6) SYS CLOCK/SINGLE PULSE at SYSCLOCK
(7) Press MEM ADDR/DATA REG CLR

The first three digits will be the current EPROM address and the next two digits is the content of this address. Press UPCOUNT or DOWNCOUNT to check the content of the EPROM.

3.3.2 RAM Read and Write Test
(A) Write Test
    (1) Power up system
    (2) LOCAL/REMOTE at LOCAL
    (3) IOW ON/OFF at OFF
    (4) SYS CLOCK/SINGLE PULSE at SYSCLOCK
    (5) MW ON/OFF at OFF
    (6) MEM/DATA at MEM
    (7) Press MEMADDR/DATA REG CLR
    (8) Enter the desired address to be written, address can be anyone 400 to 4FF.
    (9) MEM/DATA at DATA
    (10) MW ON/OFF at ON
    (11) Press MEMADDR/DATA REG CLR
    (12) Enter desired data. Each datum is 8 bits long and is divided into two 4-bit hexidecimal code. The higher order 4-bit code is enter first then the lower order 4-bit code. The memory address will automatically increment when the second 4-bit is entered.

(B) Read Test

   After all the data at the desired addresses are write we can go back
   to read what we have just written.

   (13) MW ON/OFF at OFF

   (14) MEM/DATA at MEM

   (15) Press MEM ADDR/DATA CLR

   (16) Enter the desired address and check its corresponding content.

   3.3.3 Use of on-line program to test PIO's.

      If 3.3.1 to 3.3.2 are working correctly, PIOs and CTC can then be
checked on-line. The USERINTERRUPT switch is intended for this operation.
The procedure is same as memory write. The format is as follows:

RAM ADDR	CODE	PROGRAM
403	CDD202	CALL PUSHPAR
406	Codes for the cor- responding program	
		End of program
	C3AF02	JP POPPAR

   3.3.3.1 Testing the Display LED

   This program can select and display each LED individually.

RAM ADDR	CODE	PROGRAM
403	CDD202	CALL PUSHPAR
406	3E XY	LD A, XY
408	D3 11	OUT (11), A
40A	06 02	LD B, 02
40C	11 FFFF	LD, DE, -1
40F	2139DE	Loop1: LD HL, 14814 H
412	19	Loop2: ADD HL, DE
413	38FD	JR C, LOOP2
415	10F8	DJNZ, LOOP1
417	C3AF02	JP POPPAR

x = digit select, $0 \le x \le 9$

y = content to be displayed $0 \le y \le 9$

Select REMOTE

Once the program is entered, depressing the USER INTERRUPT switch once should display the selected digit with the desired content for approximately 2 seconds.

3.3.3.2 Test MARK statement or mark the tape locally

(1) Enter

RAMADDR	CONTENT
4E6	# of bytes to be marked
4E7	
4E8	# records to be marked
4E9	$0 < \# \le 255$

RAMADDR	CODE	PROGRAM
403	CDD202	CALL PUSHPAR
406	CD7C03	CALL MARK N,X
409	C3AF02	JP POPPAR

(2) Select REMOTE

(3) Press USERINTERRUPT

3.3.3.3 Test FIND statement or finding the tape locally

(1) Enter

RAM ADDR	CONTENT
4F7	Record No. for user's programmable
4F8	"FIND" switch

(2) Select REMOTE

(3) Press FIND RECORD switch

3.3.3.4. Test FIND statement using USER INTERRUPT switch

(1) Enter

RAM ADDR	CONTENT
4F5	Record # to be found
4F6	

RAM ADD	CODE	PROGRAM
403	CDD202	CALL PUSHPAR
406	CD5E03	CALL FINDN
409	C3AF02	CALL POPPAR

(2) Select REMOTE

(3) Press USERINTERRUPT switch

3.3.3.5 Test WBYTE statement or writing data using USERINTERRUPT switch

(1) Enter

RAM ADDR	CONTENT
4A0	length of data in Binary
4A1 to X	data, x ≤ what 4A0 specified
4F4	79 ;this is the op code for WBYTE

RAM ADDR	CODE	PROGRAM
403	CDD202	CALL PUSHPAR
406	21A004	LD HL, A004H
409	3AA004	LD A, (04A0H)
40C	47	LD B, A
40D	3E79	LD A, 79

40F	32F404	LD(04F4H), A
412	CD6001	CALL HANSHAKE 1
415	CD3F03	CALL WBYTE
418	CD9601	CALL UNTKLN
41B	C3AF02	CALL POPPAR

(2) Select REMOTE

(3) Press USERINTERRUPT 1.

3.3.3.6 Conclusion

Using the programs described above, the USERINTERRUPT1 switch can perform any combinations of statements like FIND, MARK and WYBTE. With a little practice and imagination, the DBC can be programmed to perform numerous functions like generating test patterns to providing various timing signals. I shall leave this for my users.

Byron C. Cheung
August 6, 1979 at MIT

APPENDIX E

CROSS-CELL VELOCITY MEASUREMENTS

In order to quantify the three-dimensional effects occuring at the
top of the test-cell, detailed measurements were made between the Plexi-
glas face plates on a horizontal plane located approximately at the
I=24 level in Fig. C.1. These measurements were made by R. W. Sawdye and
are recorded in Tables E.1 and E.2.

The data show a definite three-dimensional structure that includes
substantial down-flow occurring near the face plates across the entire
cell, which explains the failed centerplane mass balance that is described
in Chapter Three. It appears that the inlet jet impinges on the cross-
piece that forms the top boundary of the test cell and rolls outward and
down, in a fairly even fashion, along both face-plates. Further, the
maximum vertical velocities no longer occur at the cell centerplane, but
are displaced a few millimeters to one side. The horizontal velocities,
on the other hand, generally maintain their peaks on the centerplane
between the two face plates.

Table E.1

Vertical Velocities

Measurements by: R. W. Sawdye

FFTF Test Cell
Flow Rate = 37.8 GPM (steady-state)
Temp. = 110°F
Vertical Position, I = 24

	Off-Center Distance (mm)						
	15	10	5	0 ($\mathcal{C}$)	5	10	15
Approx. Chimney Center							
	-.361	-.328	.439	.494	.577	.441	-.206
	-.336	-.351	.431	.494	.604	.408	-.243
	-.347	-.351	.452	.484	.573	.368	-.279
	-.323	.338	.455	.474	.520	.348	-.311
	-.332	.305	.468	.461	.483	.323	-.322
Plexiglas	-.340	.273	.466	.423	.437	.276	-.336
Face	-.329	.222	.429	.366	.386	.215	-.344
Plate	-.322	.169	.334	.303	.314	.146	-.343
	-.315	.092	.241	.234	.232	.078	-.334
	-.287	.028	.157	.158	.149	.017	-.308
	-.272	-.029	.082	.092	.072	-.037	-.287
	-.262	-.076	.014	-.025	-.007	-.089	-.279
	-.293	-.167	-.064	-.054	-.104	-.171	-.300
	-.332	-.289	-.219	-.202	-.229	-.273	-.336
	-.316	-.318	-.322	-.342	-.347	-.336	-.338

////// Approx. Cell Side-Piece Location ////////

Table E.1 Measured Vertical Velocities (m/sec.) on a
Horizontal Plane Between Plexiglas Face Plates.

Table E.2

Horizontal Velocities

Measurements by: R. W. Sawdye
Conditions: Same as Table E.1

	Off-Center Distance (mm)						
	15	10	5	0	5	10	15

Approx.
Chimney
Center

	15	10	5	0	5	10	15
	.019	.021	.034	.022	.013	.032	.064
	.072	.090	.112	.112	.102	.124	.124
	.148	.148	.196	.201	.187	.188	.171
	.228	.224	.279	.287	.280	.264	.199
	.275	.287	.365	.374	.361	.306	.239
Plexiglas	.306	.346	.447	.447	.430	.329	.259
Face	.343	.358	.508	.501	.479	.352	.259
Plate	.337	.363	.522	.522	.487	.323	.257
	.313	.306	.468	.496	.456	.270	.239
	.283	.259	.407	.446	.389	.226	.252
	.263	.180	.331	.383	.310	.192	.270
	.263	.150	.241	.321	.245	.178	.292
	.275	.162	.184	.243	.203	.194	.313
	.253	.191	.180	.190	.192	.211	.300
	.148	.184	.160	.152	.161	.180	.218
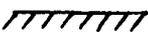
/////// Approx. Cell Side-Piece Location ///////////

Table E.1 Measured Horizontal Velocities (m/sec.) on a
Horizontal Plane Between Plexiglas Face Plates.

APPENDIX F

PLOTS OF TURBULENCE FIELD PARAMETERS VS. TIME

The following 39 pages of plots, one page for each I-J
position marked with a (+) in Figs. 5.14 - 17, portray the
turbulence field data (+'s) and computed transient behavior (solid
lines) as a function of time during the transient. Each parameter,
both data and calculation, are normalized to one (1.0) at their
individual maximum values (usually occurring at the time origin).
These normalization constants are printed above each graph with the
convention that the maximum data value lies over the maximum calculated
value. The labeling scheme is demonstrated on the first page
(I = 5, J = 6).

Note that turbulent kinetic energy (K) is designated (Q) on
the plots in Appendix F. Thus QMAX is the normalization factor for
turbulent kinetic energy as a function of time.

Typical values of the standard deviations obtained from the
ensembles are depicted on the plots of page 252. Precise values of
the standard deviations at each point in time for each position are
given in Section 2 of Appendix C.

I=5
J=10
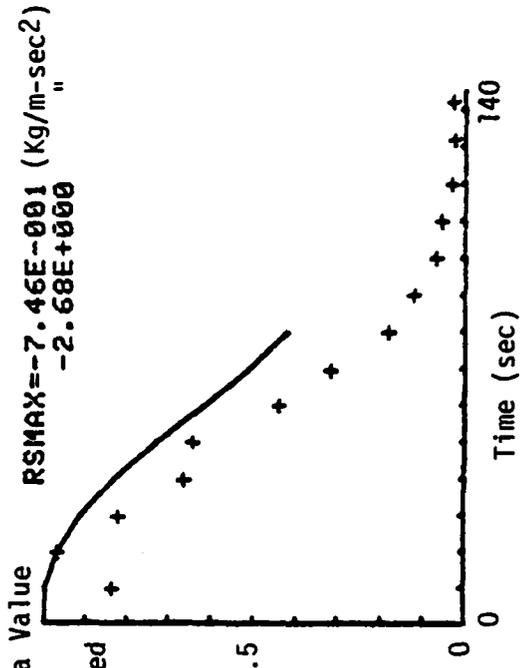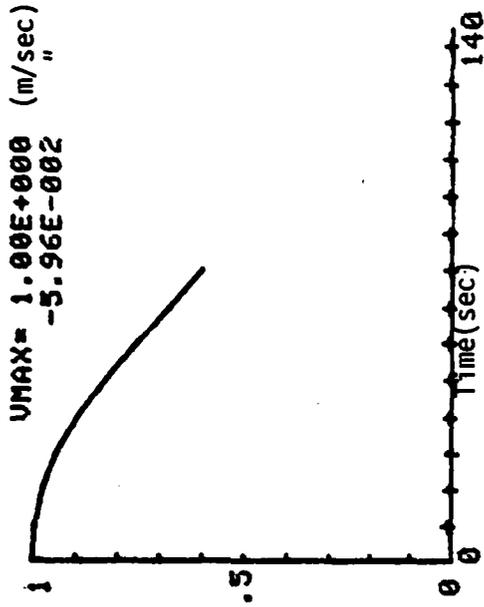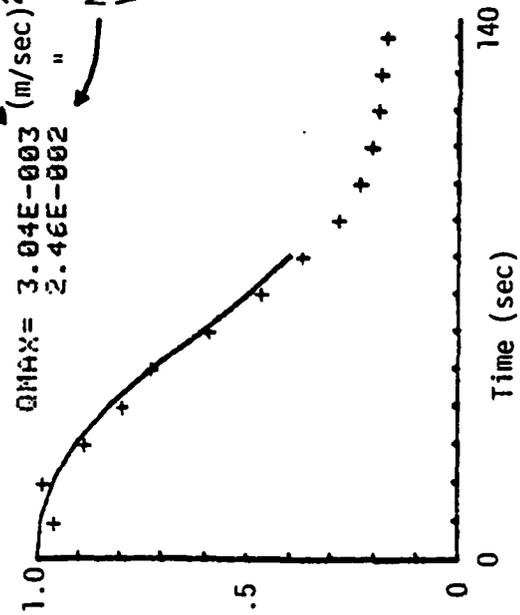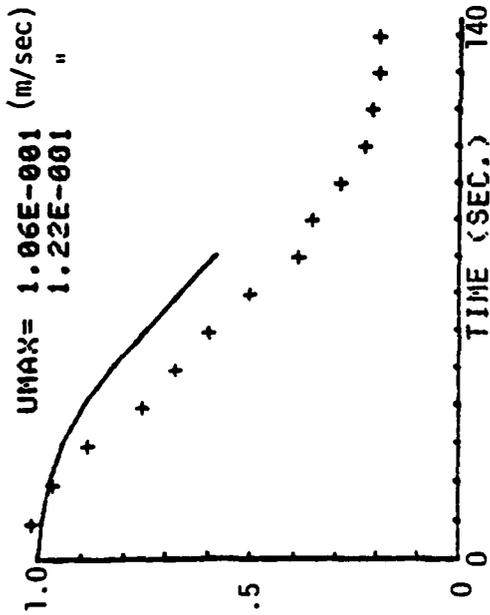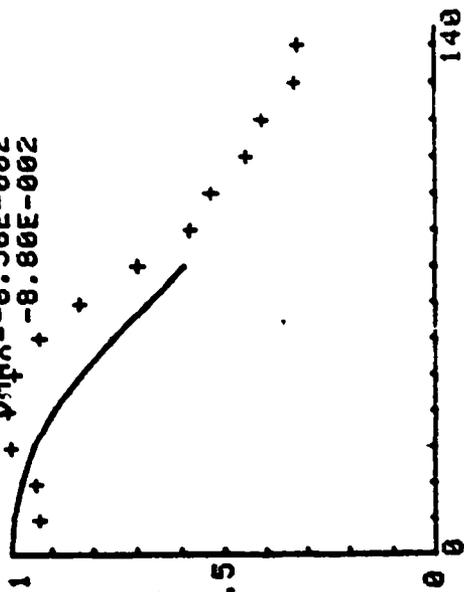
UMAX=-1.35E-001
5.68E-003

VMAX=-6.56E-002
-8.86E-002

RSMAX= 9.93E+002
-2.36E+000
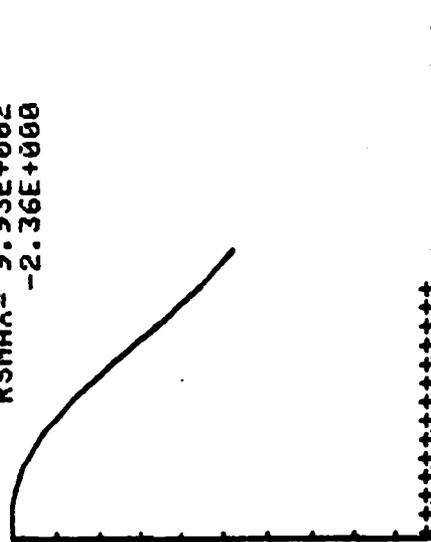
QMAX= 5.80E-003
2.49E-002

TIME (SEC.)

UMAX= 2.67E-002
1.45E-001

RSMAX=-2.14E+000
-2.62E+000

I=5
J=14

UMAX=-3.93E-001
-2.67E-001

QMAX= 1.01E-002
6.27E-002

TIME (SEC.)

VMAX= 6.23E-001
       1.22E+000

RSMAX=-7.24E-001
       1.36E+002

VMAX=-4.77E-001
      -3.54E-001

QMAX= 3.28E-003
      3.27E-001

I=5
J=17

TIME (SEC.)

140

.5

0

1

UMAX=-4.74E-002
     -7.76E-002

RSMAX=-5.72E-001
      -3.39E+000

I=6
J=8

UMAX= 3.05E-002
      8.09E-002

QMAX= 4.32E-003
      2.09E-002

TIME (SEC.)

140

.5

0

UMAX=-6.56E-002
      -1.64E-002

RSMAX=-8.69E-001
       -7.79E+000

I=6
J=12

UMAX=-2.82E-001
      -1.36E-001
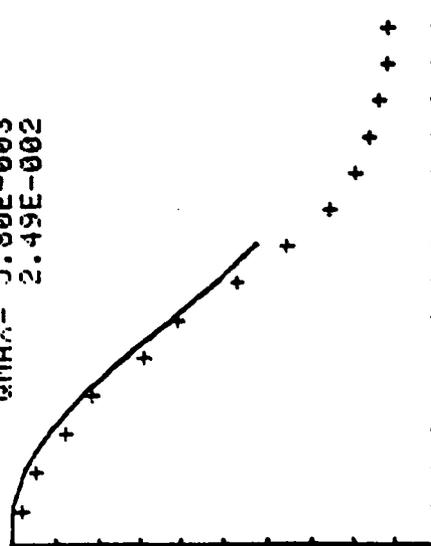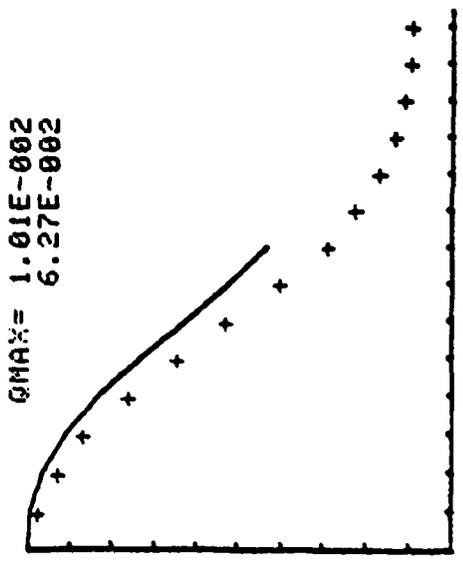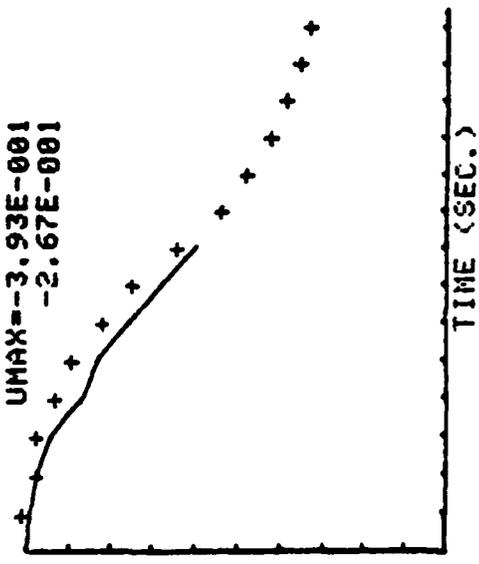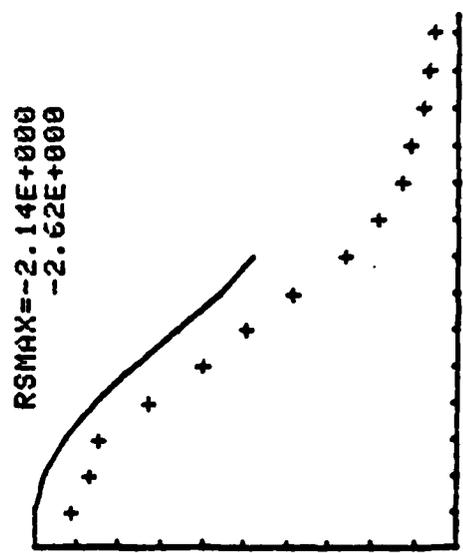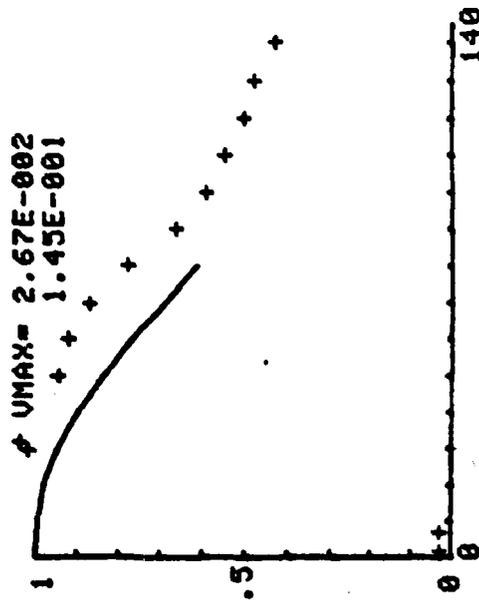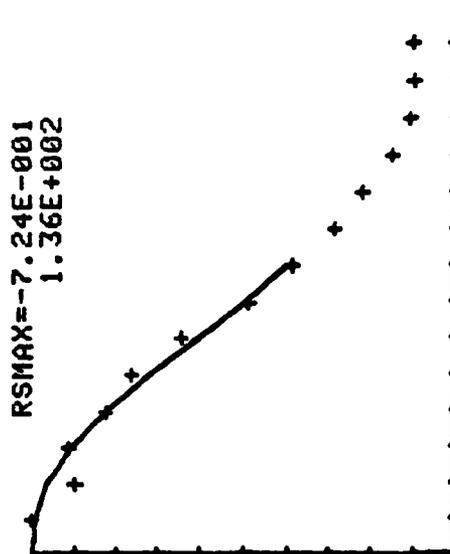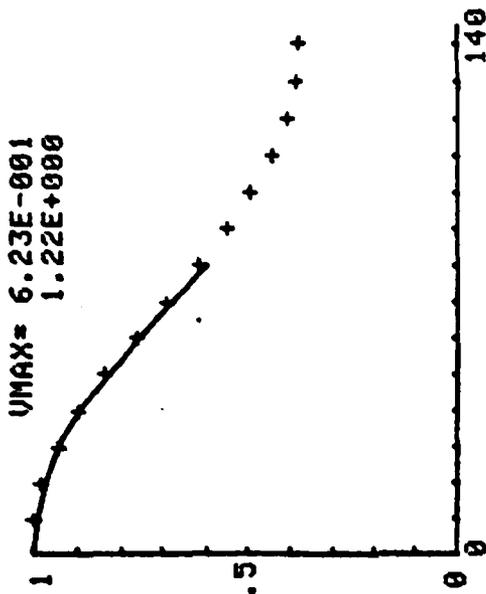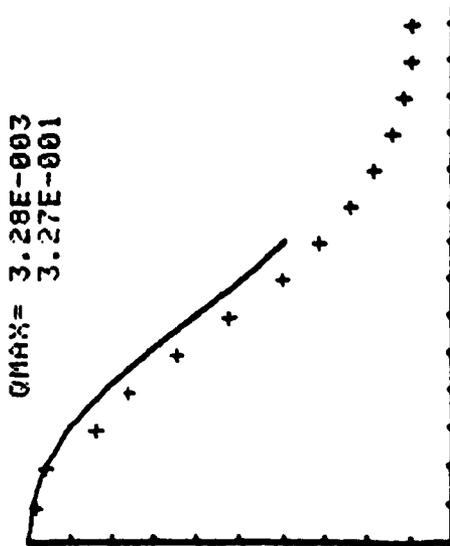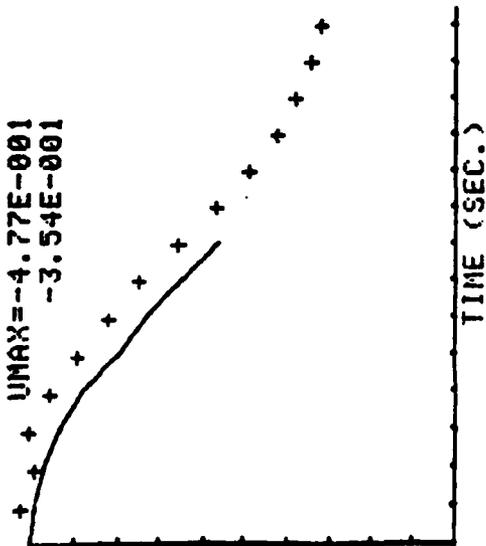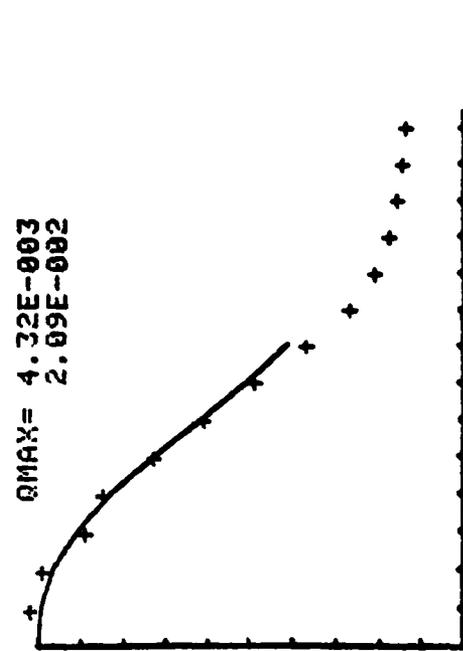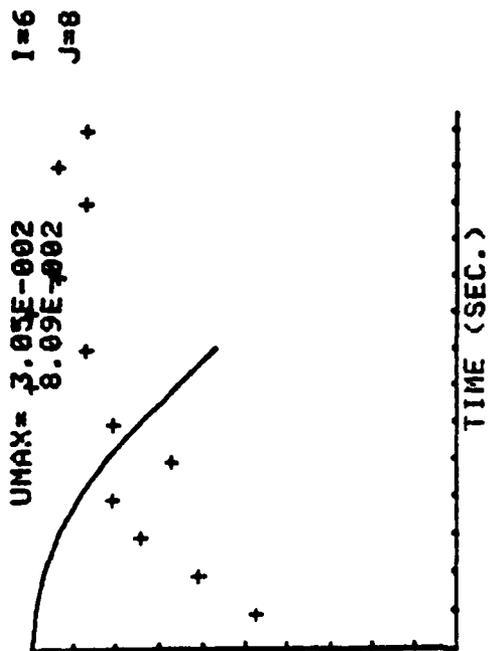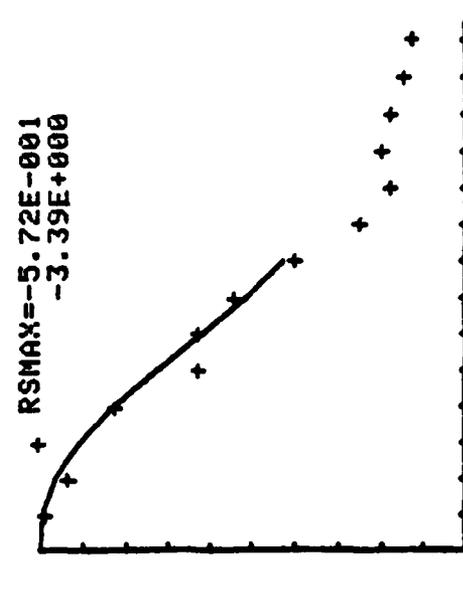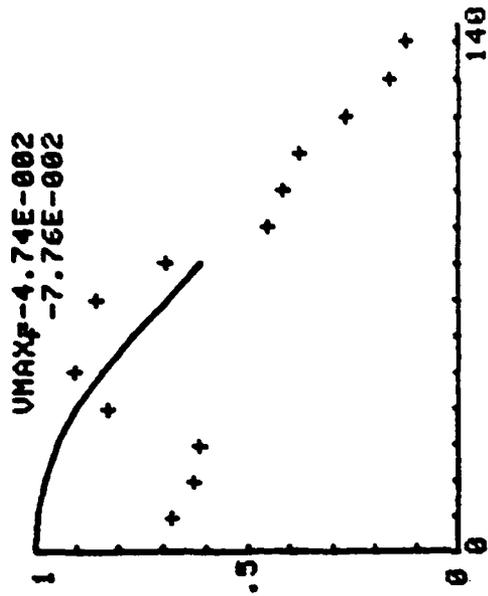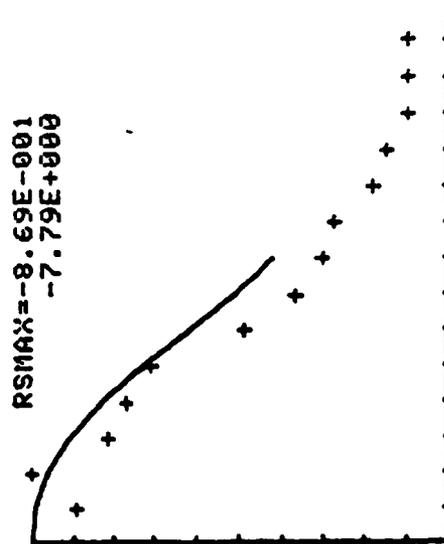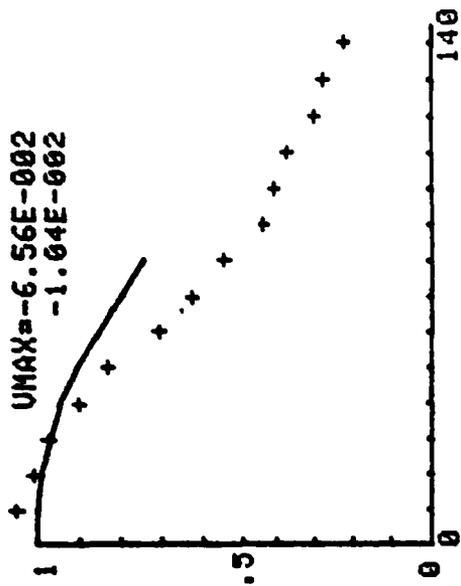
QMAX= 7.28E-003
      2.72E-002
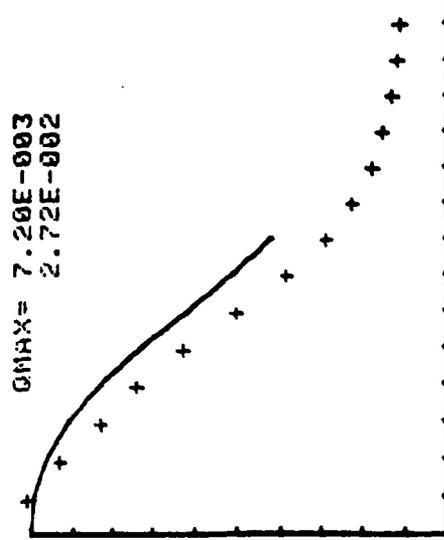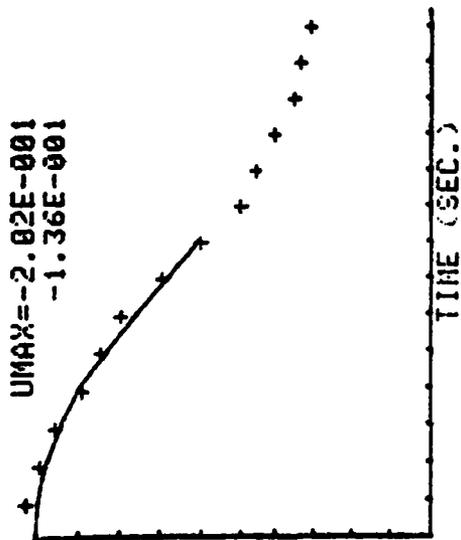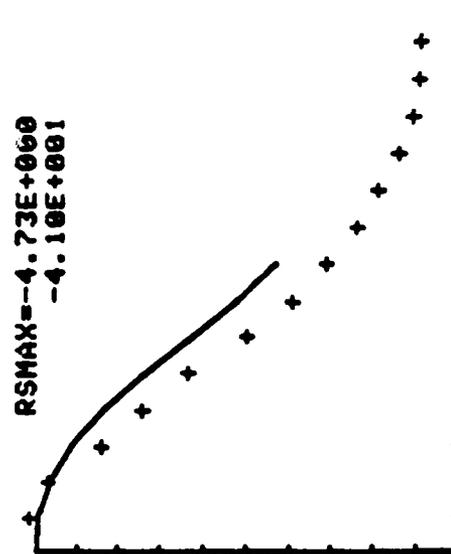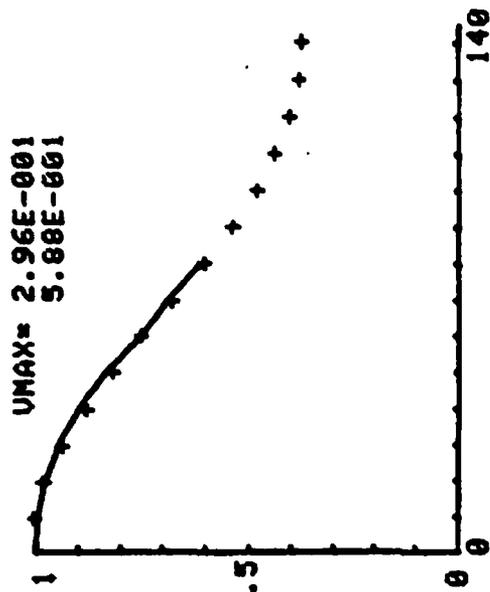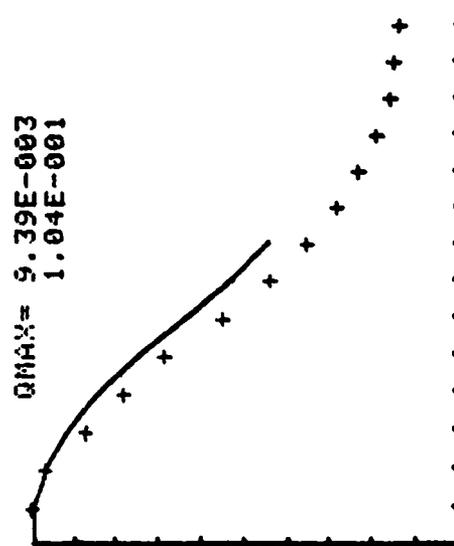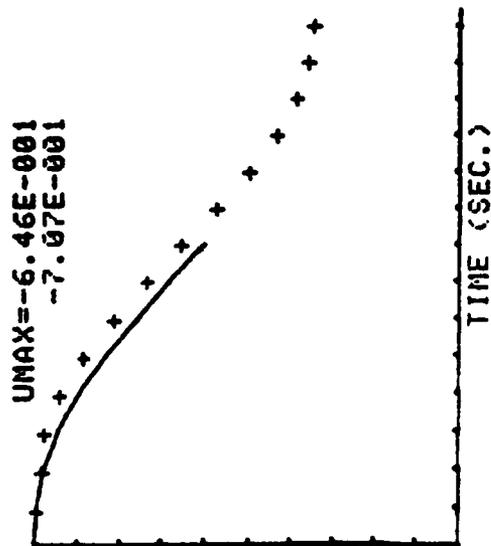
TIME (SEC.)

UMAX= 1.00E+000
-5.07E-002

140
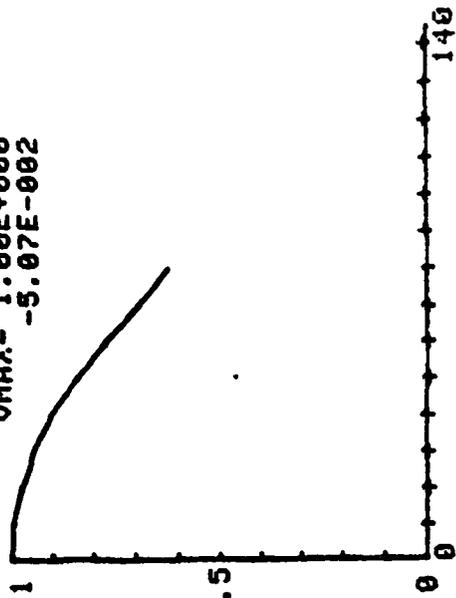
RSMAX=-8.17E-001
-5.15E+000
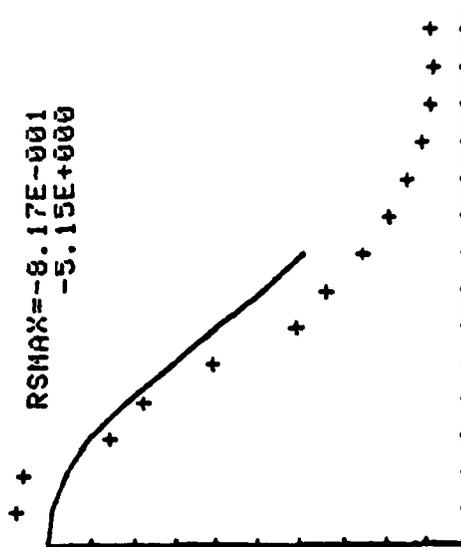
I=8
J=6

UMAX= 1.60E-001
1.71E-001
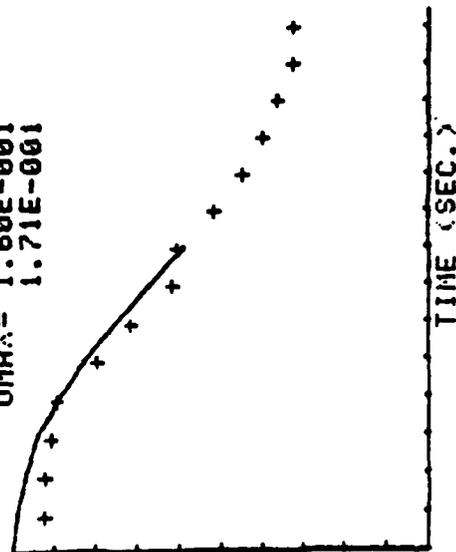
TIME (SEC.)

QMAX= 3.35E-003
2.28E-002

UMAX=-4.73E-002
     -4.32E-002

RSMAX=-6.71E-001
      -6.13E+000
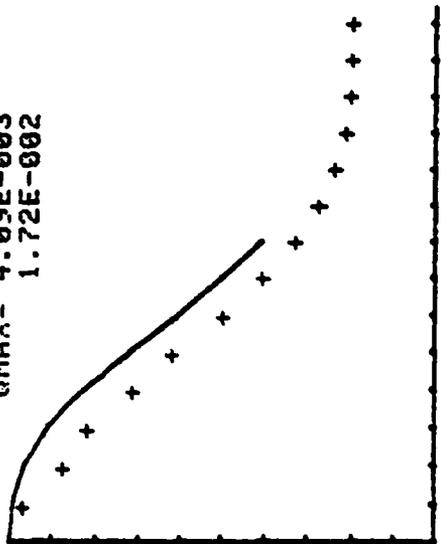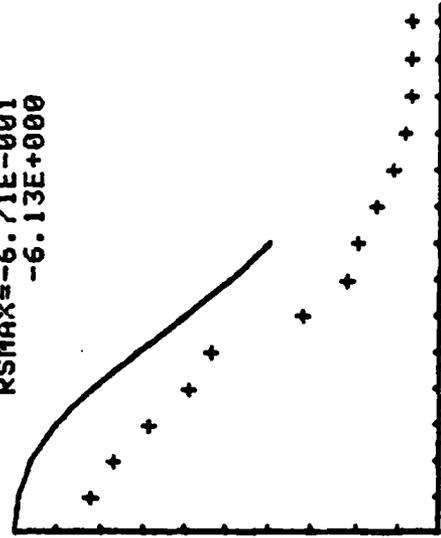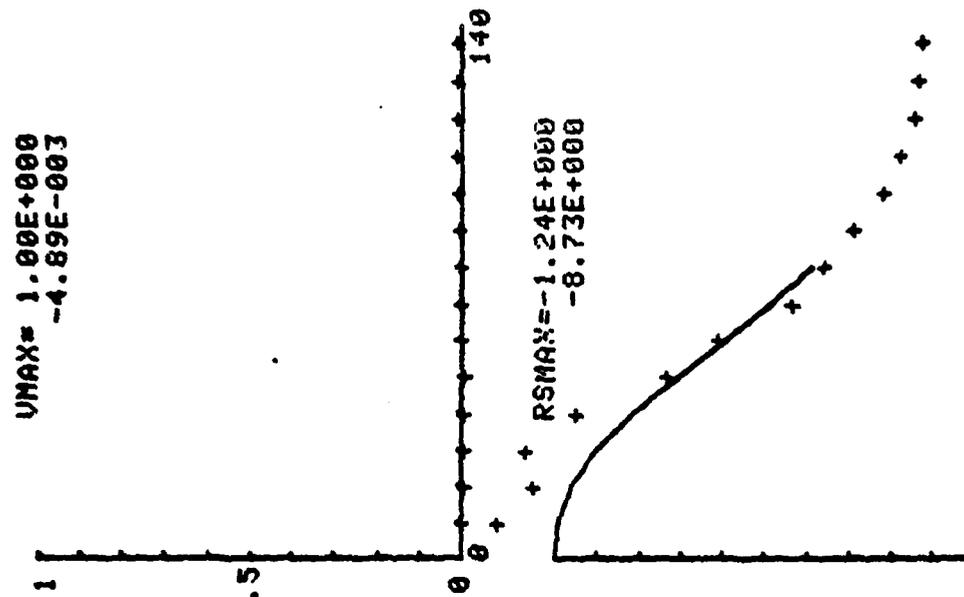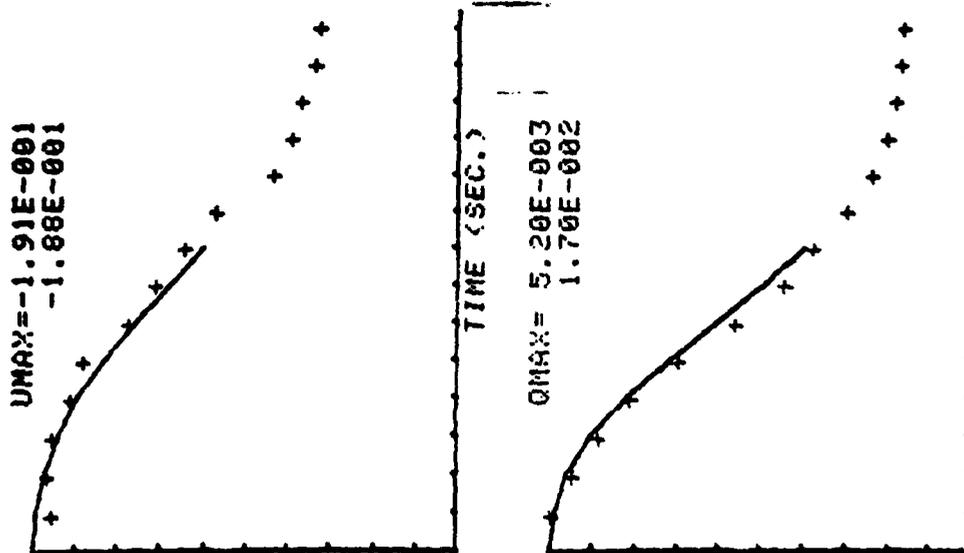
140

.5

0

I=8
J=10

UMAX= 1.00E+000
     -2.38E-002

QMAX= 4.09E-003
      1.72E-002

TIME (SEC.)

VMAX= 7.21E-002
       4.45E-002

RSMAX=-2.62E+000
      -4.79E+000

I=8
J=16

UMAX=-7.59E-001
     -6.87E-001

QMAX= 5.62E-003
      6.87E-003

TIME (SEC.)

UMAX= 1.37E-002
       -1.11E-003

RSMAX= 5.06E-002
        6.25E-002

I=18
J=2

140

.5

0

UMAX= 7.98E-001
       8.13E-001

TIME (SEC.)

QMAX= 3.83E-004
       1.40E-002
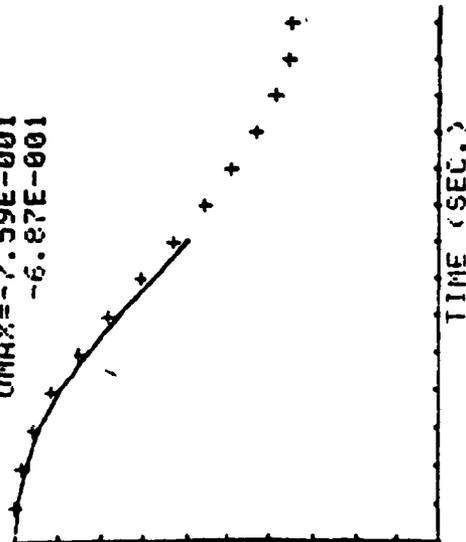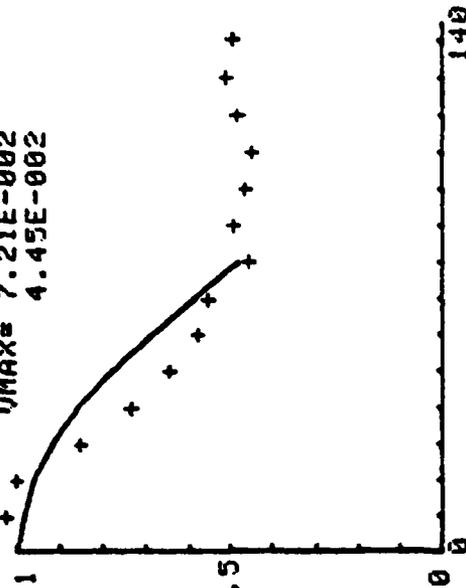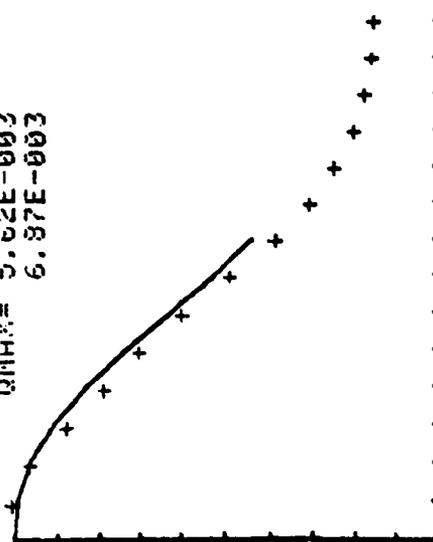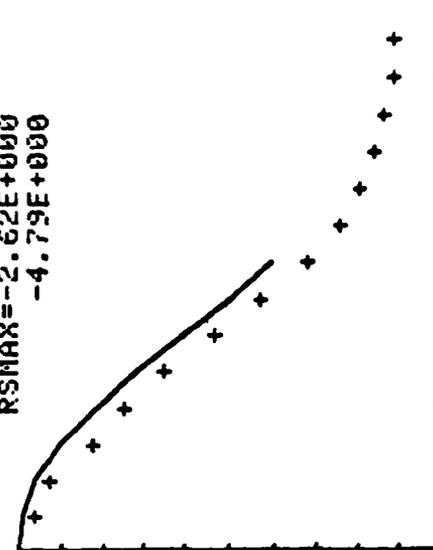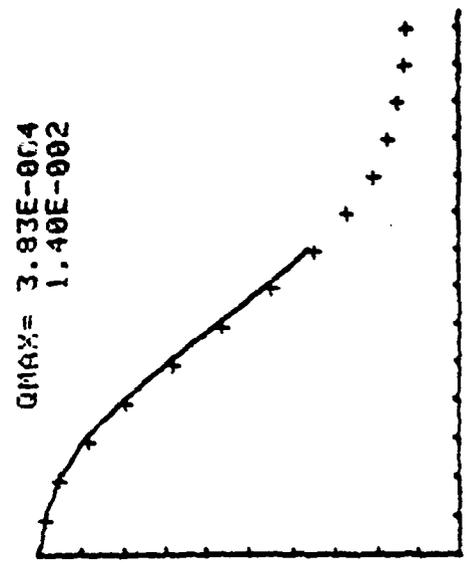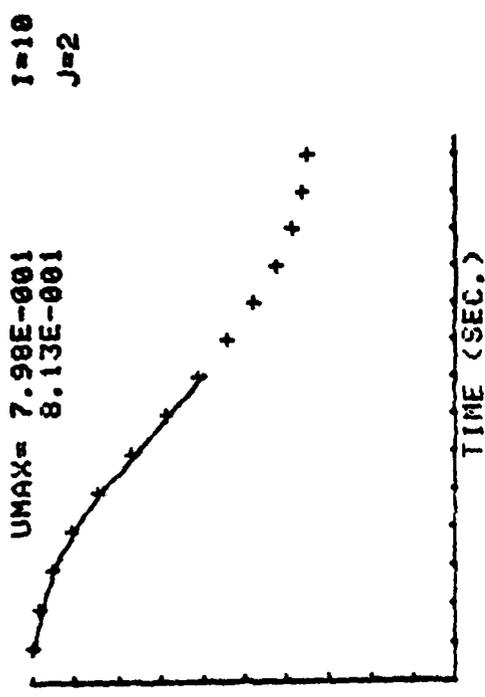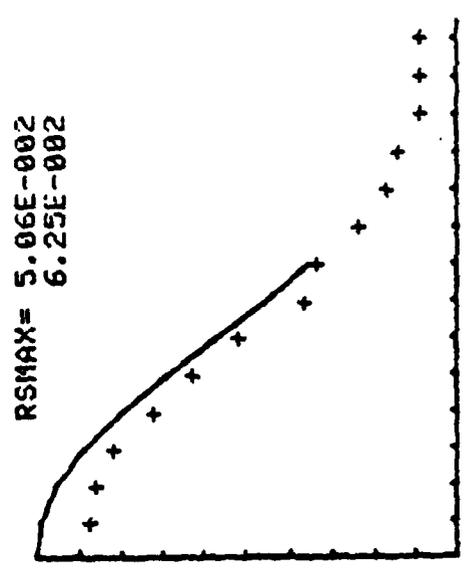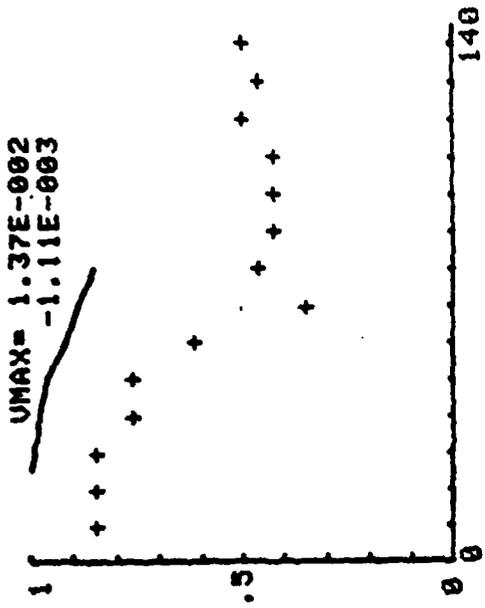
UMAX= 4.19E-002
8.00E-003
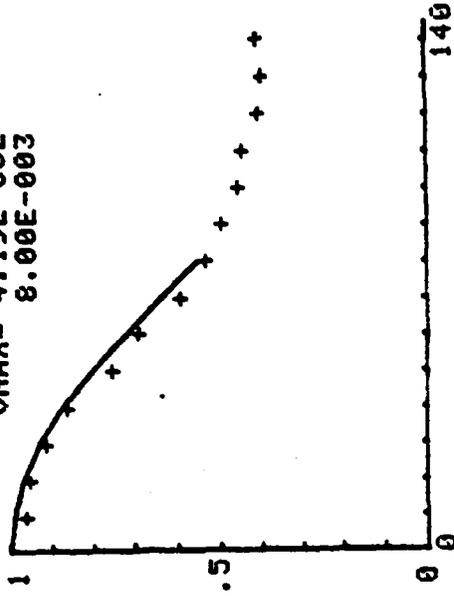
RSMAX=-4.95E-001
-1.88E+000
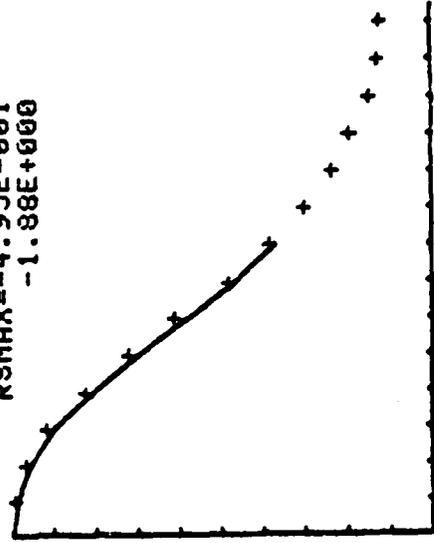
I=10
J=4

UMAX= 7.62E-001
7.38E-001
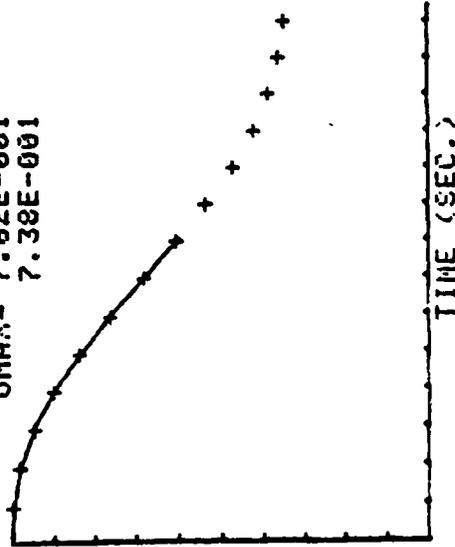
TIME (SEC.)

QMAX= 1.72E-003
1.45E-002
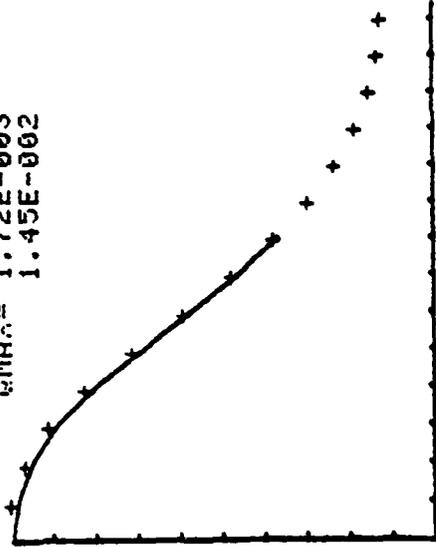
UMAX= 1.00E+000
-3.89E-002
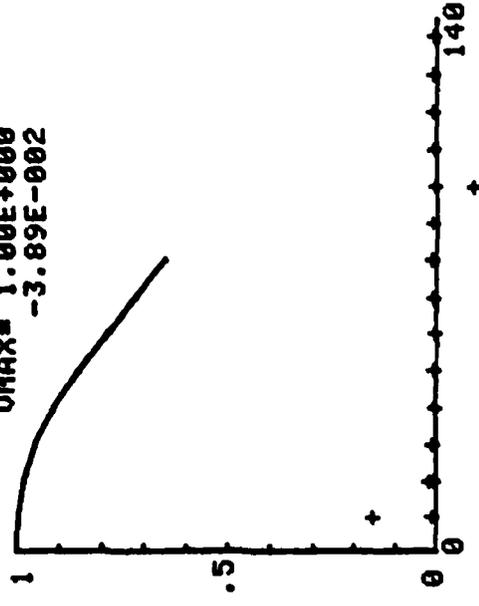
+ RSMAX=-2.50E-001
-4.62E+000

I=10
J=8
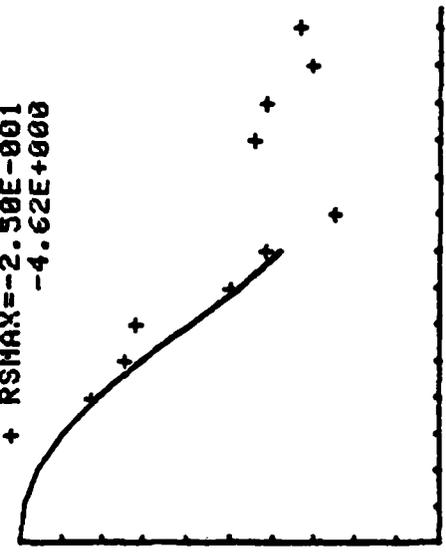
UMAX= 9.24E-002
8.42E-002
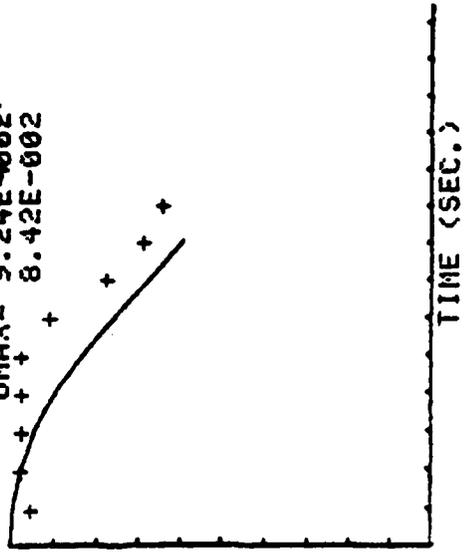
TIME (SEC.)

QMAX= 2.97E-003
1.55E-002
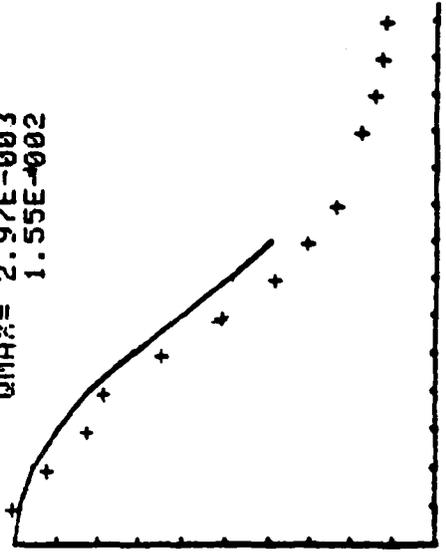
UMAX= 1.00E+000
1.61E-002
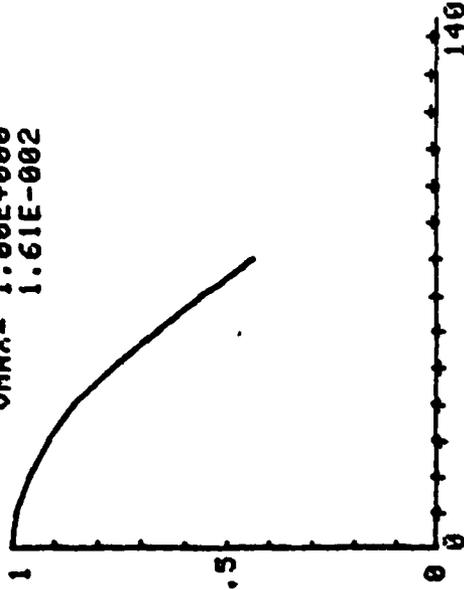
RSMAX=-3.22E+000
-3.90E+000

I=10
J=14
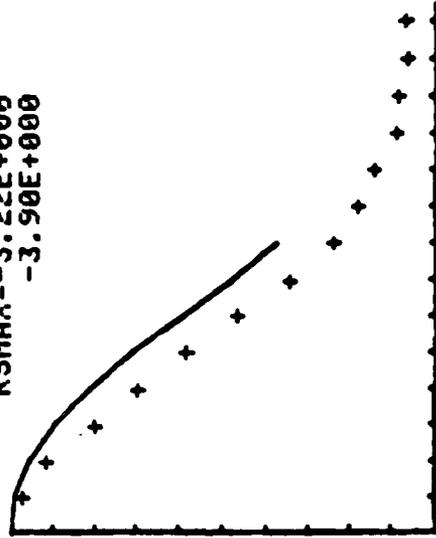
UMAX=-4.75E-001
-4.58E-001

TIME (SEC.)

QMAX= 7.52E-003
5.93E-003

UMAX=-6.24E-003
4.46E-003

RSMAX= 2.26E-002
5.66E-002

I=12
J=2

UMAX= 7.78E-001
8.07E-001

TIME (SEC.)

QMAX= 3.64E-004
7.87E-003
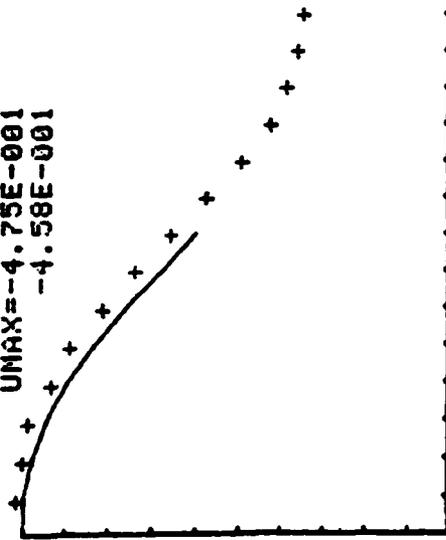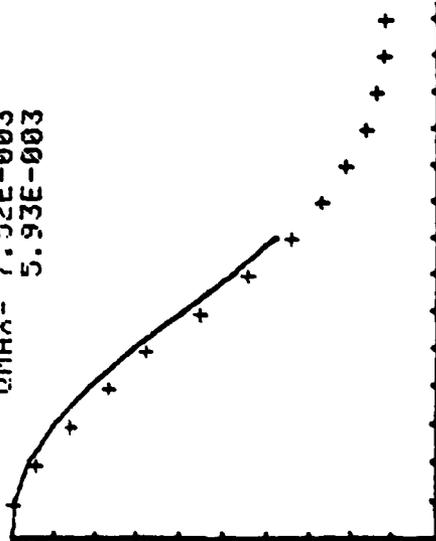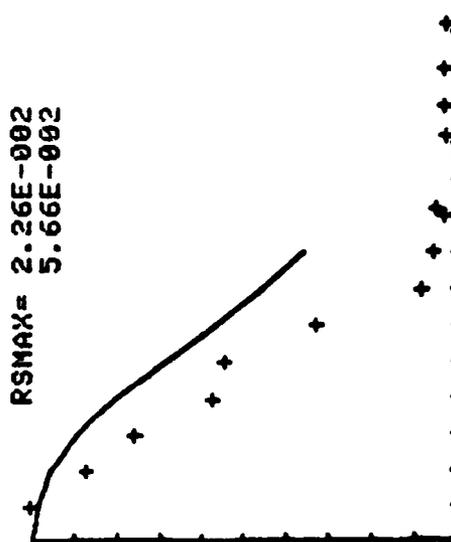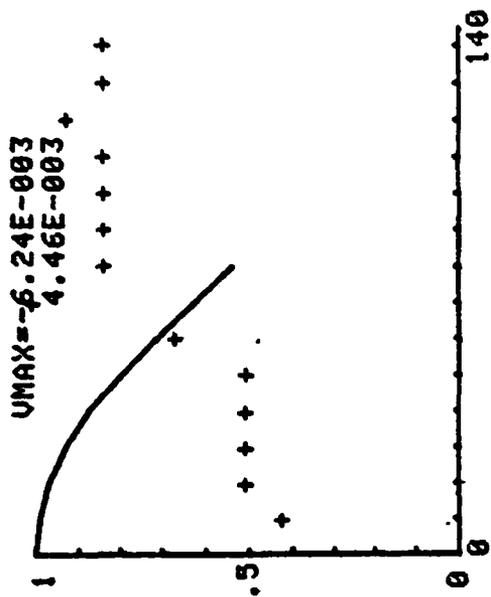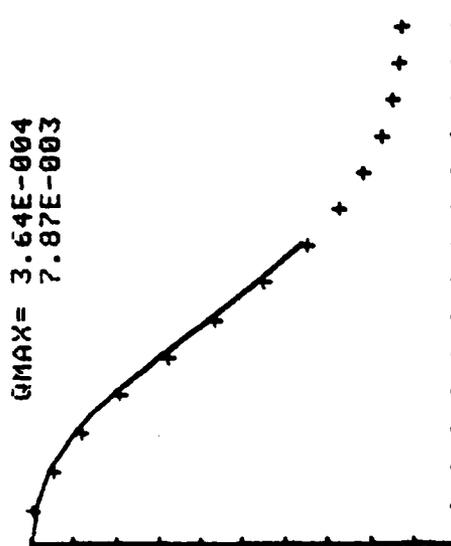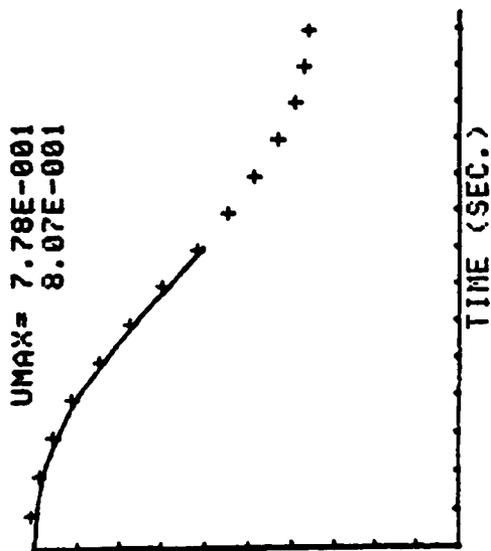
VMAX= 1.00E+000
-1.73E-002
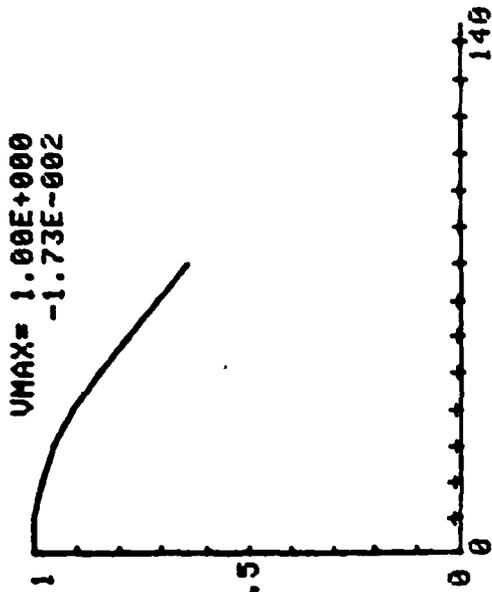
RSMAX=-3.20E-001
-5.83E+000

I=12
J=6

140

0

.5

0
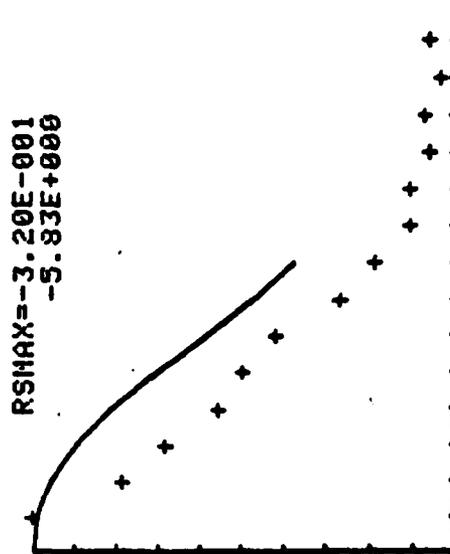
UMAX= 1.54E-001
2.23E-001
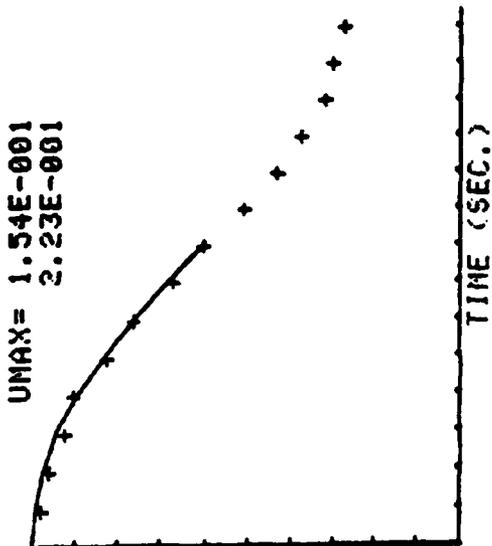
QMAX= 2.44E-003
1.73E-002

TIME (SEC.)

UMAX= 2.41E-002
       -1.42E-002

RSMAX=-3.85E-001
      -5.59E+000

I=12
J=10

UMAX=-3.63E-002
      -4.85E-002

TIME (SEC.)

QMAX= 1.83E-003
      1.18E-002
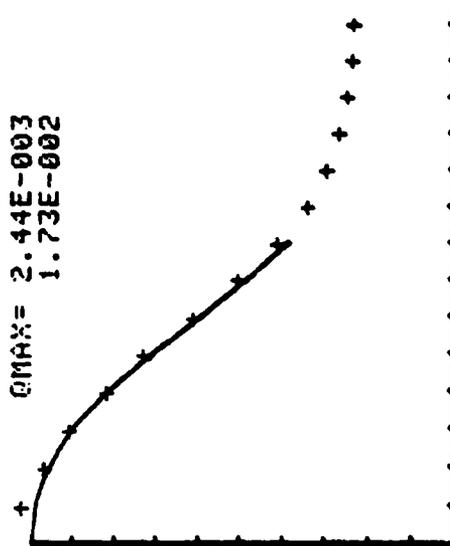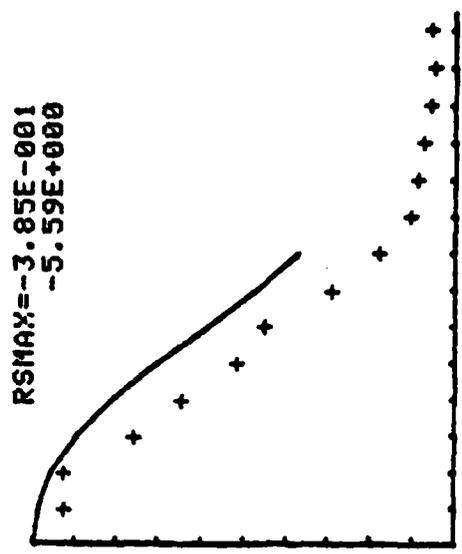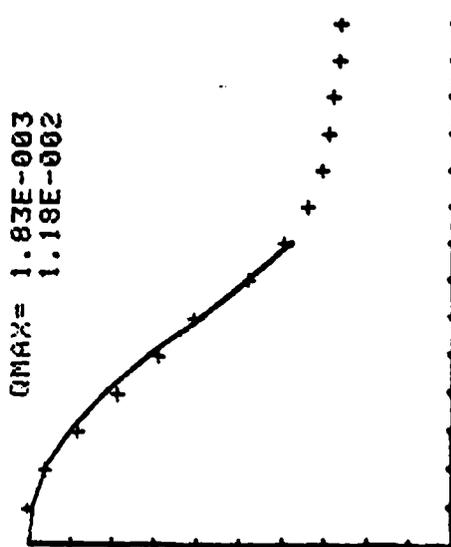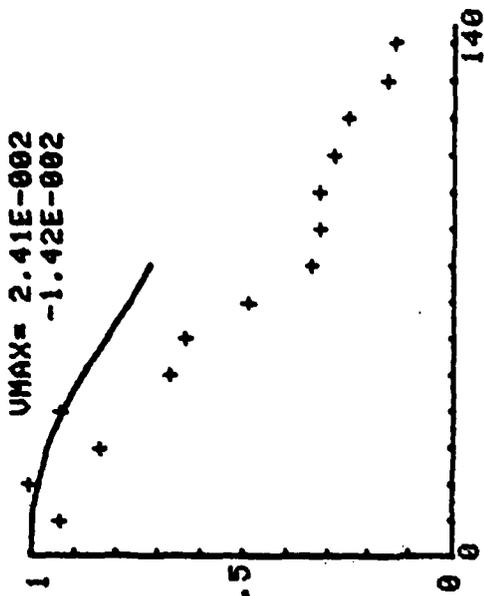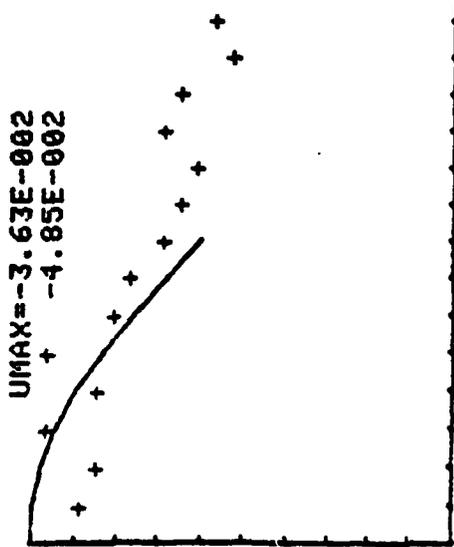
UMAX=-2.24E-002
1.35E-002
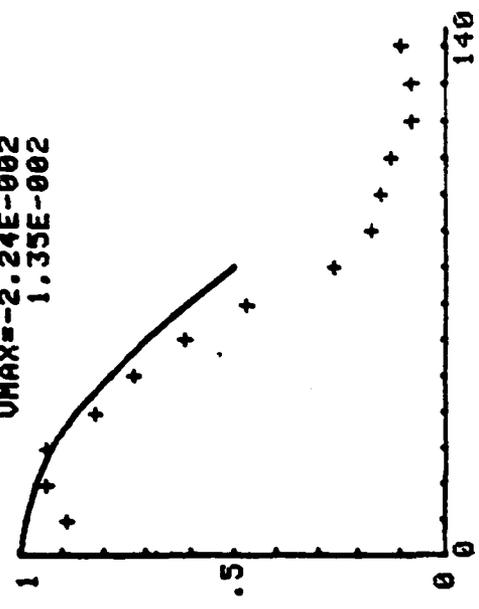
RSMAX=-2.52E+000
-2.52E+000

I=12
J=14

140

.5

0

1
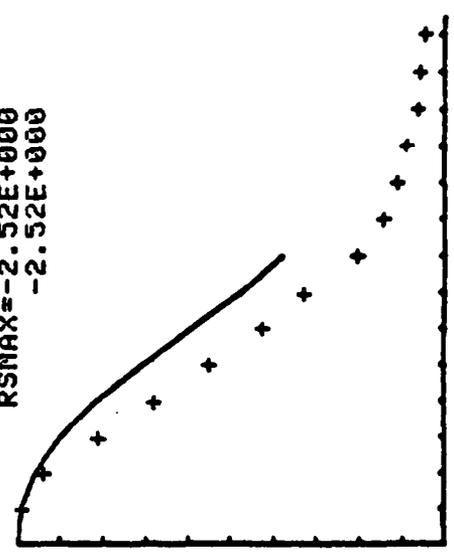
UMAX=-5.10E-001
-4.67E-001
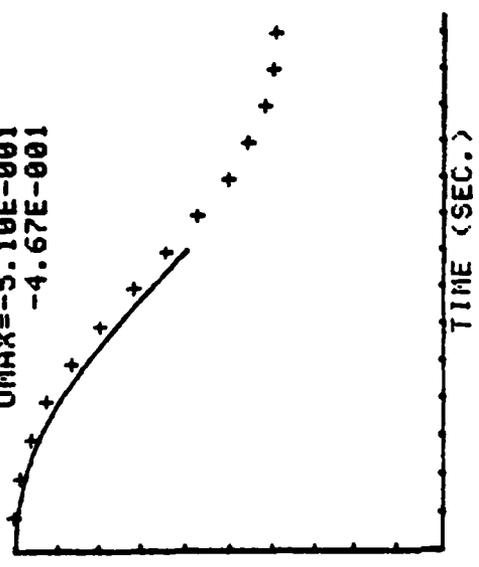
TIME (SEC.)

QMAX= 7.73E-003
4.14E-003
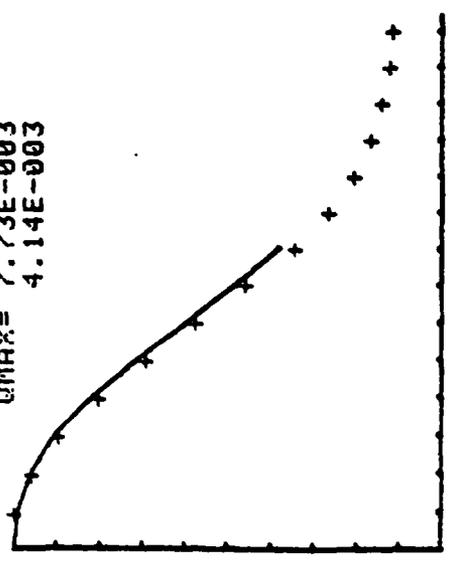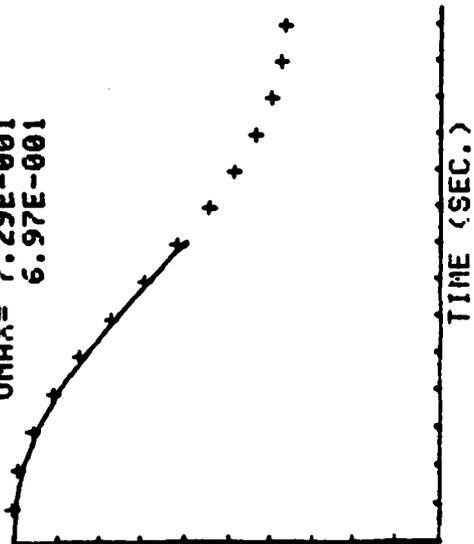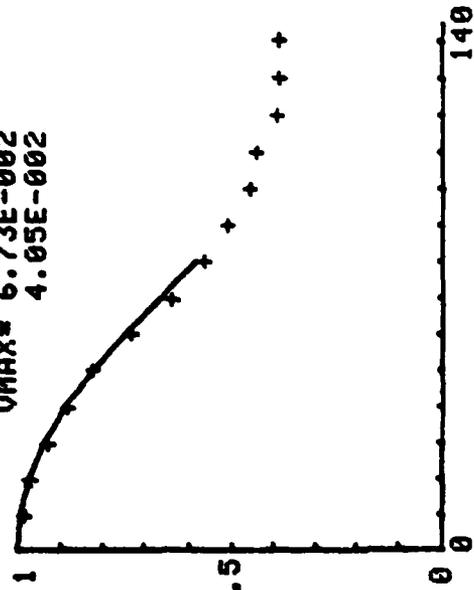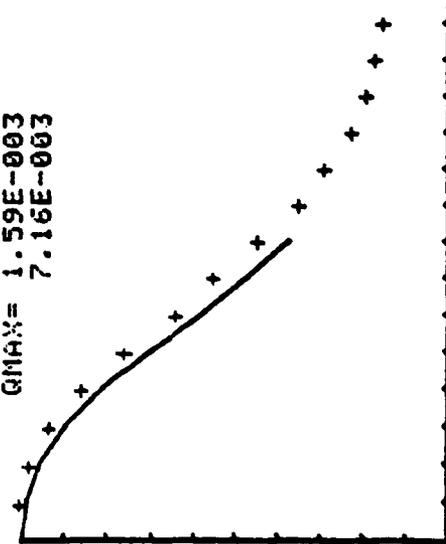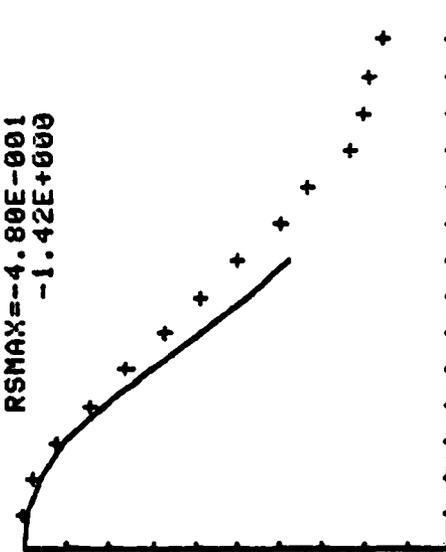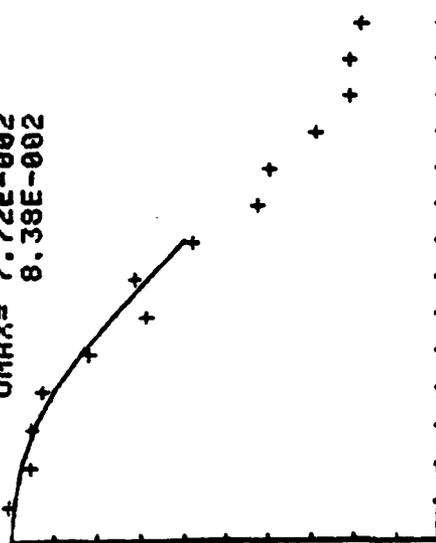
UMAX= 3.18E-002
      1.60E-003

140
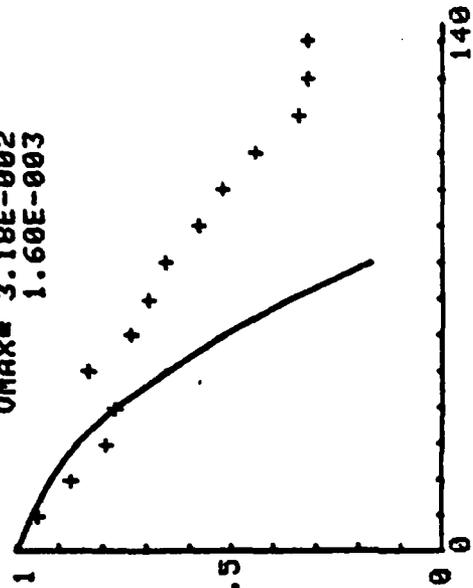
UMAX= 7.72E-002
      8.38E-002

RSMAX=-1.93E-001
      -3.79E+000

TIME (SEC.)

UMAX= 1.68E-003
      1.15E-002

I=14
J=8

UMAX= 2.59E-002
      2.55E-002

RSMAX=-1.97E+000
      -3.61E+000

I=14
J=12

UMAX=-2.67E-001
     -2.53E-001

QMAX= 6.10E-003
      6.19E-003

TIME (SEC.)

UMAX=-3.49E-002
      1.06E-002
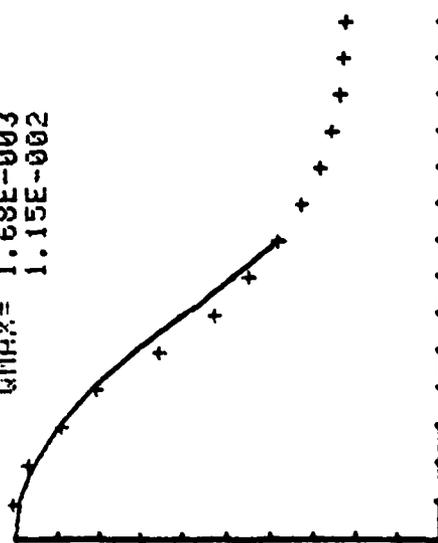
RSMAX=-1.48E+000
       -9.69E-001
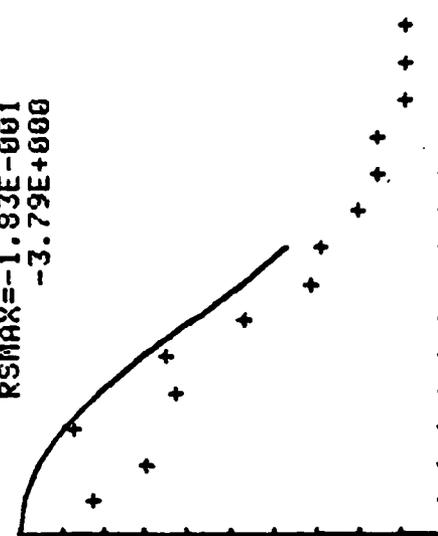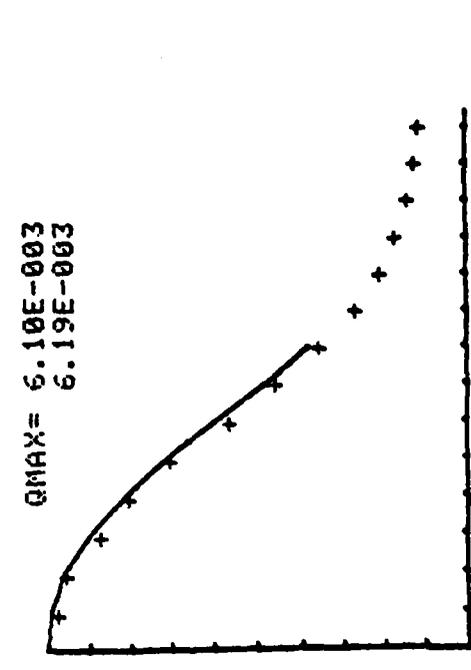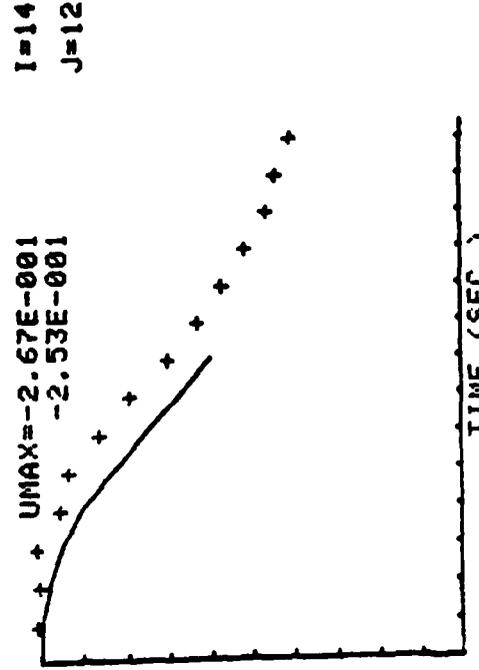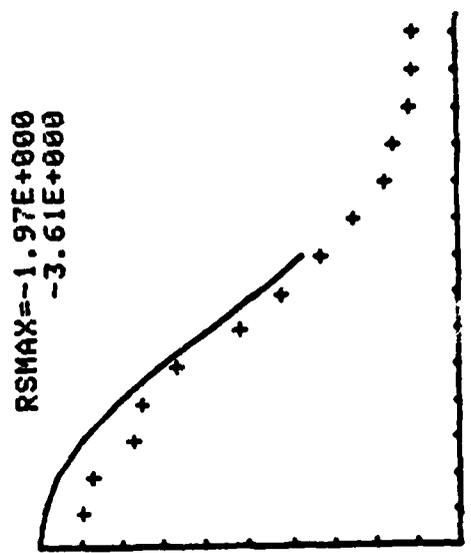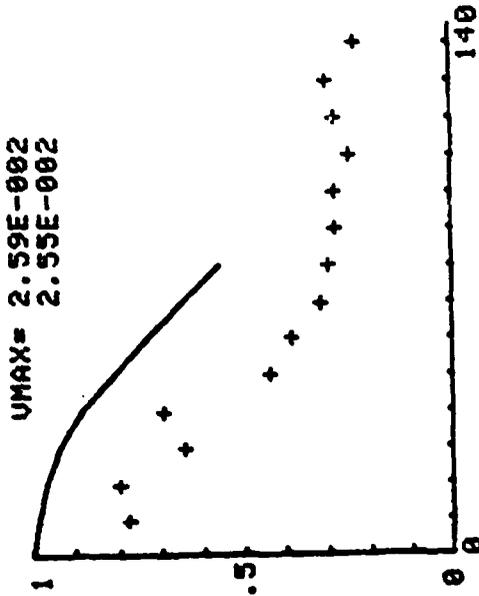
I=14
J=16

UMAX=-6.72E-001
      -6.45E-001

TIME (SEC.)

QMAX= 5.23E-003
      3.15E-003

VMAX= 9.15E-002
       8.18E-002

RSMAX=-4.32E-001
       -1.07E+000

UMAX= 7.29E-001
       6.58E-001

QMAX= 1.53E-003
       5.55E-003

I=16
J=4

TIME (SEC.)

140

0

1

.5

0

UMAX= 3.23E-002
       4.90E-002
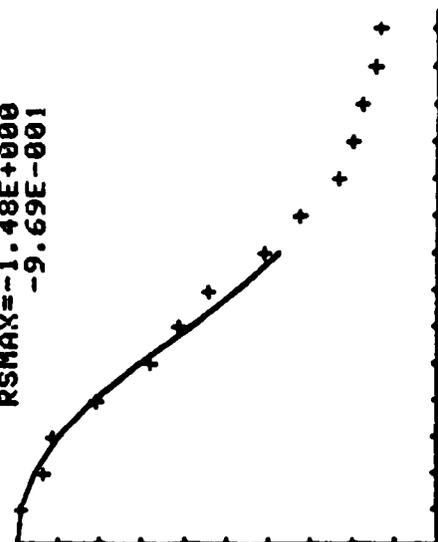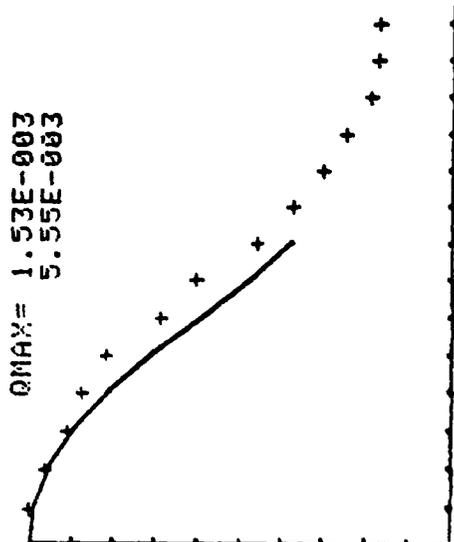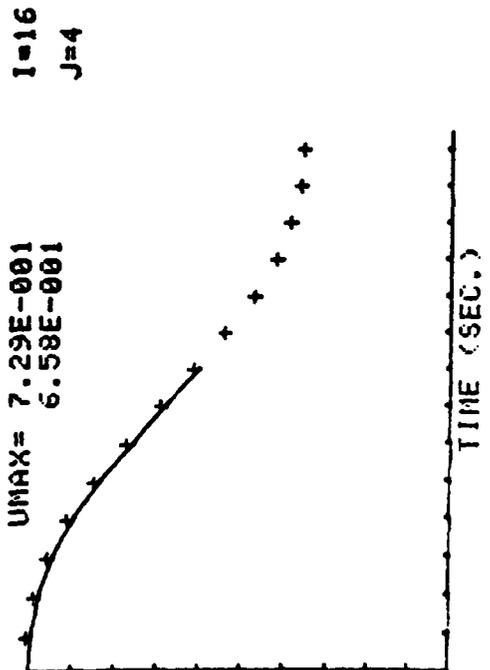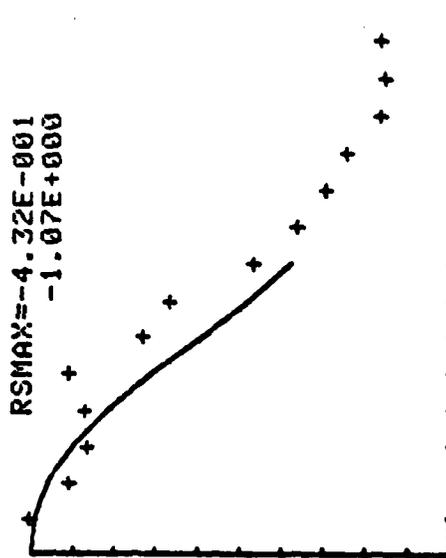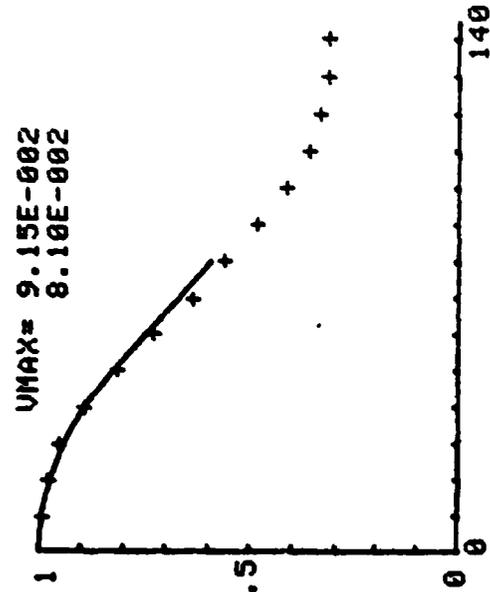
RSMAX=-1.36E-001
       -2.40E+000

UMAX= 5.59E-002
       8.42E-002

QMAX= 1.43E-003
       9.47E-003

I=16
J=8

TIME (SEC.)

UMAX= 3.08E-002
        6.74E-002

RSMAX=-2.07E+000
        -2.04E+000
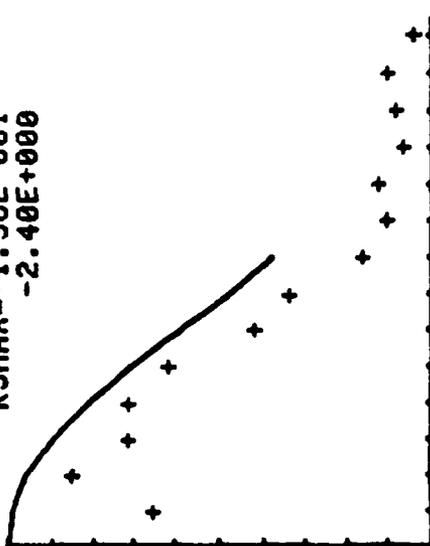
I=16
J=12

UMAX=-2.97E-001
        -2.60E-001
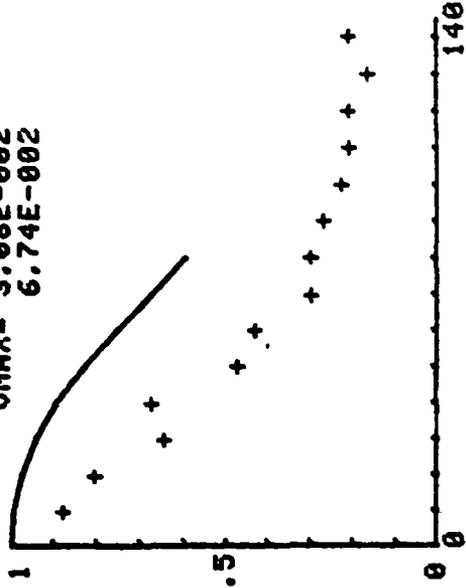
QMAX= 7.41E-003
        4.39E-003

TIME (SEC.)

0   140

UMAX= 1.03E-001
1.49E-001

RSMAX=-2.82E+000
-2.12E+000

I=18
J=6

UMAX= 2.35E-001
2.92E-001

QMAX= 6.40E-003
8.82E-003

TIME (SEC.)

UMAX= 5.77E-002
1.47E-001
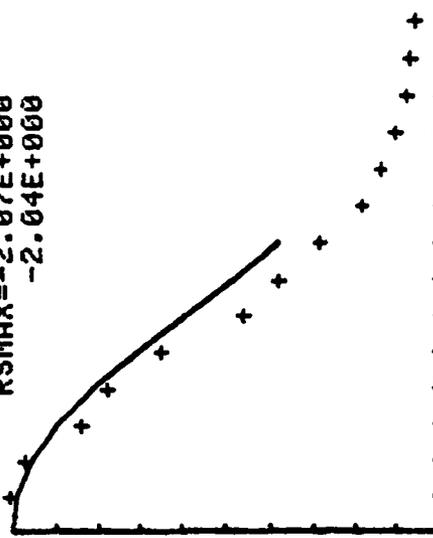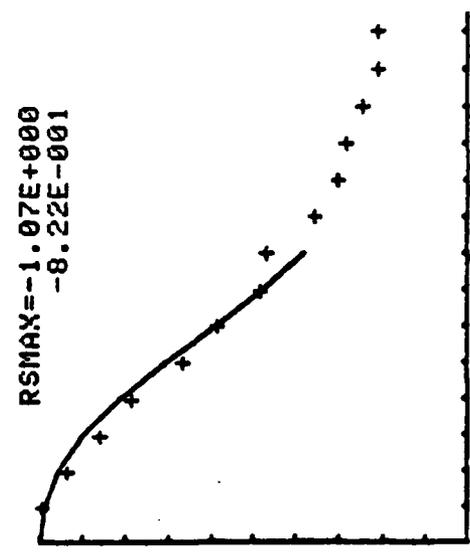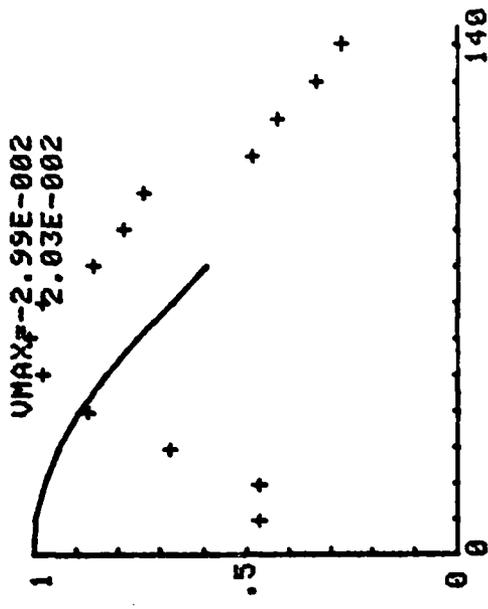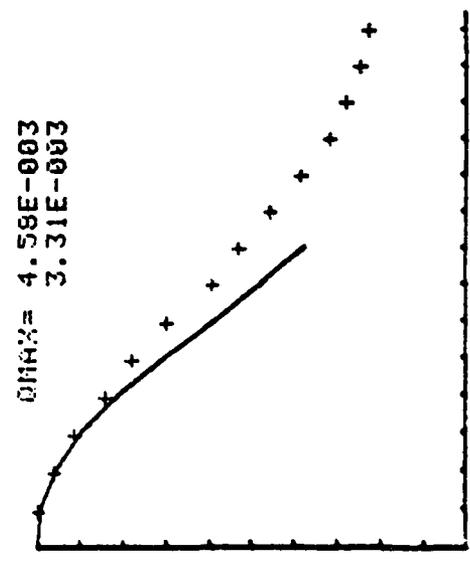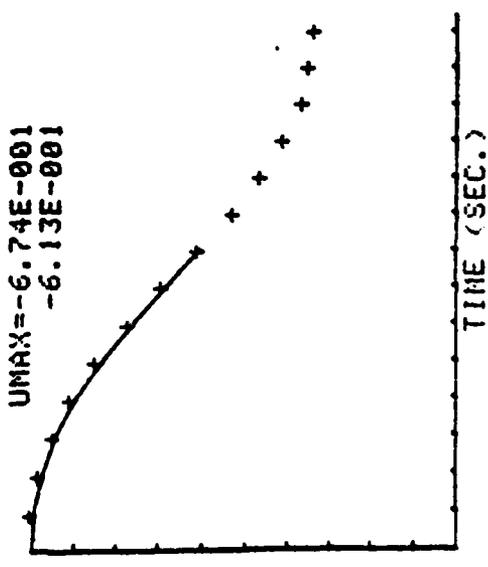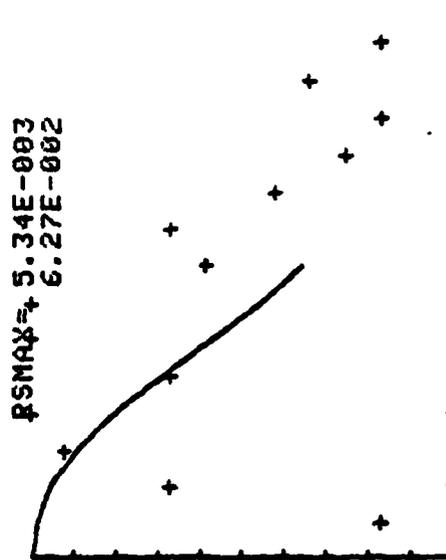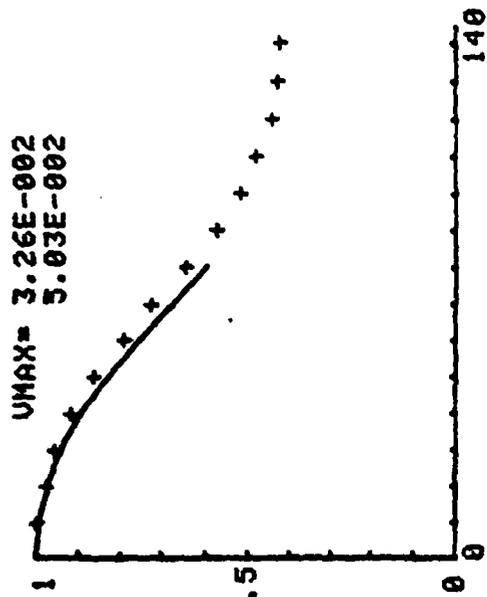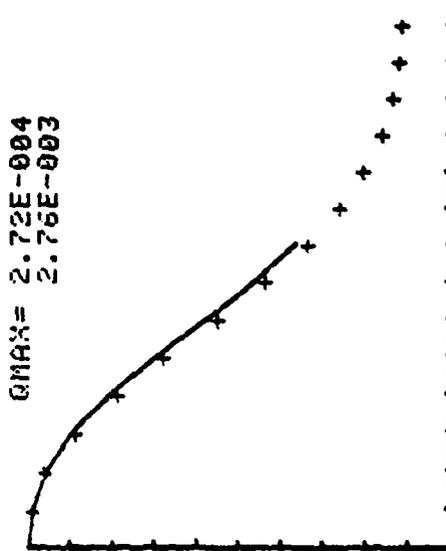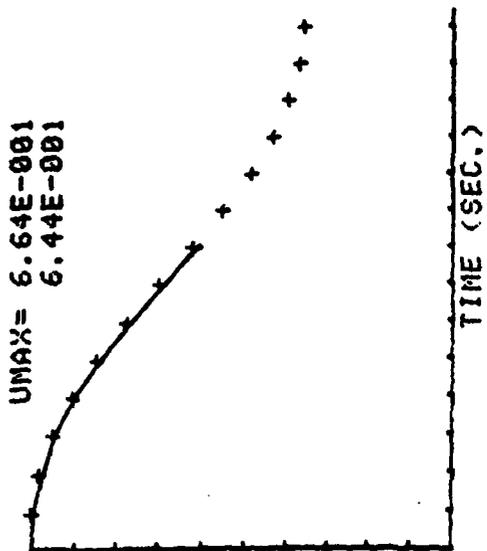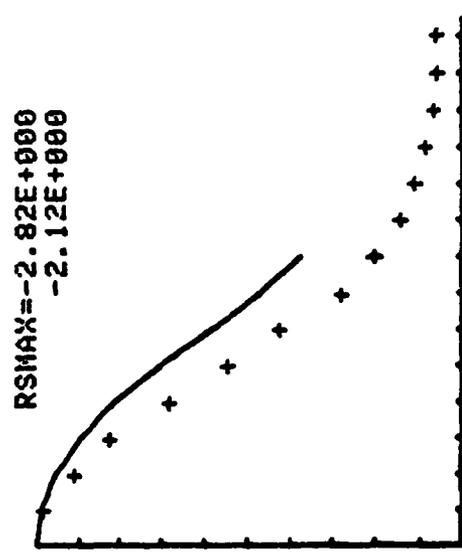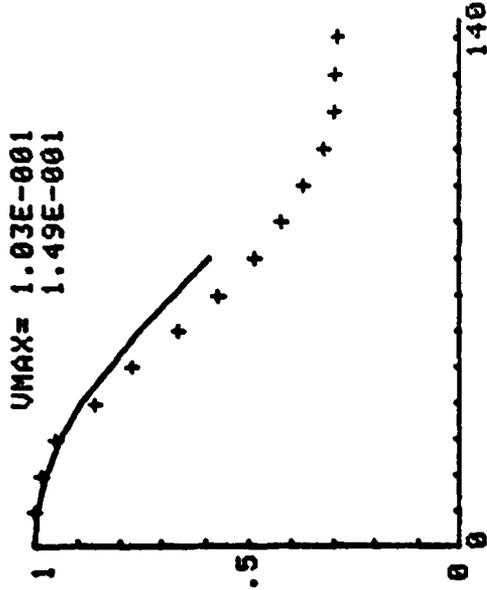
RSMAX=-3.92E-001
-8.77E-001
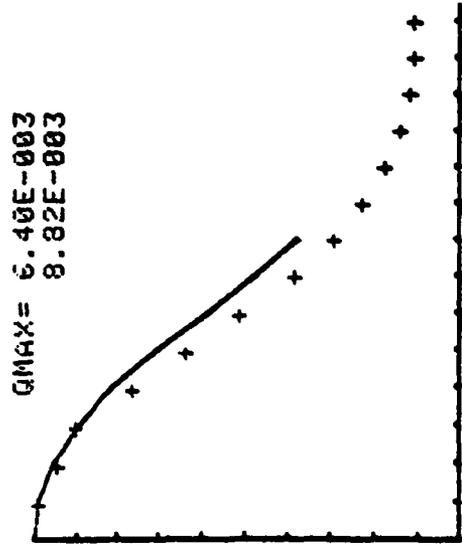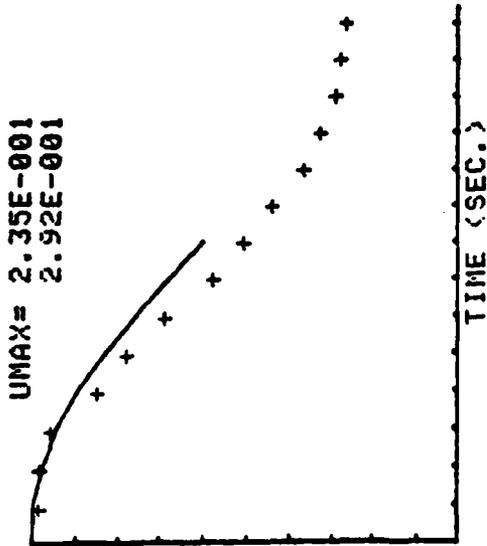
I=18
J=10

UMAX=-6.50E-002
-8.04E-002
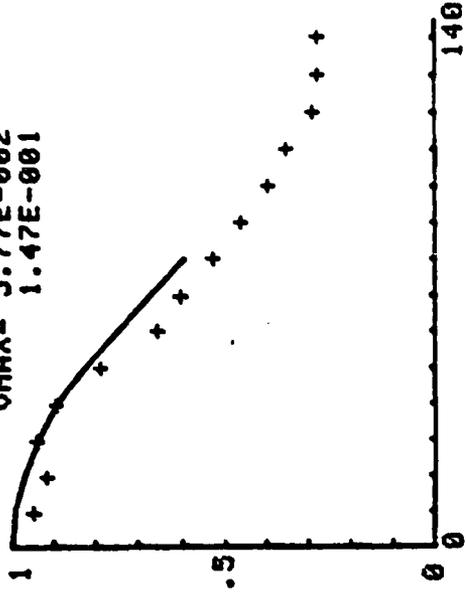
QMAX= 1.50E-003
5.19E-003

TIME (SEC.)

140

1

.5

0

UMAX= 5.26E-002
9.93E-002

RSMAX=-4.12E-001
-6.72E-001
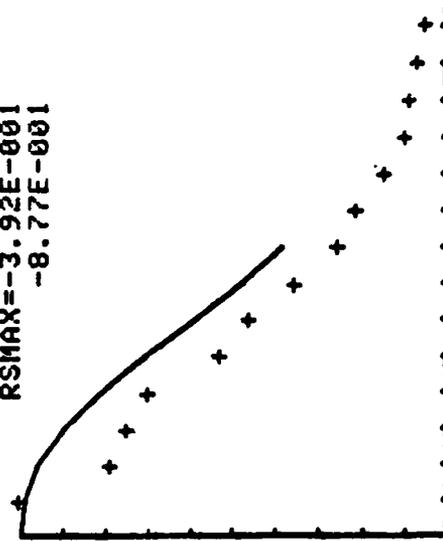
I=18
J=14

UMAX=-4.12E-001
-4.13E-001
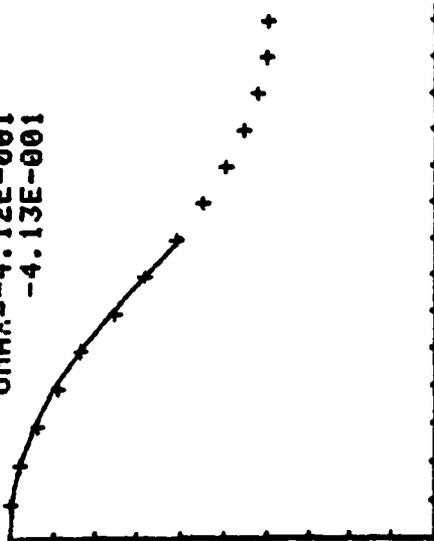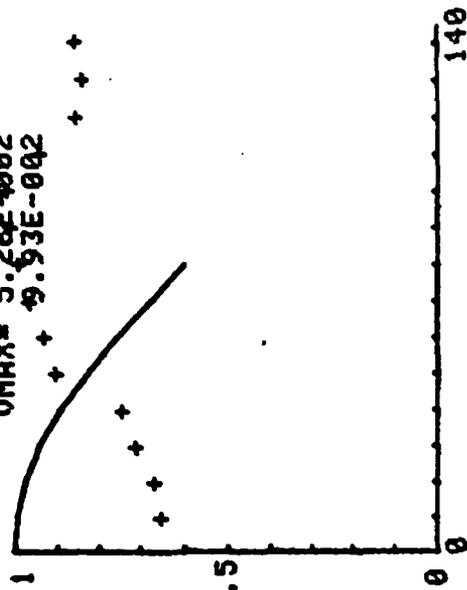
TIME (SEC.)

UMAX= 1.01E-002
2.54E-003
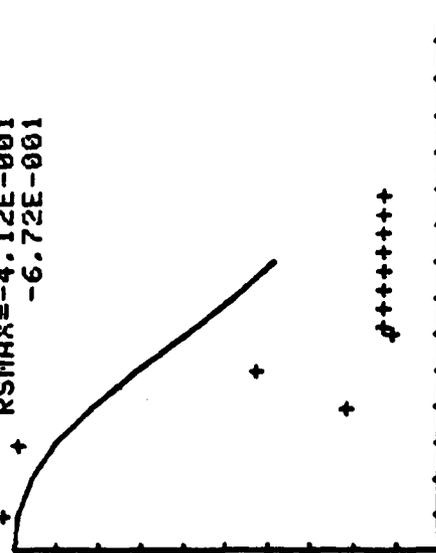
VMAX= 2.03E-001
      2.12E-001
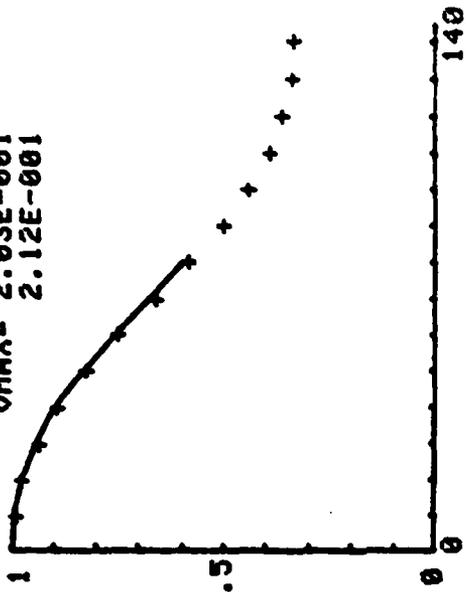
RSMAX= 1.49E-002
      -3.43E-001

I=20
J=4
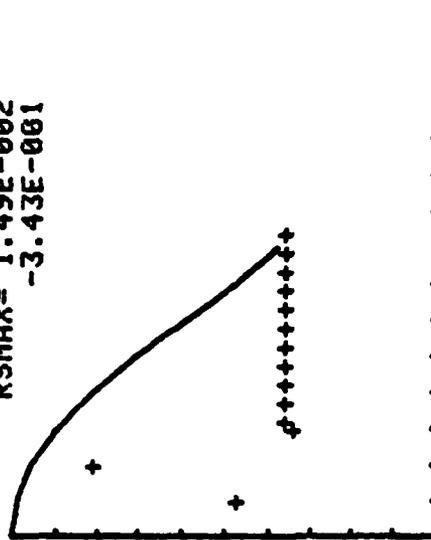
UMAX= 6.03E-001
      4.72E-001

TIME (SEC.)

QMAX= 5.85E-004
      3.12E-003

140

.5

0

UMAX= 1.34E-001
2.83E-001

RSMAX=-4.48E-001
-2.60E-001

I=20
J=8

UMAX= 7.31E-002
8.31E-002

QMAX= 2.74E-003
5.10E-003
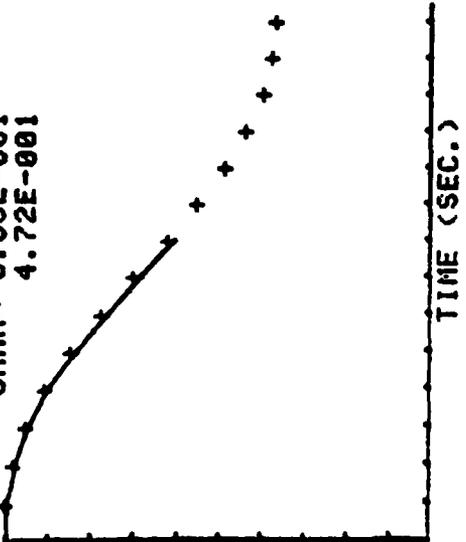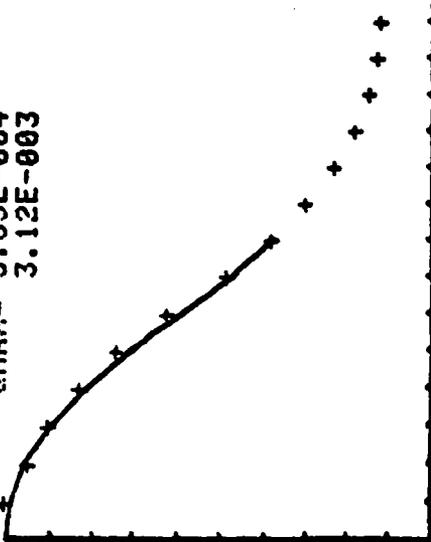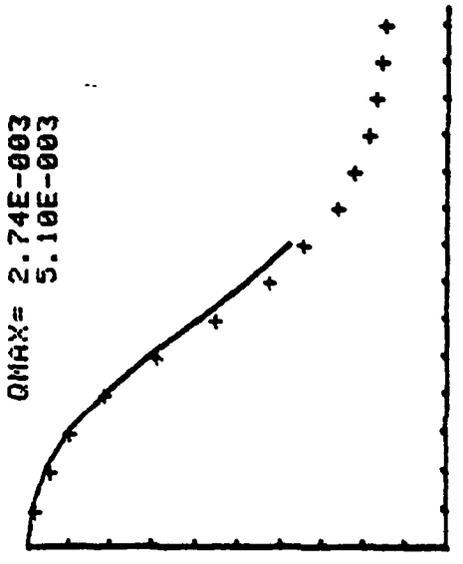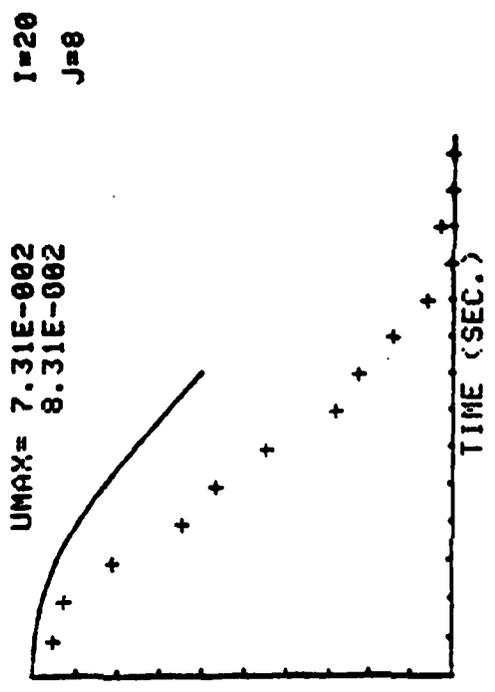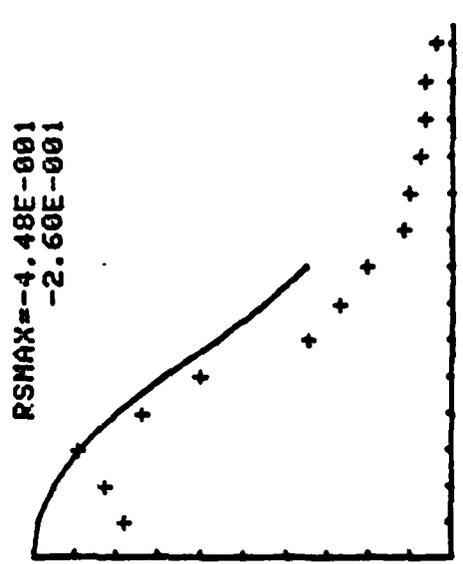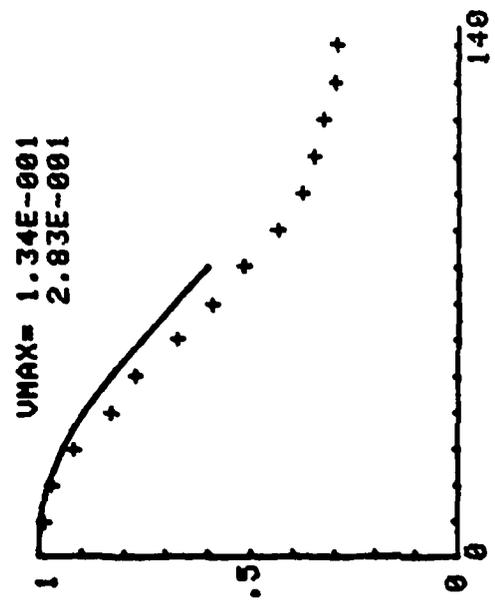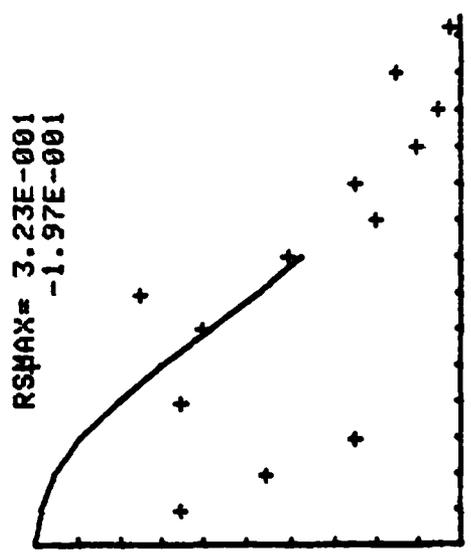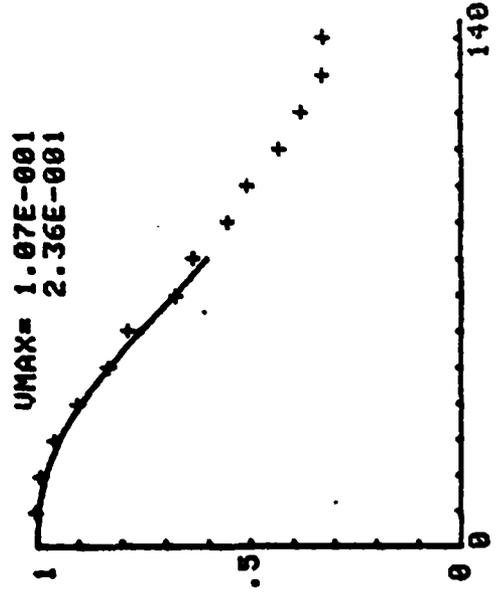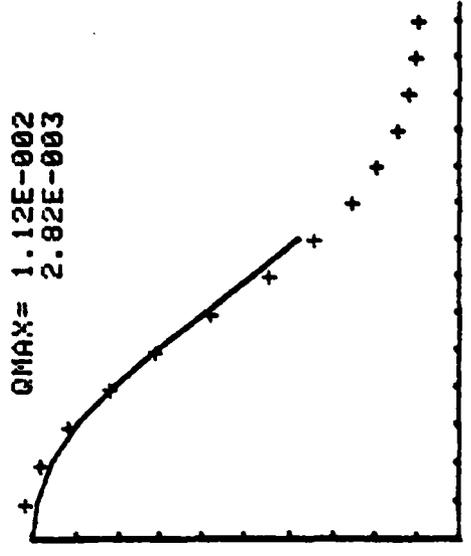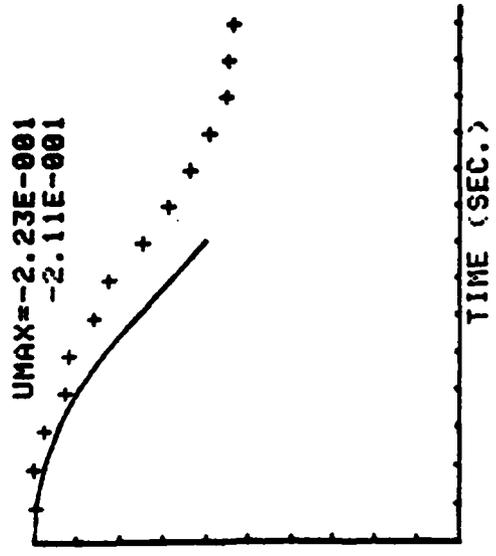
TIME (SEC.)

UMAX= 1.00E+000
5.81E-002
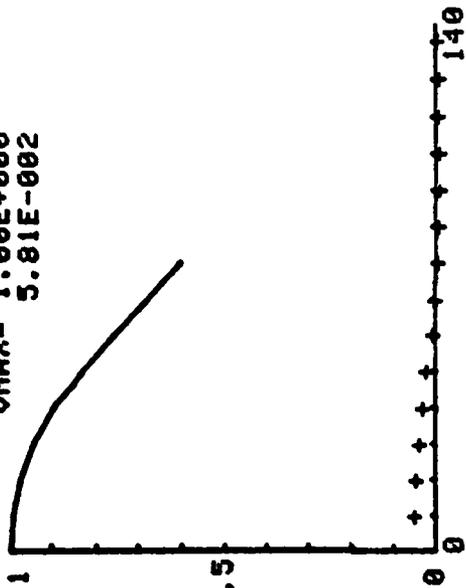
RSMAX= 7.35E-002
-4.91E-001
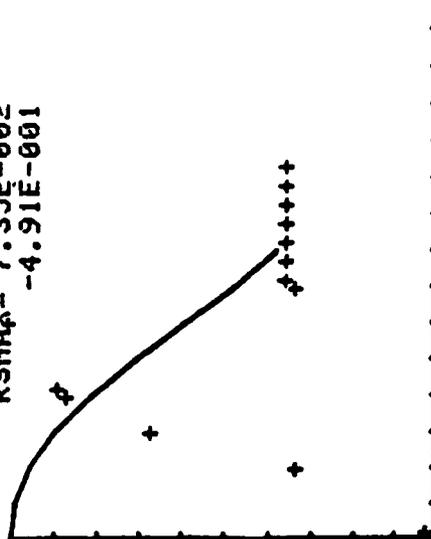
UMAX=-5.60E-001
-4.54E-001

I=20
J=16
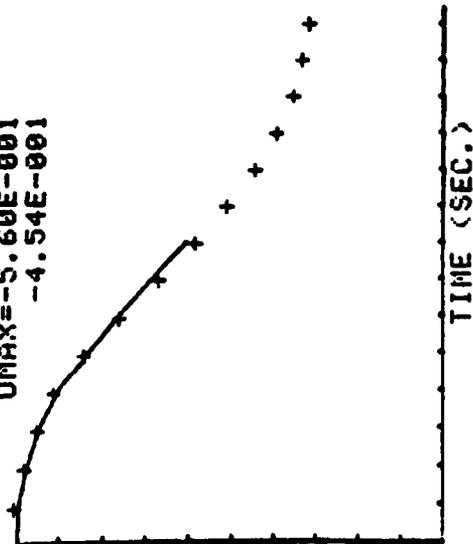
QMAX= 3.04E-003
3.98E-003

TIME (SEC.)

UMAX= 4.84E-002
9.48E-002
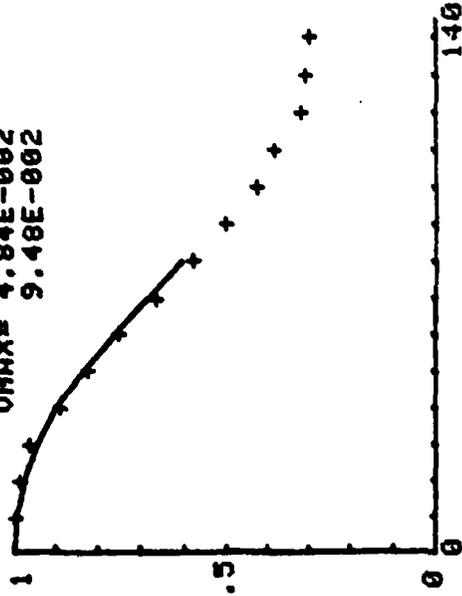
RSMAX= 1.56E-002
5.03E-002

I=22
J=2

UMAX= 4.49E-001
3.29E-001

TIME (SEC.)

OMAX= 3.01E-004
2.12E-003

140
.5
0

UMAX= 4.42E-001
      3.88E-001

RSMAX= 9.93E+002
      -2.60E-001

I=22
J=6

UMAX= 4.45E-001
      1.87E-001

QMAX= 1.25E-003
      3.30E-003

TIME (SEC.)

140

0

.5

1

UMAX= 2.60E-001
       4.14E-001

RSMAX= 1.51E-001
        9.51E-002

I=22
J=10

UMAX= 1.00E+000
      -4.54E-002

QMAX= 5.05E-003
       2.58E-003

TIME (SEC.)
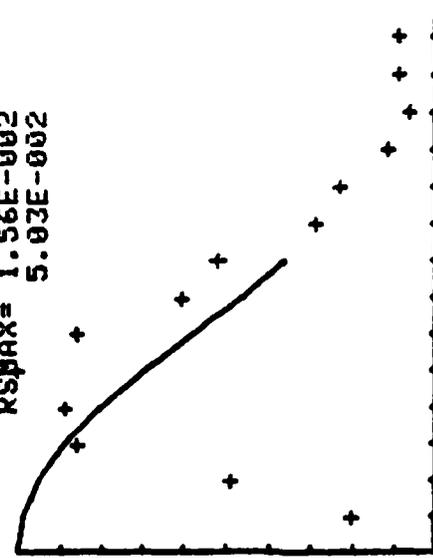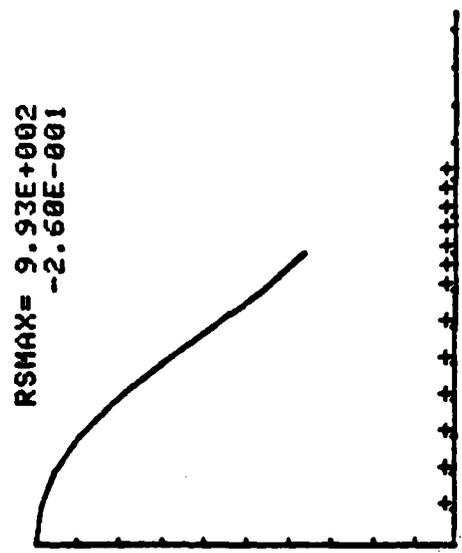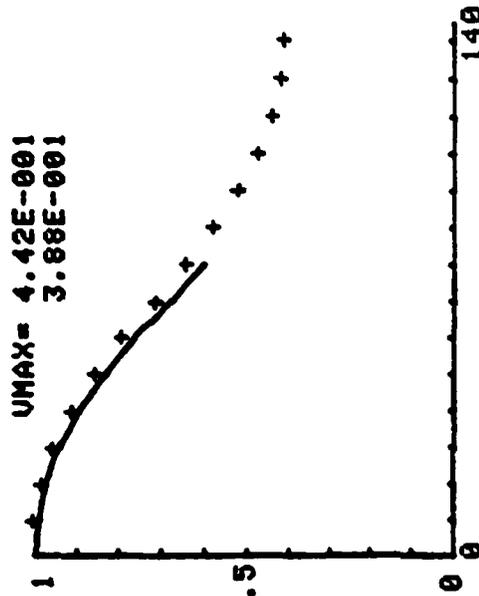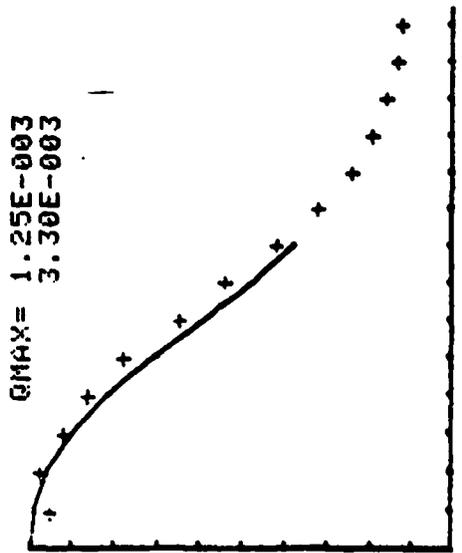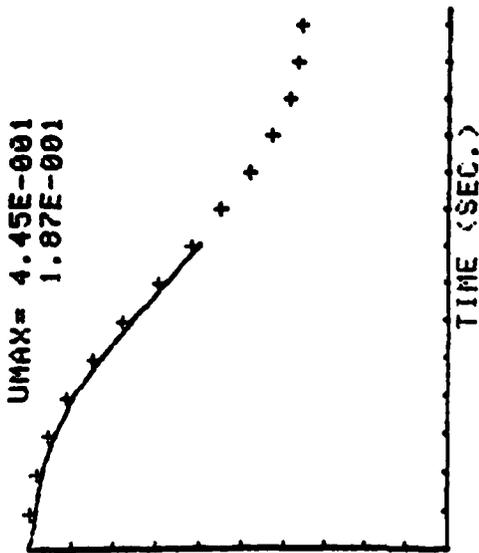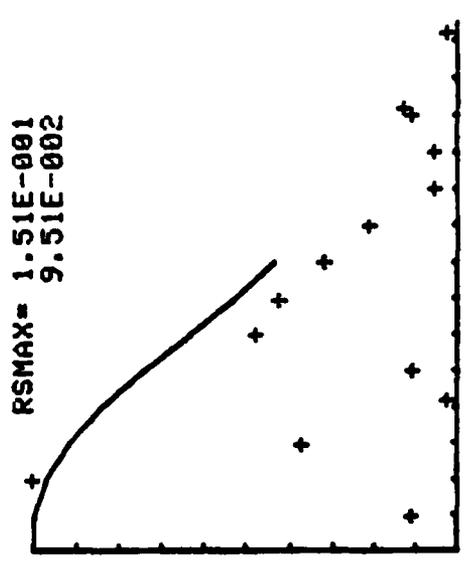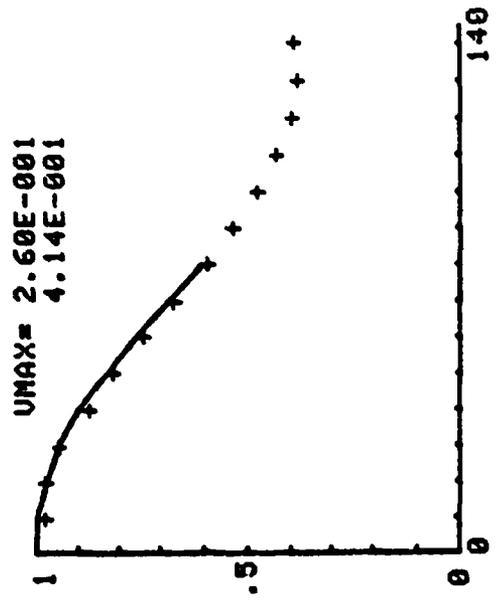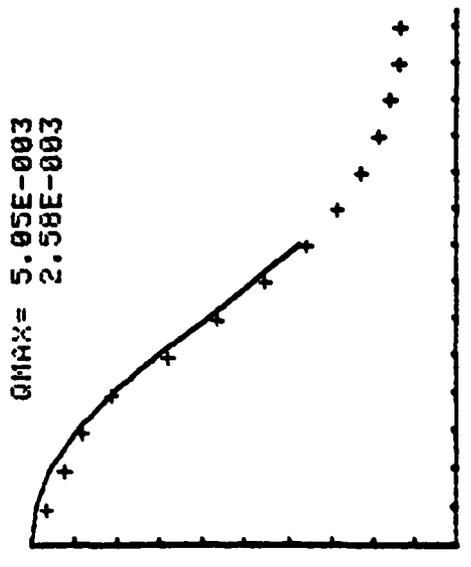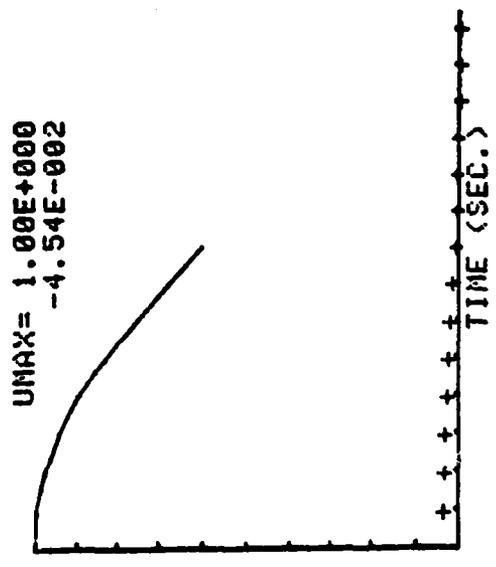
UMAX= 1.82E-001
2.35E-001
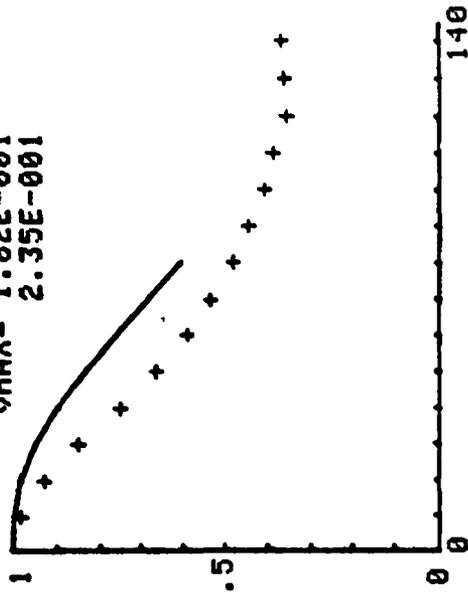
RSMAX= 3.87E-001
-4.85E-002

140

1

.5

0

0
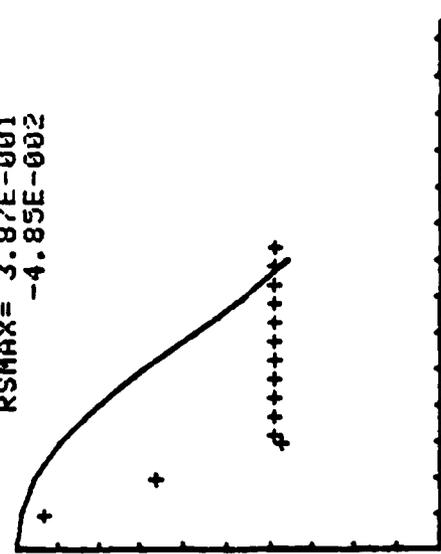
I=22
J=14

UMAX=-2.37E-001
-2.25E-001
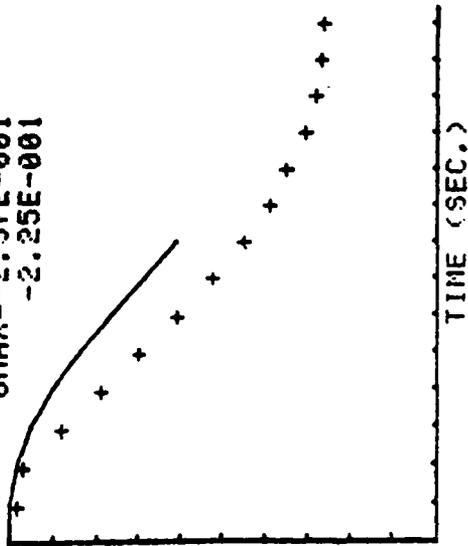
QMAX= 6.06E-003
2.30E-003

TIME (SEC.)
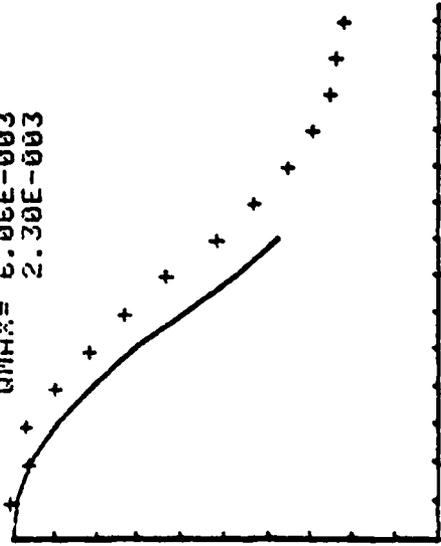
APPENDIX G

NOTES ON LDA OPERATIONS

A number of general statements in Chapter Three regarding LDA theory are addressed here with emphasis on the specific technique and equipment used in this experiment. In particular, this appendix expands on the following three sections:

> 3.2.3.2 Light Scattering Particles
>
> 3.2.3.3 Optical Arrangement
>
> 3.2.3.4 Point Positioning

Light Scattering Particles

In cases where demineralized water with artificial seeding is used, the scattering particle size can be controlled and optimized. When using the fringe mode, the particle diameter should be smaller than the fringe spacing to obtain maximum signal modulation. Generally, particle diameters on the order of ten to thirty percent of the fringe spacing are recommended. In the reference beam mode, the virtual fringe spacing may be used for the particle diameter calculation. The half-micron latex particles that were used successfully in a previous experiment [Chen] were used again in this experiment, and no further particle-size optimization was attempted.

The scattering particle concentration in the reference beam mode can be much higher than that used in the fringe mode. In the

latter case, one particle per measuring volume is the ideal homogeneous concentration. In this reference beam experiment, a concentration of approximately ten to one hundred particles per measuring volume was found to give an easily tracked and continuous Doppler signal. The so-called "Doppler ambiguity," introduced by the simultaneous presence of many particles in the measuring volume, is discussed and accounted for in Appendix B.

Optical Arrangement

In order to measure two orthogonal velocity components simultaneously, it is necessary to discriminate between the Doppler signals that correspond to each direction. This is usually accomplished by using either different polarization or different wavelengths (colors) for the two velocity directions to be measured. In the dual-beam or fringe mode of LDA operation, polarization rotators must be added to the optics package or else a two-color laser modification (as well as new optics) are required. The expense of such charges is avoided in this experimental set-up by using the reference beam mode. In such a case, the existing optics package and inexpensive polarized lens covers on each of the two photomultiplier tubes may be used to provide a dual channel measurement capability.

It is noted in Section 3.2.3.3 that vibration and alignment problems are reduced when the reference beams are directed to pass through the measuring volume. Although it is not necessary for the reference beams to pass through the measuring volume, the existing

optics package is designed to operate in such a fashion. To split off
the reference beams, guide them around the test-cell, and redirect
them accurately down the bore of the photo-multiplier tubes would be
an unnecessary complication. Such a procedure would require numerous
mirrors and lenses to be anchored on different parts of the experimental
apparatus. These components would require frequent tedious adjustments
and would be subject to different sources of vibration. The existing
set-up anchors the entire optics package at a single point which
eliminates the problem of differential vibrations and greatly simpli-
fies alignment.

Point Positioning

The converted milling-machine used for point positioning and
described in Sec. 3.2.3.4 is highly accurate when used properly.
However, a possible measurement error can be introduced when
reversing the direction of travel because of play in the threaded
translation mechanism. This phenomenon, known as "backlash" to
experienced machinists, must be compensated for in order to maintain
positioning accuracy.

For a particular translation axis, the backlash is removed as
follows:

(1) Before reversing direction, one must note the dial
indicator reading and then turn the crank slowly
in the new direction until the play is taken up and
the threads just begin to bite (generally on the

order of 10 hash-marks on the indicator).

(2) Next, one loosens the knurled knob that locks the indicator dial and rotates the dial to a new baseline on the indicator ("0" is usually most convenient).

(3) Finally, one tightens the knurled knob and continues cranking in the new direction until he has translated the desired distance.

With practice, this technique can provide consistent positioning accuracy on the order of 0.5 millimeters.